CHEMICAL ABUNDANCE ANALYSIS OF VARIOUS POPULATIONS IN THE MILKY WAY

A Dissertation

by

DANIEL Q NAGASAWA

Submitted to the Office of Graduate and Professional Studies of
Texas A&M University
in partial fulfillment of the requirements for the degree of

DOCTOR OF PHILOSOPHY

Chair of Committee,	Jennifer L. Marshall
Committee Members,	Darren L. DePoy
	Casey Papovich
	Sherry Yennello
Head of Department,	Grigory Rogachev

August 2018

Major Subject: Astronomy

ABSTRACT

We perform chemical abundance analysis of two populations of stars to better understand the chemical evolution history the Milky Way. We take two approaches to answer this question, intending to add to the growing body of knowledge that comprises the field of galactic archaeology.

In the first approach, we provide a means by which we can improve current methods to measure the metallicity of M-dwarf stars, useful tracers of the chemical evolution of the Milky Way. The measurement of M-dwarf metallicity relies on the use of empirical relationships calibrated with F/G/K+M binary pairs. We have measured the radial velocity of 77 F/G/K stars and 62 M-dwarfs previously identified by common proper motion to be potentially in F/G/K+M binaries. Of the 63 candidate pairs where we have observed both the F/G/K primary and the M-dwarf secondary, we have identified 47 F/G/K+M-dwarf binaries using a 2-σ agreement in their measured radial velocities.

In order to indirectly measure the metallicity of the M-dwarf secondaries, we have performed chemical abundance analysis of 58 F/G/K stars, 47 of which were identified by radial velocity as F/G/K+M-dwarf binaries. Our sample of confirmed binaries spans a metallicity range of $-1.94 <$ [Fe/H] $< +0.01$. This allows the extension of these empirically calibrated relationships used to determine metallicity to more metal-poor M-dwarfs, enabling this tracer population to probe further back into the chemical history of the Milky Way.

Our second approach is to study the chemical abundance of an ultra-faint dwarf galaxy, allowing us to study the chemical evolution of similar Milky Way progenitors and to probe early Universe nucleosynthesis. We have performed a detailed chemical abundance analysis of three stars in the ultra-faint dwarf Horologium I. We have found that despite its metal-poor nature, there is an unexpected lack of α-element enrichment. We discuss possible scenarios that could cause this abundance pattern and discuss the stochasticity of early nucleosynthesis that these scenarios suggest.

By understanding the chemical abundance of these two populations, we can probe the chemical

history of the Galaxy and the origin of the elements, learning how the Milky Way evolved into its present chemical state.

DEDICATION

To my parents, from whom all that is good in me originates. To my dear friends, whose cheerful company and comforting support I have enjoyed and relied on all my life. To my teachers, who never gave up on me and inspired me to always be curious about the world around. To my beloved, whose love has lit my darkest days and my brightest moments. This work is yours.

ACKNOWLEDGMENTS

The author wishes to thank C. Sneden for his insight and his training in using the MOOG spectral synthesis software. He would also like to thank K.V. Tran and N. B. Suntzeff for productive conversations.

Funding for the DES Projects has been provided by the U.S. Department of Energy, the U.S. National Science Foundation, the Ministry of Science and Education of Spain, the Science and Technology Facilities Council of the United Kingdom, the Higher Education Funding Council for England, the National Center for Supercomputing Applications at the University of Illinois at Urbana-Champaign, the Kavli Institute of Cosmological Physics at the University of Chicago, the Center for Cosmology and Astro-Particle Physics at the Ohio State University, the Mitchell Institute for Fundamental Physics and Astronomy at Texas A&M University, Financiadora de Estudos e Projetos, Fundação Carlos Chagas Filho de Amparo à Pesquisa do Estado do Rio de Janeiro, Conselho Nacional de Desenvolvimento Científico e Tecnológico and the Ministério da Ciência, Tecnologia e Inovação, the Deutsche Forschungsgemeinschaft and the Collaborating Institutions in the Dark Energy Survey.

The Collaborating Institutions are Argonne National Laboratory, the University of California at Santa Cruz, the University of Cambridge, Centro de Investigaciones Energéticas, Medioambientales y Tecnológicas-Madrid, the University of Chicago, University College London, the DES-Brazil Consortium, the University of Edinburgh, the Eidgenössische Technische Hochschule (ETH) Zürich, Fermi National Accelerator Laboratory, the University of Illinois at Urbana-Champaign, the Institut de Ciències de l'Espai (IEEC/CSIC), the Institut de Física d'Altes Energies, Lawrence Berkeley National Laboratory, the Ludwig-Maximilians Universität München and the associated Excellence Cluster Universe, the University of Michigan, the National Optical Astronomy Observatory, the University of Nottingham, The Ohio State University, the University of Pennsylvania, the University of Portsmouth, SLAC National Accelerator Laboratory, Stanford University, the University of Sussex, Texas A&M University, and the OzDES Membership Consortium.

Based in part on observations at Cerro Tololo Inter-American Observatory, National Optical Astronomy Observatory, which is operated by the Association of Universities for Research in Astronomy (AURA) under a cooperative agreement with the National Science Foundation.

The DES data management system is supported by the National Science Foundation under Grant Numbers AST-1138766 and AST-1536171. The DES participants from Spanish institutions are partially supported by MINECO under grants AYA2015-71825, ESP2015-88861, FPA2015-68048, SEV-2012-0234, SEV-2016-0597, and MDM-2015-0509, some of which include ERDF funds from the European Union. IFAE is partially funded by the CERCA program of the Generalitat de Catalunya. Research leading to these results has received funding from the European Research Council under the European Union's Seventh Framework Program (FP7/2007-2013) including ERC grant agreements 240672, 291329, and 306478. We acknowledge support from the Australian Research Council Centre of Excellence for All-sky Astrophysics (CAASTRO), through project number CE110001020.

IRAF is distributed by the National Optical Astronomy Observatory, which is operated by the Association of Universities for Research in Astronomy (AURA) under a cooperative agreement with the National Science Foundation.

CONTRIBUTORS AND FUNDING SOURCES

Contributors

This work was supported by a dissertation committee consisting of Professor Jennifer L. Marshall, Professor Darren L. DePoy, and Professor Casey Papovich of the Department of Physics and Astronomy and Professor Sherry Yennello of the Department of Chemistry.

The raw data analyzed for Chapter 2 and Chapter 3 was provided by Professor Jennifer L. Marshall. These observations were performed by Professor Jennifer L. Marshall and Doctor Katharine Schlesinger. Data reduction was performed by Professor Jennifer L. Marshall.

Analysis and writing of Chapter 2 was additionally reviewed by Professor Nicholas Suntzeff.

The UVES observations using Chapter 4 were obtained by Doctor Eduardo Balbinot. Observations using the MIKE spectrograph was principally proposed by Doctor Rebecca Bernstein. Observations were performed by Professor Jennifer L. Marshall and the student.

Chapter 4 underwent collaboration-wide review by the Dark Energy Survey. Writing of Chapter 4 was done by Professor Jennifer Marshall and the student. The radial velocities presented were measured by Craig Pellegrino. An initial review was performed by Doctor Ting Li, Doctor Josh Simon, and Doctor Terese Hansen. Further review was performed by the Dark Energy Survey Working Group, including Doctor Rebecca Bernstein, Doctor Eduardo Balbino, Doctor Alex Drlica-Wagner, Doctor Andrew Pace, Professor Louis Strigari, Professor Darren L. DePoy, Professor Nicholas Suntzeff, and Doctor Keith Bechtol. Final reading and Dark Energy Survey collaboration approval was performed by Doctor Alistair Walker. Additional comments were provided by Astrophysical Journal referee Professor Christopher Sneden.

Funding Sources

Graduate study was supported by the graduate student Heep Fellowship, awarded by the Texas Institute of Advanced Study. This also work was supported supported by NSF award AST-1411678, “Measuring the Metallicities of M Dwarf Stars”, proposed by Professor Jennifer L. Marshall. This

work was also supported by a NASA WIYN PI Data Award, administered by the NASA Exoplanet Science Institute (Contract 1542413), and proposed for by the student.

NOMENCLATURE

dM	M-dwarf star (metal rich)
sdM	subdwarf M star
esdM	extreme subdwarf M star
usdM	ultra-subdwarf M star
DES	The Dark Energy Survey
Hor I	Horologium I
$T_{\rm eff}$	effective temperature [K]
log g	stellar surface gravity measured [dex]
$v_{\rm micro}$	microturbulence velocity [km s^{-1}]

TABLE OF CONTENTS

Page

LIST OF FIGURES

FIGURE Page

LIST OF TABLES

TABLE Page

1. INTRODUCTION AND LITERATURE REVIEW

For over a hundred years, astronomers have been using spectroscopic observations of astronomical phenomena to study their underlying physics and thereby better understand the Universe in which we live. Since the original discovery of the dark lines in the spectra of the sun in 1824 by Joseph Fraunhofer, scientists have used them to study individual stars. They found that spectra differ from star to star (Fraunhofer, 1905, summary work published posthumously), and thus enabled the first comparative studies between stars.

It can be argued that the field of stellar astrophysics was founded when the collaborative efforts of Gustav Kirchoff and Robert Bunsen found that Fraunhofer's dark lines were due to atomic absorption in the stellar atmosphere (Kirchhoff, 1860; Kirchhoff & Bunsen, 1860). This discovery allowed the initial identification of elements in the solar atmosphere. It was this work that allowed William Huggins to determine that the sun was composed of the same elements as found on Earth and that the relative shift in these lines could be used to determine whether an object is moving toward or away from Earth (Huggins, 1868). With these discoveries, astronomers could use physics to roughly understand the composition and the motion of distant celestial objects.

This culminated in the development of stellar chemical abundance analysis methods by Cecilia Payne in 1925. Payne (1925) applied the ionization theory developed by Meghnad Saha (1921) to measure the relative abundance of individual elements in the solar atmosphere. She found that the sun was composed primarily of hydrogen, a discovery which at the time was dismissed as wrong due to the preponderance of iron lines in the solar spectrum but would later be proven correct (Payne, 1925). This would eventually lead to the fundamental conclusion that hydrogen is the most abundant element in the Universe.

In developing these techniques, Payne enabled the measurement of the relative metal, or elements heavier than helium, content of a star (metallicity) and formed the basis of spectroscopic chemical abundance studies performed ever since. Though the manner and the methods in which chemical abundances are calculated have improved over the years as our understanding of physics

and astrophysics has advanced, the basic principles of the methodology remains the same. Astrophysicists identify element lines in a stellar atmosphere. Using Saha's equations and a model of the stellar atmosphere, the abundance of element are measured with respect to hydrogen.

Though this methodology has remained largely intact, new scientific questions have arisen that can be answered using these techniques. These questions motivate this dissertation. By applying these historically significant techniques to modern problems, we hope to contribute to the solution to some of these profound and interesting questions.

1.1 Motivations for this Study

There are many unanswered questions about the Galaxy: How does the 13 billion-year history of the Milky Way manifest itself in modern observations of its structure? How does each of the progenitors of the Milky Way influence the chemical makeup of the Galaxy that astronomers observe today? Does the chemical makeup of the stars in the Galaxy affect the formation of the Galaxy as a whole? Of structures found within the Galaxy? Of the formation of planets around the stars? These questions have formed the basis of the field of galactic archaeology.

The focus of galactic archaeology is the understanding of the complex history of the Milky Way. Since Searle & Zinn (1978) found that the halo of the Milky Way was formed by the infall of smaller structures, hierarchal merging has become the leading theory of the formation of the Galaxy. This view has been supported by modern simulations of the Universe with dark energy and dark matter (ΛCDM), our best understanding of the composition of the Universe.

Much work has been done to understand this primordial population of Milky Way progenitors and how they affect the Galaxy formation (Johnston et al., 1996; Bullock & Johnston, 2005, and subsequent work) from a kinematic perspective. These N-body dark matter simulations demonstrate that the Milky Way, rather than being one homogeneous structure, is in actually at heterogeneous combination of thousands of independent structures. Some are progenitors falling from outside of the Milky Way and are subsequently disrupted while others are star clusters native to the Milky Way formed from the gas of previously disrupted progenitors.

From a chemical analysis standpoint, this heterogeneity presents an interesting avenue for re-

search. In principle, every Milky Way progenitor and every Milky Way birth cluster had its own chemical evolution history prior to its infall and eventual disruption by the Milky Way. The chemical abundance of every star is a fossil record of the chemical composition of its birth environment. Therefore, studying the chemical composition of Milky Way stars can help untangle the evolution of the Milky Way by tracing its progenitors or its birth star cluster (Freeman & Bland-Hawthorn, 2002). This methodology, called chemical tagging, has gained traction in the field. Hogg et al. (2016) tested this methodology's capability to track individual populations by abundance alone with some success. With larger spectroscopic surveys such as APOGEE (Majewski et al., 2017) measuring more elements in a greater number of stars, this is a field posed to make interesting discoveries in the coming years.

Another way to study the primordial progenitors of the Milky Way is to study objects similar to them that still remain undisrupted by the Galactic gravitational potential. ΛCDM N-body simulations predict a large number of satellite galaxies to the Milky Way . A focus in recent years has been finding (i.e. Bechtol et al., 2015; Drlica-Wagner et al., 2015) and characterizing (i.e. Koposov et al., 2015b; Simon et al., 2017) such ultra-faint dwarf satellite galaxies.

These objects present an interesting laboratory to study the chemical evolution of the progenitors of the Milky Way. Ultra faint dwarfs are composed of old, isolated stellar populations. Because of the age and the early halt of star formation in these objects (Brown et al., 2014; Wetzel et al., 2015; Jeon et al., 2017), these objects are likely influenced by only a few nucleosynthetic events and preserve the chemical signature of those events. Therefore, studying the chemical abundance of these ultra-faint dwarfs can help improve our understanding of the early history of the Universe and the population of small galaxies that would merge to become the Milky Way.

These two different avenues of research using chemical abundances, studying the stars within the Milky Way to untangle its disparate populations and studying the stars that compose objects similar to the progenitors of the Milky Way, both attempt to probe the complex history of the Galaxy. Understanding the chemical evolution of the Milky Way is the prime motivation behind this dissertation. Therefore, we attempt to use both techniques to contribute to our knowledge of

the history of the Galaxy.

In studying stars within the Milky Way itself, late-type low temperature main sequence stars known as M-dwarfs can be used as a tracer population. These stars are the most numerous in the Milky Way and can potentially be used to study the kinematics and the metallicity of the Milky Way disk and halo. Metal-poor M-dwarfs in particular are an interesting population to study in that they are likely compose most of the closest metal-poor stars. Therefore, the first part of this dissertation is dedicated to finding ways to improve the study of this population of stars.

The second part of this dissertation involves the study of stars in an ultra-faint dwarf galaxy. Analysis of stars in these objects provides us a look into the nucleosynthetic history of Milky Way progenitors and the highly stochastic nature of early Universe element formation. Through the measurement of the abundance of various elements in these objects, we hope to understand how these objects came to be and whether some stars in the Milky Way halo originated in objects with a similar nucleosynthetic history.

1.2 Literature Review

We discuss some of the previous work performed in these fields. We divide this literature review into literature involving the measurement of M-dwarf metallicity and literature involving the chemical abundance analysis of ultra-faint dwarfs.

1.2.1 Studies of M-dwarfs and their Metallicities

Modern surveys such as the Sloan Digital Sky Survey (York et al., 2000) have allowed the construction of large catalogs of M-dwarfs for both photometric study (Bochanski et al., 2010) and spectroscopic study (West et al., 2011). This has allowed the study of the distribution of M-dwarfs in the galaxy (Bochanski et al., 2010) and their kinematics (Bochanski et al., 2007; Fuchs et al., 2009). This work has led to the use of M-dwarfs as tracers of Galactic populations. The next logical step is the measurement of their metal content.

M-dwarfs have become even more appealing targets for study in the field of exoplanet studies. Due to their low-mass, they have a higher Doppler response to the influence of an orbiting planet.

Due to their faintness, planet transits are more dramatic and therefore easier to detect. Given previously established planet-metallicity relationship found by Fischer & Valenti (2005) in F/G/K stars, studying the metallicity of these M-dwarf exoplanet hosts has been a key goal of M-dwarf metallicity measurement attempts.

However, the need to measure M-dwarf metallicities is belied by its difficulty. The coolness of the M-dwarf stellar atmosphere allow the formation of molecular species whose features dominate their spectra (Bessell, 1991). In particular, hydrides such as CaH and oxides such as TiO and VO complicate the study of M-dwarf metallicity due to the lack of laboratory transition studies for these species.

This has led some to measure the metallicity of M-dwarfs without the use of spectra. Work done by (Bonfils et al., 2005) used 20 wide visual binaries to calibrate a photometric method to determine M-dwarf metallicity. Using absolute magnitudes, this was able to achieve a [Fe/H] precision of ± 0.2 dex in M-dwarf metallicity measurements. However, the inherent drawback of this method is that it relies on distance measurements, limiting its application to nearby stars with known parallaxes.

Another approach was tried by Marshall (2008) using a combination of proper motions and precise photometric measurements to determine the metallicity of M-dwarfs. In this work, a reduced proper motion diagram was used to find extreme subdwarfs (esdM), very metal-poor M-dwarfs stars, in the Galactic halo. They concluded that with precise enough photometry and proper motions, these metal-poor stars can be identified. The drawback of this is that it requires the measurement of proper motions. While significant gains have been made in the measurement of proper motions across the whole sky, including the recent Gaia mission (Tian et al., 2017), this still limits the applicability of this technique to stars where proper motion has been measured.

Some who have attempted to use spectra to study M-dwarfs have turned the molecular species that complicate analysis to their advantage. Mould (1976) first measured the band strengths of CaH and TiO and offered a theoretical calibration of TiO to metallicity and CaH to surface gravity. Importantly, Mould (1976) created a theoretical model atmosphere grid for M-dwarfs, incorporat-

ing effective temperature, surface gravity, and metallicity. Originally, this was used to study the difference between halo M-dwarfs and disk M-dwarfs.

This initial calculation would be refined by Bessell (1982). In this work, TiO and CaH bands found at optical wavelengths were used as a secondary metallicity check. In studying M-dwarfs with strong hydride bands, namely CH, MgH, and CaH, Bessell (1982) developed what they called an "equivalent spectral type " for a set of different metallicities, i.e. an M-dwarf with an effective temperature of 3000K and $Z/Z_{\odot} = 0.01$ would have a TiO5 absorption feature similar to that of a spectral type M5. This drawing of comparisons is a qualitative determination of metallicity which was a useful first step in analyzing M-dwarf spectroscopy.

The use of molecular features that dominate the spectra of M-dwarfs to characterize these stars was further improved by Reid et al. (1995). Through the Palomar/MSU spectroscopic survey, Reid et al. (1995) obtained optical spectroscopy of 1746 stars. In their attempt to quantitatively measure these molecular features, they defined a number of flux ratios to serve as molecular indices to measure the absorption strength of CaH and TiO, the same species identified by Mould (1976) to be sensitive to surface gravity and metal content. This allowed them to apply quantitative analysis to their large sample and would form the basis of future analyses.

Additional molecular indices were defined by Kirkpatrick et al. (1995), specifically for the molecular species VO. This particular molecular species is observed in very late-type M-dwarfs (M7V-M9V), where VO absorption is greater than that of earlier types M-dwarfs. Thus, the molecular index they defined is useful in identifying these late type stars. However, the indices developed by Reid et al. (1995) remain the most widely used for M-dwarf classification schemes.

The CaH and TiO indices defined by Reid et al. (1995) were used by Lépine et al. (2003) to roughly classify M-dwarfs into metallicity classes. The sample of M-dwarfs used in their classification was composed of 104 high proper motion stars and spanning a wide range of metallicites. Using plots of various CaH molecular indices against the measured absorption of TiO, M-dwarfs could be divided into metal-rich dwarfs (dM) stars, slightly metal-poor subdwarfs (sdM) stars, and the most metal-poor extreme subdwarfs (esdM) stars. They used empirically drawn bounds to clas-

sify their M-dwarfs into these subgroups. However, this classification scheme fails in cases of low TiO absorption. While it can adequately separate the populations when TiO absorption is strong, when the TiO band is weak, it is more difficult for this classification scheme to separate metal-poor M-dwarfs from metal-rich.

Lépine et al. (2007) identified a few of the inherent weaknesses in this classification scheme and attempted to rectify it by defining a new classification scheme. In their work to address these weaknesses, they created a new metallicity index $\zeta_{\text{TiO/CaH}}$ where they defined $\zeta = 1$ as stars of roughly solar metallicity in the disk. To elucidate, ζ was determined by a TiO molecular band and a theoretically calculated TiO band for a star of solar metallicity. The metallicity classes dM, sdM, esdM, and the additional class of the most metal-poor ultra subdwarfs (usdM) could then defined quantitatively by ζ.

This ζ metallicity parameter was futher refined by Dhital et al. (2012) using the SLoWPoKES catalog of low-mass binaries. They found that the original calibration developed by (Lépine et al., 2007) had a small systematic bias for earlier type M-dwarfs. By recalibrating to eliminate this systematic bias, Dhital et al. (2012) claimed that ζ is a good predictor of iso-metallicity for M-dwarfs.

To calibrate M-dwarf metallicites, some studies used binary pairs comparing the metallicites of M dwarfs with those of F/G/K-type partners. While the work using the molecular features for classification into metallicity subtypes has been useful as a qualitative study of M-dwarf metallicity, some have approached the problem by using spectral features as a direct proxy for [Fe/H]. Woolf & Wallerstein (2006) used F/G/K+M binaries to calibrate a relationship between the metal content of the M-dwarf (as measured in the F/G/K-type partner) to optical wavelength CaH and TiO features. Using 76 binaries with a metallicity range of $-1.0 <$ [Fe/H] $< +0.05$, they were able to determine the metallicity of M-dwarfs within this range to an accuracy of ± 0.3 dex.

More work creating these proxy measurements using binary pairs has been done at near-infrared wavelengths. Approaches using near-infrared have focused on the use of strong atomic features rather than molecular bandpasses. Rojas-Ayala et al. (2012) used 18 F/G/K+M binaries with previously measured metallicites to develop and calibrate a relationship between the metallic-

ity of the M-dwarf with the equivalent width of Na I, the Ca I triplet, and the H_2O-K2 molecular index. This allowed the use of medium-resolution near-infrared spectroscopy to determine the metal content of an M-dwarf within the range of their calibration sample, $-0.69 <$ [Fe/H] $< +0.31$.

An improvement to this method was developed by Newton et al. (2014) who used more M-dwarfs and a larger metallicity range as a calibration sample for their proxy measurement. Using 36 common proper motion F/G/K+M binaries with a metallicity range from $-1.0 <$ [Fe/H] $< +0.35$, they developed a relationship between metallicity and the 2.2 μm Na I doublet. Using this method, one can use moderate-resolution spectra ($R \sim 2,000$) to determine the metallicity of M-dwarfs to an accuracy of 0.12 dex.

Some of the most recent work using infrared spectra has attempted to expand the range of species for which we can determine abundance in an M-dwarf to include Ti. Up until this point, these empirical metallicity relationships have solely focused on the determination of [Fe/H]. Veyette et al. (2017) attempted to create an empirically calibrated relationship to measure not only [Fe/H] but [Ti/H] as well using high resolution ($R \sim 25,000$) near-infrared spectra. They used 33 F/G/K+M binaries with a metallicity range of $-0.7 <$ [Fe/H] $< +0.3$ to calibrate their method which uses both the equivalent widths of near-infrared Fe I and Ti I and the latest M-dwarf spectroscopic models available, the BT-SETTL models from Allard (2016). With this, it is now possible to measure [Fe/H] and an a refractory element, [Ti/H], in the atmosphere of an M-dwarf.

At present, the ability to precisely determine the metallicity of an M-dwarf is largely limited to near-infrared wavelengths. An optical wavelength counterpart to the work of Rojas-Ayala et al. (2012) and Newton et al. (2014) has yet to determined. It is the ultimate goal of this work to develop such as calibration in order to utilize the prolific optical spectroscopic surveys such as SDSS to study the metallicity and the kinematics of M-dwarf populations, especially metal-poor halo stars.

To develop an optical wavelength metallicity relationship for M-dwarfs, more F/G/K+M binaries are needed for use in empirical calibration. All of these relationships to measure [Fe/H] have relied on F/G/K+M binaries to determine the metallicity of the M-dwarf for use in their empirical

calibrations. This prompts the development of a high fidelity sample of F/G/K+M binaries that cover a larger range of metallicities to extend the reach of these methods to more metal-poor stars.

1.2.2 Ultra-Faint Dwarf Metallicity Studies

The study of the chemical abundance of ultra-faint dwarfs has expanded rapidly in recent years. This has been largely due to the increased effort to discover and characterize satellite galaxies to the Milky Way in an attempt to reconcile the prediction of a large number of these satellites by ΛCDM N-body simulations with observations. McConnachie (2012) provided a summary of work done using the SDSS survey in characterizing the positional, structural, and dynamical parameters of over 100 dwarf galaxies around the Milky Way, 27 of which were dark matter dominated satellites bound to the Milky Way potential.

Recently, the Dark Energy Survey (DES; The Dark Energy Survey Collaboration, 2005), a five-year survey of the Southern hemisphere, has discovered a large number of new ultra-faint dwarf galaxies. In the first two years of DES, 22 new candidate satellites were discovered using DES data (Bechtol et al., 2015; Koposov et al., 2015a; Drlica-Wagner et al., 2015; Kim & Jerjen, 2015; Kim et al., 2015; Luque et al., 2016, 2017). This has greatly expanded the number of satellites to the Milky Way, enabling a range of analyses.

In particular, the discovery of so many ultra-faint dwarf galaxies has enabled the study of the varying chemical histories of these objects and how they relate to the history of the Milky Way. This has led to efforts using high-resolution spectroscopy to measure a variety of elemental species to characterize these objects through their member stars.

The first work to perform high resolution spectroscopic observations to measure chemical abundances was done by Koch et al. (2008b) with additional follow-up work performed by Koch et al. (2013) and François et al. (2016) on the Hercules dwarf spheroidal galaxy (Her), orginally found using SDSS. They found a moderately low metallicity of [Fe/H] ~ -2 and a high α-element abundance, consistent with an older population of stars. They concluded that the member stars of Her were similar to metal-poor Milky Way halo stars.

Bootes I (Boo I) was discovered in 2006 by Belokurov et al. (2006) using SDSS data. Subse-

quent chemical abundance studies were performed by Norris et al. (2010), Ishigaki et al. (2014), Gilmore et al. (2013), and Frebel et al. (2016). These studies found that overall abundance ratios for light elements and Fe-peak elements resemble the Milky Way halo, with a slight deficiency in neutron-capture element abundance. The ultimate conclusion of Frebel et al. (2016) was that Boo I was one of the earliest assembled systems, but not a pristine first galaxy unaffected by later chemical evolution.

Frebel et al. (2010) studied two ultra-faint dwarfs using high resolution spectroscopy, Coma Berenices (ComBer) and Ursa Major II (UMa II). Medium resolution spectra of member stars in these objects indicated that these stars were likely more metal-poor than Her. This ultimately was proven in their analysis using high resolution abundance analysis of the α-elements and the Fe-peak elements. Critically, however, they came to the conclusion that their results suggested that much more massive dwarf galaxies were the origin of the metal-rich stars in the Galactic halo while objects like ComBer and UMa II were the origin of the most metal-poor stars.

This idea was further reinforced by the study of another ultra-faint dwarf galaxy. The ultra-faint dwarf Leo IV was studied by Simon et al. (2010) with a follow-up study performed by François et al. (2016). The conclusion of Simon et al. (2010) was that the brightest star in Leo IV had a chemical abundance pattern consistent with nucleosynthesis from the explosion of a Population III star, the first stars in the Universe that formed with primordial chemical abundances from Big Bang nucleosynthesis. This work laid the foundation of using nucleosynthetic models of Population III stars to understand the presently observable population of ultra-faint dwarf member stars.

The lack of substantial chemical evolution these objects was shown in the analysis of Segue 1 by Frebel et al. (2014). In this work, Frebel et al. (2014) performed chemical abundance analysis on every red giant in Segue 1, finding a metallicity range of $-3.8 <$ [Fe/H] < -1.4 and a high α-enhancement. However, in their analysis of the neutron-capture element abundance, they found a deficiency that suggested as few as one nucleosynthetic event. They ultimately concluded that Segue 1 had one generation of star formation before quenching, which preserved this nucleosynthetic record.

This is contrasted by the study of Segue 2, which was studied by Roederer & Kirby (2014). They measured the chemical abundance of the brightest star using high resolution spectroscopy. They reached similar conclusions to Frebel et al. (2010) in that the abundance of Segue 2 was similar to that of the Milky Way halo with the exception of this deficiency in neutron-capture elements. However, they concluded that this abundance pattern was not due to a single generation, but rather multiple generations of Type II supernovae. This suggested that Segue 2 must have been more massive in the past than it is presently observed to be.

This deficiency in neutron-capture elements as compared to the Galactic halo was later found to be even greater in the analysis of Bootes II (Boo II). Ji et al. (2016d) found that neutron-capture elements were practically undetectable in Boo II, which had the lowest upper limits on this abundance yet seen. The remaining elements suggested only a few generations of star formation in Boo II resulting in a low metallicity. The most important conclusion of this work though was that the discrepancy in neutron-capture element abundance between halo stars and these ultra-faint dwarf members was too great for the neutron-capture elements in the halo to have originated in ultra-faint dwarfs.

Further insight into the origin of these heavy neutron-capture elements was gained in the analysis of Canes Venatici II (CVn II) by François et al. (2016). In their chemical analysis, they found that lighter neutron-capture elements were more abundant than heavier neutron-capture elements, evidenced by a high [Sr/Ba] ratio. They surmised that these two groups may have different origins, suggesting that neutron star mergers may be responsble for this high ratio.

Observation proof of this theory that neutron-capture elements had a different nucleosynthetic origin came with the study of Reticulum II (Ret II) by Ji et al. (2016c) with additional follow-up performed by Roederer et al. (2016). In these works, a ~ 2 dex overabundance in neutron-capture elements was found in a majority of the stars studied in Ret II, meaning these stars were r-II stars, stars enriched in r-process elements (definition by Beers & Christlieb, 2005). This was suggested to be due to a single event with a high nucleosynthetic yield of neutron-capture elements, particularly r-process elements. This was one of the first hints that the chemical evolution of ultra-faint

dwarfs was highly variable.

This idea was bolstered by the study of Tucana II (Tuc II) by Ji et al. (2016b) with additional follow-up work by Chiti et al. (2018). These works suggest that the chemical history of Tuc II was influenced by two nucleosynthetic events in order to explain the various abundances of α-elements, neutron-capture elements, and C abundance. Chiti et al. (2018) suggested that that the two events are made possible by an extended chemical evolution. This result adds to the growing body of evidence that the early Universe nucleosynthesis differed greatly from ultra-faint dwarf to ultra-faint dwarf.

Triangulum II (Tri II), studied by Venn et al. (2017) and Kirby et al. (2017), presents another unusual chemical abundance signature. However, the noteworthy difference is in the spread of the metallicity distribution. Kirby et al. (2017) found that Tri II presents a wide variety of metallicites, indicating that supernovae ejecta, usually dispersed from ultra-faint dwarfs due to their inherently low masses, may have been retained and enriched subsequent populations. They concluded that Tri II may have been more massive in the past, a similar case to Segue 2. They also indicated that the dark matter halo may have impacted nucleosynthesis in retaining the supernovae ejecta.

Tucana III (Tuc III) is another ultra-faint dwarf with chemically peculiar stars. Tuc III is noteworthy among the ultra-faint dwarfs studied to date in that it is undergoing tidal disruption. Studied by Hansen et al. (2017), Tuc III presents a neutron-capture element enrichment similar to Ret II though not as high, making them r-I stars, stars enriched with r-process elements though not enriched to the extent of r-II stars. This was considered surprising given the relatively low luminosity of Tuc III. They suggested that objects similar to Tuc III are the source of r-I stars in the halo, and propose several possible formation mechanisms.

The wide variety of mechanisms and solutions invoked to explain the assorted chemical abundance patterns observed in these ultra-faint dwarfs hint at the stochasticity of the nucleosynthesis processes in the early Universe when these objects were still star forming. These previous studies have raised questions about the origin of the elements and how they relate to the Milky Way halo. The study of the chemical abundance of additional ultra-faint dwarfs will allow us to understand

the extent of this stochasticity and how the element formed and affected the formation of the Milky Way.

1.3 Summary and Structure of This Study

The structure of this dissertation is divided into three chapters. The first two chapters relate to the study of M-dwarfs through the analysis of a binary partner. The third chapter describes the detailed chemical abundance analysis of an ultra-faint dwarf and possible explanations of its chemical abundance patter.

In Chapter 2, we present a sample of wide-separation F/G/K+M stars likely to be binary pairs, identified using a combination of proper motion and radial velocity measurements. A large, sample of F/G/K+M binaries can be used to evaluate existing methodologies to parameterize M-dwarf metallicity and to develop new techniques. Li et al. (2014) assembled a sample of 81 pairs of common proper motion stars likely to be an F/G/K+M binary system. We have measured radial velocities of both stars in the candidate binary using high resolution spectra of the solar-like primary and low resolution spectra of the M-dwarf secondary for 52 candidate binaries. By comparing the radial velocity of the primary and secondary stars, we have determined that 47 of the 52 candidate binaries observed are true binaries.

In Chapter 3, we present measurements of the Fe, Ca, and Ti abundance of 59 of the 81 F/G/K stars identified as candidate primaries in an F/G/K+M system by Li et al. (2014). Of the 58 stars studied, 42 were confirmed in Chapter 2 to have an M-dwarf partner. We found that the abundance pattern of these stars matches that of the Milky Way halo. We have also found that the metallicites of the majority of our sample would classify them as subdwarfs, consistent with findings from a reduced proper motion diagram.

In Chapter 4, we present chemical abundance measurements of three stars in the ultra-faint dwarf galaxy Horologium I, a Milky Way satellite discovered by the Dark Energy Survey. Using high resolution spectroscopic observations we measure the metallicity of the three stars as well as abundance ratios of several α-elements, iron-peak elements, and neutron-capture elements. The abundance pattern is relatively consistent among all three stars, which have a low average

metallicity of [Fe/H] ~ -2.6 and are not α-enhanced ([α/Fe] ~ 0.0). This result is unexpected when compared to other low-metallicity stars in the Galactic halo and other ultra-faint dwarfs and suggests the possibility of a different mechanism for the enrichment of Hor I compared to other satellites. We discuss possible scenarios that could lead to this observed nucleosynthetic signature including extended star formation, enrichment by a Population III supernova, and or an association with the Large Magellanic Cloud.

In Chapter 5, we conclude with a summary of the findings in this work. We also discuss challenges in performing this work as well as potential avenues of future exploration.

2. HIGH FIDELITY SAMPLE OF F/G/K+M-DWARF BINARY PAIRS

2.1 Introduction

Low-mass main sequence stars known as M-dwarfs are the most prevalent types of stars in the Galaxy. They form 60-70% of the main sequence stars in the Galaxy (Chabrier, 2003; Bochanski et al., 2010). Because of this ubiquity, they form an independent tracer for the evolution of the structure, dynamics, and chemistry of the Milky Way. Surveys such as the Sloan Digital Sky Survey (SDSS York et al., 2000) and the Two Micron All-Sky Survey (2MASS; Skrutskie et al., 2006) have enabled the study of the spatial distribution (Bochanski et al., 2010) and the kinematic properties (Fuchs et al., 2009) of M-dwarfs. Studies such as these have opened up a large portion of discovery space using these stars to study the enrichment and merger history of the Galaxy through the chemistry and the kinematics of these objects.

However, the metallicities of M-dwarfs are difficult to determine. Techniques and programs exist to model and measure the metal content of solar-like stars (i.e. Sneden, 1973). Additionally, modeling the atmosphere to measure the metal content of an M-dwarf has been attempted (e.g. Bean et al., 2006; Allard, 2016). However, use of either methodology are hampered by the lack of detailed laboratory studies of the molecular species such as CaH and TiO found in the M-dwarf atmospheres, a problem particular to the study of low mass stars.

As a result, astronomers have turned to indirect methods using photometry (Bonfils et al., 2005; Marshall, 2008) and spectroscopy (Lépine et al., 2007; Dhital et al., 2012). Though unable to directly measure the metallicity of M-dwarfs, astronomers have used these empirically based methodologies to bypass the analysis difficulties caused by these molecular features. A promising method is the use of F/G/K+M binaries to determine empirical relationships between the metallicity of the primary F/G/K star and molecular spectral indices in the M-dwarf secondary known to be sensitive to metallicity (Woolf & Wallerstein, 2006; Rojas-Ayala et al., 2012).

Recent work has been done on developing such empirical relationships using infrared spec-

tra of an M-dwarf to determine similar empirically calibrated relationships between strong atomic feature and metallicity. This has been done using Fe I and Ti I lines (Veyette et al., 2017) and Na I lines (Newton et al., 2014). These relationships have also been calibrated through the use of F/G/K+M binary pairs.

The core assumption of these indirect methods is that the F/G/K-type star and its M-dwarf companion have identical chemical abundances. Therefore, one can use techniques developed to measure the chemical abundance of the solar-like primary to infer the detailed metal content of its M-dwarf partner (i.e. Rojas-Ayala et al., 2012). Having a large, pure sample of F/G/K+M binaries can be used to evaluate the effectiveness of existing methodologies and develop new techniques to measure M-dwarf metallicity.

In this chapter, we have assembled a sample of common proper motion F/G/K+M candidate binaries and performed radial velocity measurements to confirm binarity. This paper is organized as follows: in Chapter 2.2, we discuss the criteria used to identify likely wide separation, common proper motion F/G/K+M binary pairs. In Chapter 2.3, we discuss the observations and data reduction of the high resolution spectra taken of the solar-type primary stars and low resolution spectra taken of the M-dwarf secondaries. In Chapter 2.4, we discuss how we measured the radial velocities of all stars observed in this work. In Chapter 2.5, we present our measured radial velocities. In Chapter 2.6, we compare these measurements to literature measurements and discuss our criteria for determining binarity.

2.2 Sample Selection

The sample was constructed as described by Li et al. (2014). In summary, we selected stars from the LSPM-South and LSPM-North high proper motion catalog of Lépine & Shara (2005a, private communication) and Lépine (2005), both catalogs being subsets of the SUPERBLINK proper motion survey (Lépine & Shara, 2005b; Lépine, 2008), and the published list of halo binaries in the revised New Luyten Two-Tenths Catalog (rNLTT) by Chanamé & Gould (2004). Potential binaries from both catalogs were selected by finding pairs of stars with a separation of 3 arcsec $< \Delta\theta <$ 900 arcsec and a common proper motion. We require that the binaries have $\Delta\mu$, or the

difference in the measured proper motion of the candidate primary and secondary,$<$ 20 mas yr^{-1}. The candidates were further required to be dwarfs or subdwarfs via their placement on a reduced proper motion diagram (Li et al., 2014, Fig. 1). The final requirement is that the primary star of the pair has $V - J < 2.5$ and the secondary has $V - J > 3.0$, to ensure that the primaries are F, G, or K dwarfs or subdwarfs while the secondaries are M dwarfs and subdwarfs. These criteria yield a list of 81 pairs of stars observable from the Las Campanas Observatory, where these observations were performed.

2.3 Observations and Data Reduction

From the original sample of 81 candidate pairs, 77 candidate primary stars and 66 candidate secondary stars were observed with the Magellan-Clay 6.5m and du Pont 2.5m telescopes at the Las Campanas Observatory in 2007-2008 and 2016. Photometric measurements of the 81 selected pairs are presented by Li et al. (2014).

2.3.1 High Resolution Spectroscopy of Primary Stars

We obtained high-resolution spectra of 77 F/G/K primary stars using the MIKE spectrograph on the Magellan-Clay telescope and the Echelle spectrograph on the 100" du Pont telescope from 2007 to 2008 and 2016.

MIKE observations were made at a resolution of $R = \lambda/\Delta\lambda \sim$22,000 ($\Delta\lambda = 0.25$ Å at 5500Å) using a 0.7 arcsec slit and 2x2 pixel binning on the CCD. Raw spectra were reduced using the pipeline provided by Kelson (2003). With this pipeline, the data were bias corrected, flat fielded, extracted, wavelength calibrated, sky subtracted, and combined.

The resulting spectra covered a wavelength range of 3340 Å $< \lambda < 5100$ Å in the blue and 4825 Å $< \lambda < 9650$ Å in the red. During several periods of observations, the blue CCD of MIKE malfunctioned, resulting in the loss of spectral data in that wavelength range. Therefore, for these nights, only data obtained using the red CCD were usable; in total, this affected spectra for 41 F/G/K-type targets.

Spectra were also obtained using the echelle spectrograph on the 100" du Pont telescope (for

simplicity, henceforth referred to Echelle-100). These spectra were bias corrected, flat-fielded, extracted, wavelength calibrated, sky-subtracted, and stacked using IRAF[1] tasks.

This resulting spectra had a resolution of $R = \lambda/\Delta\lambda$ ∼26,000 ($\Delta\lambda = 0.19$ Å at 5000Å) and wavelength coverage from 3500 Å $< \lambda < 10400$ Å.

We present five representative spectra from both MIKE and Echelle-100 in Figure 3.1. These are also representative of the high dispersion spectra used in the abundance analysis in Chapter 3.

2.3.2 Low Resolution Spectroscopy of M-dwarf Secondaries

Spectroscopic observations of 62 M dwarf stars were obtained with the B&C spectrograph on the 100-inch du Pont telescope at Las Campanas Observatory over four observing runs in 2007 and 2008. We used the 600 l/mm grating blazed at 7500 Å with a tilt angle of 13°45′ and order-sorting filter GG-495 yielding a wavelength coverage of roughly 5500Å $< \lambda <$ 8500Å. A 2″ slit yielded a resolution of $R = \lambda/\Delta\lambda \sim$ 2000 at 6400Å.

Multiple exposures of the target stars were required to obtain an adequate signal-to-noise ratio (S/N). The following procedure was used for each observation individually, i.e. a flat field and comparison lamp spectrum were obtained every 15 minutes of a multi-hour exposure in order to account for instrument flexure during tracking and to remove fringing in each exposure.

The spectral images were reduced using the IRAF[1] software package beginning with subtraction of bias as measured using the overscan region of the detector. Flat fields were constructed for each individual exposure, using the flat field exposures acquired before and after each target spectrum. The two flat fields were averaged and the overscan-subtracted target image was divided by the normalized combined flat field. Spectra were then extracted from the target images. When multiple exposures were obtained of a single target, the spectra were extracted individually with the individual images being averaged together after extraction, applying cosmic ray rejection during the averaging. The resulting spectra were then flux calibrated using a flux standard star observed on each night. Figure 2.1 shows a representative sample of spectra of the M dwarf secondary stars

[1]IRAF is distributed by the National Optical Astronomy Observatories, which are operated by the Association of Universities for Research in Astronomy, Inc., under cooperative agreement with the National Science Foundation.

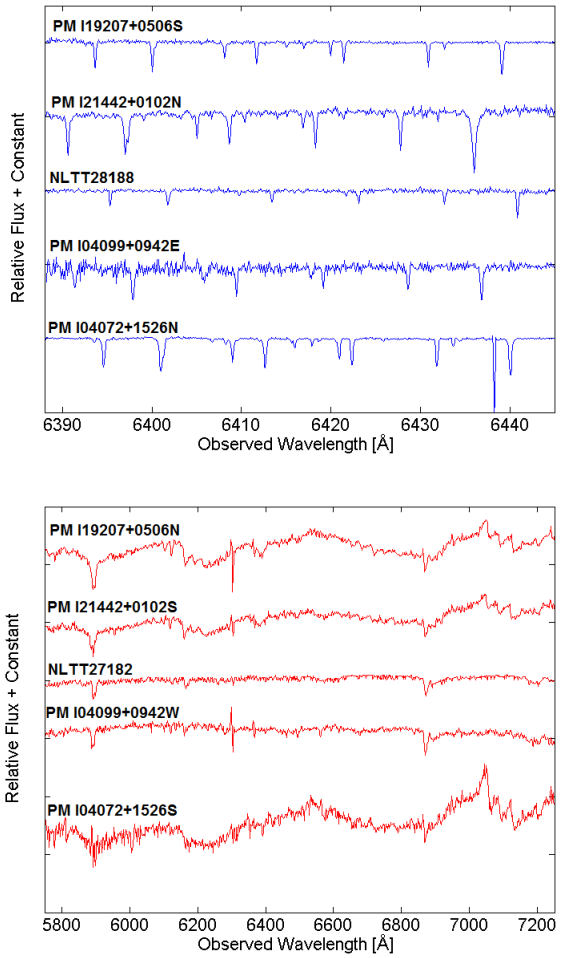

Figure 2.1 Left: Observed spectra of five confirmed F/G/K+M binary pairs in our sample. We show PM I04072+1526N from Echelle-100, order 44. The other stars presented are from MIKE, order 17. Right: The M-dwarf spectra presented span a wide range of achieved S/N. PM I04072+1526S had a $S/N = 16$ while PM I19207+0506N had $S/N = 192$.

in the sample.

2.4 Radial Velocities

Radial velocity measurements of the F/G/K primary stars were performed using the IRAF *fxcor* task (Alpaslan, 2009), which utilizes a Fourier cross-correlation analysis to determine the relative velocity $R_{\rm rel}$ between a reference with known velocity $R_{\rm ref}$ and a target star. To compute the

Table 2.1 Summary of Observing Runs

UT Dates	Telescope	Instrument
26-Aug-2007 to 30-Aug-2007	du Pont	echelle spectrograph
16-Feb-2008 to 20-Feb-2008	du Pont	echelle spectrograph
19-Mar-2007 to 23-Mar-2007	du Pont	B&C spectrograph
05-Sep-2007 to 10-Sep-2007	du Pont	B&C spectrograph
01-Feb-2008 to 05-Feb-2008	du Pont	B&C spectrograph
30-Aug-2008 to 07-Sep-2008	du Pont	B&C spectrograph
09-Feb-2007 to 10-Feb-2007	Magellan-Clay	MIKE spectrograph
20-Nov-2007 to 23-Nov-2007	Magellan-Clay	MIKE spectrograph
24-Apr-2008 to 25-Apr-2008	Magellan-Clay	MIKE spectrograph
23-Jul-2008	Magellan-Clay	MIKE spectrograph
13-Nov-2008 to 16-Nov-2008	Magellan-Clay	MIKE spectrograph
09-Dec-2008 to 11-Dec-2008	Magellan-Clay	MIKE spectrograph
05-Aug-2016	Magellan-Clay	MIKE spectrograph

heliocentric velocity correction, the *rvcor* task was used, which calculates the heliocentric velocity correction of the target star $R^{\text{tar}}_{\text{helio}}$ and the reference star $R^{\text{ref}}_{\text{helio}}$. Based on these, the radial velocity of the target star R_{tar} can be determined by use of Equation 2.1:

$$R_{\text{tar}} = R_{\text{rel}} + (R_{\text{ref}} - R^{\text{ref}}_{\text{helio}}) + R^{\text{tar}}_{\text{helio}} \tag{2.1}$$

2.4.1 Relative Velocities for High Resolution Spectra Using Telluric Features

To ensure that the relative velocities measured using this method was not affected by any systematic offsets, for every night of observation, we performed Fourier cross correlation between a reference star and each star observed using an order dominated by telluric absorption lines.

Because the telluric lines should have the same wavelength in every spectra, any relative velocity measured using these lines would systematically affect the relative velocities as we measure them using stellar absorption lines. We focused these tests on the molecular O_2 A-band absorption feature at 7594Å - 7621Å. We selected a wavelength range of 7550Åto 7700Åto perform this cross-correlation. Ideally, cross-correlation using this feature of any observed spectra should produce a relative velocity difference = 0 km s^{-1}.

For each night of observation, an star was arbitrarily selected as reference. Fourier cross-correlation was performed on every star observed that night using this reference and limited to the wavelength range of 7600 Å $< \lambda < 7800$Å.

For MIKE, across all nights, the average relative velocity measured using the telluric feature was -0.11 km s^{-1} with a standard deviation of 0.40 km s^{-1}. These values spanned a range of -1.31 km s^{-1} to 0.88 km s^{-1}.

For Echelle-100, across all nights of observations, the average velocity was -0.16 km s^{-1} with a standard deviation of 0.63 km s^{-1}. These spanned a range of -1.85 km s^{-1} to 0.93 km s^{-1}.

We conclude that the wavelength calibration is good to at least ~ 2 km s^{-1}.

2.4.2 Primary Stars

To demonstrate how we measure the radial velocities and determine the associated errors, we present an example of an analysis of a night of observation.

2.4.2.1 Example MIKE Analysis of Observations Made on 09 February 2007 and 24 April 2008

For the night of 09 February 2007, we observed two radial velocity standard stars: HD108177 and HD140283 (radial velocities from Latham et al., 2002). Of the 34 spectral orders in the blue and the 34 spectral orders in the red provided by MIKE, 11 orders in the blue and 6 orders in the red were selected for use in Fourier cross-correlation. We selected these orders based on S/N considerations at bluer wavelengths and to avoid telluric lines in redder orders. Our selected orders covered a wavelength range of 4100Å to 4640Å, 4975Å to 5440Å, and 6450Å to 6722Å.

Using HD108177 as a reference for Fourier cross-correlation, we measured the relative velocity of HD140283 for each of the 17 orders we selected. We added the literature value for the radial velocity of HD108177 to these 17 relative velocities and performed a heliocentric correction to calculate heliocentric radial velocities using each order individually. The 17 radial velocities had a mean of -169.9 km s^{-1} and a standard deviation of 0.5 km s^{-1}.

In comparison to existing literature values for the radial velocity of HD140283, Latham et al. (2002) listed the radial velocity of this star as -171.12 ± 0.29 km s^{-1} yielding a difference between

our measurement and that of in the literature of $\Delta v = 1.22$ km s^{-1}.

We obtain multiple radial velocity standards on two nights with MIKE. We repeat this same analysis for this second night, 24 April 2008, using NLTT22848 as reference to measure the velocity of HD99109. On this night, however, a malfunction in the blue CCD of MIKE resulted in the loss of all spectral data, leaving only 6 orders in the red for use in Fourier cross-correlation. Using the same methods as on 09 February 2007, we determined the velocity of HD99109 to be 34.6 km s^{-1} with a standard deviation of 0.8 km s^{-1}. HD99109 has a literature radial velocity of 33.02 ± 0.02 km s^{-1} as measured by Nidever et al. (2002) which gives a velocity difference of $\Delta v = 1.6$ km s^{-1} when compared to literature.

2.4.2.2 Other Primaries Observed Using MIKE

We repeat this procedure for our target F/G/K primaries. On nights when only one radial velocity standard was observed, we use this as a reference for Fourier cross correlation to measure the relative velocity of our target stars. On nights when two radial velocity stars are observed, we choose the reference star based on when the observation was taken, preferring to minimize time between observations of target and reference. For each program star, from multiple orders, we determine a mean radial velocity and a standard deviation. We present the mean radial velocity for our primary stars in Table 2.2. We also present the combined quadrature error of the systematic and the statistical errors associated with the measurement (see Chapter 2.4.3.1 for a description of how this was calculated).

2.4.2.3 Example Echelle-100 Analysis of Observations Made on 16 February 2008

For the night of 16 February 2008, we observed 3 radial velocity standards: NLTT19164, NLTT15871, and NLTT25424 (radial velocities from Nidever et al., 2002). Of the 64 spectral orders provided by Echelle-100, we selected 34 orders, from orders 13 through 46 covering a wavelength range of 4200Å to 6761Å, for using in Fourier cross-correlation. This selection was motivated by S/N considerations at bluer wavelengths and fringing at redder wavelengths.

We measured the radial velocity of standard star NLTT19164 using NLTT15871 and NLTT25424

separately as reference for Fourier cross-correlation. Relative radial velocities for each of the 34 orders were obtained using each reference. These relative velocity measurements were converted to heliocentric radial velocities in the same manner previously described for MIKE. Using NLTT15871 as a template and the literature values for these templates from Nidever et al. (2002), we measured the radial velocity of NLTT19164 based on the mean of the 34 orders to be 53.2 km s^{-1} with a standard deviation of 0.4 km s^{-1}. With NLTT25424, we measured a mean of 52.5 km s^{-1} and a standard deviation of 0.2 km s^{-1}. We compare the radial velocity to the literature radial velocity measurement of NLTT19164 as measured by Nidever et al. (2002), 51.74 ± 0.09 km s^{-1}. We plot a histogram of Δv for the 34 orders in Figure 2.2. The mean value of this histogram was -1.2 km s^{-1} with a standard deviation of 0.4 km s^{-1}.

Since multiple radial velocity standards were observed each night, we were able to perform this analysis for every night of Echelle-100 observations. We found that the systematic errors of Echelle-100 were consistent from a night-to-night basis (varied < 1 km s^{-1}). Therefore, we approximate the systematic errors of Echelle-100 as 1.2 km s^{-1} for our measurements.

2.4.2.4 Remaining Primaries Observed Using Echelle-100

For each night of observations, we selected one radial velocity standard as the reference for Fourier cross-correlation. We selected the reference based on which of the standard stars observed that night was the closest in recreating literature values. We then measured a relative velocity for each of 34 orders using Fourier cross-correlation, which we convert to a heliocentric radial velocity. The mean of these 34 measurements are reported as radial velocities in Table 2.2. In this table, we also show the combined quadrature error of the systematic and the statistical errors associated with the measurement (see Chapter 2.4.3.1 for further details on the calculation of this error).

2.4.3 Comparison of Stars Observed with Both MIKE and Echelle-100

Between the observations made with MIKE and Echelle-100, there were 20 program stars in common, enabling an analysis of the difference in radial velocity measurements from the two stars.

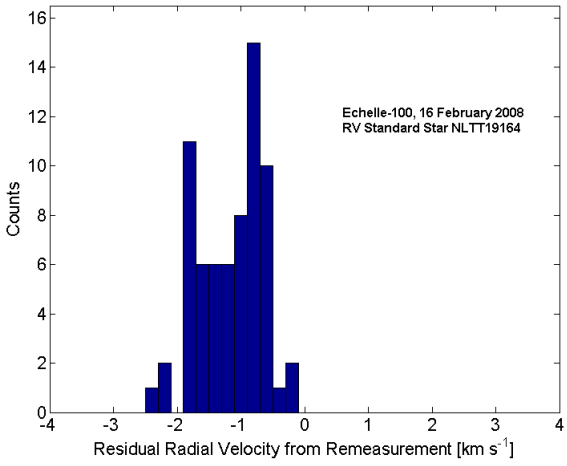

Figure 2.2 Example radial velocity remeasurement of radial velocity standard star NLTT19164 using Echelle-100. Using the other two radial velocity standard observed that night as reference, we measured the radial velocity of NLTT19164. We present a histogram of the difference between the calculated radial velocity for each individual order and the literature radial velocity for NLTT19164 for the night of 16 February 2008. This example is a typical example of the residual velocities calculated for each night using Echelle100. Based on this analysis, we have determined our systematic error in radial velocity measurements to be ~ 1.2 km s^{-1}.

We present a comparison of the radial velocities determined using MIKE and Echelle-100 in Figure 2.3. We note that while the two instruments are in reasonably good agreement with each other (i.e. within 3-σ), there is 1 point that does not agree within errors.

Spectra of PM I02225+1531S was obtained using MIKE on 16 November 2008 and using Echelle-100 on 27 August 2007. Radial velocity measurements using these spectra yield -58.1 ± 1.4 km s^{-1} and -50.6 ± 1.4 km s^{-1} respectively, a $\Delta v = -7.5$ km s^{-1}. This is a 3.75-σ discrepancy. We cannot explain this discrepancy, but we will use the MIKE measurement in further analysis due to its higher S/N.

We present the radial velocity difference between the two instruments against the measured radial velocity using MIKE in Figure 2.3 for all 20 comparison stars, including PM I02225+1531S. The mean $\Delta v = +0.3$ km s^{-1}, with a standard deviation of 2.4 km s^{-1}. However, 19 stars are in agreement within 3-σ. We conclude that this is consistent with a minimal systematic offset between the radial velocity measurements of the primary stars using these two instruments.

2.4.3.1 Errors in Primary Radial Velocity Measurements

When determining the errors associated with these measurements, we will consider the systematic error and the statistical error separately.

Our determination of the systematic errors associated with MIKE are based on the remeasurement of radial velocity standard star HD140283 on 09 February 2007 and of HD99109 on 24 April 2008 (see Section 2.4.2.1 for details). We have determined that we can match the literature radial velocities of these two stars to 1.22 km s^{-1} and 1.6 km s^{-1} respectively.

A rough estimate of the total error in our MIKE measurements would be the quadrature sum of the associated error of our measurement σ_m and the literature measurements σ_l respectively. This would be ≤ 0.9 km s^{-1}. If we compare this error estimate against the measured radial velocity of HD140283 and HD99109 as compared to their literature values, there is an unaccounted-for error of < 1.3 km s^{-1}. Therefore, in order to be conservative with our error estimates, we will assume the error in the zero point (or the calibration of our relative velocity measurements to heliocentric radial velocities) of our velocity scale to be 1.3 km s^{-1} for MIKE.

For our Echelle-100 measurements, the determination of our systematic errors are also based upon the remeasurement of the radial velocity of standards (see Section 2.4.2.3). Based on histograms of residual radial velocities such as Figure 2.2, we were able to recreate the literature radial velocity value of a standard star to within 1.2 km s^{-1}; we take this as an upper limit to the systematic errors in the zero point of our velocity scale. To estimate our errors conservatively, we will consider the systematic errors associated with Echelle-100 to be 1.2 km s^{-1}.

For each star, each order was individually used to calculate the radial velocity. This would be 17 orders for MIKE measurements or 34 orders for Echelle-100 producing 17 and 34 measurements of the radial velocity respectively. Our reported radial velocity was measured by taking the mean of the radial velocities as calculated by each individual order. The standard deviation of these individual order measurements is taken to be our statistical error.

We take the quadrature sum of the systematic and statistical errors to determine the total error

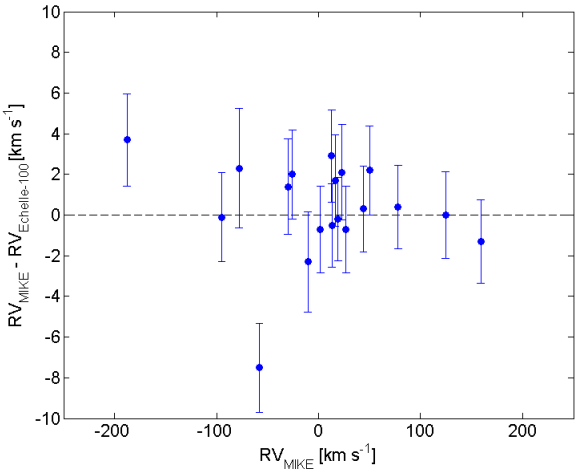

Figure 2.3 Comparison of measured radial velocities of the F/G/K primary star using the MIKE spectrograph on the Magellan telescope and the du Pont 100 inch Echelle spectrograph. We note that for these 20 comparison stars, the mean $\Delta v = +0.3$ km s^{-1}. The velocities measured by the two instruments are in 3-σ agreement with each other. The one outlying point is PM I02225+1531S with a $\Delta v = -7.5$ km s^{-1}, a 3.75-σ discrepancy (see text for a discussion of this measurement).

associated with our measurement. We present this total error for each primary star observed in Table 2.2.

2.4.4 Secondary Stars

Radial velocities of the secondary stars were measured by cross-correlating the reduced, wavelength-calibrated spectra with spectra of M-type radial velocity standard stars (Nidever et al., 2002) observed on the same night. On each night an effort was made to observe at least one early-M dwarf (M0-M2) and one late-M dwarf (M3-M5) standard star in order to be able to match the spectral shape during cross-correlation of the target stars across the range of M dwarf spectral classes in our sample (M0–M5). On most nights, 3–5 radial velocity standard stars were observed; on all nights at least two M-dwarf radial velocity standards were observed.

The cross-correlation was performed using the IRAF task *fxcor*. Care was taken to select an appropriate spectral range over which to conduct the cross-correlation, centering on spectral features in the M dwarf spectra that would be present across a range of spectral types as well as avoiding strong telluric lines. Two spectral ranges were selected: $6000 < \lambda < 6500$ Å and $7000 < \lambda <$

7300 Å. Cross-correlation was performed on each target star against the a standard star observed on the same night. The standard selected for use in Fourier cross-correlation was the standard that was closest in $V - J$ color to ensure that the spectral types between target and standard were as close as possible. $V - J$ color for our targets were taken from Li et al. (2014), while the color of our standards were sourced from *SIMBAD*.

In order to filter out low frequency noise and improve our measurement, a high-pass filter was employed during Fourier cross-correlation. The filter settings were chosen such that in correlating one radial velocity standard star to another, the literature value of the radial velocity star was most closely reproduced. The *fxcor* filter used was a ramp function that began at wavenumber $k = 50$ and reached full value at $k = 250$. The filter begins to decrease at $k = 350$, reaching zero at $k = 650$.

Visual inspection of the spectra revealed that, in some cases, there were noticeable residuals from sky subtraction and cosmic ray subtraction in the spectral ranges selected. These features were edited out manually by interpolation for the purposes of Fourier cross correlation. However, we have identified these spectra as potentially problematic and, though we do measure their radial velocities, we indicate that these measurements may be suspect.

The resulting relative velocities measured using *fxcor* were corrected to heliocentric values using heliocentric corrections and the literature value of the radial velocity of the standard. In cases of multiple observations of the same target , the average of the multiple observations were taken as the radial velocity of the target star. These velocities are presented in Table 2.3. We also indicate which stars had noticeable residuals of sky lines and cosmic rays, and therefore have suspect radial velocities.

2.4.4.1 Error Analysis of Secondary Velocities

For a low-resolution spectrograph with $R = \lambda/\Delta\lambda \sim 2000$, it is reasonable to measure radial velocity to a precision of $\sim 1/10$ of a resolution element, or in this case, $c/R \times 1/10 \sim 15$ km s^{-1}. This can serve as a first order, highly simplistic estimation of our expected error.

To determine the error more rigorously, we estimate the error on the radial velocity measure-

ments by considering the measurement and systematic components of the error independently. The measurement error was determined using *fxcor*, which determines the error in a single radial velocity measurement using the method developed by Tonry & Davis (1979), which calculates a velocity error based on the fitted peak of the correlation function used by *fxcor* to determine the relative velocity and the antisymmetric noise.

The systematic error is measured by cross-correlating each radial velocity standard star spectrum against the other radial velocity standards observed on the same night. On nights when three or more radial velocity standards were observed, these systematic and measurement error estimates agree within roughly 10%; both values are generally between 10 and 15 km s^{-1} on all nights, except in a few cases. We therefore conservatively estimate the maximum error on all measurements to be < 20 km s^{-1} except in cases in which *fxcor* indicates a larger measurement error.

In some cases, the measurement errors calculated by Tonry & Davis (1979) method were unreasonably low. In order to determine a more conservative estimation of our measurement error, we estimate our noise "floor" using the radial velocity standards taken each night. For every night, we measure the relative velocity between two standards and compare that to the difference in the literature radial velocities. In perfect conditions, the mean difference between the measured relative velocity and the difference in literature radial velocities across all nights should be zero. Our measured mean difference is 3.2 km s^{-1} with a standard deviation of 11.4 km s^{-1}. We take 11.4 km s^{-1} to be a conservative estimate of our minimum measurement error.

Table 2.3 presents the errors for every M-dwarf radial velocity measurement. If more than two standard stars were observed we report an error that is the quadrature sum of the measurement and systematic errors determined as described above.

2.5 Results

In this work, we intend to construct a high-fidelity binary sample of F/G/K+M binaries to evaluate and improve empirically-based techniques used to determine M-dwarf metallicity. In order to confirm the binary status of a sample of 81 common proper motion, wide separation F/G/K+M binary candidates, we have performed spectroscopic observations of both the primary and the sec-

ondary to measure their radial velocities.

We have measured the radial velocity of 77 F/G/K-type primary stars. We report the radial velocities and the total radial velocity error of each star in Table 2.2. In cases where we have both MIKE and Echelle-100 data, we will preferentially use MIKE data in future analyses due its better S/N.

We have measured the radial velocity of 62 M-dwarf partners using low-resolution spectroscopy. We report the radial velocities and the total error associated with the measurement in Table 2.3. Excluding the 9 stars where, due to the presence of residuals from sky and cosmic ray subtraction, the radial velocities should be considered suspect, this sample includes 53 M-dwarf candidate partners with radial velocity measurements unhindered by this particular issue. From this point forward, we will not consider the velocities measured in those 9 suspect stars as suitable for use in determining binarity.

We have measured the radial velocity of both the primary and the secondary of 52 of the original 81 candidate binaries. We have compared the measured radial velocity for the primary and secondary stars, which we present in Table 2.4. We show a histogram of Δv, the calculated difference between the measured radial velocity of the primary and secondary candidate, in Figure 2.4. We determine based upon the Δv whether the candidate pair is a true binary or not. The largest source of uncertainty in this binary determination is the errors associated with the measurement of the radial velocities of the M-dwarfs using low dispersion spectroscopy. We utilize a 2-σ agreement between the velocity measured for the F/G/K primary and the M-dwarf secondary as our criterion for identifying a "true" binary.

Based on this criterion, of the 52 pairs where we have measured the radial velocity of both primary and secondary, 47 are "true binaries" (90.4%). Based on this, the false positive rate, the percentage of pairs identified as binaries based on proper motion but are revealed to be possible chance alignments through radial velocity, is 9.6%.

2.6 Discussion

2.6.1 Comparison with Literature Values

Previous surveys have performed radial velocity measurements of several of the stars in this sample. Prior radial velocity measurements have reported in the SIMBAD database for 9 of the primary stars and 1 secondary star, including work from Latham et al. (2002), Kunder et al. (2017), Soubiran et al. (2013), and Newton et al. (2014).

We plot our measured radial velocities against literature measurements in Figure 2.5. First, we see that the measured radial velocities match reasonably well for eight of the nine primaries. The one exception to this is NLTT14407, which we discuss independently.

For the eight remaining primaries, the mean of the difference Δv between our measured radial velocities and the literature is $\langle \Delta v \rangle = -1.2$ km s^{-1} with a standard deviation of 2.7 km s^{-1}. We therefore consider that our measurements for the primaries are consistent with existing measurements.

Our measured radial velocity for the M-dwarf secondary PM I03150+0103 of 74.4 ± 13.8 km s^{-1} based on low dispersion spectra is in overall agreement with the previously measured radial velocity of this star by Newton et al. (2014), 87 ± 5 km s^{-1}. Due to the larger errors associated with our measurement, this discrepancy is within 1-σ agreement with the literature values.

2.6.1.1 NLTT14407

One out of nine primaries had a much larger discrepancy between what we measured and literature values. We observed NLTT14407 on 22 November 2007 using MIKE. Only 6 orders were usable due to the malfunction in the blue CCD. Using these 6 orders, we measured a radial velocity of 88.9 km s^{-1} with a standard deviation of 0.3 km s^{-1}. Combined with the presumed systematic errors associated with MIKE, we estimate a combined total error of 1.2 km s^{-1}.

Kunder et al. (2017) previously measured the radial velocity of this star and reported 66.01 ± 7.2 km s^{-1}, which is a 3-σ difference from our measurement. While we do not know the exact source

of this discrepancy, we will use our own measurement in this paper.

2.6.2 Sample Binary Fidelity

We now consider the fidelity of the F/G/K+M binary sample we have assembled in comparison to other work. Previous work, such as the AstroLux Survey (Janson et al., 2012), have used multi-epoch imaging data to find M-dwarf companionship using common proper motions. A secondary method of confirming binarity is therefore crucial in the distinguishing the chance alignment of field stars with true physical binary systems. In the AstroLux Survey, the color of the companion was used as additional basis for determining binarity following a selection criteria developed by Bergfors et al. (2010) based on the expected color-magnitude relationship of a physical companion. Janson et al. (2012) found only 2 stars out of a sample of 134 common proper motion pairs failed to meet this secondary criteria, concluding a contamination of their multiplicity fraction by $\pm 1\%$.

The MinMS survey, a volume-limited infrared survey of K7-M6 dwarfs, utilized common proper motion as their binarity confirmation after identifying candidate pairs using high resolution imaging data (Ward-Duong et al., 2015). In order to quantify the number of background contaminants in their binary sample, they utilized two statistical methods. The first counted sources within their detection apertures and determined a contamination of a "a few to 10%" for wide separation candidates. The second was a likelihood analysis of background stars sharing 2-dimensional proper motion with their candidate primaries using the stellar population models. They similarly concluded that the background source contamination was $< 1\%$.

The SLoWPoKES catalog published by Dhital et al. (2012) for extremely close pairs (< 8 AU) used radial velocity to confirm binarity. For M0-M3 stars, they found that 12.6% of their sample of comoving objects has > 3-σ difference in their measured velocities. They did find that this seemed to be correlated with the S/N of their spectra, where the lowest S/N spectra seemed to have the greatest differences between the two stars in the candidate binary. They postulate that undiscovered spectroscopic binary partners may be the cause some of the discrepancies, though that could not be confirmed at the time using low resolution spectroscopy.

By combining proper motions with radial velocities, our technique uses the three dimensional

space motion to confirm binarity. Using this sample, we can also determine how many binary pair candidates identified using common proper motion are in reality false positives.

In contrast with the SLoWPoKes catalog, this work has high resolution spectroscopy of the more massive F/G/K-type primary star, allowing for a more precise measurement.

We have determined that, from our initial sample of 81 common proper motion pairs, 47 of 52 pairs where we have both primary and secondary observations had radial velocities that were within 2-σ of each other, or 90.4% percent.

For comparison, we have simulated what the difference between the measured radial velocity of a primary and a secondary (Δv) for a pure binary sample composed of 10^6 pairs. For each simulated pair, we simulated an observation of a primary and a secondary by sampling a normal distribution with a standard deviation of a randomly selected error in our sample, an error in a primary measurement for a simulated primary and an error in a secondary measurement for a simulated secondary. We then take the difference in the observed velocity of the primary and the observed velocity of the secondary for each simulated pair. In an ideal case with no measurement error, this would have produced a delta function centered at zero. With our measurement errors, we have simulated a distribution of what Δv should be for a pure binary sample observed with our errors. We show this simulated distribution in Figure 2.4.

By visual inspection, our observed distribution of difference in radial velocity looks similar to our simulated binary sample. Using a 2-σ rejection criterion on this simulated pure binary sample, we find that 95.3% of simulated pairs pass this cut. This is not inconsistent with the 90.4% percent pass rate of our observed binary sample.

2.6.3 Comparison with Results from Li et al. (2014)

In their photometric measurements of these 81 candidate F/G/K+M binaries, Li et al. (2014) constructed updated reduced proper motion (RPM) diagrams. On an RPM diagram, the expectation is that a line connecting the positions of candidate binaries should be parallel to the main sequence or subdwarf track if the candidate were true binaries. If this line was not parallel, then

the pair contained either a white dwarf companion or was a chance alignment.

Based on an arbitrary slope criterion, Li et al. (2014) determined that out of 74 candidate pairs with updated V-band photometry, 68 were likely to be "true" wide separation binary pairs. We have radial velocity measurements for both primary and secondary stars of 4 of the 6 candidate pairs that Li et al. (2014) identified as unlikely to be binary.

Two of these unlikely binary candidates, PM I14475+1134 / PM I14476+1134 and PM I19420+2014S / PM I19420+2014N, were determined by our 2-σ criterion to not be binaries. With Δv of -191.4 km s^{-1} and 52.1 km s^{-1} respectively and the quadrature combined errors of both the primary and the secondary of 15.8 km s^{-1} and 20.4 km s^{-1}, it is unlikely that these two are binaries, in agreement with Li et al. (2014).

Two candidate binaries we observed, PM I03256-3333E / PM I03256-3333Wn and PM I21536+0010S / PM I21536+0010N, were designated by Li et al. (2014) to be unlikely binaries. However, these two binary candidates passed our 2-σ criterion for determining binarity. However, based upon the analysis of Li et al. (2014) and the slope of the connecting line between the two stars on a reduced proper motion diagram, it is unlikely that the primary and secondary candidates are at a common distance. However, for the purposes of this work, we will consider them as binaries.

Overall, the identification of 90.4% of our sample of 52 candidates as actual binaries is in broad agreement with the work done by Li et al. (2014). Of the 5 candidate pairs that failed our 2-σ criterion and had no residual features in their spectra, two were PM I14475+1134/PM I14476+1134 and PM I19420+2014S/PM I19420+2014N, which were unlikely to be binaries. The remaining 3 may be chance alignments. This could also be resolved by achieving higher precision radial velocities for the M-dwarf secondaries, allowing a second check of their velocities.

2.7 Conclusions

We have assembled a high fidelity sample of 47 confirmed F/G/K+M binary pairs for the purposes of evaluating and improving existing techniques to measure M-dwarf metallicity in Table 2.4. Based on high resolution spectroscopic observations, we have determined the radial velocity

of the F/G/K-type primary stars to a systematic precision of 1.3 km s^{-1} using MIKE and 1.2 km s^{-1} using Echelle-100.

Using low resolution spectroscopic observations of the M-dwarf partners, we were able to determine radial velocity to roughly ~ 20 km s^{-1} precision, making them the key limitation in our determination of binarity.

We have measured the radial velocity of 77 F/G/K-type primary stars and 62 M-dwarf secondaries. Comparisons of our radial velocity measurements to existing literature values for 8 F/G/K primaries (excluding the particular case of NLTT14407) and 1 M-dwarf secondary reveal that we have reproduced previous measurements within errors.

When comparing the measured radial velocities of the primary and the secondary star and using a 2-σ agreement criterion, we have determined that out of the original 81 candidate binary pairs identified using common proper motion, 47 of the 52 pairs we observed are likely to be binaries, leading to a false identification rate of 9.6% percent if solely using common proper motions.

This high fidelity sample of F/G/K+M binaries will form the basis of our future work to evaluate current techniques for metallicity measurements using optical and near-infrared low dispersion spectra as well as to develop new techniques usable at optical wavelengths. It is the intent of the creation of this sample to assist the use of M-dwarf spectroscopy to probe interesting discovery space especially the chemical evolution of the Milky Way.

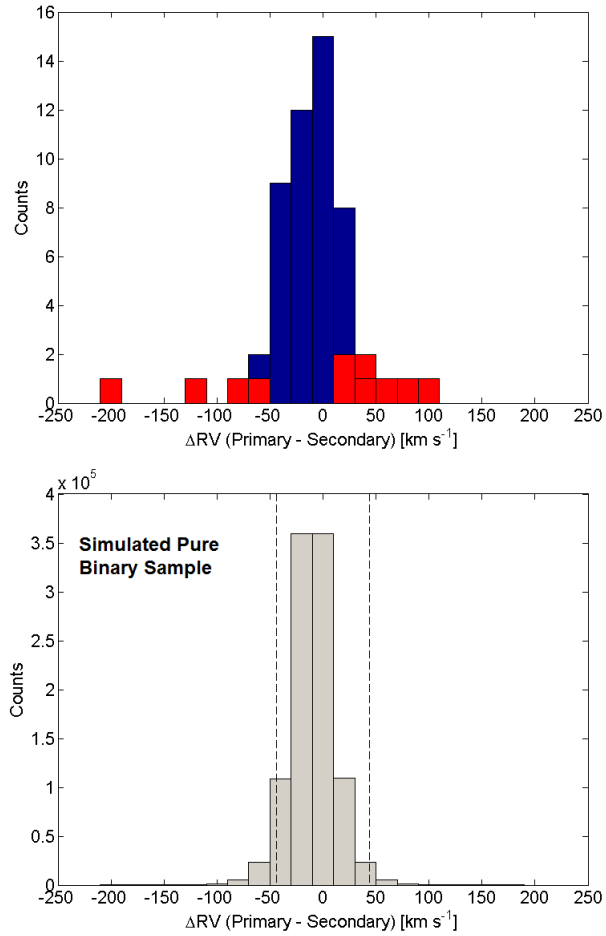

Figure 2.4 Histogram of the difference between the measured radial velocity of the candidate primary F/G/K star and its candidate secondary M-dwarf. Blue represents candidates we consider to be binaries based on a 2-σ agreement between the measured velocities where σ is the quadrature combined error of the primary and secondary radial velocities. Red represents those that did not meet this criteria. We include in the rejected category candidates any pair where the spectrum of the candidate secondary was considered suspect due to the presence of residuals from sky subtraction or cosmic ray rejection. For comparison, we also present a simulation of the difference between the measured radial velocity for a pure binary sample composed of 10^6 pairs that was observed with our errors, plotted with the 2-σ boundaries, which includes 95.2% of all simulated binaries.

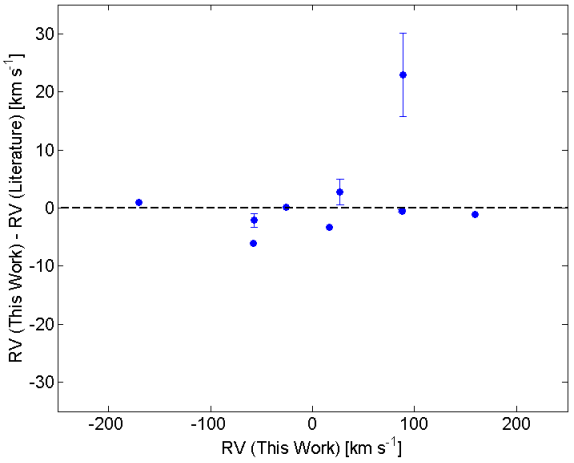

Figure 2.5 Comparison of literature radial velocity measurements and the measurements made in this work for the 9 primaries with existing literature velocities. We have found literature radial velocities for 9 primary stars in our sample from Latham et al. (2002), Kunder et al. (2017), Soubiran et al. (2013), and Newton et al. (2014). Nine F/G/K primary stars had previously measured radial velocities. The one outlying F/G/K primary measurement was of NLTT14407 (see text for discussion of this measurement). Excluding the specific case of NLTT14407, the mean difference of the remaining eight primaries Δv between our measured radial velocities and the literature is $\langle \Delta v \rangle = -1.2$ km s^{-1} with a standard deviation of 2.7 km s^{-1}

Table 2.2: F/G/K Primary Observing Log and Radial Velocities

Primary Name	R.A.	Dec.	MIKE (Magellan-Clay)			Echelle-100 (du Pont)		
	J2000	J2000	UT Date	RV	Error	UT Date	RV	Error
			Observed	km s^{-1}	km s^{-1}	Observed	km s^{-1}	km s^{-1}
PM I00025-4644	00:02:35.66	−46:44:52.0	13-Nov-08	−77.8 [b]	1.4	···	···	···
PM I00329+1805	00:32:55.80	+18:05:52.9	14-Nov-08	49.6 [b]	1.6	···	···	···
PM I00422+0731E	00:42:15.23	+07:31:18.7	14-Nov-08	−21.5 [b]	1.4	···	···	···
PM I00592+0705N	00:59:17.81	+07:05:56.4	16-Nov-08	−152.5 [b]	1.3	···	···	···
NLTT 3847	01:09:28.97	−05:07:25.3	23-Nov-07	−2.3	1.4	···	···	···
PM I01227+1409	01:22:43.29	+14:09:34.5	16-Nov-08	−30.1 [b]	1.3	28-Aug-07	−31.5 [a]	1.8
PM I01266-4842W	01:26:37.33	−48:42:51.0	23-Nov-07	12.9	1.4	27-Aug-07	10.0 [a]	1.5
NLTT 4817	01:26:55.17	+12:00:25.9	9-Dec-08	−170.6 [b]	1.4	···	···	···
PM I01352+0538N	01:35:14.71	+05:38:24.7	23-Nov-07	16.2	1.4	28-Aug-07	14.5 [a]	1.5
PM I01430-4959W	01:43:00.68	−49:59:26.8	21-Nov-07	67.8	1.3	···	···	···
PM I02012+0218	02:01:15.09	+02:18:25.8	13-Nov-08	57.5 [b]	1.4	···	···	···
PM I02225+1531S	02:22:34.06	+15:31:09.9	16-Nov-08	−58.1 [b]	1.4	27-Aug-07	−50.6[a]	1.4
PM I02267-4214	02:26:47.96	−42:14:58.9	16-Nov-08	57.9 [b]	1.5	···	···	···
NLTT 8753	02:42:05.13	−24:45:16.3	20-Nov-07	69.0	1.5	···	···	···
PM I02548+2057W	02:54:49.43	+20:57:34.8	9-Dec-08	−199.7 [b]	1.4	···	···	···
PM I02569-5831N	02:56:55.71	−58:31:24.3	13-Nov-08	17.5 [b]	1.6	···	···	···
PM I03150+0102	03:15:04.76	+01:02:15.2	···	···	···	28-Aug-07	87.6	1.5
PM I03256-3333E	03:25:41.79	−33:33:34.6	21-Nov-07	−31.0	1.4	···	···	···
NLTT 12296	03:59:04.27	−06:56:03.2	23-Nov-07	−154.5	1.3	···	···	···
PM I04072+1526N	04:07:16.36	+15:26:42.8	···	···	···	29-Aug-07	76.9	1.3
PM I04099+0942E	04:09:54.30	+09:42:58.8	20-Nov-07	−101.3	1.3	···	···	···
PM I04254-4601	04:25:28.74	−46:01:23.9	13-Nov-08	37.5 [b]	1.4	···	···	···
PM I04325-5657N	04:32:32.44	−56:57:04.3	···	···	···	20-Feb-08	190.0	1.3
					1.3	17-Feb-08	190.7 [a]	1.6

[a] This measurement was not used in further analysis.

[b] During this measurement, the blue CCD of MIKE failed, resulting in a loss of spectral data from 3340 Å $< \lambda <$ 5100 Å. As a result, only 6 orders were used in this measurement.

Table 2.2: F/G/K Primary Observing Log and Radial Velocities *(continued)*

Primary Name	R.A.	Dec.	MIKE (Magellan-Clay)			Echelle-100 (du Pont)		
	J2000	J2000	UT Date	RV	Error	UT Date	RV	Error
			Observed	km s^{-1}	km s^{-1}	Observed	km s^{-1}	km s^{-1}
PM I04327+0820	04:32:45.59	+08:20:05.5	16-Nov-08	-134.3 [b]	1.3	···	···	···
PM I04332+0013	04:33:17.84	+00:13:59.8	···	···	···	28-Aug-07	-21.3	1.5
PM I04477-3044W	04:47:42.65	-30:44:03.2	···	···	···	20-Feb-08	89.2	1.3
					1.3	19-Feb-08	88.7 [a]	1.3
NLTT 14407	05:02:20.19	-19:32:04.4	22-Nov-07	88.9 [b]	1.3	···	···	···
PM I05137+0647W	05:13:46.03	+06:47:01.0	16-Nov-08	83.7 [b]	1.3	···	···	···
PM I05195+0903E	05:19:34.77	+09:03:46.3	16-Nov-08	63.4 [b]	1.3	···	···	···
PM I05484-3617Nn	05:48:28.64	-36:17:06.7	13-Nov-08	69.0 [b]	1.4	···	···	···
PM I06032+1921N	06:03:14.87	+19:21:38.6	22-Nov-07	-187.8 [b]	1.3	17-Feb-08	-191.5 [a]	1.6
PM I06050+0723S	06:05:03.52	+07:23:30.5	23-Nov-07	102.9	1.4	···	···	···
PM I06394-3030E	06:39:24.52	-30:30:50.9	···	···	···	···	···	···
PM I06436+0851	06:43:36.55	+08:51:44.4	16-Nov-08	-7.5 [a,b]	1.5	···	···	···
PM I08152-6337	08:15:17.60	-63:37:18.4	24-Apr-08	27.0 [b]	1.4	20-Feb-08	27.7 [a]	1.3
PM I08239-7549W	08:23:54.94	-75:49:34.3	11-Dec-08	13.0 [b]	1.4	20-Feb-08	13.5 [a]	1.3
					1.3	16-Feb-08	13.4 [a]	1.6
PM I08386-3856	08:38:36.72	-38:56:55.7	11-Dec-08	19.0 [b]	1.3	20-Feb-08	19.2 [a]	1.3
					1.3	19-Feb-08	19.4 [a]	1.3
PM I09502+0509E	09:50:13.89	+05:09:02.4	24-Apr-08	-25.8 [b]	1.3	16-Feb-08	-27.8 [a]	1.5
PM I10105+1203W	10:10:34.78	+12:03:17.6	25-Apr-08	50.0 [b]	1.4	16-Feb-08	47.8 [a]	1.5
PM I10520+1521N	10:52:02.16	+15:21:18.6	24-Apr-08	30.6	2.0	···	···	···
PM I11110-4414	11:11:04.09	-44:14:15.9	25-Apr-08	17.8 [b]	1.4	···	···	···
PM I11125-3512	11:12:30.07	-35:12:35.0	9-Feb-07	-48.4	1.7	···	···	···
NLTT 27188	11:22:26.44	-27:13:35.2	10-Feb-07	124.6	1.5	20-Feb-08	124.6 [a]	1.3
PM I11263+2047Ee	11:26:21.55	+20:47:22.7	25-Apr-08	-77.8 [b]	1.6	16-Feb-08	-80.1 [a]	2.4

[a] This measurement was not used in further analysis.

[b] During this measurement, the blue CCD of MIKE failed, resulting in a loss of spectral data from 3340 Å $< \lambda <$ 5100 Å. As a result, only 6 orders were used in this measurement.

Table 2.2: F/G/K Primary Observing Log and Radial Velocities *(continued)*

Primary Name	R.A.	Dec.	MIKE (Magellan-Clay)			Echelle-100 (du Pont)		
	J2000	J2000	UT Date	RV	Error	UT Date	RV	Error
			Observed	km s^{-1}	km s^{-1}	Observed	km s^{-1}	km s^{-1}
PM I11330+1318N	11:33:02.86	+13:18:33.2	···	···	···	19-Feb-08	33.5	1.4
PM I11392-4118N	11:39:12.23	−41:18:15.1	25-Apr-08	−10.4	1.5	17-Feb-08	−8.1 [a]	1.7
PM I11584-4155E	11:58:27.99	−41:55:19.3	25-Apr-08	159.2	1.3	20-Feb-08	160.5 [a]	1.3
					1.3	17-Feb-08	162.9 [a]	1.4
PM I12170+0742E	12:17:05.76	+07:42:30.3	9-Feb-07	80.0	1.4	···	···	···
PM I12237+0625	12:23:43.48	+06:25:10.3	9-Feb-07	11.7	1.4	···	···	···
PM I12277+1334	12:27:43.78	+13:34:16.2	25-Apr-08	−94.5 [b]	1.6	···	···	···
PM I12283+1222S	12:28:18.28	+12:22:36.4	···	···	···	19-Feb-08	57.2	1.5
PM I12440+0625E	12:44:02.57	+06:25:46.9	···	···	···	20-Feb-08	122.5	1.7
PM I12508+0757	12:50:48.80	+07:57:56.7	···	···	···	16-Feb-08	30.8	1.4
PM I13116+1106	13:11:41.81	+11:06:24.8	···	···	···	···	···	···
NLTT 33282	13:13:09.08	−07:42:15.2	9-Feb-07	54.3	1.7	···	···	···
PM I13133-4153N	13:13:20.50	−41:53:14.0	25-Apr-08	−95.0 [b]	1.4	16-Feb-08	−94.9 [a]	1.4
PM I13167+0810E	13:16:47.28	+08:10:27.4	25-Apr-08	77.9 [b]	1.3	19-Feb-08	77.5 [a]	1.3
PM I13372-4244E	13:37:14.25	−42:44:54.8	···	···	···	···	···	···
PM I14055+0244S	14:05:30.97	+02:44:23.4	9-Feb-07	29.0	1.6	···	···	···
PM I14124+0517S	14:12:28.75	+05:17:28.5	10-Feb-07	174.0	1.4	···	···	···
PM I14136-3634E	14:13:41.61	−36:34:39.2	6-Aug-16	255.1	1.4	···	···	···
PM I14475+1134	14:47:35.80	+11:34:13.7	25-Apr-08	88.3 [b]	1.3	···	···	···
PM I15413+1349N	15:41:19.36	+13:49:28.5	9-Feb-07	−87.0	2.3	···	···	···
PM I16008+0146E	16:00:53.85	+01:46:16.5	25-Apr-08	43.9 [b]	1.4	27-Aug-07	43.6 [a]	1.3
PM I16519-4806N	16:51:58.19	−48:06:13.7	6-Aug-16	25.2 [b]	1.4	···	···	···
PM I17135+1909	17:13:30.36	+19:09:57.2	23-Jul-08	1.9 [b]	1.4	29-Aug-07	2.6 [a]	1.4
PM I19207+0506S	19:20:46.74	+05:06:26.5	25-Apr-08	28.5 [b]	1.3	···	···	···

[a] This measurement was not used in further analysis.

[b] During this measurement, the blue CCD of MIKE failed, resulting in a loss of spectral data from 3340 Å $< \lambda <$ 5100 Å. As a result, only 6 orders were used in this measurement.

Table 2.2: F/G/K Primary Observing Log and Radial Velocities *(continued)*

Primary Name	R.A.	Dec.	MIKE (Magellan-Clay)			Echelle-100 (du Pont)		
	J2000	J2000	UT Date	RV	Error	UT Date	RV	Error
			Observed	km s^{-1}	km s^{-1}	Observed	km s^{-1}	km s^{-1}
PM I19420+2014S	19:42:00.86	+20:14:05.0	6-Aug-16	37.6 [b]	1.5	···	···	···
PM I20072-3519E	20:07:13.51	−35:19:50.0	25-Apr-08	−4.3 [b]	2.0	···	···	···
PM I20343+1151	20:34:22.72	+11:51:59.5	···	···	···	29-Aug-07	15.3	1.4
NLTT 49474	20:34:31.48	−22:19:24.3	···	···	···	27-Aug-07	−57.4	1.3
PM I20487+1406	20:48:42.08	+14:06:59.1	23-Jul-08	23.0 [b]	1.4	28-Aug-07	20.9 [a]	1.8
PM I21175-4142E	21:17:32.29	−41:42:17.3	23-Jul-08	52.3	1.5	···	···	···
PM I21442+0102N	21:44:15.64	+01:02:09.1	15-Nov-08	−171.4 [b]	1.5	···	···	···
PM I21536+0010S	21:53:39.95	+00:10:20.8	···	···	···	27-Aug-07	−57.7	1.6
NLTT 52532	21:57:35.98	−03:28:09.2	23-Nov-07	−46.3	1.4	···	···	···
PM I22296+0620	22:29:41.07	+06:20:02.8	···	···	···	28-Aug-07	−33.6	1.8
PM I22487-5613W	22:48:44.33	−56:13:37.0	16-Nov-08	−28.0 [b]	1.3	···	···	···
PM I23033-5311	23:03:23.47	−53:11:23.1	16-Nov-08	−59.2 [b]	1.3	···	···	···
NLTT 57827	23:44:27.89	−30:55:16.9	23-Jul-08	−59.2 [b]	1.7	···	···	···

[a] This measurement was not used in further analysis.

[b] During this measurement, the blue CCD of MIKE failed, resulting in a loss of spectral data from 3340 Å $< \lambda <$ 5100 Å. As a result, only 6 orders were used in this measurement.

Table 2.3: M-Dwarf Secondary Observing Log and Radial Velocities

Secondary Name	RA	Dec	B&C Spectrograph (du Pont 100")		
			Date	RV km s^{-1}	Error km s^{-1}
PM I00026-4644	00:02:36.21	-46:44:57.9	31-Aug-08	-67.1	27.9
PM I00329+1805-2	00:32:56.85	+18:05:56.5	7-Sep-08	88.9	24.4
PM I00422+0731W	00:42:14.35	+07:31:19.9	30-Aug-08	13.8	19.5
PM I00592+0705S	00:59:17.38	+07:05:47.0	...	...	...
NLTT 3849	01:09:29.34	-05:07:30.6	7-Sep-07	7.2	18.4
PM I01226+1409E	01:22:41.13	+14:09:28.8	7-Sep-08	-22.0	73.3
PM I01266-4842E	01:26:38.28	-48:42:54.9	1-Sep-08	57.9[a]	16.9
NLTT 4814	01:26:54.13	+12:00:06.8	1-Sep-08	-183.4	14.4
PM I01352+0538S	01:35:14.24	+05:38:12.0	8-Sep-07	2.2	18.8
PM I01430-4959E	01:43:01.27	-49:59:22.1	9-Sep-07	-3.4[a]	29.8
PM I02012+0217	02:01:17.12	+02:17:29.7	11-Sep-07	-26.6	11.4
PM I02225+1531N	02:22:33.00	+15:31:47.8	8-Sep-07	-86.1	20.6
PM I02267-4215	02:26:46.85	-42:15:06.8	...	...	...
NLTT 8759	02:42:14.98	-24:44:18.0	10-Sep-07	64.4	22.7
PM I02548+2057E	02:54:50.04	+20:57:32.1	...	...	...
PM I02569-5831S	02:56:56.81	-58:31:36.6	30-Aug-08	33.3	27.3
PM I03150+0103	03:15:00.92	+01:03:08.3	7-Sep-08	74.4	13.8
PM I03256-3333Wn	03:25:40.93	-33:33:25.3	10-Sep-07	-33.2	24.0
NLTT 12294	03:59:02.49	-06:56:33.8	11-Sep-07	-176.1	35.9
PM I04072+1526S	04:07:15.45	+15:26:20.2	8-Sep-07	69.7	23.2
PM I04099+0942W	04:09:54.07	+09:42:56.4	5-Feb-08	-99.5	11.4
PM I04255-4601	04:25:30.84	-46:01:22.7	...	...	...
PM I04325-5657S	04:32:31.79	-56:57:14.6	4-Feb-08	175.0	13.1
PM I04327+0820-2	04:32:46.10	+08:20:14.6	...	...	...
PM I04333+0014	04:33:18.67	+00:14:14.0	...	...	...
PM I04477-3044E	04:47:44.22	-30:44:02.5	5-Feb-08	42.8[a]	12.8
NLTT 14408	05:02:20.95	-19:32:01.9	3-Feb-08	62.0	11.4
PM I05137+0647E	05:13:47.17	+06:47:08.6	...	...	...
PM I05195+0903W	05:19:34.09	+09:03:36.8	...	...	...
PM I05484-3617S	05:48:29.65	-36:17:19.5	3-Feb-08	45.0	24.0
PM I06032+1921S	06:03:14.51	+19:21:34.0	...	...	...
PM I06050+0723N	06:05:03.39	+07:23:39.1	2-Feb-08	90.7	11.4
PM I06394-3030W	06:39:24.03	-30:30:55.3	2-Feb-08	234.2	12.9
PM I06436+0851-2	06:43:35.88	+08:51:40.8	...	...	...
PM I08153-6337	08:15:18.03	-63:37:04.5	5-Feb-08	32.9	11.4
PM I08239-7549E	08:23:58.54	-75:49:32.4	5-Feb-08	3.6	11.4
PM I08386-3857	08:38:37.73	-38:57:14.4	3-Feb-08	313.0[a]	25.9
PM I09502+0509W	09:50:12.89	+05:09:08.2	21-Mar-07	-47.7	15.2

[a] There were noticeable residuals in the sky subtraction and cosmic ray subtraction in the spectrum. Therefore, this radial velocity is suspect.

Table 2.3: M-Dwarf Secondary Observing Log and Radial Velocities *(continued)*

Secondary Name	RA	Dec	B&C Spectrograph (du Pont 100")		
			Date	RV km s^{-1}	Error km s^{-1}
PM I10105+1203E	10:10:35.17	+12:03:22.9	23-Mar-07	47.8	16.7
PM I10520+1521S	10:52:01.65	+15:21:09.5	2-Feb-08	57.6	14.0
PM I11109-4416	11:10:57.83	-44:16:31.1	···	···	···
PM I11124-3512	11:12:28.92	-35:12:36.0	5-Feb-08	−52.6	13.3
NLTT 27182	11:22:23.60	-27:13:45.0	24-Mar-07	145.6	20.6
PM I11263+2047Ew	11:26:20.37	+20:47:15.0	3-Feb-08	−66.7	11.4
PM I11330+1318S	11:33:03.95	+13:18:17.1	21-Mar-07	75.1	29.6
PM I11392-4118S	11:39:12.30	-41:18:26.2	2-Feb-08	−3.1	11.4
PM I11584-4155W	11:58:26.46	-41:55:03.4	24-Mar-07	270.5[a]	11.4
PM I12170+0742W	12:17:04.98	+07:42:31.1	20-Mar-07	−27.7[a]	26.2
PM I12237+0624	12:23:44.04	+06:24:48.4	24-Mar-07	36.8	17.7
PM I12277+1336	12:27:46.62	+13:36:37.0	···	···	···
PM I12283+1222N	12:28:18.75	+12:22:50.7	···	···	···
PM I12440+0625We	12:44:00.58	+06:25:48.3	···	···	···
PM I12507+0758	12:50:47.08	+07:58:08.0	2-Feb-08	75.6	25.2
PM I13116+1105	13:11:32.30	+11:05:40.7	···	···	···
NLTT 33283	13:13:09.60	-07:42:07.8	22-Mar-07	115.4	20.5
PM I13133-4153S	13:13:21.15	-41:53:29.2	3-Feb-08	−74.7	12.0
PM I13167+0810W	13:16:45.12	+08:10:21.5	5-Feb-08	62.8	15.7
PM I13372-4244W	13:37:13.54	-42:44:54.4	···	···	···
PM I14055+0244N	14:05:31.65	+02:44:35.1	···	···	···
PM I14124+0517N	14:12:28.04	+05:17:40.1	21-Mar-07	388.9[a]	20.5
PM I14136-3634W	14:13:40.94	-36:34:43.6	20-Mar-07	206.2	28.0
PM I14476+1134	14:47:36.16	+11:34:36.3	24-Mar-07	279.7	15.7
PM I15413+1349S	15:41:19.36	+13:49:23.6	20-Mar-07	−86.1	21.4
PM I16008+0146W	16:00:53.48	+01:46:19.4	22-Mar-07	77.2	21.6
PM I16519-4806S	16:51:57.91	-48:06:19.2	23-Mar-07	−1.1	24.1
PM I17134+1910	17:13:29.74	+19:10:10.0	9-Sep-07	4.5	21.4
PM I19207+0506N	19:20:46.08	+05:06:38.5	30-Aug-08	11.9	13.6
PM I19420+2014N	19:42:00.88	+20:14:10.3	31-Aug-08	−14.5	20.3
PM I20072-3519W	20:07:13.20	-35:19:52.8	1-Sep-08	−21.2	11.7
PM I20343+1152	20:34:22.56	+11:52:03.3	10-Sep-07	33.1	17.0
NLTT 49477	20:34:33.49	-22:17:59.7	1-Sep-08	−30.5	17.1
PM I20487+1407	20:48:42.78	+14:07:01.3	30-Aug-08	−343.8[a]	27.8
PM I21175-4142W	21:17:31.42	-41:42:21.2	6-Sep-07	21.0[a]	14.6
PM I21442+0102S	21:44:15.92	+01:02:03.3	10-Sep-07	−149.0	19.3
PM I21536+0010N	21:53:39.98	+00:10:37.2	31-Aug-08	−81.7	21.2
NLTT 52538	21:57:37.93	-03:28:32.3	11-Sep-07	−50.8	11.4

[a] There were noticeable residuals in the sky subtraction and cosmic ray subtraction in the spectrum. Therefore, this radial velocity is suspect.

Table 2.3: M-Dwarf Secondary Observing Log and Radial Velocities *(continued)*

Secondary Name	RA	Dec	B&C Spectrograph (du Pont 100")		
			Date	RV km s^{-1}	Error km s^{-1}
PM I22297+0620W	22:29:42.75	+06:20:09.0	···	···	···
PM I22487-5613E	22:48:45.54	-56:13:44.0	11-Sep-07	-27.2	16.3
PM I23034-5311	23:03:25.79	-53:11:43.2	1-Sep-08	-84.7	14.8
NLTT 57823	23:44:24.90	-30:55:26.2	10-Sep-07	-97.7	38.1

[a] There were noticeable residuals in the sky subtraction and cosmic ray subtraction in the spectrum. Therefore, this radial velocity is suspect.

Table 2.4: Binary Sample Matching

Primary Name	Secondary Name	Primary RV[a] km s^{-1}	Secondary RV[a] km s^{-1}	Δv km s^{-1}	Binary? Y/N
PM I00025-4644	PM I00026-4644	-77.8 ± 1.4	-67.1 ± 27.9	-10.7	Y
PM I00329+1805	PM I00329+1805-2	49.6 ± 1.6	88.9 ± 24.4	-39.3	Y
PM I00422+0731E	PM I00422+0731W	-21.5 ± 1.4	13.8 ± 19.5	-35.3	Y
PM I00592+0705N	PM I00592+0705S	-152.5 ± 1.3	...	...	?
NLTT 3847	NLTT 3849	-2.3 ± 1.4	7.2 ± 18.4	-9.5	Y
PM I01227+1409	PM I01226+1409E	-30.1 ± 1.3	-22.0 ± 73.3	-8.1	Y
PM I01266-4842W	PM I01266-4842E	12.9 ± 1.4	57.9 ± 16.9[b]	-45.0	?
NLTT 4817	NLTT 4814	-170.6 ± 1.4	-183.4 ± 14.4	12.8	Y
PM I01352+0538N	PM I01352+0538S	16.2 ± 1.4	2.2 ± 18.8	14.0	Y
PM I01430-4959W	PM I01430-4959E	67.8 ± 1.3	-3.4 ± 29.8[b]	71.2	?
PM I02012+0218	PM I02012+0217	57.5 ± 1.4	-26.6 ± 11.4	84.1	N
PM I02225+1531S	PM I02225+1531N	-50.6 ± 1.4	-86.1 ± 20.6	35.5	Y
PM I02267-4214	PM I02267-4215	57.9 ± 1.5	...	...	?
NLTT 8753	NLTT 8759	69.0 ± 1.5	64.4 ± 22.7	4.6	Y
PM I02548+2057W	PM I02548+2057E	-199.7 ± 1.4	...	...	?
PM I02569-5831N	PM I02569-5831S	17.5 ± 1.6	33.3 ± 27.3	-15.8	Y
PM I03150+0102	PM I03150+0103	87.6 ± 1.5	74.4 ± 13.8	13.2	Y
PM I03256-3333E	PM I03256-3333Wn	-31.0 ± 1.4	-33.2 ± 24.0	2.2	Y
NLTT 12296	NLTT 12294	-154.5 ± 1.3	-176.1 ± 35.9	21.6	Y
PM I04072+1526N	PM I04072+1526S	76.9 ± 1.3	69.7 ± 23.2	7.2	Y
PM I04099+0942E	PM I04099+0942W	-101.3 ± 1.3	-99.5 ± 11.4	-1.8	Y
PM I04254-4601	PM I04255-4601	37.5 ± 1.4	...	...	?
PM I04325-5657N	PM I04325-5657S	190.0 ± 1.3	175.0 ± 13.1	15.0	Y
PM I04327+0820	PM I04327+0820-2	-134.3 ± 1.3	...	...	?
PM I04332+0013	PM I04333+0014	-21.3 ± 1.5	...	...	?
PM I04477-3044W	PM I04477-3044E	89.2 ± 1.3	42.8 ± 12.8[b]	46.4	?
NLTT 14407	NLTT 14408	88.9 ± 1.3	62.0 ± 11.4	26.9	N
PM I05137+0647W	PM I05137+0647E	83.7 ± 1.3	...	...	?
PM I05195+0903E	PM I05195+0903W	63.4 ± 1.3	...	...	?
PM I05484-3617Nn	PM I05484-3617S	69.0 ± 1.4	45.0 ± 24.0	24.0	Y
PM I06032+1921N	PM I06032+1921S	-187.8 ± 1.3	...	...	?
PM I06050+0723S	PM I06050+0723N	102.9 ± 1.4	90.7 ± 11.4	12.2	Y
PM I06394-3030E	PM I06394-3030W	...	234.2 ± 12.9	...	?
PM I06436+0851	PM I06436+0851-2	-7.5 ± 1.4	...	...	?
PM I08152-6337	PM I08153-6337	27.0 ± 1.4	32.9 ± 11.4	-5.9	Y
PM I08239-7549W	PM I08239-7549E	13.0 ± 1.4	3.6 ± 11.4	9.4	Y
PM I08386-3856	PM I08386-3857	19.0 ± 1.3	313.0 ± 25.9[b]	-294.0	?
PM I09502+0509E	PM I09502+0509W	-25.8 ± 1.3	-47.7 ± 15.2	21.9	Y

[a]Errors reported here are the statistical and systematic errors added in quadrature.
[b] There were noticeable residuals in the sky subtraction and cosmic ray subtraction in the spectrum. Therefore, this radial velocity is suspect.

Table 2.4: Binary Sample Matching *(continued)*

Primary Name	Secondary Name	Primary RV[a] km s^{-1}	Secondary RV[a] km s^{-1}	Δv km s^{-1}	Binary? Y/N
PM I10105+1203W	PM I10105+1203E	50.0 ± 1.4	47.8 ± 16.7	2.2	Y
PM I10520+1521N	PM I10520+1521S	30.6 ± 2.0	57.6 ± 14.0	-27.0	Y
PM I11110-4414	PM I11109-4416	17.8 ± 1.4	...	...	?
PM I11125-3512	PM I11124-3512	-48.4 ± 1.7	-52.6 ± 13.3	4.2	Y
NLTT 27188	NLTT 27182	124.6 ± 1.5	145.6 ± 20.6	-21.0	Y
PM I11263+2047Ee	PM I11263+2047Ew	-77.8 ± 1.6	-66.7 ± 11.4	-11.1	Y
PM I11330+1318N	PM I11330+1318S	33.5 ± 1.4	75.1 ± 29.6	-41.6	Y
PM I11392-4118N	PM I11392-4118S	-10.4 ± 1.5	-3.1 ± 11.4	-7.3	Y
PM I11584-4155E	PM I11584-4155W	159.2 ± 1.3	270.5 ± 11.4[b]	-111.3	?
PM I12170+0742E	PM I12170+0742W	80.0 ± 1.4	-27.7 ± 26.2[b]	107.7	?
PM I12237+0625	PM I12237+0624	11.7 ± 1.4	36.8 ± 17.7	-25.1	Y
PM I12277+1334	PM I12277+1336	-94.5 ± 1.6	...	...	?
PM I12283+1222S	PM I12283+1222N	57.2 ± 1.5	...	...	?
PM I12440+0625E	PM I12440+0625We	122.5 ± 1.7	...	...	?
PM I12508+0757	PM I12507+0758	30.8 ± 1.4	75.6 ± 25.2	-44.8	Y
PM I13116+1106	PM I13116+1105	...	...	...	?
NLTT 33282	NLTT 33283	54.3 ± 1.7	115.4 ± 20.5	-61.1	N
PM I13133-4153N	PM I13133-4153S	-95.0 ± 1.4	-74.7 ± 12.0	-20.3	Y
PM I13167+0810E	PM I13167+0810W	77.9 ± 1.3	62.8 ± 15.7	15.1	Y
PM I13372-4244E	PM I13372-4244W	...	...	...	?
PM I14055+0244S	PM I14055+0244N	29.0 ± 1.6	...	...	?
PM I14124+0517S	PM I14124+0517N	174.0 ± 1.4	388.9 ± 20.5[b]	-214.9	?
PM I14136-3634E	PM I14136-3634W	255.1 ± 1.4	206.2 ± 28.0	48.9	Y
PM I14475+1134	PM I14476+1134	88.3 ± 1.3	279.7 ± 15.7	-191.4	N
PM I15413+1349N	PM I15413+1349S	-87.0 ± 2.3	-86.1 ± 21.4	-0.9	Y
PM I16008+0146E	PM I16008+0146W	43.9 ± 1.4	77.2 ± 21.6	-33.3	Y
PM I16519-4806N	PM I16519-4806S	25.2 ± 1.4	-1.1 ± 24.1	26.3	Y
PM I17135+1909	PM I17134+1910	1.9 ± 1.4	4.5 ± 21.4	-2.6	Y
PM I19207+0506S	PM I19207+0506N	28.5 ± 1.3	11.9 ± 13.6	16.6	Y
PM I19420+2014S	PM I19420+2014N	37.6 ± 1.5	-14.5 ± 20.3	52.1	N
PM I20072-3519E	PM I20072-3519W	-4.3 ± 2.0	-21.2 ± 11.7	16.9	Y
PM I20343+1151	PM I20343+1152	15.3 ± 1.4	33.1 ± 17.0	-17.8	Y
NLTT 49474	NLTT 49477	-57.4 ± 1.3	-30.5 ± 17.1	-26.9	Y
PM I20487+1406	PM I20487+1407	23.0 ± 1.4	-343.8 ± 27.8[b]	366.8	?
PM I21175-4142E	PM I21175-4142W	52.3 ± 1.5	21.0 ± 14.6[b]	31.3	?
PM I21442+0102N	PM I21442+0102S	-171.4 ± 1.5	-149.0 ± 19.3	-22.4	Y
PM I21536+0010S	PM I21536+0010N	-57.7 ± 1.6	-81.7 ± 21.2	24.0	Y
NLTT 52532	NLTT 52538	-46.3 ± 1.4	-50.8 ± 11.4	4.5	Y

[a]Errors reported here are the statistical and systematic errors added in quadrature.

[b] There were noticeable residuals in the sky subtraction and cosmic ray subtraction in the spectrum. Therefore, this radial velocity is suspect.

Table 2.4: Binary Sample Matching *(continued)*

Primary Name	Secondary Name	Primary RV[a] km s^{-1}	Secondary RV[a] km s^{-1}	Δv km s^{-1}	Binary? Y/N
PM I22296+0620	PM I22297+0620W	-33.6 ± 1.8	$\cdots$	$\cdots$	?
PM I22487-5613W	PM I22487-5613E	-28.0 ± 1.3	-27.2 ± 16.3	-0.8	Y
PM I23033-5311	PM I23034-5311	-59.2 ± 1.3	-84.7 ± 14.8	25.5	Y
NLTT 57827	NLTT 57823	-59.2 ± 1.7	-97.7 ± 38.1	38.5	Y

[a]Errors reported here are the statistical and systematic errors added in quadrature.
[b] There were noticeable residuals in the sky subtraction and cosmic ray subtraction in the spectrum. Therefore, this radial velocity is suspect.

3. METALLICITY MEASUREMENTS OF F/G/K PRIMARIES WITH M-DWARF SECONDARIES

3.1 Introduction

M-dwarf stars are cool, main sequence stars that compose up a majority of the stars in the Milky Way (Chabrier, 2003; Bochanski et al., 2010). Due to their intrinsically low-masses, they have main sequence lifespan longer than the age of the Universe (Laughlin et al., 1997). Because of this ubiquity and their long lived natures, the distribution of M-dwarfs in the galaxy (Bochanski et al., 2010) and their kinematics (Bochanski et al., 2007; Fuchs et al., 2009) have been used as tracer to probe the history of the Galaxy through the thin and thick disk. Given this usefulness as a tracer of Galactic evolution, measuring the metallicity of M-dwarfs would allow the tracing of the chemical evolution of the Milky Way. Since stars preserve a fossil record of the chemical conditions in which they formed, we can use M-dwarfs to study the the early history of the Galaxy.

In addition to these Galactic archaeology studies, efforts to discover an Earth-sized exoplanet in the habitable zone have made M-dwarfs a key focus in exoplanet search programs. The relative ease of finding smaller exoplanets around M-dwarfs compared to larger, Sun-like stars due to the more dramatic transit depths and the larger reflex motion due to orbiting planets has made them attractive targets for these efforts (Gould et al., 2003). Additionally, the closeness of the habitable zone to the M-dwarf increases the geometric likelihood of observing the transit of a habitable zone planet on a timescale conducive to survey efforts (Nutzman & Charbonneau, 2008a). Surveys such as the MEarth project (Nutzman & Charbonneau, 2008b) have leveraged these advantages in the search for terrestrial exoplanets around late-type stars such as M-dwarfs (i.e. Charbonneau et al., 2009; Irwin et al., 2009). Therefore, M-dwarfs have become the subject of interest for testing the metallicity dependence of planet formation, especially for terrestrial planets (Schlaufman & Laughlin, 2011).

However, the relative coolness of M-dwarfs makes spectroscopic study of these stars a chal-

lenging problem. The lower temperature of the M-dwarf stellar atmosphere allows the formation of molecular species that complicate analysis. Reid et al. (1995) identified these molecular features and developed a methodology to measure their strength. However, methodologies developed using atomic transitions in Sun-like atmospheres are rendered unusable since these molecular species lack detailed laboratory transition studies. Even the study of the atomic transitions in these stars is a complex problem since these molecular features make identifying the spectral continuum difficult at best.

Because of these molecular features, measuring the metallicity of an M-dwarf has been approached indirectly through a variety of methodologies. Some bypass using spectra entirely, relying on absolute magnitudes (Bonfils et al., 2005) or high precision photometry and proper motions to determine metallicity (Marshall, 2008). These useful relations rely on the subtle effects that metals, or a lack thereof, in the stellar atmosphere have on the color and magnitude of a star.

Spectroscopic efforts to measure M-dwarf metallicity have depended on identifying features in the M-dwarf spectra and empirically linking them to metal content. F/G/K+M binaries have been used to calibrate these empirical relationships. Spectroscopic analysis methods developed for solar-like stars are used to study the metal content of the F/G/K primary. Then, by assuming that the binary primary and secondary have identical metallicities, the metallicity of the M-dwarf secondary is known and can therefore be used to calibrate these relationships.

Such relationships have been developed using a range of spectroscopic resolutions, from low- to high-resolution spectra. M-dwarf spectroscopic features found at optical wavelengths (Woolf & Wallerstein, 2006) and near-infrared wavelengths (Rojas-Ayala et al., 2012; Newton et al., 2014; Veyette et al., 2017) have been empirically linked to metallicity.

In each of these previous studies, the sample of F/G/K+M binaries selected to calibrate these empirical relationships had [Fe/H] > -1. In order to study M-dwarfs with lower metallicities, these empirical relationships must be extended. This necessitates the creation of a high fidelity, F/G/K+M binary sample with known metallicities extending to [Fe/H] ~ -2.0 to calibrate this extension.

We present a metallicity measurements of 42 F/G/K stars confirmed by radial velocities to be the primary in an F/G/K+M binary pair (see Chapter 2). These 42 stars span a metallicity range of $-1.94 <$ [Fe/H] $< +0.01$. Our sample is heavily weighted towards the metal-poor end as $\sim 70\%$ of our sample are subdwarfs. It is our intent that these stars be used to extend these empirically-based relationships used to measure M-dwarf metallicities to the metal-poor regime.

This chapter is organized as follows: we describe our selection of candidate F/G/K+M binaries in Section 3.2. We detail our observations and the reduction of the data in Section 3.3. We discuss our measurements of the metallicity of the F/G/K stars in Section 3.4. We present the metallicity measurement of 58 F/G/K stars including the 47 confirmed primaries with M-dwarf partners in Section 3.5. We discuss these results and how they compare to previous works in Section 3.6. We conclude with a summary of the results and their importance in Section 3.7.

3.2 Sample Selection

The sample was selected by Li et al. (2014) and described in detail in Chapter 2.2. To ensure the fidelity of our binary sample, we measured radial velocities of both the primary and the secondary to confirm that both stars were moving together in three dimensional space. This we describe in Chapter 2. A criterion of a 2-σ agreement between the measured velocities of the primary and the secondary yielded a sample of 47 primary stars with M-dwarf secondaries with which we could perform chemical abundance measurements.

3.3 Observations and Data Reduction

For this sample, observations were performed using the MIKE spectrograph on the Magellan-Clay 6.5m telescope and the echelle spectrograph on the du Pont 2.5m telescope at Las Campanas Observatory (henceforth referred to as Echelle-100). We discuss the observations and data reduction in detail in Chapter 2.3.2.

We used the previously measured radial velocities (see Chapter 2 for an in depth discussion of the methodology) to shift all spectra to rest wavelengths. We used the *dopcor* task of IRAF to perform this shift.

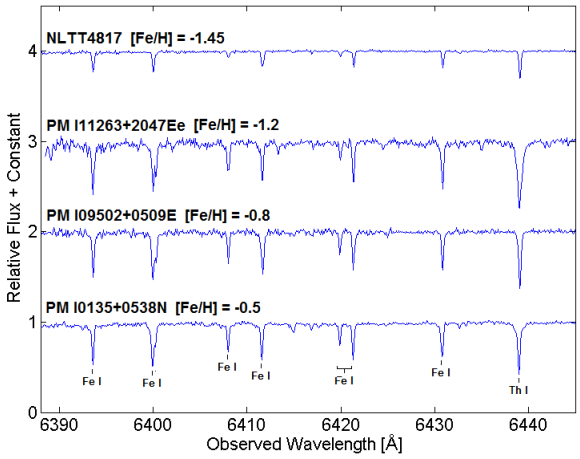

Figure 3.1 Rest wavelength spectra of four confirmed F/G/K+M binary pairs in our sample. Strong Fe I and an unused Th I line are identified for convenience.

3.4 Chemical Abundance Analysis

We performed a chemical abundance analysis of these F/G/K+M primaries using the *MOOG* program developed by Sneden (1973). We utilized a line list produced by Bensby et al. (2003). We performed equivalent width measurements using the *SPECTRE* program (Sneden et al., 2012) and performed a secondary quantitative check of each equivalent width using the IRAF task *splot*. In cases where the two measurements disagreed, we favored the *splot* measurement. We will assume that the species measured in the work are in local thermodynamic equilibrium (LTE).

3.4.1 Determination of Stellar Parameters

We utilized equivalent width measurements of Fe I and Fe II to determine the stellar parameters of program stars. In particular, we used a number of Fe I lines spanning a range of excitation potentials (E.P.) and transition probabilities (log(gf)) to minimize any bias in our measurements. Abundance calculations were done using the *abfind* package of the *MOOG* program (Sneden, 1973) and the Castelli & Kurucz 1D non-α-enhanced plane-parallel models and their 2004 opacity distribution functions (Castelli & Kurucz, 2004a).

Using a set of stellar parameters (effective temperature ($T_{\rm eff}$), surface gravity (log g), and mi-

crotubulence velocity (v_{micro})), we calculated an $\log_{10}(\epsilon_{Fe})$ abundance for each line of Fe I and Fe II. We iterated over these stellar parameters until trends in calculated $\log_{10}(\epsilon_{Fe})$ were minimized across excitation potential and reduced equivalent width. We also required 1-σ agreement between the abundance calculated for Fe I and Fe II, where σ is the combined quadrature error in the measurement of $\log_{10}(\epsilon_{Fe})$ using Fe I and Fe II. Then a mean $\log_{10}(\epsilon_{Fe})$ was calculated and converted to [Fe/H] using measurements of solar abundances from Asplund et al. (2009).

For 35 of 58 stars where Fe I lines were measured, Fe II lines were identified and measured to calculate its abundance. The 1-σ agreement between the abundance calculated for Fe I and Fe II provided feedback into our determination of surface gravity based on the ionization balance between the two species. However, Fe II lines were much generally much weaker than Fe I lines. In 23 of the 58 stars studied, the Fe II could not be distinguished clearly distinguished from noise, causing either large measurement errors or preventing measurement entirely. Therefore, we used a different method of determining the surface gravity.

For star where Fe II lines could not be distinguished, we used the photometry from Li et al. (2014) to calculate an approximate photometric temperature. We use the Dartmouth isochrones (Dotter et al., 2008) with an age of $\tau = 8$ Gyrs to determine a surface gravity using that approximate photometric temperature assuming that these stars are all main sequence (i.e $\log g > 4.0$). We selected 8 Gyrs as the age of the isochrone based on the work of Hayden et al. (2017) who used [Mg/Fe] to determine the age of the thick and thin disks.

We then use that surface gravity as an input into our calculation of $\log_{10}(\epsilon_{Fe})$ abundance for each line of Fe I. We then minimize trends in calculated abundance of Fe I across excitation potential and reduced equivalent width to spectroscopically derive an effective temperature, which we then use to determine a surface gravity using the Dartmouth isochrones. We iterate this process until our spectroscopic temperature, our photometric temperature, and the surface gravity determined using the isochrone are self-consistent. We note which stars have surface gravities derived in this manner in Table 3.2.

Once a set of stellar parameters was determined, we measured the equivalent width of Ca I to

calculate α-enhancement. This is done in order to determine whether an α-enhanced stellar atmosphere model should be used instead of a non-α-enhanced model. For every Ca I line, a $\log_{10}(\epsilon_{\rm Ca})$ was calculated. We determined the mean $\log_{10}(\epsilon_{\rm Ca})$ and similarly converted to [Ca/H] and [Ca/Fe] using Asplund et al. (2009) and our measurement of [Fe/H]. We took [Ca/Fe] as an approximate measure of [α/Fe]. If [Ca/Fe] < 0.3, then the star was considered non-α-enhanced and the determined stellar parameters were accepted for future analyses.

If [Ca/Fe] > 0.3, then the star was identified as α-enhanced, which required reanalysis using the α-enhanced variants of the Castelli & Kurucz atmosphere models (Castelli & Kurucz, 2004a). Of the 58 stars analyzed in this study, 31 were found to be α-element enhanced. Using these α-enhanced atmosphere models, we redetermined the stellar parameters using the same methods. As expected, stellar parameters changed as Fe II abundances were systematically reduced compared to their non-α-enhanced analysis. Consequently, surface gravities for these stars are higher than originally calculated using non α-enhanced stellar atmospheres. We note which stars are α-element enhanced in Table 3.2.

We determine the uncertainty in our stellar parameters by varying the stellar model and examining the resulting trends in excitation potential and reduced equivalent width. We present our stellar parameters for these stars and their associated errors in Table 3.2. We also present plots of the $V - J$ color of these stars from Li et al. (2014) against the spectroscopically determined effective temperature in Figure 3.2, a plot of the effective temperature against surface gravity in Figure 3.3 compared to the Dartmouth isochrones, and a plot of the surface gravity compared to the microturbulence velocity in Figure 3.4.

3.4.2 Equivalent Width Analysis

We measured the equivalent widths of species with strong, unblended absorption lines: Fe I, Fe II, Ca I, and Ti I. For each line, we calculated an $\log_{10}(\epsilon_X)$ abundance using the determined stellar parameters. We take the mean value of these line abundances of each species as the abundance for the species. Outliers greater than 3-σ were discarded; these in general were saturated lines, lines that were indistinguishable from noise, or blended. This abundance is then converted

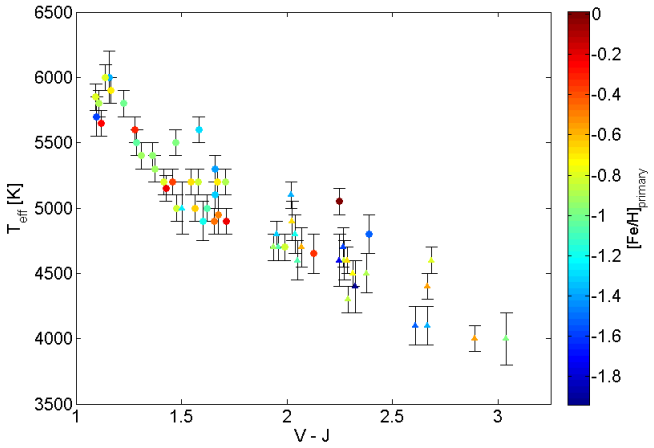

Figure 3.2 $V - J$ color of the primary candidates sourced from Li et al. (2014) compared to the spectroscopically determined effective temperature. Each point is colored by the measured [Fe/H] abundance. We see a clear trend between the spectroscopically determined effective temperatures and the *V-J* colors, increasing our confidence in our effective temperatures used for calculating abundances. Triangles indicate stars where surface gravity was derived using isochrones and the $V-J$ photometry. Circles indicate stars with measurable Fe II lines that could be used to determine surface gravity through an ionization balance between Fe I and Fe II.

into familiar [X/H] and [X/Fe] notation using $\log_{10}(\epsilon_{X,\odot})$ provided by Asplund et al. (2009).

We selected these particular species for analysis to ensure that the metallicity of the primary star is understood at least to first order and to ensure that the appropriate atmosphere models are utilized. Fe I and Fe II are measured in order to determine [Fe/H] and to ensure a robust measurement of the surface gravity of the primary star. Ca I and Ti I can be measured to determine [Ca/Fe] and [Ti/Fe], both indicative of the overall α-element abundance. We only used [Ca/Fe] as a proxy for [α/Fe] when selecting an α-enhanced or a non-α-enhanced stellar atmosphere model from (Castelli & Kurucz, 2004a). Abundances calculated using Ti I served as a secondary check of the α-enhancement.

We present the measured Fe, Ca, and Ti abundance of 58 F/G/K stars in Table 3.3 and Table 3.4. Of these 58 F/G/K stars, 42 have been confirmed to be primaries in an F/G/K+M binary system (see Chapter 2 for a full discussion). We present individual line measurements in Appendix Table B.1 along with the calculated abundance for each line.

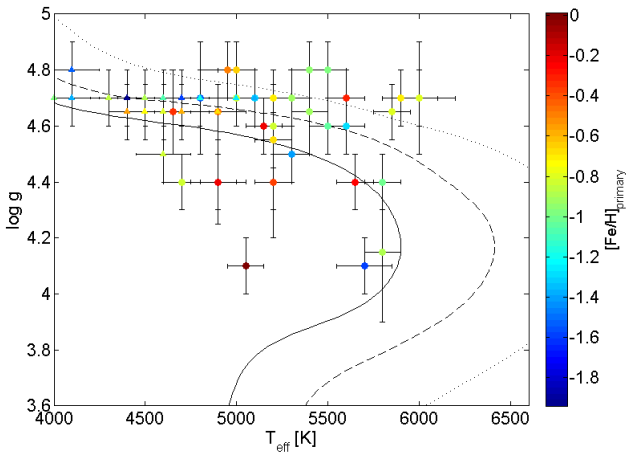

Figure 3.3 Effective temperature of the star compared to the surface gravity for the F/G/K stars studied in this work. Each point is colored by the measured [Fe/H] from equivalent width analysis. Also plotted are 3 Dartmouth isochrones (Dotter et al., 2008) with age of $\tau = 8$ Gyrs, and [Fe/H] = 0 (solid line), [Fe/H] = -1 (dashed line), and [Fe/H] = -2 (dotted line). Triangles indicate stars where surface gravity was derived using these isochrones. Circles indicate stars with measurable Fe II lines that could be used to determine surface gravity through ionization balance.

We have determined stellar parameters and chemical abundances for 42 of the 47 binaries we have confirmed using radial velocity measurements. We could not determine stellar parameters for five of these confirmed F/G/K primaries. We did obtain high resolution spectra which was sufficient for radial velocity analysis. However, while this S/N is sufficient for Fourier cross-correlation, it was too low for a detailed chemical analysis. Therefore, despite being confirmed binaries, we will not use them in further analyses.

In order to demonstrate the validity of our method, we have present 3 example spectra of relatively high, relatively low, and the median metallicity of our sample in Figure 3.5. We have generated synthetic spectra using the *synth* package in *MOOG* and used Gaussian smoothing to match the resolution of the spectrographs. We synthesized a spectrum with a wavelength range of $6140\text{Å} - 6190\text{Å}$for each star using its determined stellar parameters and used the abundances of Fe I, Fe II, Ca I, and Ti I calculated using equivalent width analysis as the abundance of the spectral synthesis. We see that we can recreate our observations using the derived stellar parameters and the measured abundances.

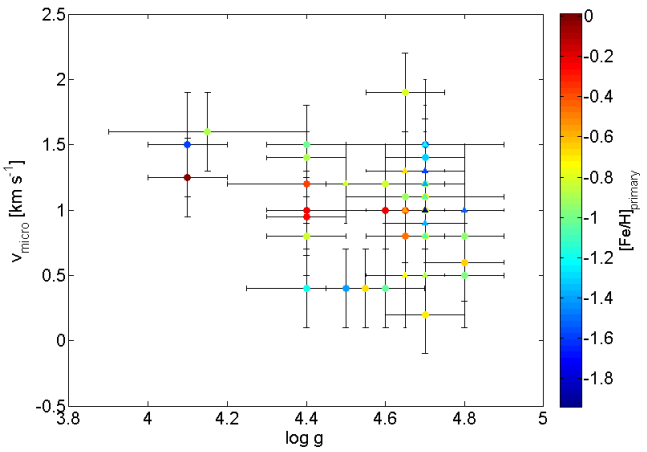

Figure 3.4 Microturbulence velocity compared to the surface gravity for the F/G/K primary candidates, with each point color coded to the measured [Fe/H]. It should be noted that there are overlapping points in this plot. There is a known correlation between microturbulence and surface gravity especially for giant stars, but because this sample is composed entirely of main sequence stars this trend should not be and is not visible.

3.4.3 Error Analysis

We use an approach similar to McWilliam & Rich (1994) in considering the errors associated with this measurement. We will account for the statistical and the systematic errors independently. While McWilliam & Rich (1994) determined the error for all stars in their sample based upon a presumed systematic error of ± 100 K in effective temperature, ± 0.3 km s^{-1} in microturbulence velocity and ± 0.3 dex in log g, we determine the error for each star individually.

For Fe I, Fe II, Ca I, and Ti I, we calculated the mean abundance of each species using several lines. We take the dispersion σ around this mean for each species and divide by $\sqrt{N}$, where N is the number of lines used to calculate the abundance, to determine the statistical error of our equivalent width measurements.

To evaluate the effect that our stellar atmosphere model has on our calculated abundances, we vary the stellar models individually by the uncertainty of each stellar parameter: $T_{\rm eff}$, log g, and $v_{\rm micro}$. We then calculate a new abundance using this perturbed model and, by comparison to our original value, calculate $\Delta \log_{10}(\epsilon_X)$.

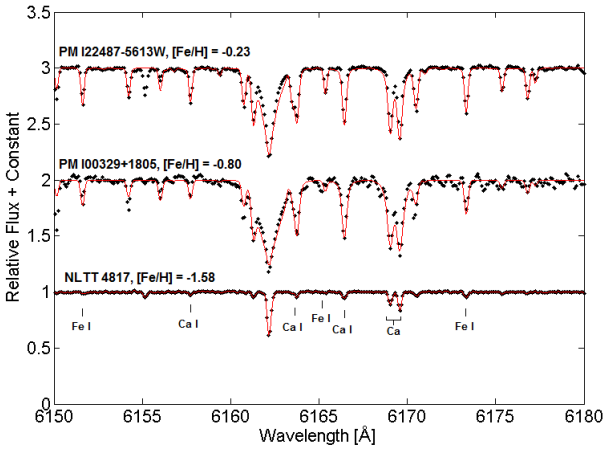

Figure 3.5 Spectra of PM I22487-5613W, PM I00329+1805, and NLTT 4817 (black points) compared to synthesized spectra (red line) over a wavelength range of $6140\text{Å}-6190\text{Å}$. The location of Fe I and Ca I lines are identified for ease of comparison. PM I22487-5613W and NLTT 4817 had measurable Fe II lines and therefore we used an ionization balance between Fe I and Fe II to determine surface gravity. We could not do the same for PM I00329+1805 and therefore used photometry and an isochrone to determine it surface gravity. We see that we are able to recreate our observational data using the stellar parameters we derived and the abundances we have calculated, increasing our confidence in the validity of these methods, including our method of determining the surface gravity of the star using an isochrone and the $V - J$ color.

We report $\Delta \log_{10}(\epsilon_X)$ for each stellar parameter and each star in Table 3.5 and Table 3.6. The total error in our abundance measurement is the quadrature sum of the $\Delta \log_{10}(\epsilon_X)$ for all stellar parameters and our statistical error $\sigma/\sqrt{N}$.

3.4.3.1 Effect of the Isochrone on the Uncertainty in the Determination of Surface Gravity

In using an isochrone to determine the surface gravities of some of our sample, we must evaluate how the input parameters of the isochrone affect our determination of surface gravity. Based on our methodology, the three parameters that could affect the surface gravity as determined by the isochrone are the age used to generate the isochrone, the metallicity of the isochrone, and the effective temperature used to determine the surface gravity.

We tested the dependence of the surface gravity as determined by the isochrone on each of these parameters. We first tested the age dependence, holding effective temperature and metallicity fixed while varying the age of the isochrone by ± 2 Gyrs. This changed the surface gravity on

order of ~ 0.01 dex, ranging from 0.004 to 0.012. In holding the age and metallicity constant and varying the temperature by the uncertainty in the effective temperature, we changed the surface gravity by an average of ~ 0.02 dex, ranging from 0.003 to 0.08. Finally, by varying the metallicity by the uncertainty in our [Fe/H] measurement and holding the remaining parameters constant, we changed the surface gravity by an average of ~ 0.02 dex, ranging from 0.006 to 0.0264.

The quadrature sum of the average of these errors would be 0.03 dex. Even if we take the extreme case and use the maximum value of each error, we get an error in our surface gravity of 0.085. In order to conservatively estimate our error in the surface gravity, we will assume that the error in surface gravity determined using photometry and isochrones is ± 0.1.

3.4.3.2 Effect of α-enhancement of the Stellar Atmosphere on the Abundance Uncertainty

We did not consider the uncertainty in our determination of [Ca/Fe] when selecting an α-enhanced or a non-α-enhanced stellar atmosphere model from (Castelli & Kurucz, 2004a) for use in our analysis. However, we did perform a comparison of the difference in stellar parameters and in calculated abundance when using an α-enhanced and non-α-enhanced atmosphere model. For all stars where with measurable Fe I and Fe II lines, we determined stellar parameters and measured [Fe/H] using both the non-α-enhanced atmosphere model and the α-enhanced model using the same measured equivalent widths.

We found that using an α-enhanced model systematically changed the measured $\log_{10}(\epsilon_{\text{Fe II}})$ by ~ -0.1 dex compared to a non-α-enhanced model, with a maximum variation of -0.2 dex. This resulted in a higher surface gravity $\log g$, an increase of ~ 0.1 dex, in order to ensure agreement between $\log_{10}(\epsilon_{\text{Fe I}})$ and $\log_{10}(\epsilon_{\text{Fe II}})$. This affected the measured [Fe/H] by ~ -0.1 dex and changed the measured [Ca/Fe] by ~ -0.05 dex. While we do not incorporate this potential source of error into our error determination, if we misidentified a star in its α-element content and subsequently used the wrong stellar atmosphere model, the increased uncertainty in our determination of $\Delta \log_{10}(\epsilon_{\text{Fe I}})$ would be on order of ~ -0.1 dex and $\Delta \log_{10}(\epsilon_{\text{Ca I}})$ would be on order of ~ -0.05 dex.

3.5 Results

We have performed high resolution spectroscopic observations of 58 primaries of candidate F/G/K+M binaries. Using previously measured radial velocities, we have shifted these obtained spectra to rest wavelengths. We have measured the equivalent widths of a number of Fe I, Fe II, Ca I, and Ti I lines identified in the spectra. Using Fe I and Fe II equivalent widths, we have determined the stellar parameters of 58 F/G/K stars, 42 of which have been previously confirmed by radial velocity to be primaries in an F/G/K+M binary system. We have also measured the α-element species Ca I and Ti I to ensure that we use the appropriate α-enhancement in our stellar atmosphere models. We present the measured Fe abundance in Table 3.3 and the Ca and Ti abundance in Table 3.4. We show [Ca/Fe] and [Ti/Fe] compared to [Fe/H] in Figure 3.6.

This sample of 42 confirmed F/G/K primaries will be used to evaluate the current methods used to empirically determine M-dwarf metallicity. We also intend, in future work, to develop an empirical relationship between the [Fe/H] as measured from the F/G/K primary to molecular features at optical wavelengths known to be metal-sensitive.

3.5.1 Comparison of Stars Observed using both MIKE and Echelle-100

We have both MIKE and Echelle-100 observations for 20 of the 77 observed F/G/K stars from our original sample. Of those 20 stars observed with both instruments, we could determine stellar parameters for 19 stars.

The five stars where we could not determine stellar parameters using Echelle-100 were PM I01266-4842W, PM I02225+1531S, PM I08386-3856, PM I13133-4153N, and PM I13167+0810E. Using the Echelle-100 spectra, we were able to measure relative velocities. However, the achieved S/N using Echelle-100 was insufficient to measure the equivalent width of Fe II lines, which are relatively weaker than Fe I. Without Fe II, we could not determine surface gravity spectroscopically in these five stars using Echelle-100.

For the remaining 14 stars, we compare the measured [Fe/H] to ensure there is no systematic offset between the abundances determined using these instruments. We plot the measured [Fe/H]

using MIKE against Δ[Fe/H], defined as the difference in the determined [Fe/H] for MIKE and Echelle-100 in Figure 3.7. The mean Δ[Fe/H]$= +0.06$ dex with a standard deviation of 0.17 dex. The measurements are all in agreement to 1.3-σ, where σ is the quadrature combined error of the [Fe/H] abundance measurement made with MIKE and with Echelle-100. Based on this, we conclude that the offset between [Fe/H] measurements made with MIKE and those made with Echelle-100 is minimal and can be ignored.

A similar test using [Ca/Fe] and [Ti/Fe] was also performed, which we plot in Figure 3.7. The mean Δ[Ca/Fe] $= +0.08$ dex with a standard deviation of 0.38, and the mean Δ[Ti/Fe] $= -0.03$ dex with a standard deviation of 0.26. The measurements of [Ca/Fe] and [Ti/Fe] for all 14 stars were in agreement to 1.8-σ and 1.1-σ respectively. We therefore conclude that there is also a minimal systematic offset in our measurements of [Ca/Fe] and [Ti/Fe] using MIKE and those using Echelle-100 which we can ignore.

3.6 Discussion

3.6.1 Comparison with Literature Values

In our sample of 58 F/G/K stars with measured stellar parameters, there were seven stars with literature [Fe/H] values found in SIMBAD (Wenger et al., 2000): NLTT 4817, PM I03150+0102, PM I11584-4155E. We present our measurements of [Fe/H] alongside literature value from Axer et al. (1994), Ramírez et al. (2013), Battistini & Bensby (2016), Franchini et al. (2014) and the RAVE survey (Kordopatis et al., 2013) in Figure 3.8.

We see that all but one of our measurements of [Fe/H] are in $\leq$ 1-σ agreement with these literature values for all three stars, where σ is the error determined in our measurement (see Table 3.5 for a complete breakdown of our error). The one exception, PM I08152-6337, is reproduced to 2.1-σ. We conclude that both MIKE and Echelle-100 can reproduce literature values to within error. This increases our confidence in our methodology and our measurements.

3.6.2 Comparison with Reduced Proper Motion Diagram from Li et al. (2014)

In their work precisely measuring the photometry of these F/G/K+M binary candidates, Li et al. (2014) constructed improved reduced proper-motion diagrams that could discern between dwarfs and subdwarfs. Using a criterion drawn from Salim & Gould (2003), they found that approximately 30% of their total sample were likely to be metal-rich dwarfs and the remainder were likely to be metal-poor subdwarfs. This criterion η is a function of the reduced proper motion of the star H_V, its galactic latitude b (which we assume to be $\pm 30^\circ$), and its $V-J$ color, as can be seen in Equation 3.1.

$$\eta = H_V - 3.1(V-J) - 1.47|\sin b| - 7.73 \tag{3.1}$$

Redder stars with lower reduced proper motions would ($\eta < 0$) are classified as main sequence dwarfs. Bluer stars with higher reduced proper motions ($0 < \eta < 5.15$) would be classified as subdwarfs. Salim & Gould (2003) noted that this separation between dwarfs and subdwarfs is not perfect. However, it has been previously demonstrated that with proper motions and high precision photometry, metal-rich dwarfs, likely to be kinematically associated with the disk, can be distinguished from the metal-poor subdwarfs likely to be halo stars (Marshall, 2008).

We calculate η for all 58 F/G/K stars with measured stellar parameters. Of this sample, 17 F/G/K stars have $\eta < 0$, classifying them as dwarfs. The average [Fe/H] of these 17 dwarfs is -0.58 dex. The average [Fe/H] of the subdwarf stars ($0 < \eta < 5.15$) is -1.02 dex. This is unsurprising since by definition subdwarfs are more metal-poor than the dwarfs since these subdwarfs are more likely to be halo stars.

When considering only those F/G/K stars confirmed to be primaries in an F/G/K+M binary, 15 primaries satisfy the criterion set by Salim & Gould (2003) to be considered dwarfs; the remainder of the sample are classified as subdwarfs. This is consistent with conclusions of Li et al. (2014) that approximately 30% of the sample are dwarfs.

We reproduce the reduced proper motion diagram of Li et al. (2014) incorporating radial velocity confirmation of the binary pairs and the measured [Fe/H] of the primaries in Figure 3.9.

We also present the calculated η from Equation 3.1 compared to the measured [Fe/H] in Figure 3.10. We see that as η becomes smaller, the metallicity of the star tends to increase as expected. The wide range of metallicities covered by our sample will be an asset in our future calibration to determine M-dwarf metallicity using low resolution optical spectroscopy.

3.6.3 Metallicity Range of the High Fidelity Sample

The use of spectroscopy to determine the metallicity of M-dwarf stars has been performed using both high-resolution spectroscopy (i.e Woolf & Wallerstein, 2005; Bean et al., 2006; Veyette et al., 2017) and using lower resolution spectroscopy (i.e Woolf & Wallerstein, 2006; Rojas-Ayala et al., 2012; Newton et al., 2014). Efforts to develop these techniques, however, have been primarily focused on the use of near-infrared spectra to determine M-dwarf stellar parameters due to the lower temperature of these stars, though some attempts have been made using optical wavelength spectra.

Woolf & Wallerstein (2006) was one of the first efforts to develop such a calibration, using the molecular features CaH2 and TiO5. These two optical wavelength features had been previously used to measure the CaH and TiO band strengths (Reid et al., 1995). Woolf & Wallerstein (2006) developed empirically calibrated the relation between the [Fe/H] of the M-dwarf and the strength of these molecular features, using 76 observed F/G/K+M binaries. Their final relationship was able to estimate M-dwarf metallicity for $-1.0 <$ [Fe/H] $< +0.05$ to an accuracy of ± 0.3 dex.

Rojas-Ayala et al. (2012) utilized moderate resolution ($R \sim 2,700$) near-infrared spectroscopy to develop their methodology. They used 18 F/G/K+M binaries with known metallicities from Fischer & Valenti (2005) to calibrate a relation between the measured equivalent width of the Na I doublet and the Ca I triplet and scaled by the H_2O-K2 molecular index to determine the metallicity of M-dwarfs. This calibration sample of 18 F/G/K+M binaries were relatively metal-rich, ranging $-0.69 <$ [Fe/H] $< +0.31$.

In their work to determine the metallicity of M-dwarfs, Newton et al. (2014) used 36 common proper motion F/G/K+M binary pairs with known literature metallicities as a calibration sample. Using moderate resolution near-infrared spectra ($R \sim 2,000$), they used the 2.2 μm Na I doublet

to determine M-dwarf metallicity. Their empirically calibrated relation is valid for metallicites $-1.0 <$ [Fe/H] $< +0.35$ and can determine [Fe/H] to an accuracy of 0.12 dex.

Using high-resolution ($R \sim 25,000$) near-infrared spectra, Veyette et al. (2017) developed a calibration using 33 F/G/K+M binaries drawn from Mann et al. (2013). Their work focused on using both spectroscopic models developed for M-dwarfs and the equivalent widths of near-infrared Fe I and Ti I lines to determine metallicity. Their method is valid for $-0.7 <$ [Fe/H] $< +0.3$, limiting its application to metal-rich dwarfs.

These previous works selected F/G/K+M binary pairs with [Fe/H]> -1 for to calibrate their samples, allowing us to trace the chemical evolution of the Milky Way to the time when the protostellar gas had this metallicity. In order to probe further back in time, these relationships should be extended to a encompass more metal-poor M-dwarfs. When constructing this sample, we intentionally included both metal-rich dwarfs and metal-poor subdwarfs in order to develop a metallicity calibration that could cover a wide range of metallicities. Our calibration sample spans a metallicity range of $-1.94 <$ [Fe/H] $< +0.01$. The metal-rich dwarfs in our sample can serve as a link to these previously developed methodologies and additionally serve as a way to evaluate them. The majority of our sample, the metal-poor subdwarfs, will be useful in extending these empirical calibrations to lower metallicites. This will allow the study of metal-poor M-dwarfs in the disk and halo M-dwarfs passing through the disk, allowing up to probe further back into the chemical evolution history of the Milky Way.

3.7 Conclusions

We have performed chemical abundance measurements of 58 F/G/K stars with high proper motions using high dispersion spectroscopy. Of these 58 stars, 42 were previously determined to be the primary star in a F/G/K+M binary system. We have derived stellar parameters and measured the abundance of Fe, Ca, and Ti to provide accurate determinations of [Fe/H] and [α/Fe] in the binary pair. We have shown that we can reproduce literature [Fe/H] abundances within error for 7 stars in our sample. We also have shown that our sample is constituted primarily of metal-poor subdwarf stars. We have also shown that our sample can extend the applicability of empirically

calibrated relations used to measure the metallicity of M-dwarfs to the metal-poor regime.

Future work using this sample include the evaluation of current methodologies used to classify M-dwarfs into metallicity classes (Lépine et al., 2007; Dhital et al., 2012). However, we will primarily be focused on the development of a method based on Woolf & Wallerstein (2006) to measure the metallicity of M-dwarfs using low-resolution optical spectroscopy. By developing a methodology using optical spectroscopy, we hope to use the myriad of optical spectroscopic surveys to study the metallicity distribution of M-dwarfs in the Galaxy, both the metal-rich disk and the metal-poor halo populations.

We also intend that this calibration sample be used to improve existing methods of determining metallicity of M-dwarf exoplanet hosts. In particular, the extension of these methods to metal-poor M-dwarfs can allow the probing of the planet-metallicity relation (Fischer & Valenti, 2005) at the low-mass, metal-poor end. Given the growing interest in formation theories of terrestrial planets and the recent programs specifically targeting M-dwarfs to find terrestrial planets in the habitable zone, we anticipate the need to measure metallicites of metal-poor M-dwarf hosts.

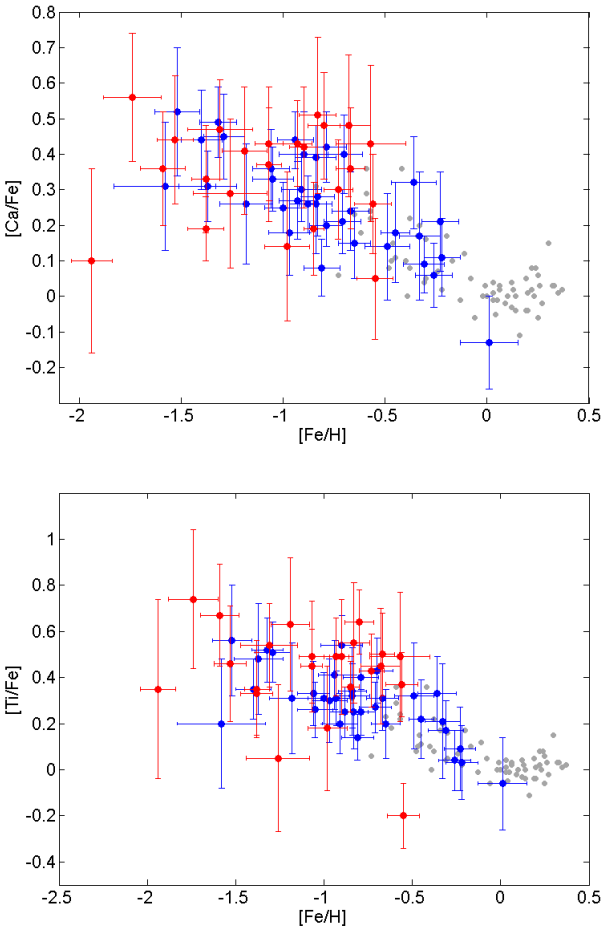

Figure 3.6 [Ca/Fe] and [Ti/Fe] of F/G/K stars plotted against [Fe/H] for all 58 stars analyzed in this study. Blue points represent stars where the surface gravity was determined using Fe I and Fe II ionization balance. Red points represent stars where the surface gravity was determined by photometry and comparison to an isochrone. Grey points are Milky Way stars studied by Bensby et al. (2003). We note that the α-enhancement of some stars seems high; however, these points also have very high measurement errors.

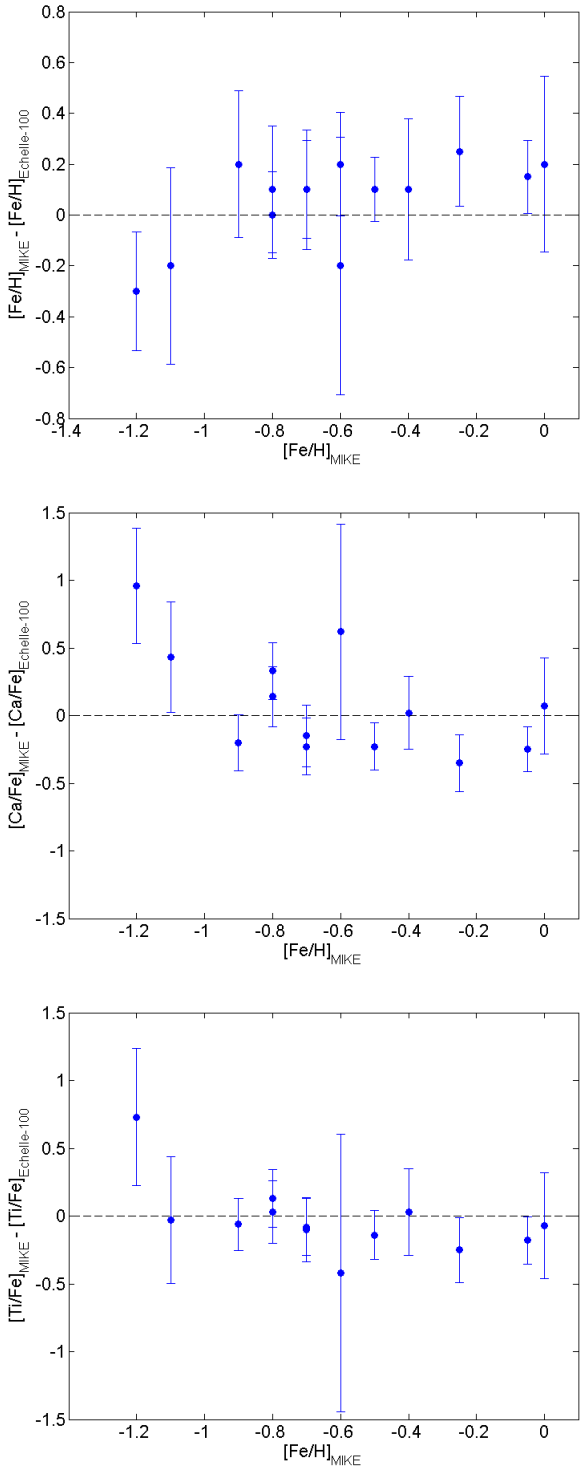

Figure 3.7 Comparison of the [Fe/H], [Ca/Fe], and [Ti/Fe] determined using MIKE and Echelle-100 independently. We determined stellar parameters (including [Fe/H]) for both MIKE and Echelle-100 for 14 stars. The error bars are the quadrature sum of the total errors in the abundance measurement (see Table 3.5 for details). The mean Δ[Fe/H] = $[\mathrm{Fe/H}]_{\mathrm{MIKE}} - [\mathrm{Fe/H}]_{\mathrm{Echelle\text{-}100}} = +0.06$ dex. There is a < 1.3-σ agreement between the measurements for all stars. We therefore conclude that the systematic offset between the measurements of [Fe/H] using MIKE spectra and using Echelle-100 spectra is minimal and can be ignored.

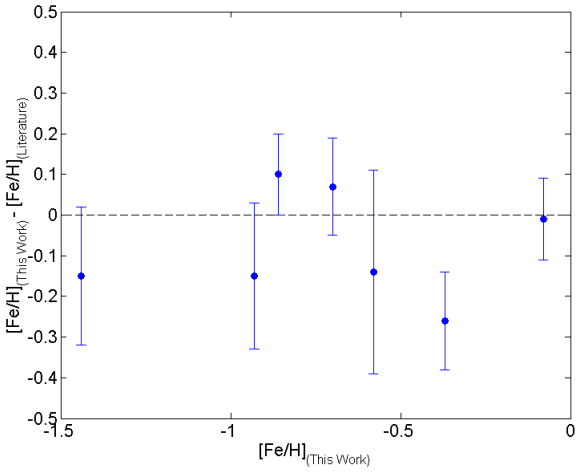

Figure 3.8 Comparison of our [Fe/H] measurements with those in the literature for seven F/G/K stars in our sample. Literature [Fe/H] measurements are sourced from Axer et al. (1994), Ramírez et al. (2013), Battistini & Bensby (2016), Kordopatis et al. (2013), and Franchini et al. (2014). The error bars are our error in the measurement of [Fe/H], σ. We see that all but one star is reproduced within $\leq$ 1-σ.The outlying star is reproduced within 2.1-σ. We see that we can reproduce literature values to within error and are therefore confident in our measurements.

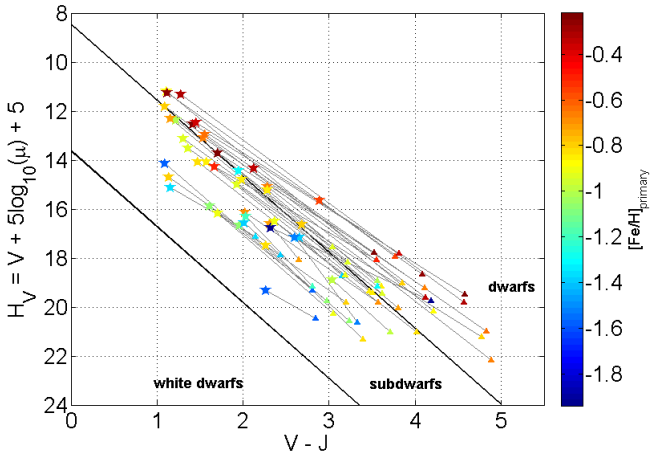

Figure 3.9 Reduced proper motion diagram for all confirmed binaries. Photometry used for the proper motion diagram is sourced from Li et al. (2014). Each point is colored according to the measured [Fe/H]. Five-point stars are the confirmed primaries of an F/G/K+M binary pair. M-dwarf secondaries of these confirmed pairs are plotted as triangles and are connected to their primaries by a grey line. Our boundary between dwarf, subdwarf, and white dwarf groups are $\eta = 0$ and $\eta = 5.15$ discrimination lines from Salim & Gould (2003). We see that of our sample of common proper motion binaries, about 30% of our sample are dwarfs and the remainder are subdwarfs. However, it should be noted that this separation between dwarfs and subdwarfs is not perfect (Salim & Gould, 2003) meaning stars at close to the $\eta = 0$ may be misclassified.

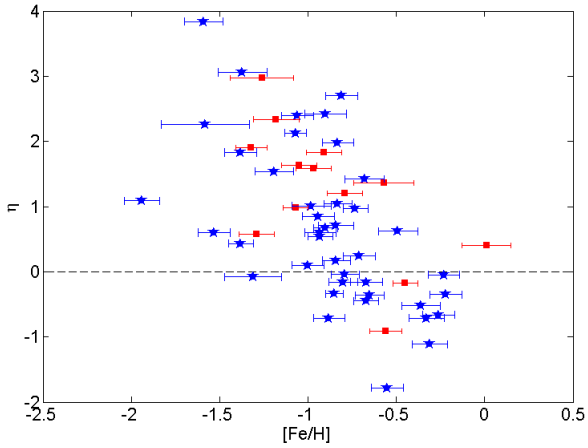

Figure 3.10 η as calculated from Equation 3.1 compared to measured [Fe/H]. Blue stars represent confirmed binaries. Red squares are unconfirmed binary candidates. Photometry and proper motions uses to calculate η are presented in Li et al. (2014). We also show $\eta = 0$ boundary line separating the dwarf ($\eta < 0$) and the subdwarf ($\eta > 0$) populations. We see that as [Fe/H] increases, η decreases as expected. We also see that the majority of of stars are classified as metal-poor subdwarf stars.

Table 3.1: F/G/K Star Observing Details

Primary Name	R.A. J2000	Dec. J2000	Instrument	UT Date Obs.	S/N at 5500Å	η^{b}	Notes
PM I00025-4644	00:02:35.66	−46:44:52.0	MIKE	13-Nov-08	30	1.98	[a]
PM I00329+1805	00:32:55.80	+18:05:52.9	MIKE	14-Nov-08	41	-0.16	[a]
PM I00422+0731E	00:42:15.23	+07:31:18.7	MIKE	14-Nov-08	45	2.42	[a]
PM I00592+0705N	00:59:17.81	+07:05:56.4	MIKE	16-Nov-08	15	1.74	
NLTT 3847	01:09:28.97	−05:07:25.3	MIKE	23-Nov-07	12	-0.38	[a]
PM I01227+1409	01:22:43.29	+14:09:34.5	MIKE	16-Nov-08	70	-0.71	[a]
PM I01266-4842W	01:26:37.33	−48:42:51.0	MIKE	23-Nov-07	28	-0.91	
NLTT 4817	01:26:55.17	+12:00:25.9	MIKE	9-Dec-08	120	2.26	[a]
PM I01352+0538N	01:35:14.71	+05:38:24.7	MIKE	23-Nov-07	95	-0.16	[a]
PM I01430-4959W	01:43:00.68	−49:59:26.8	MIKE	21-Nov-07	35	2.34	
PM I02012+0218	02:01:15.09	+02:18:25.8	MIKE	13-Nov-08	15	···	
PM I02225+1531S	02:22:34.06	+15:31:09.9	MIKE	16-Nov-08	75	···	[a]
PM I02267-4214	02:26:47.96	−42:14:58.9	MIKE	16-Nov-08	11	···	
NLTT 8753	02:42:05.13	−24:45:16.3	MIKE	20-Nov-07	17	2.64	[a]
PM I02548+2057W	02:54:49.43	+20:57:34.8	MIKE	9-Dec-08	34	···	
PM I02569-5831N	02:56:55.71	−58:31:24.3	MIKE	13-Nov-08	36	-0.45	[a]
PM I03150+0102	03:15:04.76	+01:02:15.2	Echelle100	28-Aug-07	120	0.6	[a]
PM I03256-3333E	03:25:41.79	−33:33:34.6	MIKE	21-Nov-07	32	0.97	[a]
NLTT 12296	03:59:04.27	−06:56:03.2	MIKE	23-Nov-07	46	2.13	[a]
PM I04072+1526N	04:07:16.36	+15:26:42.8	Echelle100	29-Aug-07	130	-1.11	[a]
PM I04099+0942E	04:09:54.30	+09:42:58.8	MIKE	20-Nov-07	22	1.83	[a]
PM I04254-4601	04:25:28.74	−46:01:23.9	MIKE	13-Nov-08	47	1.9	
PM I04325-5657N	04:32:32.44	−56:57:04.3	Echelle100	20-Feb-08	67	0.85	[a]
PM I04327+0820	04:32:45.59	+08:20:05.5	MIKE	16-Nov-08	65	0.58	
PM I04332+0013	04:33:17.84	+00:13:59.8	Echelle100	28-Aug-07	13	0.24	
PM I04477-3044W	04:47:42.65	−30:44:03.2	Echelle100	20-Feb-08	13	0.62	

[a] This star is the primary in a binary pair confirmed using radial velocity (see Chapter 2).

[b] Calculated from Equation 3.1 using data presented in Li et al. (2014).

Table 3.1: F/G/K Star Observing Details *(continued)*

Primary Name	R.A. J2000	Dec. J2000	Instrument	UT Date Obs.	S/N at 5500Å	η[b]	Notes
NLTT 14407	05:02:20.19	−19:32:04.4	MIKE	22-Nov-07	91	0.98	
PM I05137+0647W	05:13:46.03	+06:47:01.0	MIKE	16-Nov-08	10	0.69	
PM I05195+0903E	05:19:34.77	+09:03:46.3	MIKE	16-Nov-08	12	2.15	
PM I05484-3617Nn	05:48:28.64	−36:17:06.7	MIKE	13-Nov-08	47	2.39	[a]
PM I06032+1921N	06:03:14.87	+19:21:38.6	MIKE	22-Nov-07	120	1.63	
PM I06050+0723S	06:05:03.52	+07:23:30.5	MIKE	23-Nov-07	33	0.43	[a]
PM I06394-3030E	06:39:24.52	−30:30:50.9	···	···	···	-0.21	
PM I06436+0851	06:43:36.55	+08:51:44.4	···	···	···	-2.12	
PM I08152-6337	08:15:17.60	−63:37:18.4	MIKE	24-Apr-08	26	-0.71	[a]
PM I08239-7549W	08:23:54.94	−75:49:34.3	MIKE	11-Dec-08	86	-0.35	[a]
PM I08386-3856	08:38:36.72	−38:56:55.7	MIKE	11-Dec-08	48	-0.18	
PM I09502+0509E	09:50:13.89	+05:09:02.4	MIKE	24-Apr-08	31	1.04	[a]
PM I10105+1203W	10:10:34.78	+12:03:17.6	MIKE	25-Apr-08	25	0.71	[a]
PM I10520+1521N	10:52:02.16	+15:21:18.6	MIKE	24-Apr-08	8	2.37	[a]
PM I11110-4414	11:11:04.09	−44:14:15.9	MIKE	25-Apr-08	10	2.64	
PM I11125-3512	11:12:30.07	−35:12:35.0	MIKE	9-Feb-07	23	1.42	[a]
NLTT 27188	11:22:26.44	−27:13:35.2	MIKE	10-Feb-07	43	3.06	[a]
PM I11263+2047Ee	11:26:21.55	+20:47:22.7	MIKE	25-Apr-08	30	-0.34	[a]
PM I11330+1318N	11:33:02.86	+13:18:33.2	Echelle100	19-Feb-08	140	-0.66	[a]
PM I11392-4118N	11:39:12.23	−41:18:15.1	MIKE	25-Apr-08	18	-1.78	[a]
PM I11584-4155E	11:58:27.99	−41:55:19.3	MIKE	25-Apr-08	31	···	
PM I12170+0742E	12:17:05.76	+07:42:30.3	MIKE	9-Feb-07	18	2.97	
PM I12237+0625	12:23:43.48	+06:25:10.3	MIKE	9-Feb-07	29	0.54	[a]
PM I12277+1334	12:27:43.78	+13:34:16.2	MIKE	25-Apr-08	14	2.85	
PM I12283+1222S	12:28:18.28	+12:22:36.4	Echelle100	19-Feb-08	12	···	
PM I12440+0625E	12:44:02.57	+06:25:46.9	Echelle100	20-Feb-08	10	2.1	
PM I12508+0757	12:50:48.80	+07:57:56.7	Echelle100	16-Feb-08	130	-0.04	[a]

[a] This star is the primary in a binary pair confirmed using radial velocity (see Chapter 2).

[b] Calculated from Equation 3.1 using data presented in Li et al. (2014).

Table 3.1: F/G/K Star Observing Details *(continued)*

Primary Name	R.A. J2000	Dec. J2000	Instrument	UT Date Obs.	S/N at 5500Å	η[b]	Notes
PM I13116+1106	13:11:41.81	+11:06:24.8	···	···	···	2.06	
NLTT 33282	13:13:09.08	−07:42:15.2	MIKE	9-Feb-07	12	1.27	
PM I13133-4153N	13:13:20.50	−41:53:14.0	MIKE	25-Apr-08	32	-0.08	[a]
PM I13167+0810E	13:16:47.28	+08:10:27.4	MIKE	25-Apr-08	32	-0.36	[a]
PM I13372-4244E	13:37:14.25	−42:44:54.8	···	···	···	2.52	
PM I14055+0244S	14:05:30.97	+02:44:23.4	MIKE	9-Feb-07	17	1.36	
PM I14124+0517S	14:12:28.75	+05:17:28.5	MIKE	10-Feb-07	43	1.83	
PM I14136-3634E	14:13:41.61	−36:34:39.2	MIKE	6-Aug-16	34	1.54	[a]
PM I14475+1134	14:47:35.80	+11:34:13.7	MIKE	25-Apr-08	41	1.2	
PM I15413+1349N	15:41:19.36	+13:49:28.5	MIKE	9-Feb-07	25	1.01	[a]
PM I16008+0146E	16:00:53.85	+01:46:16.5	MIKE	25-Apr-08	23	0.17	[a]
PM I16519-4806N	16:51:58.19	−48:06:13.7	MIKE	6-Aug-16	23	1.09	[a]
PM I17135+1909	17:13:30.36	+19:09:57.2	MIKE	23-Jul-08	34	-0.52	[a]
PM I19207+0506S	19:20:46.74	+05:06:26.5	MIKE	25-Apr-08	55	0.1	[a]
PM I19420+2014S	19:42:00.86	+20:14:05.0	MIKE	6-Aug-16	12	0.13	
PM I20072-3519E	20:07:13.51	−35:19:50.0	MIKE	25-Apr-08	6	-1.89	[a]
PM I20343+1151	20:34:22.72	+11:51:59.5	Echelle100	29-Aug-07	54	0.62	[a]
NLTT 49474	20:34:31.48	−22:19:24.3	Echelle100	27-Aug-07	100	0.24	[a]
PM I20487+1406	20:48:42.08	+14:06:59.1	MIKE	23-Jul-08	115	0.4	
PM I21175-4142E	21:17:32.29	−41:42:17.3	MIKE	23-Jul-08	57	1.58	
PM I21442+0102N	21:44:15.64	+01:02:09.1	MIKE	15-Nov-08	22	0.67	[a]
PM I21536+0010S	21:53:39.95	+00:10:20.8	Echelle100	27-Aug-07	9	1.14	[a]
NLTT 52532	21:57:35.98	−03:28:09.2	MIKE	23-Nov-07	24	0.6	[a]
PM I22296+0620	22:29:41.07	+06:20:02.8	Echelle100	28-Aug-07	8	-1.5	
PM I22487-5613W	22:48:44.33	−56:13:37.0	MIKE	16-Nov-08	105	-0.05	[a]
PM I23033-5311	23:03:23.47	−53:11:23.1	MIKE	16-Nov-08	53	2.7	[a]
NLTT 57827	23:44:27.89	−30:55:16.9	MIKE	23-Jul-08	22	3.84	[a]

[a] This star is the primary in a binary pair confirmed using radial velocity (see Chapter 2).

[b] Calculated from Equation 3.1 using data presented in Li et al. (2014).

Table 3.2: F/G/K Star Stellar Parameters Used in Atmosphere Model

Primary Name	$T_{\rm eff}$ (K)	log(g) (dex)	$v_{\rm micro}$ (km s^{-1})	[Fe/H] (dex)	α-Enhancement	Notes
PM I00025-4644	4600 ± 150	4.5 ± 0.1[b]	1.2 ± 0.3	-0.83 ± 0.09	α-enhanced	[a]
PM I00329+1805	4600 ± 100	4.65 ± 0.1[b]	1.3 ± 0.2	-0.80 ± 0.08	α-enhanced	[a]
PM I00422+0731E	5200 ± 100	4.4 ± 0.1	1.4 ± 0.2	-0.90 ± 0.12	α-enhanced	[a]
PM I00592+0705N	...	...	...	...	...	
NLTT 3847	...	...	...	...	...	[a]
PM I01227+1409	5800 ± 100	4.15 ± 0.25	1.6 ± 0.3	-0.88 ± 0.09	non-α-enhanced	[a]
PM I01266-4842W	4400 ± 100	4.65 ± 0.1[b]	0.5 ± 0.4	-0.56 ± 0.09	non-α-enhanced	
NLTT 4817	5700 ± 150	4.1 ± 0.1	1.5 ± 0.4	-1.58 ± 0.25	α-enhanced	[a]
PM I01352+0538N	5200 ± 100	4.55 ± 0.1	0.4 ± 0.3	-0.67 ± 0.09	non-α-enhanced	[a]
PM I01430-4959W	4900 ± 150	4.4 ± 0.15	0.4 ± 0.3	-1.18 ± 0.13	non-α-enhanced	
PM I02012+0218	4600 ± 200	4.7 ± 0.1[b]	1 ± 0.3	-1.74 ± 0.14	α-enhanced	
PM I02225+1531S	5300 ± 100	4.5 ± 0.1	0.4 ± 0.3	-1.40 ± 0.10	α-enhanced	[a]
PM I02267-4214	...	...	...	...	...	
NLTT 8753	...	...	...	...	...	[a]
PM I02548+2057W	4800 ± 150	4.7 ± 0.2	1.5 ± 0.4	-1.52 ± 0.11	α-enhanced	
PM I02569-5831N	4600 ± 100	4.7 ± 0.1[b]	0.8 ± 0.3	-0.67 ± 0.07	α-enhanced	[a]
PM I03150+0102	5400 ± 100	4.65 ± 0.15	1.1 ± 0.3	-0.93 ± 0.09	non-α-enhanced	[a]
PM I03256-3333E	4500 ± 100	4.65 ± 0.1[b]	0.5 ± 0.3	-0.73 ± 0.07	α-enhanced	[a]
NLTT 12296	4700 ± 100	4.7 ± 0.1[b]	0.8 ± 0.3	-1.07 ± 0.06	α-enhanced	[a]
PM I04072+1526N	5600 ± 100	4.7 ± 0.1	0.8 ± 0.3	-0.31 ± 0.10	non-α-enhanced	[a]
PM I04099+0942E	5100 ± 100	4.7 ± 0.1[b]	0.9 ± 0.3	-1.38 ± 0.09	non-α-enhanced	[a]
PM I04254-4601	5100 ± 100	4.7 ± 0.1	1.4 ± 0.3	-1.32 ± 0.09	α-enhanced	
PM I04325-5657N	5400 ± 100	4.8 ± 0.1	0.8 ± 0.3	-0.94 ± 0.09	α-enhanced	[a]
PM I04327+0820	5600 ± 100	4.6 ± 0.1	1 ± 0.3	-1.29 ± 0.10	α-enhanced	
PM I04332+0013	...	...	...	...	...	
PM I04477-3044W	...	...	...	...	...	
NLTT 14407	4600 ± 150	4.7 ± 0.1[b]	1.1 ± 0.4	-1.07 ± 0.07	α-enhanced	
PM I05137+0647W	...	...	...	...	...	
PM I05195+0903E	...	...	...	...	...	
PM I05484-3617Nn	5000 ± 100	4.7 ± 0.1	1.1 ± 0.3	-1.06 ± 0.09	α-enhanced	[a]
PM I06032+1921N	5500 ± 100	4.6 ± 0.1	0.4 ± 0.3	-1.05 ± 0.10	α-enhanced	
PM I06050+0723S	4100 ± 150	4.7 ± 0.1[b]	1.2 ± 0.4	-1.38 ± 0.07	α-enhanced	[a]
PM I06394-3030E	...	...	...	...	...	
PM I06436+0851	...	...	...	...	...	
PM I08152-6337	4650 ± 150	4.65 ± 0.15	1 ± 0.4	-0.33 ± 0.10	non-α-enhanced	[a]
PM I08239-7549W	5150 ± 100	4.6 ± 0.1	1 ± 0.3	-0.22 ± 0.09	non-α-enhanced	[a]
PM I08386-3856	4900 ± 100	4.65 ± 0.1	0.8 ± 0.3	-0.45 ± 0.07	non-α-enhanced	
PM I09502+0509E	5000 ± 100	4.7 ± 0.1	0.8 ± 0.3	-0.83 ± 0.08	non-α-enhanced	[a]

[a] This star is the primary in a binary pair confirmed using radial velocity (see Chapter 2).
[b] This surface gravity was derived using an isochrone instead of using an ionization balance between Fe I and Fe II.

Table 3.2: F/G/K Star Stellar Parameters Used in Atmosphere Model *(continued)*

Primary Name	$T_{\rm eff}$ (K)	log(g) (dex)	$v_{\rm micro}$ (km s^{-1})	[Fe/H] (dex)	α-Enhancement	Notes
PM I10105+1203W	5200 ± 100	4.6 ± 0.15	1.2 ± 0.3	-0.84 ± 0.10	α-enhanced	[a]
PM I10520+1521N	...	...	...	...	...	[a]
PM I11110-4414	...	...	...	...	...	
PM I11125-3512	4900 ± 150	4.65 ± 0.1[b]	1.3 ± 0.3	-0.68 ± 0.11	α-enhanced	[a]
NLTT 27188	6000 ± 200	4.7 ± 0.2	1.1 ± 0.4	-1.37 ± 0.14	α-enhanced	[a]
PM I11263+2047Ee	4300 ± 100	4.7 ± 0.1[b]	0.5 ± 0.3	-0.85 ± 0.05	non-α-enhanced	[a]
PM I11330+1318N	5650 ± 100	4.4 ± 0.1	0.95 ± 0.3	-0.26 ± 0.09	non-α-enhanced	[a]
PM I11392-4118N	4000 ± 100	4.7 ± 0.1[b]	1 ± 0.3	-0.55 ± 0.09	non-α-enhanced	[a]
PM I11584-4155E	5200 ± 100	4.7 ± 0.1	1.1 ± 0.3	-0.70 ± 0.09	α-enhanced	
PM I12170+0742E	5000 ± 200	4.7 ± 0.1[b]	1.5 ± 0.5	-1.26 ± 0.18	non-α-enhanced	
PM I12237+0625	4700 ± 100	4.7 ± 0.1[b]	1.3 ± 0.3	-0.93 ± 0.07	α-enhanced	[a]
PM I12277+1334	...	...	...	...	...	
PM I12283+1222S	...	...	...	...	...	
PM I12440+0625E	...	...	...	...	...	
PM I12508+0757	5850 ± 100	4.65 ± 0.1	1.9 ± 0.3	-0.79 ± 0.08	non-α-enhanced	[a]
PM I13116+1106	...	...	...	...	...	
NLTT 33282	...	...	...	...	...	
PM I13133-4153N	4800 ± 100	4.7 ± 0.1[b]	1.5 ± 0.3	-1.31 ± 0.16	α-enhanced	[a]
PM I13167+0810E	5000 ± 100	4.8 ± 0.1	0.6 ± 0.3	-0.65 ± 0.08	non-α-enhanced	[a]
PM I13372-4244E	...	...	...	...	...	
PM I14055+0244S	4700 ± 150	4.65 ± 0.1[b]	1 ± 0.5	-0.57 ± 0.17	α-enhanced	
PM I14124+0517S	5300 ± 100	4.7 ± 0.1	1.2 ± 0.3	-0.91 ± 0.10	α-enhanced	
PM I14136-3634E	4800 ± 150	4.7 ± 0.1[b]	1.5 ± 0.5	-1.19 ± 0.11	α-enhanced	[a]
PM I14475+1134	5200 ± 100	4.4 ± 0.1	1 ± 0.3	-0.79 ± 0.10	α-enhanced	
PM I15413+1349N	4000 ± 200	4.7 ± 0.1[b]	1 ± 0.5	-0.98 ± 0.11	non-α-enhanced	[a]
PM I16008+0146E	4700 ± 100	4.4 ± 0.1	0.8 ± 0.3	-0.84 ± 0.08	non-α-enhanced	[a]
PM I16519-4806N	4400 ± 200	4.7 ± 0.1[b]	1 ± 0.5	-1.94 ± 0.10	non-α-enhanced	[a]
PM I17135+1909	5200 ± 100	4.4 ± 0.2	1.2 ± 0.3	-0.36 ± 0.11	α-enhanced	[a]
PM I19207+0506S	5800 ± 100	4.4 ± 0.1	1.5 ± 0.3	-1.00 ± 0.09	non-α-enhanced	[a]
PM I19420+2014S	...	...	...	...	...	
PM I20072-3519E	...	...	...	...	...	[a]
PM I20343+1151	4950 ± 150	4.8 ± 0.1	0.5 ± 0.4	-0.49 ± 0.11	non-α-enhanced	[a]
NLTT 49474	5900 ± 100	4.7 ± 0.1	0.2 ± 0.3	-0.71 ± 0.09	non-α-enhanced	[a]
PM I20487+1406	5050 ± 100	4.1 ± 0.1	1.25 ± 0.3	0.01 ± 0.14	non-α-enhanced	
PM I21175-4142E	5500 ± 100	4.8 ± 0.1	0.5 ± 0.4	-0.97 ± 0.10	non-α-enhanced	
PM I21442+0102N	4500 ± 150	4.7 ± 0.1[b]	0.5 ± 0.3	-0.90 ± 0.07	α-enhanced	[a]
PM I21536+0010S	...	...	...	...	...	[a]
NLTT 52532	4100 ± 150	4.8 ± 0.1[b]	1 ± 0.5	-1.53 ± 0.09	α-enhanced	[a]
PM I22296+0620	...	...	...	...	...	

[a] This star is the primary in a binary pair confirmed using radial velocity (see Chapter 2).

[b] This surface gravity was derived using an isochrone instead of using an ionization balance between Fe I and Fe II.

Table 3.2: F/G/K Star Stellar Parameters Used in Atmosphere Model *(continued)*

Primary Name	$T_{\rm eff}$ (K)	log(g) (dex)	$v_{\rm micro}$ (km s^{-1})	[Fe/H] (dex)	α-Enhancement	Notes
PM I22487-5613W	4900 ± 100	4.4 ± 0.1	1 ± 0.3	-0.23 ± 0.09	non-α-enhanced	[a]
PM I23033-5311	6000 ± 100	4.7 ± 0.1	1 ± 0.3	-0.81 ± 0.09	non-α-enhanced	[a]
NLTT 57827	4700 ± 150	4.7 ± 0.1[b]	1.3 ± 0.4	-1.59 ± 0.11	α-enhanced	[a]

[a] This star is the primary in a binary pair confirmed using radial velocity (see Chapter 2).
[b] This surface gravity was derived using an isochrone instead of using an ionization balance between Fe I and Fe II.

Table 3.3: F/G/K Star Measured Element Abundances - Fe I and Fe II

Primary Name	Secondary Name	Fe I				Fe II				Notes
		N	$\log_{10}(\epsilon_X)$	[Fe/H]	Error	N	$\log_{10}(\epsilon_X)$	[Fe/H]	Error	
PM I00025-4644	PM I00026-4644	27	6.69	−0.83	0.09	···	···	···	···	[a]
PM I00329+1805	PM I00329+1805-2	21	6.72	−0.80	0.08	···	···	···	···	[a]
PM I00422+0731E	PM I00422+0731W	28	6.62	−0.90	0.12	6	6.62	−0.90	0.19	[a]
PM I00592+0705N	PM I00592+0705S	···	···	···	···	···	···	···	···	
NLTT 3847	NLTT 3849	···	···	···	···	···	···	···	···	[a]
PM I01227+1409	PM I01226+1409E	21	6.64	−0.88	0.09	6	6.67	−0.85	0.12	[a]
PM I01266-4842W	PM I01266-4842E	22	6.96	−0.56	0.09	···	···	···	···	
NLTT 4817	NLTT 4814	11	5.94	−1.58	0.25	4	5.91	−1.61	0.09	[a]
PM I01352+0538N	PM I01352+0538S	32	6.85	−0.67	0.09	6	6.82	−0.70	0.09	[a]
PM I01430-4959W	PM I01430-4959E	17	6.34	−1.18	0.13	2	6.43	−1.09	0.18	
PM I02012+0218	PM I02012+0217	7	5.78	−1.74	0.14	···	···	···	···	
PM I02225+1531S	PM I02225+1531N	20	6.12	−1.40	0.10	4	6.04	−1.48	0.11	[a]
PM I02267-4214	PM I02267-4215	···	···	···	···	···	···	···	···	
NLTT 8753	NLTT 8759	···	···	···	···	···	···	···	···	[a]
PM I02548+2057W	PM I02548+2057E	18	6.00	−1.52	0.11	1	6.01	−1.51	0.25	
PM I02569-5831N	PM I02569-5831S	19	6.85	−0.67	0.07	···	···	···	···	[a]
PM I03150+0102	PM I03150+0103	21	6.59	−0.93	0.09	4	6.54	−0.98	0.09	[a]
PM I03256-3333E	PM I03256-3333Wn	19	6.79	−0.73	0.07	···	···	···	···	[a]
NLTT 12296	NLTT 12294	16	6.45	−1.07	0.06	···	···	···	···	[a]
PM I04072+1526N	PM I04072+1526S	27	7.21	−0.31	0.10	6	7.16	−0.36	0.09	[a]
PM I04099+0942E	PM I04099+0942W	12	6.14	−1.38	0.09	···	···	···	···	[a]
PM I04254-4601	PM I04255-4601	21	6.20	−1.32	0.09	2	6.14	−1.38	0.09	
PM I04325-5657N	PM I04325-5657S	14	6.58	−0.94	0.09	2	6.58	−0.94	0.08	[a]
PM I04327+0820	PM I04327+0820-2	17	6.23	−1.29	0.10	4	6.22	−1.30	0.07	
PM I04332+0013	PM I04333+0014	···	···	···	···	···	···	···	···	
PM I04477-3044W	PM I04477-3044E	···	···	···	···	···	···	···	···	
NLTT 14407	NLTT 14408	16	6.45	−1.07	0.07	···	···	···	···	

[a] This star is the primary in a binary pair confirmed using radial velocity (see Chapter 2).

Table 3.3: F/G/K Star Measured Element Abundances - Fe I and Fe II *(continued)*

Primary Name	Secondary Name	Fe I				Fe II				Notes
		N	$\log_{10}(\epsilon_X)$	[Fe/H]	Error	N	$\log_{10}(\epsilon_X)$	[Fe/H]	Error	
PM I05137+0647W	PM I05137+0647E	···	···	···	···	···	···	···	···	
PM I05195+0903E	PM I05195+0903W	···	···	···	···	···	···	···	···	
PM I05484-3617Nn	PM I05484-3617S	23	6.46	−1.06	0.09	3	6.38	−1.14	0.10	[a]
PM I06032+1921N	PM I06032+1921S	21	6.47	−1.05	0.10	6	6.5	−1.02	0.08	
PM I06050+0723S	PM I06050+0723N	11	6.14	−1.38	0.07	···	···	···	···	[a]
PM I06394-3030E	PM I06394-3030W	···	···	···	···	···	···	···	···	
PM I06436+0851	PM I06436+0851-2	···	···	···	···	···	···	···	···	
PM I08152-6337	PM I08153-6337	16	7.19	−0.33	0.10	1	7.24	−0.28	0.32	[a]
PM I08239-7549W	PM I08239-7549E	40	7.30	−0.22	0.09	5	7.3	−0.22	0.12	[a]
PM I08386-3856	PM I08386-3857	36	7.07	−0.45	0.07	4	7.03	−0.49	0.13	
PM I09502+0509E	PM I09502+0509W	26	6.69	−0.83	0.08	2	6.65	−0.87	0.11	[a]
PM I10105+1203W	PM I10105+1203E	24	6.68	−0.84	0.10	3	6.67	−0.85	0.12	[a]
PM I10520+1521N	PM I10520+1521S	···	···	···	···	···	···	···	···	[a]
PM I11110-4414	PM I11109-4416	···	···	···	···	···	···	···	···	
PM I11125-3512	PM I11124-3512	19	6.84	−0.68	0.11	···	···	···	···	[a]
NLTT 27188	NLTT 27182	6	6.15	−1.37	0.14	3	6.09	−1.43	0.07	[a]
PM I11263+2047Ee	PM I11263+2047Ew	14	6.67	−0.85	0.05	···	···	···	···	[a]
PM I11330+1318N	PM I11330+1318S	26	7.26	−0.26	0.09	6	7.26	−0.26	0.08	[a]
PM I11392-4118N	PM I11392-4118S	17	6.97	−0.55	0.09	···	···	···	···	[a]
PM I11584-4155E	PM I11584-4155W	26	6.82	−0.70	0.09	4	6.75	−0.77	0.09	
PM I12170+0742E	PM I12170+0742W	7	6.26	−1.26	0.18	···	···	···	···	
PM I12237+0625	PM I12237+0624	19	6.59	−0.93	0.07	···	···	···	···	[a]
PM I12277+1334	PM I12277+1336	···	···	···	···	···	···	···	···	
PM I12283+1222S	PM I12283+1222N	···	···	···	···	···	···	···	···	
PM I12440+0625E	PM I12440+0625We	···	···	···	···	···	···	···	···	
PM I12508+0757	PM I12507+0758	21	6.73	−0.79	0.08	5	6.72	−0.80	0.06	[a]
PM I13116+1106	PM I13116+1105	···	···	···	···	···	···	···	···	

[a] This star is the primary in a binary pair confirmed using radial velocity (see Chapter 2).

Table 3.3: F/G/K Star Measured Element Abundances - Fe I and Fe II *(continued)*

Primary Name	Secondary Name	Fe I				Fe II				Notes
		N	$\log_{10}(\epsilon_X)$	[Fe/H]	Error	N	$\log_{10}(\epsilon_X)$	[Fe/H]	Error	
NLTT 33282	NLTT 33283	...	...	...	...	...	...	...	...	
PM I13133-4153N	PM I13133-4153S	13	6.21	−1.31	0.16	...	...	...	...	[a]
PM I13167+0810E	PM I13167+0810W	27	6.87	−0.65	0.08	4	6.85	−0.67	0.09	[a]
PM I13372-4244E	PM I13372-4244W	...	...	...	...	...	...	...	...	
PM I14055+0244S	PM I14055+0244N	12	6.95	−0.57	0.17	...	...	...	...	
PM I14124+0517S	PM I14124+0517N	20	6.61	−0.91	0.10	3	6.63	−0.89	0.09	
PM I14136-3634E	PM I14136-3634W	12	6.33	−1.19	0.11	...	...	...	...	[a]
PM I14475+1134	PM I14476+1134	27	6.73	−0.79	0.10	4	6.74	−0.78	0.12	
PM I15413+1349N	PM I15413+1349S	5	6.54	−0.98	0.11	...	...	...	...	[a]
PM I16008+0146E	PM I16008+0146W	26	6.68	−0.84	0.08	2	6.7	−0.82	0.13	[a]
PM I16519-4806N	PM I16519-4806S	7	5.58	−1.94	0.10	...	...	...	...	[a]
PM I17135+1909	PM I17134+1910	32	7.16	−0.36	0.11	4	7.2	−0.32	0.23	[a]
PM I19207+0506S	PM I19207+0506N	19	6.52	−1.00	0.09	5	6.53	−0.99	0.05	[a]
PM I19420+2014S	PM I19420+2014N	...	...	...	...	...	...	...	...	
PM I20072-3519E	PM I20072-3519W	...	...	...	...	...	...	...	...	[a]
PM I20343+1151	PM I20343+1152	26	7.03	−0.49	0.11	3	6.98	−0.54	0.16	[a]
NLTT 49474	NLTT 49477	17	6.81	−0.71	0.09	4	6.75	−0.77	0.09	[a]
PM I20487+1406	PM I20487+1407	36	7.53	0.01	0.14	5	7.51	−0.01	0.14	
PM I21175-4142E	PM I21175-4142W	21	6.55	−0.97	0.10	4	6.43	−1.09	0.06	
PM I21442+0102N	PM I21442+0102S	16	6.62	−0.90	0.07	...	...	...	...	[a]
PM I21536+0010S	PM I21536+0010N	...	...	...	...	...	...	...	...	[a]
NLTT 52532	NLTT 52538	10	5.99	−1.53	0.09	...	...	...	...	[a]
PM I22296+0620	PM I22297+0620W	...	...	...	...	...	...	...	...	
PM I22487-5613W	PM I22487-5613E	39	7.29	−0.23	0.09	6	7.28	−0.24	0.15	[a]
PM I23033-5311	PM I23034-5311	18	6.71	−0.81	0.09	5	6.68	−0.84	0.06	[a]
NLTT 57827	NLTT 57823	11	5.93	−1.59	0.11	...	...	...	...	[a]

[a] This star is the primary in a binary pair confirmed using radial velocity (see Chapter 2).

Table 3.4: F/G/K Star Measured Element Abundances - Ca I and Ti I

Primary Name	Ca I					Ti I					Notes
	N	$\log_{10}(\epsilon_X)$	[Ca/H]	[Ca/Fe]	Error	N	$\log_{10}(\epsilon_X)$	[Ti/H]	[Ti/Fe]	Error	
PM I00025-4644	5	6.02	−0.32	+0.51	0.22	7	4.67	−0.28	+0.55	0.26	[a]
PM I00329+1805	2	6.02	−0.32	+0.48	0.15	2	4.79	−0.16	+0.64	0.14	[a]
PM I00422+0731E	4	5.84	−0.50	+0.40	0.12	7	4.59	−0.36	+0.54	0.13	[a]
PM I00592+0705N	...	...	...	...	...	...	...	...	...	...	
NLTT 3847	...	...	...	...	...	...	...	...	...	...	[a]
PM I01227+1409	3	5.72	−0.62	+0.26	0.08	3	4.32	−0.63	+0.25	0.11	[a]
PM I01266-4842W	2	6.04	−0.30	+0.26	0.14	5	4.76	−0.19	+0.37	0.14	
NLTT 4817	3	5.07	−1.27	+0.31	0.18	2	3.57	−1.38	+0.20	0.28	[a]
PM I01352+0538N	5	5.91	−0.43	+0.24	0.11	6	4.59	−0.36	+0.31	0.14	[a]
PM I01430-4959W	4	5.42	−0.92	+0.26	0.17	5	4.08	−0.87	+0.31	0.24	
PM I02012+0218	3	5.16	−1.18	+0.56	0.18	4	3.95	−1.00	+0.74	0.30	
PM I02225+1531S	3	5.38	−0.96	+0.44	0.14	4	3.90	−1.05	+0.35	0.13	[a]
PM I02267-4214	...	...	...	...	...	...	...	...	...	...	
NLTT 8753	...	...	...	...	...	...	...	...	...	...	[a]
PM I02548+2057W	4	5.34	−1.00	+0.52	0.18	5	3.99	−0.96	+0.56	0.24	
PM I02569-5831N	2	6.03	−0.31	+0.36	0.17	5	4.78	−0.17	+0.50	0.18	[a]
PM I03150+0102	3	5.68	−0.66	+0.27	0.11	5	4.33	−0.62	+0.31	0.12	[a]
PM I03256-3333E	3	5.91	−0.43	+0.30	0.14	5	4.65	−0.30	+0.43	0.16	[a]
NLTT 12296	3	5.64	−0.70	+0.37	0.16	5	4.33	−0.62	+0.45	0.16	[a]
PM I04072+1526N	4	6.12	−0.22	+0.09	0.08	4	4.81	−0.14	+0.17	0.13	[a]
PM I04099+0942E	3	5.15	−1.19	+0.19	0.09	2	3.90	−1.05	+0.33	0.18	[a]
PM I04254-4601	3	5.51	−0.83	+0.49	0.10	4	4.15	−0.80	+0.52	0.14	
PM I04325-5657N	3	5.84	−0.50	+0.44	0.08	3	4.42	−0.53	+0.41	0.15	[a]
PM I04327+0820	3	5.50	−0.84	+0.45	0.12	4	4.17	−0.78	+0.51	0.13	
PM I04332+0013	...	...	...	...	...	...	...	...	...	...	
PM I04477-3044W	...	...	...	...	...	...	...	...	...	...	
NLTT 14407	4	5.70	−0.64	+0.43	0.16	5	4.37	−0.58	+0.49	0.24	

[a] This star is the primary in a binary pair confirmed using radial velocity (see Chapter 2).

Table 3.4: F/G/K Star Measured Element Abundances - Ca I and Ti I *(continued)*

Primary Name	Ca I					Ti I					Notes
	N	$\log_{10}(\epsilon_X)$	[Ca/H]	[Ca/Fe]	Error	N	$\log_{10}(\epsilon_X)$	[Ti/H]	[Ti/Fe]	Error	
PM I05137+0647W	...	...	...	...	...	...	...	...	...	...	
PM I05195+0903E	...	...	...	...	...	...	...	...	...	...	
PM I05484-3617Nn	4	5.64	−0.70	+0.36	0.11	6	4.22	−0.73	+0.33	0.14	[a]
PM I06032+1921N	5	5.62	−0.72	+0.33	0.09	5	4.16	−0.79	+0.26	0.12	
PM I06050+0723S	2	5.29	−1.05	+0.33	0.15	4	3.92	−1.03	+0.35	0.21	[a]
PM I06394-3030E	...	...	...	...	...	...	...	...	...	...	
PM I06436+0851	...	...	...	...	...	...	...	...	...	...	
PM I08152-6337	3	6.18	−0.16	+0.17	0.18	5	4.83	−0.12	+0.21	0.25	[a]
PM I08239-7549W	4	6.23	−0.11	+0.11	0.11	6	4.76	−0.19	+0.03	0.16	[a]
PM I08386-3856	3	6.07	−0.27	+0.18	0.14	6	4.72	−0.23	+0.22	0.17	
PM I09502+0509E	4	5.79	−0.55	+0.28	0.11	6	4.37	−0.58	+0.25	0.16	[a]
PM I10105+1203W	4	5.89	−0.45	+0.39	0.09	6	4.43	−0.52	+0.32	0.14	[a]
PM I10520+1521N	...	...	...	...	...	...	...	...	...	...	[a]
PM I11110-4414	...	...	...	...	...	...	...	...	...	...	
PM I11125-3512	3	6.14	−0.20	+0.48	0.20	4	4.72	−0.23	+0.45	0.25	[a]
NLTT 27188	2	5.28	−1.06	+0.31	0.10	1	4.06	−0.89	+0.48	0.24	[a]
PM I11263+2047Ee	2	5.68	−0.66	+0.19	0.13	4	4.46	−0.49	+0.36	0.11	[a]
PM I11330+1318N	4	6.14	−0.20	+0.06	0.09	4	4.73	−0.22	+0.04	0.13	[a]
PM I11392-4118N	2	5.84	−0.50	+0.05	0.17	5	4.20	−0.75	−0.20	0.14	[a]
PM I11584-4155E	5	6.04	−0.30	+0.40	0.11	6	4.68	−0.27	+0.43	0.14	
PM I12170+0742E	2	5.37	−0.97	+0.29	0.21	1	3.74	−1.21	+0.05	0.32	
PM I12237+0625	3	5.84	−0.50	+0.43	0.12	5	4.51	−0.44	+0.49	0.17	[a]
PM I12277+1334	...	...	...	...	...	...	...	...	...	...	
PM I12283+1222S	...	...	...	...	...	...	...	...	...	...	
PM I12440+0625E	...	...	...	...	...	...	...	...	...	...	
PM I12508+0757	3	5.75	−0.59	+0.20	0.06	4	4.41	−0.54	+0.25	0.10	[a]
PM I13116+1106	...	...	...	...	...	...	...	...	...	...	

[a] This star is the primary in a binary pair confirmed using radial velocity (see Chapter 2).

Table 3.4: F/G/K Star Measured Element Abundances - Ca I and Ti I *(continued)*

Primary Name	Ca I					Ti I					Notes
	N	$\log_{10}(\epsilon_X)$	[Ca/H]	[Ca/Fe]	Error	N	$\log_{10}(\epsilon_X)$	[Ti/H]	[Ti/Fe]	Error	
NLTT 33282	...	...	...	...	...	...	...	...	...	...	
PM I13133-4153N	3	5.50	−0.84	+0.47	0.14	6	4.18	−0.77	+0.54	0.18	[a]
PM I13167+0810E	4	5.84	−0.50	+0.15	0.10	5	4.50	−0.45	+0.20	0.15	[a]
PM I13372-4244E	...	...	...	...	...	...	...	...	...	...	
PM I14055+0244S	2	6.20	−0.14	+0.43	0.22	5	4.87	−0.08	+0.49	0.28	
PM I14124+0517S	5	5.73	−0.61	+0.30	0.09	4	4.24	−0.71	+0.20	0.13	
PM I14136-3634E	3	5.56	−0.78	+0.41	0.18	4	4.39	−0.56	+0.63	0.29	[a]
PM I14475+1134	4	5.97	−0.37	+0.42	0.10	6	4.56	−0.39	+0.40	0.15	
PM I15413+1349N	2	5.50	−0.84	+0.14	0.21	2	4.15	−0.80	+0.18	0.27	[a]
PM I16008+0146E	5	5.76	−0.58	+0.26	0.14	7	4.45	−0.50	+0.34	0.19	[a]
PM I16519-4806N	1	4.50	−1.84	+0.10	0.26	1	3.36	−1.59	+0.35	0.39	[a]
PM I17135+1909	5	6.30	−0.04	+0.32	0.13	7	4.92	−0.03	+0.33	0.16	[a]
PM I19207+0506S	3	5.59	−0.75	+0.25	0.07	3	4.26	−0.69	+0.31	0.11	[a]
PM I19420+2014S	...	...	...	...	...	...	...	...	...	...	
PM I20072-3519E	...	...	...	...	...	...	...	...	...	...	[a]
PM I20343+1151	4	5.99	−0.35	+0.14	0.15	5	4.78	−0.17	+0.32	0.23	[a]
NLTT 49474	3	5.84	−0.50	+0.21	0.09	3	4.51	−0.44	+0.27	0.11	[a]
PM I20487+1406	4	6.22	−0.12	−0.13	0.13	6	4.90	−0.05	−0.06	0.20	
PM I21175-4142E	2	5.55	−0.79	+0.18	0.12	2	4.28	−0.67	+0.30	0.18	
PM I21442+0102N	3	5.86	−0.48	+0.42	0.17	5	4.54	−0.41	+0.49	0.25	[a]
PM I21536+0010S	...	...	...	...	...	...	...	...	...	...	[a]
NLTT 52532	2	5.25	−1.09	+0.44	0.18	3	3.88	−1.07	+0.46	0.25	[a]
PM I22296+0620	...	...	...	...	...	...	...	...	...	...	
PM I22487-5613W	5	6.32	−0.02	+0.21	0.14	6	4.81	−0.14	+0.09	0.18	[a]
PM I23033-5311	3	5.61	−0.73	+0.08	0.08	4	4.28	−0.67	+0.14	0.10	[a]
NLTT 57827	3	5.11	−1.23	+0.36	0.16	3	4.03	−0.92	+0.67	0.22	[a]

[a] This star is the primary in a binary pair confirmed using radial velocity (see Chapter 2).

Table 3.5: F/G/K Star Element Abundances Error Analysis - Fe I and Fe II

Primary Name	Fe I						Fe II						Notes
			$\Delta\log_{10}(\epsilon_X)$						$\Delta\log_{10}(\epsilon_X)$				
	N	σ	$\Delta T_{\rm eff}$	Δ log(g)	$\Delta v_{\rm micro}$	Total[b]	N	σ	$\Delta T_{\rm eff}$	Δ log(g)	$\Delta v_{\rm micro}$	Total[b]	
PM I00025-4644	27	0.17	+0.05	+0.01	−0.06	0.09	···	···	···	···	···	···	[a]
PM I00329+1805	21	0.24	+0.02	+0.01	−0.05	0.08	···	···	···	···	···	···	[a]
PM I00422+0731E	28	0.11	+0.11	+0.03	−0.01	0.12	6	0.17	+0.05	+0.14	+0.09	0.19	[a]
PM I00592+0705N	···	···	···	···	···	···	···	···	···	···	···	···	
NLTT 3847	···	···	···	···	···	···	···	···	···	···	···	···	[a]
PM I01227+1409	21	0.06	+0.09	+0.01	−0.02	0.09	6	0.04	−0.06	+0.04	−0.09	0.12	[a]
PM I01266-4842W	22	0.22	−0.01	+0.02	−0.07	0.09	···	···	···	···	···	···	
NLTT 4817	11	0.25	+0.12	−0.21	−0.01	0.25	4	0.04	−0.01	+0.09	−0.01	0.09	[a]
PM I01352+0538N	32	0.11	+0.08	+0.01	−0.04	0.09	6	0.08	−0.05	+0.06	−0.02	0.09	[a]
PM I01430-4959W	17	0.17	+0.11	+0.01	−0.05	0.13	2	0.15	−0.13	+0.06	−0.03	0.18	
PM I02012+0218	7	0.25	+0.09	+0.03	−0.02	0.14	···	···	···	···	···	···	
PM I02225+1531S	20	0.12	+0.09	+0.01	−0.02	0.10	4	0.17	−0.04	+0.05	−0.01	0.11	[a]
PM I02267-4214	···	···	···	···	···	···	···	···	···	···	···	···	
NLTT 8753	···	···	···	···	···	···	···	···	···	···	···	···	[a]
PM I02548+2057W	18	0.12	+0.09	+0.03	−0.04	0.11	1	0.20	−0.11	+0.11	−0.01	0.25	
PM I02569-5831N	19	0.15	+0.02	+0.01	−0.06	0.07	···	···	···	···	···	···	[a]
PM I03150+0102	21	0.15	+0.07	+0.01	−0.04	0.09	4	0.05	−0.06	+0.06	−0.03	0.09	[a]
PM I03256-3333E	19	0.18	+0.01	+0.01	−0.05	0.07	···	···	···	···	···	···	[a]
NLTT 12296	16	0.10	+0.03	+0.01	−0.05	0.06	···	···	···	···	···	···	[a]
PM I04072+1526N	27	0.09	+0.07	−0.01	−0.07	0.10	6	0.08	−0.05	+0.04	−0.05	0.09	[a]
PM I04099+0942E	12	0.10	+0.08	+0.01	−0.03	0.09	···	···	···	···	···	···	[a]
PM I04254-4601	21	0.13	+0.08	+0.01	−0.03	0.09	2	0.05	−0.06	+0.05	−0.01	0.09	
PM I04325-5657N	14	0.09	+0.08	+0.01	−0.04	0.09	2	0.03	−0.06	+0.04	−0.03	0.08	[a]
PM I04327+0820	17	0.12	+0.09	+0.01	−0.01	0.10	4	0.10	−0.03	+0.04	−0.02	0.07	
PM I04332+0013	···	···	···	···	···	···	···	···	···	···	···	···	

[a] This star is the primary in a binary pair confirmed using radial velocity (see Chapter 2).

[b] This is the combined quadrature error of the statistical ($\sigma/\sqrt{N}$) and the systematic shift from $\Delta T_{\rm eff}$, Δ log(g), and $\Delta v_{\rm micro}$.

Table 3.5: F/G/K Star Element Abundances Error Analysis - Fe I and Fe II *(continued)*

Primary Name	Fe I						Fe II						Notes
			$\Delta\log_{10}(\epsilon_X)$						$\Delta\log_{10}(\epsilon_X)$				
	N	σ	$\Delta T_{\rm eff}$	Δ log(g)	$\Delta v_{\rm micro}$	Total[b]	N	σ	$\Delta T_{\rm eff}$	Δ log(g)	$\Delta v_{\rm micro}$	Total[b]	
PM I04477-3044W	···	···	···	···	···	···	···	···	···	···	···	···	
NLTT 14407	16	0.06	+0.03	+0.01	−0.06	0.07	···	···	···	···	···	···	
PM I05137+0647W	···	···	···	···	···	···	···	···	···	···	···	···	
PM I05195+0903E	···	···	···	···	···	···	···	···	···	···	···	···	
PM I05484-3617Nn	23	0.13	+0.07	+0.01	−0.05	0.09	3	0.09	−0.06	+0.06	−0.01	0.10	[a]
PM I06032+1921N	21	0.11	+0.09	+0.01	−0.03	0.10	6	0.13	−0.02	+0.05	−0.02	0.08	
PM I06050+0723S	11	0.16	−0.01	+0.03	−0.04	0.07	···	···	···	···	···	···	[a]
PM I06394-3030E	···	···	···	···	···	···	···	···	···	···	···	···	
PM I06436+0851	···	···	···	···	···	···	···	···	···	···	···	···	
PM I08152-6337	16	0.13	+0.02	+0.01	−0.09	0.10	1	0.20	−0.22	+0.10	−0.04	0.32	[a]
PM I08239-7549W	40	0.08	+0.06	+0.01	−0.07	0.09	5	0.07	−0.09	+0.06	−0.05	0.12	[a]
PM I08386-3856	36	0.09	+0.04	+0.01	−0.06	0.07	4	0.11	−0.10	+0.06	−0.03	0.13	
PM I09502+0509E	26	0.09	+0.06	+0.01	−0.05	0.08	2	0.08	−0.08	+0.05	−0.03	0.11	[a]
PM I10105+1203W	24	0.12	+0.08	+0.01	−0.05	0.10	3	0.11	−0.06	+0.08	−0.03	0.12	[a]
PM I10520+1521N	···	···	···	···	···	···	···	···	···	···	···	···	[a]
PM I11110-4414	···	···	···	···	···	···	···	···	···	···	···	···	
PM I11125-3512	19	0.16	+0.07	+0.01	−0.07	0.11	···	···	···	···	···	···	[a]
NLTT 27188	6	0.13	+0.13	+0.01	−0.01	0.14	3	0.02	−0.01	+0.07	−0.02	0.07	[a]
PM I11263+2047Ee	14	0.09	−0.02	+0.02	−0.04	0.05	···	···	···	···	···	···	[a]
PM I11330+1318N	26	0.05	+0.07	−0.01	−0.06	0.09	6	0.09	−0.05	+0.03	+0.04	0.08	[a]
PM I11392-4118N	17	0.24	−0.04	+0.02	−0.06	0.09	···	···	···	···	···	···	[a]
PM I11584-4155E	26	0.08	+0.07	+0.01	−0.05	0.09	4	0.05	−0.07	+0.05	−0.03	0.09	
PM I12170+0742E	7	0.15	+0.16	+0.01	−0.06	0.18	···	···	···	···	···	···	
PM I12237+0625	19	0.14	+0.04	+0.01	−0.05	0.07	···	···	···	···	···	···	[a]
PM I12277+1334	···	···	···	···	···	···	···	···	···	···	···	···	

[a] This star is the primary in a binary pair confirmed using radial velocity (see Chapter 2).

[b] This is the combined quadrature error of the statistical ($\sigma/\sqrt{N}$) and the systematic shift from $\Delta T_{\rm eff}$, Δ log(g), and $\Delta v_{\rm micro}$.

Table 3.5: F/G/K Star Element Abundances Error Analysis - Fe I and Fe II *(continued)*

Primary Name	Fe I						Fe II						Notes
			$\Delta\log_{10}(\epsilon_X)$						$\Delta\log_{10}(\epsilon_X)$				
	N	σ	$\Delta T_{\rm eff}$	Δ log(g)	$\Delta v_{\rm micro}$	Total[b]	N	σ	$\Delta T_{\rm eff}$	Δ log(g)	$\Delta v_{\rm micro}$	Total[b]	
PM I12283+1222S	···	···	···	···	···	···	···	···	···	···	···	···	
PM I12440+0625E	···	···	···	···	···	···	···	···	···	···	···	···	
PM I12508+0757	21	0.10	+0.07	+0.01	−0.02	0.08	5	0.06	−0.02	+0.04	−0.02	0.06	[a]
PM I13116+1106	···	···	···	···	···	···	···	···	···	···	···	···	
NLTT 33282	···	···	···	···	···	···	···	···	···	···	···	···	
PM I13133-4153N	13	0.16	+0.12	+0.09	+0.03	0.16	···	···	···	···	···	···	[a]
PM I13167+0810E	27	0.10	+0.07	+0.01	−0.04	0.08	4	0.08	−0.07	+0.04	−0.02	0.09	[a]
PM I13372-4244E	···	···	···	···	···	···	···	···	···	···	···	···	
PM I14055+0244S	12	0.27	+0.06	+0.01	−0.14	0.17	···	···	···	···	···	···	
PM I14124+0517S	20	0.11	+0.08	+0.01	−0.05	0.10	3	0.08	−0.06	+0.04	−0.03	0.09	
PM I14136-3634E	12	0.11	+0.08	+0.01	−0.07	0.11	···	···	···	···	···	···	[a]
PM I14475+1134	27	0.15	+0.07	+0.01	−0.06	0.10	4	0.18	−0.06	+0.03	−0.04	0.12	
PM I15413+1349N	5	0.13	−0.05	+0.02	−0.08	0.11	···	···	···	···	···	···	[a]
PM I16008+0146E	26	0.15	+0.04	+0.01	−0.06	0.08	2	0.03	−0.12	+0.03	−0.03	0.13	[a]
PM I16519-4806N	7	0.24	+0.03	+0.02	−0.03	0.10	···	···	···	···	···	···	[a]
PM I17135+1909	32	0.15	+0.07	+0.01	−0.08	0.11	4	0.38	−0.06	+0.09	−0.06	0.23	[a]
PM I19207+0506S	19	0.08	+0.08	+0.01	−0.02	0.09	5	0.03	−0.01	+0.03	−0.03	0.05	[a]
PM I19420+2014S	···	···	···	···	···	···	···	···	···	···	···	···	
PM I20072-3519E	···	···	···	···	···	···	···	···	···	···	···	···	[a]
PM I20343+1151	26	0.13	+0.09	+0.01	−0.06	0.11	3	0.15	−0.12	+0.04	−0.04	0.16	[a]
NLTT 49474	17	0.10	+0.08	+0.01	−0.02	0.09	4	0.15	−0.02	+0.04	−0.02	0.09	[a]
PM I20487+1406	36	0.11	+0.06	+0.01	−0.12	0.14	5	0.06	−0.09	+0.06	−0.08	0.14	
PM I21175-4142E	21	0.16	+0.08	+0.01	−0.04	0.10	4	0.06	−0.02	+0.04	−0.02	0.06	
PM I21442+0102N	16	0.13	+0.04	+0.01	−0.05	0.07	···	···	···	···	···	···	[a]
PM I21536+0010S	···	···	···	···	···	···	···	···	···	···	···	···	[a]

[a] This star is the primary in a binary pair confirmed using radial velocity (see Chapter 2).

[b] This is the combined quadrature error of the statistical ($\sigma/\sqrt{N}$) and the systematic shift from $\Delta T_{\rm eff}$, Δ log(g), and $\Delta v_{\rm micro}$.

Table 3.5: F/G/K Star Element Abundances Error Analysis - Fe I and Fe II *(continued)*

Primary Name	Fe I						Fe II						Notes
	$\Delta\log_{10}(\epsilon_X)$						$\Delta\log_{10}(\epsilon_X)$						
	N	σ	$\Delta T_{\rm eff}$	Δ log(g)	Δv$_{\rm micro}$	Total[b]	N	σ	$\Delta T_{\rm eff}$	Δ log(g)	Δv$_{\rm micro}$	Total[b]	
NLTT 52532	10	0.23	-0.01	$+0.02$	-0.05	0.09	...	...	...	...	...	...	[a]
PM I22296+0620	...	...	...	...	...	...	...	...	...	...	...	...	
PM I22487-5613W	39	0.10	$+0.04$	$+0.01$	-0.08	0.09	6	0.20	-0.11	$+0.03$	-0.04	0.15	[a]
PM I23033-5311	18	0.11	$+0.08$	$+0.01$	-0.02	0.09	5	0.09	$+0.00$	$+0.04$	-0.03	0.06	[a]
NLTT 57827	11	0.16	$+0.09$	$+0.02$	-0.04	0.11	...	...	...	...	...	...	[a]

[a] This star is the primary in a binary pair confirmed using radial velocity (see Chapter 2).

[b] This is the combined quadrature error of the statistical ($\sigma/\sqrt{N}$) and the systematic shift from $\Delta T_{\rm eff}$, Δ log(g), and Δv$_{\rm micro}$.

Table 3.6: F/G/K Star Element Abundances Error Analysis - Ca I and Ti I

Primary Name	Ca I						Ti I						Notes
			$\Delta\log_{10}(\epsilon_X)$						$\Delta\log_{10}(\epsilon_X)$				
	N	σ	$\Delta T_{\rm eff}$	Δ log(g)	$\Delta v_{\rm micro}$	Total[b]	N	σ	$\Delta T_{\rm eff}$	Δ log(g)	$\Delta v_{\rm micro}$	Total[b]	
PM I00025-4644	5	0.25	+0.18	−0.01	−0.05	0.22	7	0.23	+0.23	−0.01	−0.09	0.26	[a]
PM I00329+1805	2	0.15	+0.10	−0.03	−0.03	0.15	2	0.02	+0.13	−0.01	−0.06	0.14	[a]
PM I00422+0731E	4	0.10	+0.11	+0.01	−0.01	0.12	7	0.09	+0.12	−0.01	−0.04	0.13	[a]
PM I00592+0705N	...	...	...	...	...	...	...	...	...	...	...	...	
NLTT 3847	...	...	...	...	...	...	...	...	...	...	...	...	[a]
PM I01227+1409	3	0.06	+0.07	−0.01	−0.02	0.08	3	0.03	+0.11	+0.02	−0.01	0.11	[a]
PM I01266-4842W	2	0.15	+0.07	−0.03	−0.04	0.14	5	0.09	+0.11	−0.02	−0.07	0.14	
NLTT 4817	3	0.10	+0.08	−0.15	−0.01	0.18	2	0.08	+0.13	−0.24	−0.01	0.28	[a]
PM I01352+0538N	5	0.10	+0.09	−0.03	−0.03	0.11	6	0.04	+0.13	−0.02	−0.04	0.14	[a]
PM I01430-4959W	4	0.11	+0.15	−0.03	−0.03	0.17	5	0.22	+0.21	−0.02	−0.04	0.24	
PM I02012+0218	3	0.12	+0.17	−0.01	−0.02	0.18	4	0.16	+0.28	−0.01	−0.05	0.30	
PM I02225+1531S	3	0.20	+0.08	−0.01	−0.01	0.14	4	0.12	+0.11	−0.01	−0.02	0.13	[a]
PM I02267-4214	...	...	...	...	...	...	...	...	...	...	...	...	
NLTT 8753	...	...	...	...	...	...	...	...	...	...	...	...	[a]
PM I02548+2057W	4	0.17	+0.16	−0.02	−0.03	0.18	5	0.09	+0.22	−0.02	−0.07	0.24	
PM I02569-5831N	2	0.17	+0.11	−0.04	−0.04	0.17	5	0.17	+0.15	−0.03	−0.07	0.18	[a]
PM I03150+0102	3	0.14	+0.07	−0.02	−0.03	0.11	5	0.07	+0.11	−0.01	−0.03	0.12	[a]
PM I03256-3333E	3	0.13	+0.11	−0.02	−0.02	0.14	5	0.03	+0.15	−0.02	−0.05	0.16	[a]
NLTT 12296	3	0.21	+0.10	−0.03	−0.03	0.16	5	0.11	+0.14	−0.02	−0.06	0.16	[a]
PM I04072+1526N	4	0.05	+0.07	−0.02	−0.03	0.08	4	0.05	+0.11	−0.01	−0.06	0.13	[a]
PM I04099+0942E	3	0.07	+0.08	−0.01	−0.01	0.09	2	0.18	+0.12	−0.01	−0.03	0.18	[a]
PM I04254-4601	3	0.08	+0.08	−0.01	−0.02	0.10	4	0.07	+0.13	−0.01	−0.05	0.14	
PM I04325-5657N	3	0.03	+0.07	−0.02	−0.03	0.08	3	0.15	+0.11	−0.01	−0.06	0.15	[a]
PM I04327+0820	3	0.18	+0.06	−0.01	−0.02	0.12	4	0.15	+0.10	−0.01	−0.02	0.13	
PM I04332+0013	...	...	...	...	...	...	...	...	...	...	...	...	

[a] This star is the primary in a binary pair confirmed using radial velocity (see Chapter 2).

[b] This is the combined quadrature error of the statistical ($\sigma/\sqrt{N}$) and the systematic shift from $\Delta T_{\rm eff}$, Δ log(g), and $\Delta v_{\rm micro}$.

Table 3.6: F/G/K Star Element Abundances Error Analysis - Ca I and Ti I *(continued)*

Primary Name	Ca I						Ti I						Notes
	$\Delta\log_{10}(\epsilon_X)$						$\Delta\log_{10}(\epsilon_X)$						
	N	σ	$\Delta T_{\rm eff}$	Δ log(g)	$\Delta v_{\rm micro}$	Total[b]	N	σ	$\Delta T_{\rm eff}$	Δ log(g)	$\Delta v_{\rm micro}$	Total[b]	
PM I04477-3044W	...	...	...	...	...	...	...	...	...	...	...	...	
NLTT 14407	4	0.12	+0.14	−0.02	−0.04	0.16	5	0.08	+0.21	−0.02	−0.10	0.24	
PM I05137+0647W	...	...	...	...	...	...	...	...	...	...	...	...	
PM I05195+0903E	...	...	...	...	...	...	...	...	...	...	...	...	
PM I05484-3617Nn	4	0.10	+0.09	−0.02	−0.02	0.11	6	0.07	+0.13	−0.01	−0.05	0.14	[a]
PM I06032+1921N	5	0.11	+0.08	−0.01	−0.01	0.09	5	0.09	+0.11	−0.01	−0.02	0.12	
PM I06050+0723S	2	0.07	+0.14	−0.01	−0.04	0.15	4	0.19	+0.17	−0.01	−0.09	0.21	[a]
PM I06394-3030E	...	...	...	...	...	...	...	...	...	...	...	...	
PM I06436+0851	...	...	...	...	...	...	...	...	...	...	...	...	
PM I08152-6337	3	0.12	+0.15	−0.05	−0.06	0.18	5	0.04	+0.22	−0.03	−0.12	0.25	[a]
PM I08239-7549W	4	0.10	+0.08	−0.03	−0.05	0.11	6	0.14	+0.12	−0.01	−0.09	0.16	[a]
PM I08386-3856	3	0.13	+0.10	−0.04	−0.04	0.14	6	0.09	+0.14	−0.02	−0.08	0.17	
PM I09502+0509E	4	0.10	+0.09	−0.02	−0.03	0.11	6	0.15	+0.13	−0.01	−0.06	0.16	[a]
PM I10105+1203W	4	0.05	+0.07	−0.03	−0.04	0.09	6	0.11	+0.12	−0.01	−0.05	0.14	[a]
PM I10520+1521N	...	...	...	...	...	...	...	...	...	...	...	...	[a]
PM I11110-4414	...	...	...	...	...	...	...	...	...	...	...	...	
PM I11125-3512	3	0.21	+0.15	−0.04	−0.05	0.20	4	0.15	+0.21	−0.02	−0.10	0.25	[a]
NLTT 27188	2	0.02	+0.10	−0.01	−0.01	0.10	1	0.20	+0.14	−0.01	−0.01	0.24	[a]
PM I11263+2047Ee	2	0.14	+0.08	−0.02	−0.02	0.13	4	0.02	+0.10	−0.01	−0.05	0.11	[a]
PM I11330+1318N	4	0.09	+0.06	−0.01	−0.04	0.09	4	0.07	+0.10	−0.01	−0.07	0.13	[a]
PM I11392-4118N	2	0.22	+0.06	−0.02	−0.04	0.17	5	0.23	+0.07	+0.01	−0.07	0.14	[a]
PM I11584-4155E	5	0.10	+0.09	−0.02	−0.04	0.11	6	0.06	+0.12	−0.01	−0.07	0.14	
PM I12170+0742E	2	0.13	+0.18	−0.01	−0.04	0.21	1	0.20	+0.24	−0.01	−0.04	0.32	
PM I12237+0625	3	0.08	+0.10	−0.04	−0.04	0.12	5	0.13	+0.14	−0.02	−0.08	0.17	[a]
PM I12277+1334	...	...	...	...	...	...	...	...	...	...	...	...	

[a] This star is the primary in a binary pair confirmed using radial velocity (see Chapter 2).

[b] This is the combined quadrature error of the statistical ($\sigma/\sqrt{N}$) and the systematic shift from $\Delta T_{\rm eff}$, Δ log(g), and $\Delta v_{\rm micro}$.

Table 3.6: F/G/K Star Element Abundances Error Analysis - Ca I and Ti I *(continued)*

Primary Name	Ca I						Ti I						Notes
	$\Delta\log_{10}(\epsilon_X)$						$\Delta\log_{10}(\epsilon_X)$						
	N	σ	$\Delta T_{\rm eff}$	Δ log(g)	$\Delta v_{\rm micro}$	Total[b]	N	σ	$\Delta T_{\rm eff}$	Δ log(g)	$\Delta v_{\rm micro}$	Total[b]	
PM I12283+1222S	...	...	...	...	...	...	...	...	...	...	...	...	
PM I12440+0625E	...	...	...	...	...	...	...	...	...	...	...	...	
PM I12508+0757	3	0.03	+0.05	−0.01	−0.02	0.06	4	0.07	+0.09	−0.01	−0.01	0.10	[a]
PM I13116+1106	...	...	...	...	...	...	...	...	...	...	...	...	
NLTT 33282	...	...	...	...	...	...	...	...	...	...	...	...	
PM I13133-4153N	3	0.06	+0.13	+0.01	−0.01	0.14	6	0.13	+0.17	+0.01	−0.03	0.18	[a]
PM I13167+0810E	4	0.04	+0.09	−0.02	−0.02	0.10	5	0.08	+0.14	−0.01	−0.05	0.15	[a]
PM I13372-4244E	...	...	...	...	...	...	...	...	...	...	...	...	
PM I14055+0244S	2	0.16	+0.16	−0.04	−0.08	0.22	5	0.24	+0.22	−0.02	−0.13	0.28	
PM I14124+0517S	5	0.10	+0.08	−0.01	−0.02	0.09	4	0.11	+0.11	−0.01	−0.04	0.13	
PM I14136-3634E	3	0.15	+0.14	−0.03	−0.06	0.18	4	0.24	+0.23	−0.02	−0.12	0.29	[a]
PM I14475+1134	4	0.10	+0.07	−0.02	−0.05	0.10	6	0.05	+0.12	−0.01	−0.08	0.15	
PM I15413+1349N	2	0.11	+0.18	−0.02	−0.06	0.21	2	0.07	+0.22	−0.01	−0.15	0.27	[a]
PM I16008+0146E	5	0.15	+0.11	−0.03	−0.05	0.14	7	0.21	+0.15	−0.02	−0.09	0.19	[a]
PM I16519-4806N	1	0.20	+0.16	−0.01	−0.02	0.26	1	0.20	+0.33	−0.01	−0.07	0.39	[a]
PM I17135+1909	5	0.15	+0.09	−0.04	−0.06	0.13	7	0.09	+0.13	−0.02	−0.09	0.16	[a]
PM I19207+0506S	3	0.03	+0.06	−0.01	−0.02	0.07	3	0.12	+0.08	−0.01	−0.02	0.11	[a]
PM I19420+2014S	...	...	...	...	...	...	...	...	...	...	...	...	
PM I20072-3519E	...	...	...	...	...	...	...	...	...	...	...	...	[a]
PM I20343+1151	4	0.07	+0.14	−0.03	−0.03	0.15	5	0.04	+0.21	−0.02	−0.09	0.23	[a]
NLTT 49474	3	0.11	+0.06	−0.01	−0.01	0.09	3	0.10	+0.09	−0.01	−0.02	0.11	[a]
PM I20487+1406	4	0.02	+0.09	−0.02	−0.09	0.13	6	0.12	+0.13	−0.01	−0.14	0.20	
PM I21175-4142E	2	0.14	+0.07	−0.01	−0.01	0.12	2	0.20	+0.11	−0.01	−0.04	0.18	
PM I21442+0102N	3	0.11	+0.15	−0.03	−0.02	0.17	5	0.22	+0.22	−0.02	−0.05	0.25	[a]
PM I21536+0010S	...	...	...	...	...	...	...	...	...	...	...	...	[a]

[a] This star is the primary in a binary pair confirmed using radial velocity (see Chapter 2).

[b] This is the combined quadrature error of the statistical ($\sigma/\sqrt{N}$) and the systematic shift from $\Delta T_{\rm eff}$, Δ log(g), and $\Delta v_{\rm micro}$.

Table 3.6: F/G/K Star Element Abundances Error Analysis - Ca I and Ti I *(continued)*

Primary Name	Ca I						Ti I						Notes
	$\Delta\log_{10}(\epsilon_X)$						$\Delta\log_{10}(\epsilon_X)$						
	N	σ	$\Delta T_{\rm eff}$	Δ log(g)	$\Delta v_{\rm micro}$	Total[b]	N	σ	$\Delta T_{\rm eff}$	Δ log(g)	$\Delta v_{\rm micro}$	Total[b]	
NLTT 52532	2	0.13	+0.14	−0.02	−0.05	0.18	3	0.08	+0.21	−0.01	−0.12	0.25	[a]
PM I22296+0620	...	...	...	...	...	...	...	...	...	...	...	...	
PM I22487-5613W	5	0.11	+0.11	−0.02	−0.07	0.14	6	0.07	+0.13	−0.02	−0.12	0.18	[a]
PM I23033-5311	3	0.09	+0.05	−0.01	−0.02	0.08	4	0.13	+0.08	−0.01	−0.01	0.10	[a]
NLTT 57827	3	0.13	+0.14	−0.01	−0.02	0.16	3	0.05	+0.21	−0.01	−0.07	0.22	[a]

[a] This star is the primary in a binary pair confirmed using radial velocity (see Chapter 2).

[b] This is the combined quadrature error of the statistical ($\sigma/\sqrt{N}$) and the systematic shift from $\Delta T_{\rm eff}$, Δ log(g), and $\Delta v_{\rm micro}$.

4. CHEMICAL ABUNDANCE ANALYSIS OF THREE α-POOR, METAL-POOR STARS IN THE ULTRA-FAINT DWARF GALAXY HOROLOGIUM I*

4.1 Introduction

The past several decades have seen marked advancement in our understanding of how a galaxy like the Milky Way is assembled as well as how chemical enrichment processes could have evolved to produce the elements that now exist in the local Universe (e.g. Belokurov, 2013; Frebel & Norris, 2015). From the early observational work of Searle & Zinn (1978) a picture emerged that galaxies like the Milky Way most likely formed, at least in part, via hierarchical merging of smaller satellites. Modern dark energy+cold dark matter (ΛCDM) N-body simulations of the Milky Way support this picture (e.g. Bullock & Johnston, 2005; Robertson et al., 2005; Johnston et al., 2008).

The past two decades have produced an abundance of new studies to compare to theory. Most of the progress in this field has been made through modern wide-field imaging surveys and subsequent spectroscopic study of the objects found in the survey images. For example, the Sloan Digital Sky Survey (SDSS) discovered many nearby "ultra-faint" dwarf galaxies in the Milky Way halo that have lower masses and higher mass-to-light ratios than previously known Milky Way satellites (see McConnachie 2012 for a summary). More recently, new wide-field imaging surveys such as Pan-STARRS and the Dark Energy Survey (DES; The Dark Energy Survey Collaboration, 2005) have discovered even more Milky Way satellite galaxies. DES has been the most prolific of these surveys to date: the first two years of DES data alone have resulted in the discovery of 22 new candidate satellites located in and around the Milky Way halo (Bechtol et al., 2015; Koposov et al., 2015a; Drlica-Wagner et al., 2015; Kim & Jerjen, 2015; Kim et al., 2015; Luque et al., 2016, 2017). Once discovered, these candidates must be confirmed through kinematics to be gravitationally-bound stellar associations via follow-up spectroscopic observations. Spectroscopic velocity measurements also yield a measure of the mass-to-light (M/L) ratio and a determination of whether a

* Reprinted with permission from "Chemical Abundance Analysis of Three α-poor, Metal-poor Stars in the Ultra-Faint Dwarf Galaxy Horologium I" by D.Q. Nagasawa et al. 2018, The Astrophysical Journal, Volume 852, Issue 2, pg 99-115, Copyright 2018 by The Astrophysical Journal.

satellite is a dark matter-dominated dwarf galaxy or a baryon-dominated stellar cluster (see Willman & Strader 2012 for a comprehensive definition). The DES-discovered candidate satellites considered most likely to be nearby ultra-faint dwarf galaxies have been selected for follow-up spectroscopy; five have subsequently been confirmed to be highly dark matter-dominated, low luminosity satellites: Reticulum II (Ret II; Simon et al., 2015a; Koposov et al., 2015b), Tucana II and Grus I (Walker et al., 2016), Tucana III (Simon et al., 2017), Eridanus II (Li et al., 2017), and Horologium I (Hor I; Koposov et al., 2015b), the last being the subject of this chapter.

Due to their relative physical and therefore presumed chemical isolation at the time their stars were formed, ultra-faint dwarf galaxies provide opportunities to study not only the dark matter that dominates their mass profile but also the nucleosynthetic processes that occurred in the early Universe. Star formation in these low-mass objects is likely to be highly influenced by only a few nucleosynthetic events (e.g. Ji et al., 2015). And since star formation in ultra-faint dwarfs appears to have been quenched early in the history of the Universe, perhaps by reionization (Brown et al., 2014; Wetzel et al., 2015; Jeon et al., 2017), a fossil record of the early star formation history of these objects is preserved today.

Prior to the work presented here, three DES-discovered ultra-faint dwarfs have been the targets of detailed chemical study: Ret II, Tuc II, and Tuc III. In each of these galaxies a unique nucleosynthetic process is observed. The majority of stars in Ret II that have been studied to date are so-called r-II stars, signifying that they show extreme enhancement in rapid neutron-capture elements (Ji et al., 2016a; Roederer et al., 2016). This nucleosynthetic signature can be explained by a single high-yield event (e.g. a binary neutron star merger or hypernova) polluting the gas cloud from which stars in the galaxy were still forming. The chemical diversity of stars in Tuc II is somewhat unlike that observed in previously studied ultra-faint dwarfs, and could be explained by a range of phenomena, not all of which follow the standard nucleosynthetic processes (Ji et al., 2016b). Hansen et al. (2017) report the discovery of a moderately r-process enhanced (r-I) star in Tuc III, a rare chemical signature when compared to the bulk of field stars in the Milky Way halo, though not as rare as r-II stars. The diverse abundance patterns observed in these galaxies, and

the range of unusual phenomena invoked to explain them, suggests that star formation in the early Universe must have been a stochastic process that was highly variable on the mass scales of ultra-faint dwarf galaxies. If this trend holds for more of the newly discovered ultra-faint dwarfs, the study of chemical abundance patterns could provide an opportunity to improve our understanding of nucleosynthetic processes in the early Universe.

4.2 Observations and Data Reduction

Observations of Horologium I were performed using the FLAMES-UVES spectrograph (Dekker et al., 2000; Pasquini et al., 2000) on the VLT in Paranal, Chile as part of program 096.D-0967(B) (PI: E. Balbinot) and the MIKE spectrograph (Bernstein et al., 2003) at the Magellan-Clay Telescope at Las Campanas Observatory (PI: R. Bernstein).

UVES observations took place on five nights over the months of December 2015 to January 2016 in fourteen 40-minute exposures. Stars were selected for UVES observation based on DES photometry, prior confirmation from Koposov et al. (2015b), and considerations related to fiber positioning due to simultaneous observations with the FLAMES-GIRAFFE spectrograph (Li et al. *in prep.*). Two stars were selected for UVES observations: DES J025540-540807, a confirmed member from previous observations using medium resolution spectra (Koposov et al., 2015b), and DES J025543-544349, determined to be a likely member of Hor I (Bechtol et al., 2015). Spectra of UVES targets were obtained in service mode. The 580 nm configuration was used, resulting in wavelength coverage of 4800 Å $< \lambda <$ 6800 Å with a $\sim$30 Å gap in coverage around 5800 Å due to the CCD chip gap. We obtain a spectral resolution of R$\sim$47,000.

Bias subtraction, flat fielding, and spectral extraction were completed using the FLAMES-UVES Data Pipeline provided by the European Southern Observatory (Modigliani et al., 2004). Pixel oversampling (5 pixels per resolution element in the output spectrum) of the UVES spectra allowed us to boxcar-smooth the extracted spectra by 3 pixels in the wavelength dimension using the IRAF task *boxcar* without sacrificing information.

MIKE observations of DES J025535-540643, a confirmed Horologium I member star (Koposov et al., 2015b), took place on 06 August 2016 in five 30 minute exposures. Using a 0.7 arcsec

slit and 2×2 pixel binning, the resulting spectrum has a resolution of R $\sim$ 22,000 ($\Delta\lambda = 0.23$ Å) with coverage from 3310 Å$< \lambda <$5000 Å for the blue chip and 4825 Å$< \lambda <$9150 Å for the red chip. Reduction of the data, including bias correction, flat fielding, spectral extraction, wavelength calibration, and stacking were completed using the MIKE pipeline (Kelson, 2003).

4.2.1 Radial Velocity Measurements

For UVES observations of Horologium I, radial velocities were measured via Fourier cross-correlation of each exposure using the IRAF task *fxcor* with a UVES spectrum of radial velocity standard HD140283 observed on a different night (29 May 2012) with the same instrument settings as our observations. We take the statistical error to be the standard deviation of the resulting velocities derived for each of the fourteen spectra, divided by the square root of the number of exposures (fourteen). A correction was applied based on the date of the observation to shift the radial velocities to the heliocentric frame. Each exposure was then shifted to rest wavelength and the fourteen spectra were mean-combined using 3-σ rejection.

We estimate the systematic error of the radial velocities as follows. All spectra for a single star obtained on a given night were median-combined and then Fourier cross-correlated with the combined spectra for the same star obtained on another night. To minimize the influence of noise, this cross-correlation was performed over the limited wavelength range of 5100 Å $< \lambda <$ 5300 Å centered on the strong Mg triplet lines. For DES J025540-540807, this night-to-night cross correlation yielded an average relative velocity of 0.51 km s^{-1} with respect to each other. For DES J025543-544349, the average relative velocity was 0.43 km s^{-1}.

The S/N per resolution element of the two UVES spectra and measured radial velocities

Table 4.1 Details of Observations of Horologium I

ID	Instrument	S/N at 5300 Å	S/N at 6300 Å	V_{helio} (km s^{-1})
DES J025540-540807	UVES	30	40	118.6 ± 0.6
DES J025543-544349	UVES	35	40	114.3 ± 0.5
DES J025535-540643	MIKE	20	20	116.9 ± 0.5

are presented in Table 4.1. The reported radial velocity error is the quadrature combination of the statistical and systematic errors. We note that the velocity of DES J025543-544349 is consistent with the other stars in Hor I, increasing the number of confirmed Hor I member stars from five to six.

For the spectrum obtained with MIKE, the radial velocity was measured by performing Fourier cross-correlation of the target star with a spectrum of radial velocity standard HD146051 (radial velocity from Massarotti et al., 2008) observed on the same night using the IRAF task *fxcor*. A correction was applied based on the date of the observation to shift the radial velocities to the heliocentric frame. Each spectral order was considered individually; the reported radial velocity is the average value of the velocity measured in each order and the reported error is the standard deviation of the radial velocities determined in each order of the spectrum. The measured S/N per resolution element and radial velocity for DES J025535-540643 are presented in Table 4.1.

4.3 Element Abundance Analysis

We measured the equivalent widths of spectral features using the *SPECTRE* program[1] (Sneden et al., 2012), with confirmation of the measurement of each line using the IRAF task *splot*. The line list was generated from the Kurucz database (Castelli & Kurucz, 2004b) with updated laboratory transition probabilities from the NIST Atomic Line Spectra database (Kramida et al., 2018). Excitation potential, oscillator strength, and original laboratory source references for each line used in this analysis are listed in Appendix A. For this analysis, it is assumed that these species are in local thermodynamic equilibrium (LTE). For CH and CN, we use dissociation energies of 3.47 eV (Masseron et al., 2014) and 7.72 eV (Sneden et al., 2014) respectively.

4.3.1 Determination of Stellar Parameters

Stellar parameters were derived spectroscopically from Fe I and Fe II lines using the *abfind* package of the 2017 version of the *MOOG* program[2] (Sneden, 1973) and the α-enhanced 1D

[1]See http://www.as.utexas.edu/∼chris/spectre.html for the most up-to-date version of SPECTRE.
[2]See http://www.as.utexas.edu/∼chris/moog.html for the most up-to-date version of MOOG.

Table 4.2 Measured Stellar Parameters

ID	$T_{\rm eff}$ (K)	log(g) (dex)	$v_{\rm micro}$ (km s^{-1})	[Fe/H] (dex)	[Ca/Fe] (dex)
DES J025540-540807	5000 ± 100	2.0 ± 0.2	0.8 ± 0.5	-2.43 ± 0.13	-0.07 ± 0.15
DES J025543-544349	4800 ± 100	1.5 ± 0.2	1.8 ± 0.5	-2.60 ± 0.16	$+0.00 \pm 0.13$
DES J025535-540643	4500 ± 100	1.4 ± 0.2	3.5 ± 0.5	-2.83 ± 0.12	-0.02 ± 0.21

plane-parallel Castelli-Kurucz model atmospheres (Castelli & Kurucz, 2004a)[3]. We note that, although the stars studied here may not in fact turn out to be α-enhanced, we choose to use the Kurucz α-enhanced models for consistency with our previous and future work. From comparison tests using DES J025540-540807, which has an [Fe/H] $= -2.43$, we further note that at the lowest metallicities, the differences between the α-enhanced and non-α-enhanced Kurucz models are minimal, generally resulting in $\sim$0.05 dex additional change in the abundances (which is much smaller than our total adopted uncertainties).

For spectra obtained using MIKE, the abundance of every spectral feature bluer than 4500Å was calculated while accounting for continuum scattering (Sobeck et al., 2011). For species in which the majority or all of lines measured were bluer than 4500Å and therefore greatly affected by continuum scattering, this changed abundances by ~ 0.1 dex. For species where most of the lines measured were redder than 4500Å, the contribution from continuum scattering does not change the abundance significantly (< 0.05 dex). Because the UVES observations for Horologium I do not cover wavelengths bluer than 4500Å, we did not have to correct for continuum scattering for those particular spectra.

Using these models, we calculate an abundance for each Fe I and Fe II line individually. We take the mean abundance of all measured lines for each species to be the measured abundance and use the standard deviation of these abundances as a statistical error. The effective temperature was determined by iterating atmospheric models until there was no observed trend in calculated Fe I abundance with excitation potential of the Fe I lines. Surface gravity was determined by iterating until there was 1-σ agreement between abundances calculated for Fe I and Fe II. In several in-

[3]See http://kurucz.harvard.edu/grids.html for the Castelli-Kurucz model atmospheres.

stances, Fe II lines were measurable, but weak, which may contribute to a systematic error regarding the determined surface gravities. Microturbulence in the stellar atmosphere was determined by iterating microturbulent velocity until there was no observed trend in the calculated abundances of Fe I with the reduced equivalent width of the Fe I lines. The same was done for Fe II as well; the derived microturbulence for Fe II was consistent with that derived for Fe I. Due to the known discrepancy between spectroscopically-derived and photometrically-derived effective temperature for metal-poor giant stars, a correction to the effective temperature was applied following Frebel et al. (2013). This empirical correction based on spectroscopically measured effective temperature increases the effective temperature by $\sim 100\text{K}-200\text{K}$. Surface gravity, microturbulence, and abundances were then recalculated using this new effective temperature. This changed the surface gravity by $\sim +0.4$ dex and microturbulence by $\sim +0.1$ km/sec. The resulting abundances using these new parameters differed by ~ 0.2 dex. We determine the uncertainty in our stellar parameters by varying the stellar model and examining the resulting trends in excitation potential and reduced equivalent width. We calculate the final [Fe/H] of our stars from Fe I due to the greater number of lines measured. Measured stellar parameters are presented in Table 4.2.

4.3.2 Equivalent Width Analysis

In both UVES and MIKE spectra, equivalent widths were measured for several species with strong, unblended absorption lines: Fe I, Fe II, Na I, Mg I, and Ca I. For Fe I in particular, lines ranging across wavelength, excitation potential (E.P.), and transition probability log(gf) were sampled in order to minimize systematic bias in abundance calculations. For Na I, we used corrections determined by Lind et al. (2011) for the Na 5895.93Å doublet to compensate for non-local thermodynamic equilibrium (NLTE) effects .

Due to the greater wavelength coverage of the MIKE spectrum, 60 Fe I lines were measurable compared to the only 12 useful Fe I in the UVES data. To ensure that the reduced number of lines in the UVES spectra would not systematically bias our measurements, the 12 Fe I lines used in the UVES analysis were measured in the MIKE spectrum and analyzed separately from the full 60-line analysis. The difference between the two analyses in both stellar parameter determination and

abundance measurement was within the uncertainties. We conclude then that the reduced number of lines in the UVES spectral analysis of Horologium I does not systematically affect the results.

4.3.3 Measurements using Synthetic Spectra

Spectral synthesis was done for elements that either did not have a large number of measurable lines due to low S/N or due to blending and for elements where hyperfine structure and/or isotopic shifts needed to be considered. Using the stellar parameters derived, we have used spectral synthesis to measure the abundances of multiple elements in all three stars, specifically Si I, Sc II, Ti I, Cr I, Mn I, Ni I, Ba II, and Eu II.

The increased wavelength coverage in the MIKE spectrum enables measurement of additional species. For these measurements, multiple spectral lines were identified based on both their excitation potential and transition probability to be relatively strong (i.e., low excitation energies, high transition probabilities). Synthetic spectra were generated using the *synth* package of the MOOG program Sneden (1973) for a 40 Å window centered on the line of interest. The abundances of Fe and Ca from equivalent width analysis were used as input in the synthesis. Spectra were generated varying the abundance of the elements of interest in [X/H] steps of 0.10–0.125 dex. A Gaussian function was utilized in the smoothing of the synthetic spectra, which was roughly what was expected based on spectrograph resolution. If available in the 40 Å window, a Fe I or Ca I line was used to ensure that the Gaussian-smoothed synthetic spectrum using the equivalent width-derived stellar parameters was able to reproduce the observational data, generally reproducing observational data to ~ 0.10 dex. Best fit spectra were selected by eye based on the χ^2 minimization output in MOOG. Synthesis was also used to confirm the abundances derived using equivalent width analysis. Upper limits were derived by comparisons to synthetic spectra. Models of varying element abundances were generated until a model produced a clear detection that would have been distinguishable from noise but is undetected in the observed spectrum of the star. Sample synthetic spectra for elements measured using equivalent width analysis and spectral synthesis can be found in Figure 4.2 for Horolgium I, overlaid onto the observed spectra.

Abundances are calculated as $\log_{10}(\epsilon_X)$, which is defined in Equation 4.1 in terms of number density N_X. For reference, $\log_{10}(\epsilon_H)$, where N_H is the number density of hydrogen, is defined as 12.

$$\log_{10}(\epsilon_X) = \log_{10}\left(\frac{N_X}{N_H}\right) + 12 \tag{4.1}$$

Conversion into the more familiar [X/H] notation is performed using Equation 4.2 using measurements of $\log_{10}(\epsilon_{X,\odot})$ by Asplund et al. (2009). Calculation of [X/Fe] is shown in Equation 4.3.

$$[\text{X/H}]_\star = \log_{10}(\epsilon_{X,\star}) - \log_{10}(\epsilon_{X,\odot}) \tag{4.2}$$

$$[\text{X/Fe}]_\star = [\text{X/H}]_\star - [\text{Fe/H}]_\star \tag{4.3}$$

In order to reduce systematic errors, we used Fe I to calculate [X/Fe] for neutral species and Fe II to calculate [X/Fe] for ionized species. We present chemical abundance measurements in Table 4.3. We list each species measured, the number of lines measured for that species (N), $log_{10}(\epsilon_X)$, metallicity, elemental abundance compared to iron, total error on the measurement (see discussion in Section 4.3.4), and method used to measure each species. For lines for which we could only determine an upper limit, the total 1-σ uncertainty was added to the measured limit, i.e. we attempt to report a conservative estimate of the upper limit. For the UVES spectra we attempted to measure the abundances of several other elements, including Al, Co, Cu, Nd, Sr, Yb, and Zn, but could not obtain an upper limit better than [X/Fe] $< +4$ dex for these elements due to the lack of strong lines in the UVES wavelength range.

4.3.4 Error Analysis

In order to determine the uncertainty in the abundance measurements, we employ a method similar to McWilliam & Rich (1994) and account for the statistical and systematic errors separately. For lines measured using equivalent widths, we have calculated the mean abundance for multiple lines across excitation potential and transition probability space. We assume the standard deviation from this mean abundance represents our statistical error that arises from uncertainty in

our equivalent width measurements. We take this to be the uncertainty on our abundance measurement for a single, unblended spectral feature. Therefore, by dividing by $\sqrt{N}$, where N is the number of lines measured, we arrive at the statistical error in our abundance measurement that accounts for the multiple lines measured per element.

To account for systematic errors introduced by the uncertainty in stellar parameter determination, we vary the stellar atmosphere model by the uncertainty in the stellar parameters individually. We then recalculate the abundance of each element using this perturbed model and determine the variation in our abundance measurement $\Delta \log_{10}(\epsilon_X)$ caused by the perturbation. We do this for effective temperature (± 100K), surface gravity (± 0.2 dex), and microturbulence (± 0.5 km s^{-1}).

The empirical effective temperature correction from Frebel et al. (2013) to account for the discrepancy between spectroscopically and photometrically derived temperatures may have increased the uncertainty in effective temperature. Since this correction was on order $\sim 100K$, our measured error in effective temperature may be slightly larger, which may then affect the measured abundances. However, for the purposes of this paper, we adopt our stated errors solely based on the observed trends in abundance calculation across excitation potential and transition probability space.

The variation in abundance due to the perturbed stellar parameters is added in quadrature with the statistical error taken from the uncertainty in our equivalent width measurements, generating $\Delta \log_{10}(\epsilon_X)_{,\text{Total}}$.

For lines measured using spectral synthesis, we assess systematic errors as described above. However, because we use the consistency of multiple lines to measure element abundance, we cannot derive a statistical uncertainty in the same manner as the equivalent width analysis. We still remeasure abundances using a stellar atmosphere model perturbed by the uncertainty in the measured stellar parameters. Our perturbed model abundance is compared against the unperturbed abundance to determine the variation $\Delta\epsilon$, which we take to be our systematic errors based upon the errors in our stellar parameter determination. We estimate, based on S/N and the variations observed in our stellar parameter perturbation, that the statistical error associated with this mea-

surement could be as high as 0.25 dex. We therefore adopt this value as the statistical error for lines measured using synthetic spectra. The final statistical error reported for lines measured using spectral synthesis is this value divided by the square root of the number of lines measured.

4.4 Results

In Figure 4.3 we compare Hor I stars to stars in the Milky Way halo and thirteen ultra-faint dwarf galaxies for which spectroscopic abundance analysis has been performed. The three Hor I stars are all of very low metallicity, ranging from $-2.83 <$ [Fe/H] < -2.43, and have similar α-element and iron-peak element abundances. The measurement of Ba II in two stars and a consistent upper limit in the third star suggests that the abundance of neutron-capture elements in these three stars is also similar.

In comparison to most other stars in the Milky Way halo and in other ultra-faint dwarf galaxies, the α-element abundance of these three Hor I stars is low for their [Fe/H]. This can be seen in the [Ca/Fe] and [Mg/Fe] abundances. The detection of Si in one star, DES J025535-540643, is also consistent with the other α-elements. There are a few stars in other ultra-faint dwarfs with similarly low [Ca/Fe] and [Mg/Fe] (~ 0); however, these stars are generally more metal-rich, and no other ultra-faint dwarf has consistently low abundances for all α-elements among all its measured member stars.

The iron-peak elements also present some unusual patterns. The abundances of Sc and Ni seem to be similar to that of stars in the halo and the other ultra-faint dwarfs. The abundance of Cr in Hor I is slightly elevated with respect to most other ultra-faint dwarfs, but still consistent with the abundances of halo stars. However, the abundance of Mn is ~ 0.4 dex higher than most halo stars and ~ 0.6 dex higher than the abundances found in other ultra-faint dwarfs.

The abundance of Ba is similar to most other ultra-faint dwarfs. It does not present significant s-process or r-process enrichment like the stars in Ret II (Ji et al., 2016c) or Tuc III (Hansen et al., 2017). The upper limit of Eu found in DES J025535-540643 ([Eu/Fe] $< +1.02$) excludes it from being an r-II star (defined as [Eu/Fe] $> +1.0$), but does not exclude the possibility that it is an r-I star (defined as [Eu/Fe] $> +0.3$), where these definitions are taken from Beers & Christlieb (2005).

Table 4.3 Abundances of Three Confirmed Member Stars of Hor I

Species	N	$\log_{10}(\epsilon_X)$	[X/H]	[X/Fe]	Error	Method
DES J025540-540807						
Na I	2	3.54	-2.70	-0.27	0.27	Eq. Width
Mg I	2	5.15	-2.45	-0.02	0.25	Eq. Width
Si I	4	< 6.58	< -0.93	$< +1.95$	0.45	Spec. Synthesis
Ca I	4	3.84	-2.50	-0.07	0.15	Eq. Width
Sc II	1	< 0.65	< -2.50	$< +0.51$	0.44	Spec. Synthesis
Ti I	3	3.04	-1.91	$+0.52$	0.40	Spec. Synthesis
Cr I	8	3.22	-2.42	$+0.01$	0.30	Spec. Synthesis
Mn I	3	2.94	-2.49	-0.06	0.61	Spec. Synthesis
Fe I	12	5.07	-2.43	$+0.00$	0.13	Eq. Width
Fe II	4	4.93	-2.57	-0.14	0.11	Eq. Width
Ni I	2	3.80	-2.42	$+0.01$	0.41	Spec. Synthesis
Ba II	3	< -1.32	< -3.50	< -0.47	0.46	Spec. Synthesis
Eu II	2	< 0.09	< -0.43	$< +2.55$	0.41	Spec. Synthesis
DES J025543-544349						
Na I	2	2.74	-3.50	-0.90	0.32	Eq. Width
Mg I	3	4.77	-2.83	-0.23	0.25	Eq. Width
Si I	4	< 6.91	< -0.60	$< +2.45$	0.45	Spec. Synthesis
Ca I	3	3.74	-2.60	$+0.00$	0.13	Eq. Width
Sc II	1	0.70	-2.45	$+0.27$	0.50	Spec. Synthesis
Ti I	3	2.64	-2.31	$+0.29$	0.40	Spec. Synthesis
Cr I	8	2.87	-2.77	-0.17	0.31	Spec. Synthesis
Mn I	3	2.79	-2.64	-0.04	0.68	Spec. Synthesis
Fe I	12	4.90	-2.60	$+0.00$	0.16	Eq. Width
Fe II	4	4.78	-2.72	-0.12	0.11	Eq. Width
Ni I	2	3.65	-2.57	$+0.03$	0.47	Spec. Synthesis
Ba II	3	-1.47	-3.65	-0.93	0.32	Spec. Synthesis
Eu II	2	< -0.08	< -0.60	$< +2.59$	0.47	Spec. Synthesis
DES J025535-540643						
C (CH)	1	< 5.05	< -3.38	< -0.19	0.36	Spec. Synthesis
N (CN)	1	< 5.70	< -2.13	$< +1.20$	0.50	Spec. Synthesis
Na I	2	2.38	-3.86	-1.03	0.23	Eq. Width
Mg I	4	4.74	-2.86	-0.03	0.30	Eq. Width
Al I	2	2.62	-3.83	-1.00	0.22	Spec. Synthesis
Si I	1	4.80	-2.71	$+0.12$	0.48	Spec. Synthesis
Ca I	4	3.49	-2.85	-0.02	0.21	Eq. Width
Sc II	3	0.21	-2.94	$+0.00$	0.15	Spec. Synthesis
Ti I	3	2.39	-2.56	$+0.27$	0.18	Spec. Synthesis
V I	1	1.80	-2.13	$+0.70$	0.30	Spec. Synthesis
Cr I	5	2.62	-3.02	-0.19	0.38	Spec. Synthesis
Mn I	1	2.54	-2.89	-0.06	0.36	Spec. Synthesis
Fe I	60	4.67	-2.83	$+0.00$	0.12	Eq. Width
Fe II	4	4.56	-2.94	-0.11	0.19	Eq. Width
Co I	3	2.38	-2.61	$+0.22$	0.32	Spec. Synthesis
Ni I	3	3.28	-2.94	-0.11	0.35	Spec. Synthesis
Cu I	3	< 1.16	< -3.03	$< +0.12$	0.32	Spec. Synthesis
Zn I	2	< 2.30	< -2.26	$< +0.87$	0.30	Spec. Synthesis
Ga I	1	< 0.68	< -2.36	$< +0.90$	0.43	Spec. Synthesis
Rb I	2	< 2.30	< -0.22	$< +2.95$	0.34	Spec. Synthesis
Sr II	2	-0.97	-3.84	-0.90	0.33	Spec. Synthesis
Y II	4	< -0.06	< -2.27	$< +1.05$	0.38	Spec. Synthesis
Zr II	4	< 0.70	< -1.88	$< +1.40$	0.34	Spec. Synthesis
Mo II	1	< 0.52	< -1.36	$< +1.89$	0.31	Spec. Synthesis
Ba II	3	-1.75	-3.93	-0.99	0.33	Spec. Synthesis
La II	5	< -0.18	< -1.28	$< +1.98$	0.32	Spec. Synthesis
Ce II	5	< -0.45	< -2.03	$< +1.21$	0.30	Spec. Synthesis
Pr II	4	< -1.04	< -1.76	$< +1.49$	0.31	Spec. Synthesis
Nd II	6	< -0.50	< -1.92	$< +1.33$	0.31	Spec. Synthesis
Sm II	5	< -0.55	< -1.51	$< +1.75$	0.32	Spec. Synthesis
Eu II	4	< -1.84	< -2.36	$< +0.97$	0.39	Spec. Synthesis
Gd II	3	< -0.13	< -1.20	$< +2.06$	0.32	Spec. Synthesis
Tb II	3	< -0.47	< -0.77	$< +2.52$	0.35	Spec. Synthesis
Dy II	3	< -0.75	< -1.85	$< +1.43$	0.34	Spec. Synthesis
Er II	2	< -0.44	< -1.36	$< +2.01$	0.43	Spec. Synthesis

Table 4.4 Summary of Error Analysis

Species	N	σ	$\Delta\log_{10}(\epsilon_X)$ ($\Delta T = +100$K)	$\Delta\log_{10}(\epsilon_X)$ ($\Delta\log(g) = +0.2$ dex)	$\Delta\log_{10}(\epsilon_X)$ ($\Delta\xi = +0.5$ km s^{-1})	$\Delta\log_{10}(\epsilon_X)_{,\mathrm{Total}}$
DES J025540-540807						
Na I	1	0.10	+0.13	−0.06	−0.20	0.27
Mg I	2	0.13	+0.14	−0.08	−0.16	0.25
Si I	4	0.25	+0.25	+0.25	+0.25	0.45
Ca I	4	0.03	+0.08	−0.03	−0.12	0.15
Sc II	1	0.25	+0.25	+0.25	−0.10	0.44
Ti I	3	0.25	−0.25	+0.13	−0.25	0.40
Cr I	8	0.20	−0.10	−0.10	−0.25	0.30
Mn I	3	0.50	+0.25	+0.25	+0.50	0.61
Fe I	12	0.20	+0.11	−0.01	−0.05	0.13
Fe II	4	0.13	+0.05	+0.07	−0.01	0.11
Ni I	2	0.25	+0.25	+0.10	−0.25	0.41
Ba II	3	0.25	−0.25	−0.25	−0.25	0.46
Eu II	2	0.25	−0.25	−0.25	−0.10	0.41
DES J025543-544349						
Na I	1	0.19	+0.12	−0.02	−0.24	0.32
Mg I	3	0.09	+0.09	−0.06	−0.22	0.25
Si I	4	0.25	+0.25	+0.25	+0.25	0.45
Ca I	3	0.04	+0.09	−0.03	−0.08	0.13
Sc II	1	0.25	+0.25	+0.25	+0.25	0.50
Ti I	3	0.25	−0.25	−0.13	−0.25	0.40
Cr I	8	0.20	−0.10	−0.13	−0.25	0.31
Mn I	3	0.50	+0.25	+0.25	+0.50	0.68
Fe I	12	0.29	+0.13	−0.02	−0.04	0.16
Fe II	4	0.17	−0.02	+0.07	−0.01	0.11
Ni I	2	0.25	+0.25	−0.25	−0.25	0.47
Ba II	3	0.25	−0.10	−0.10	−0.25	0.32
Eu II	2	0.25	−0.25	−0.25	−0.25	0.47
DES J025535-540643						
C (CH)	1	0.25	+0.15	−0.05	−0.20	0.36
N (CN)	1	0.25	+0.25	+0.25	+0.25	0.50
Na I	1	0.08	+0.14	−0.05	−0.16	0.23
Mg I	4	0.27	+0.14	−0.08	−0.16	0.30
Al I	2	0.07	+0.15	−0.08	+0.13	0.22
Si I	1	0.25	+0.30	+0.20	+0.20	0.48
Ca I	4	0.29	+0.08	−0.03	−0.12	0.21
Sc II	3	0.12	+0.10	+0.08	−0.05	0.15
Ti I	3	0.09	+0.10	−0.10	−0.10	0.18
V I	1	0.25	+0.10	+0.10	+0.10	0.30
Cr I	5	0.35	−0.09	−0.24	−0.23	0.38
Mn I	1	0.25	+0.05	−0.20	−0.15	0.36
Fe I	60	0.20	+0.11	−0.01	−0.05	0.12
Fe II	4	0.33	+0.05	+0.07	−0.01	0.19
Co I	3	0.29	+0.22	−0.13	−0.08	0.32
Ni I	3	0.47	+0.17	+0.12	+0.08	0.35
Cu I	3	0.25	+0.15	+0.10	−0.10	0.32
Zn I	2	0.25	+0.10	+0.10	+0.10	0.30
Ga I	1	0.25	+0.20	+0.20	+0.20	0.43
Rb I	2	0.25	+0.20	+0.10	+0.05	0.34
Sr II	2	0.25	+0.13	−0.08	−0.15	0.33
Y II	4	0.25	+0.20	+0.20	+0.05	0.38
Zr II	4	0.25	−0.20	+0.05	+0.10	0.34
Mo II	1	0.25	+0.15	−0.10	+0.05	0.31
Ba II	3	0.52	+0.10	+0.07	−0.07	0.33
La II	5	0.25	+0.15	+0.10	+0.10	0.32
Ce II	5	0.25	+0.10	−0.10	−0.10	0.30
Pr II	4	0.25	+0.15	+0.10	+0.05	0.31
Nd II	6	0.25	+0.15	−0.10	−0.05	0.31
Sm II	5	0.25	+0.15	−0.10	−0.10	0.32
Eu II	4	0.25	−0.20	−0.20	−0.10	0.39
Gd II	3	0.25	−0.15	−0.10	−0.10	0.32
Tb II	3	0.25	−0.10	−0.20	−0.10	0.35
Dy II	3	0.25	−0.15	−0.15	−0.10	0.34
Er II	2	0.25	−0.20	−0.20	−0.20	0.43

However, the low [Ba/Fe] of these three stars make it unlikely that they are r-process enhanced.

Due to wavelength constraints, we could only measure C using the CH band in DES J025535-540643. Based upon the upper limit of [C/Fe] < -0.14, we can conclude that this star is not carbon-enhanced.

4.5 Discussion

We discuss possible scenarios that could lead to the observed nucleosynthetic pattern of Hor I and compare Hor I stars to stars in the Milky Way with similar abundance patterns. In Section 4.5.1, we compare the abundance pattern of Hor I to stars found in the Milky Way halo with similar nucleosynthetic patterns. In Section 4.5.2, we discuss one plausible enrichment scenario, the early onset of Type Ia supernovae in Hor I. In Section 4.5.3, we compare the peculiar abundance pattern observed in Hor I to theoretical nucleosynthetic yield models. In Section 4.5.4, we discuss a possible association with the Large Magellanic Cloud as the cause of the abundance pattern measured in Hor I. We caution that these discussions are based on the abundance measurements of only three stars, and may change with analysis of additional stars in Hor I.

4.5.1 Comparison with Stars in the Milky Way Halo

The stars in Hor I are not the first metal-poor, α-poor stars to be discovered. For example, in a detailed chemical abundance study of stars found in a search for the most metal-poor stars in the Galactic halo, Ivans et al. (2003) reported chemical abundance measurements of two additional low-α, low-metallicity stars in the Galactic halo: G4-36 and CS 22966-043, and found that these two and BD +80° 245 all have [Fe/H]~ -2 and [Ca/Fe] $\sim$ 0.5 dex below the mean halo value (Ivans et al. 2003 report [Ca/Fe] $= +0.31$ for the halo). Interestingly, these three stars also have iron-peak overabundances that are qualitatively similar to the Hor I stars, with BD +80° 245 having the most similar abundances to our stars. Additionally, BD +80° 245 has a similarly high Ti abundance despite its low α-element abundance. An emerging suggestion has arisen that posits Ti is an Fe-peak element instead of a classical α-element (Sneden et al., 2016). The abundances of stars found in Hor I may lend additional credence to that argument.

Other studies have discovered extremely metal-poor stars having peculiar abundances: Cohen et al. (2008) and Haschke et al. (2012) report discoveries of extremely low-metallicity, low-α stars; Caffau et al. (2013) found four extremely metal-poor stars ([Fe/H] ~ -3.7) with even lower [α/Fe] ratios than we measure in Hor I. Each of these studies invoke various theoretical supernova yield models to explain the observed abundance patterns, which are plausible explanations but in most cases do not perfectly match the observations.

More recently, a metal-poor ([Fe/H]=-2.5) star having low-α abundances ([α/Fe]~ -0.4), SDSS J0018-0939, was discovered in the SDSS survey (Aoki et al., 2014). The authors suggest that this star, whose observed abundance patterns are compared to theoretical nucleosynthetic yield models of a pair-instability supernova (PISN; Heger & Woosley, 2002), may represent the first observational evidence of a PISN.

Simon et al. (2015b) found 2 stars in Sculptor with similar chemical abundances but at an average [Fe/H] of ~ -3.9, which is much more metal poor than Hor I. Scl 11_1_4296 had depleted abundances of Mg, Ca, and Si. Scl 07-50 had similarly low Ca and Si, but a Mg abundance that is consistent with the Milky Way halo. They concluded that these stars were the second generation of stars formed in the galaxy and that the chemical signatures were reproducible using Population III supernovae nucleosynthetic models.

Recent models predict that the earliest stars formed that are still observable today should be very (not extremely) metal-poor stars, with [Fe/H]=-2.5 and low α abundances. Karlsson et al. (2008) constructed theoretical models for the early chemical enrichment of the Milky Way, showing that the lack of metal-free stars in the Galactic halo that are observable today is in fact expected if the first stars to form in the Universe were very massive (Bromm et al., 1999). In their model, the Galactic halo is assembled from stars formed during the assembly of "atomic-cooling halos" centered on minihalos each holding a Population III star. These models also show that stars with this chemical signature of [Fe/H]=-2.5 and low α abundances should be quite rare, about 1 star in 500 in the Galactic halo. This may not be the case in ultra-faint dwarfs. However, this picture is consistent with hierarchical structure formation as well as, at least qualitatively, with the number of

halo stars discovered to date having similarly peculiar abundance patterns. The halo stars described in the above studies are rare and unusual enough, both in observations and in theoretical models when compared to other halo stars, to warrant special attention. It is therefore quite interesting to find three very similar stars colocated in one low-mass galaxy.

We suggest that those peculiar halo stars could have formed in small galaxies like Hor I, in which pollution by a single PISN occurred early in the star formation history of the galaxy. PISN, due to the high mass of their progenitors, have a characteristically low α-element production and a characteristic odd-even effect in their nucleosynthesis pattern. Therefore, the observed abundance patterns of Aoki et al. (2014) and in Hor I may be due to a PISN (we investigate this in more detail in Section 4.5.3). Those smaller satellites would then have been accreted into the Milky Way halo, leaving small numbers of halo stars with unusual abundance patterns sprinkled throughout the halo, as is observed.

This scenario is consistent with the idea that the ultra-faint dwarfs are small contributors (by mass) to the accretion history of the Milky Way, as predicted by ΛCDM theory, and could perhaps be further confirmed if adequate numbers of similarly peculiar stars were found and their kinematic properties are consistent with having originated in the same accreted satellite. This last suggestion may be testable once Gaia proper motions are added to the measured radial velocities, enabling full position and kinematic information.

4.5.2 Possible Extended Star Formation in Horologium I

One plausible scenario that could explain the chemical abundances of Hor I is an early onset of Type Ia supernovae. In our current understanding of chemical evolution (Tinsley, 1979), as a star-forming gas cloud collapses the most massive stars form early, quickly evolving to produce Type II supernovae and thereby enriching the surrounding gas cloud with the α-elements O, Mg, Si, S, Ca and Ti. The next stars that form in this α-rich environment would then be α-enhanced stars with typical [α/Fe] values ≥ 0.3. As the stellar population continues to evolve, at some later time Type Ia supernovae, which have characteristically low yields in α-elements and greater yields of the iron-peak elements (Cr, Mn, Fe, Co, Ni, Cu), begin to dominate nucleosynthesis. The Type

Ia supernovae then enrich the surrounding environment, thereby lowering the relative abundance of α-elements and increasing the abundance of iron-peak elements. Stars formed after the transition between Type II-dominated nucleosynthesis and Type Ia-dominated nucleosynthesis would therefore present abundance ratios closer to the solar ratio (α/Fe] $\sim$ 0). This process produces a characteristic "knee" in the [α/Fe] ratios across a range of metallicities, where metallicity, or [Fe/H], increases with time as the isolated stellar population enriches itself in iron. In principle, the slope and the position of the knee can provide information about the rate and the time respectively at which this transition occurred in a given stellar population. McWilliam (1997) provides a comprehensive description of this story, which describes the observed abundances of stars in the Milky Way halo quite well.

Presumably a similar series of events to that described above occurs in all stellar populations, where the specifics of the time delay, or, equivalently, metallicity, at which the transition between α-rich to α-poor star formation is determined by the star formation rate and initial mass function of the stellar population. This effect has been observed in dwarf galaxies using both detailed abundance measurements from high-resolution spectroscopy (e.g. Venn et al., 2004; Koch et al., 2008a; Hendricks et al., 2014) as well as with medium resolution spectroscopy (Kirby et al., 2011). The trend holds for lower mass objects as well: Vargas et al. (2013) studied an ensemble of ultra-faint dwarf galaxies and determined that the transition between Type II- and Type Ia-dominated nucleosynthesis typically occurs in these objects at a "time" when [Fe/H] ~ -2.3, based on the summary properties of eight ultra-faint dwarfs. According to these results, stars in ultra-faint dwarfs that are more metal-poor than [Fe/H] ~ -2.3 generally should have formed in the α-rich environment produced by Type II supernovae and thus present super-solar α-element abundance. Conversely, stars with [Fe/H] > -2.3 were produced after Type Ia supernovae began to pollute the surrounding environment with iron-peak elements and would therefore show [α/Fe] ~ 0.

Vargas et al. (2013) also determine that star formation in ultra-faint dwarfs occurs after a minimum time delay for the onset of Type Ia supernova of at least 100 Myr. This picture is consistent with other work that places limits on the star formation histories of ultra-faint dwarf galaxies: deep

Hubble Space Telescope imaging and Keck spectroscopy of ultra-faint dwarf galaxies show that their stars were formed early, with roughly 80% of stars having formed by 12.8 Gyr ago and 100% of stars formed by 11.6 Gyr ago (Brown et al., 2014). This duration is consistent with an early but extended star formation history that would conform to the standard process of chemical evolution in a stellar population. Furthermore, the picture that has emerged to describe star formation in ultra-faint dwarf galaxies is that star formation began quickly, in some cases in a single burst of star formation (Frebel & Bromm, 2012), and was soon quenched, possibly by reionization (e.g. Brown et al., 2014; Wetzel et al., 2015; Jeon et al., 2017), leaving the stars in the ultra-faint dwarfs as a fossil record of conditions in the early Universe.

If we presume a similar chemical evolution timeline for Hor I and use [Fe/H] as an age indicator, our measurements imply that the onset of Type Ia supernovae and the subsequent chemical enrichment of the surrounding gas would have had to occur relatively earlier in Hor I than in other ultra-faint dwarfs. The lack of α-elements in even the most metal-poor star, DES J025535-540643 ([Fe/H] $= -2.8 \pm 0.2$ and [Ca/Fe] $= -0.05 \pm 0.15$), implies that the transition from Type II supernovae-dominated nucleosynthesis and Type Ia supernovae-dominated nucleosynthesis had to occur at a time when the metallicity of Hor I was [Fe/H] < -2.8. This would represent a very early transition between nucleosynthesis dominated by Type II supernovae and nucleosynthesis dominated by Type Ia supernovae compared to other ultra-faint dwarfs.

We do note that it is somewhat presumptuous to draw strong conclusions from a sample of three stars in a galaxy. Furthermore, at least one other ultra-faint dwarf galaxy has shown a spread in α-enhancement at the low end of its metallicity range, Ursa Major I (UMa I; Vargas et al., 2013). The ten stars studied by Vargas et al. (2013) span nearly two orders of magnitude in metallicity with a wide spread in α-abundance at the lowest metallicity end, i.e. UMa I contains at least two metal-poor, α-poor stars that could have chemical abundances similar to the Hor I stars. Unfortunately, the moderate-resolution spectroscopy used by Vargas et al. (2013) does not permit detailed abundance analysis of many elements. It should be noted, however, that UMa I may not fit the canonical picture of stellar populations (Jeon et al., 2017).

Limits on the duration of star formation in Hor I could be placed if it were possible to study a larger sample of member stars chemically. According to the standard picture of chemical evolution described above, some of those stars would be older than the three studied here, should have [Fe/H] < -2.8, and should show α-element enhancement consistent with the knee observed in other galaxies. Alternatively, a larger sample of stars could be studied with medium-resolution spectra using techniques such as those used by Kirby et al. (2009).

4.5.3 Comparison with Supernovae Nucleosynthetic Yield Models

Alternatively, Hor I may have been host to a rare primordial supernova such as a PISN whose nucleosynthetic signature is preserved in the presently observable population of stars. Frebel & Bromm (2012) suggest that the chemical signatures of low-mass ultra-faint dwarfs can be described by a single, long-lived, generation of stars that formed in the early Universe. In related work, Ji et al. (2015) demonstrate that the chemical abundance patterns of these single events can be preserved in the second generation of stars. Though Hor I does not have the characteristically high α-element abundance predicted by Frebel & Bromm (2012) in their "one-shot enrichment" scenario, if Aoki et al. (2014) are correct that their observed abundance patterns, which are similar to ours, are due to a PISN, then we expect that there must have been only a single nucleosynthetic event in Hor I. If there had been several generations of supernovae preceding the currently observed population, the peculiar abundance pattern produced in rare supernovae would be obscured by nucleosynthesis in other, more common Type II supernovae. By this reasoning, for the purposes of this analysis, we assume that the stars in Hor I are chemically primitive objects, and we explore the possibility that the observed abundances could be explained by the predicted yields of a single nucleosynthetic event. Therefore, in our comparison to nucleosynthetic yield models, we limit the number of events to a single Population III supernova that enriched the surrounding gas, creating the chemical abundance pattern observed today.

To explore the possibility that the observed abundance pattern of Hor I may arise from a PISN, we have compared the abundances of DES J025535-540643 to various supernova yield models for Population III stars. These models can produce low [Ca/Fe] and [Mg/Fe] abundances, such as

those observed in the three stars studied in Hor I. Since we were able to measure more elements in DES J025535-540643, we conduct this analysis only on this star.

We used the STARFIT[4] tool (Chan et al. *in prep.*; Heger & Woosley, 2010) to compare our abundance measurements with Type II supernova nucleosynthetic yield models (Heger & Woosley, 2010, and subsequent online updates in 2012) for progenitors spanning a wide range in mass (9.6-$100 M_{\odot}$) and PISN nucleosynthetic yield models (Heger & Woosley, 2002) for progenitors spanning a zero age main sequence (ZAMS) mass range of 140-$260 M_{\odot}$. The STARFIT code calculates a χ^2 statistic using abundance measurements and upper limits (see Heger & Woosley, 2010, Equation 4) and determines a best-fit supernova yield model. We used STARFIT to compare the observed abundance pattern of DES J025535-540643 against three categories of models; we present the parameters of the best fit models in Table 4.5. It should be noted that Sc and Cr are generally underproduced by yield models. Heger & Woosley (2010) assume that this is due to additional production sites that are unaccounted for and therefore discrepancies regarding these elements should be taken lightly. We therefore have STARFIT ignore them when fitting our abundance pattern.

Heger & Woosley (2010) compute yields for non-rotating, metal-free Population III stars using initial Big Bang compositions from Cyburt et al. (2001). Due to the lack of a robust model for how a core-collapse supernova explodes, these computations utilize a piston model to simulate the explosion. Heger & Woosley (2010) compute nucleosynthetic yield models for two locations of the piston (initial mass cut), one model for a piston at the base of the O shell ($S = 4$ Piston Model) and one model for a piston at the edge of the Fe core (Y_e Piston Model). We compare the abundance of DES J025535-540643 to both models using STARFIT. Using the model for a piston at the base of the O shell yields a best-fit model of a $10 M_{\odot}$ progenitor Type II supernova (mean squared residual $= 23.8$). Using the model for a piston at the edge of the Fe core yields a best-fit model of an $85 M_{\odot}$ progenitor Type II supernova (mean squared residual $= 28.2$).

The explosion mechanism of a PISN is well-understood and is simulated to obtain theoretical nucleosynthetic yields by Heger & Woosley (2002). PISN progenitors enter a regime of elec-

[4]See http://starfit.org for routine and models

tron/positron pair-production resulting in a collapse until O burning and Si burning produce enough energy to explode. This explosion results in low α-element abundances, a low C abundance, and a strong odd-even effect. Comparison to the model nucleosynthetic yields of PISN using STARFIT gives a best-fit model of a $260M_{\odot}$ ($130M_{\odot}$ He core) PISN (mean squared residual $= 64.4$). It should be noted that this is the highest available PISN model used by STARFIT. It may be that the best fitting PISN model is beyond the available mass range.

In the left panels of Figure 4.4, we show the yield models that best fit DES J025535-540643 and the abundance measurements of all three stars observed in Hor I. As can be seen in the Figure, each model has difficulties in fitting the observed abundance patterns. The $10M_{\odot}$ Type II supernova model produces too much C, Ca, Mg, and Co compared to our Hor I stars. These four elements produce contradictory requirements. The low upper limit on C and the abundances of Ca and Mg in DES J025535-540643 suggest that a higher energy explosion than provided by the $10M_{\odot}$ Type II supernova is required, while the low Co abundance requires a lower energy explosion. The $85M_{\odot}$ Type II supernova model produces too few iron-peak elements, implying that there is too much fallback and not enough iron-peak elements are synthesized and ejected. This model also does not produce enough Co, indicating that the energy of the explosion is too low. Finally, the $260M_{\odot}$ ($130M_{\odot}$ He core) PISN model produces a larger odd-even effect and a lower Co abundance than is observed in the stars of Hor I, which show essentially no odd-even effect.

We compare BD +80° 245, G4-36, CS 22966-043 (Ivans et al., 2003), and SDSS J0018-0939 (Aoki et al., 2014) to the same models that best fit DES J025535-540643 in the right panels of Figure 4.4. It should be noted that the PISN model that we present is the same model suggested by Aoki et al. (2014) as a possible fit for SDSS J0018-0939. For a common point of comparison for our best-fit models, we also used STARFIT to determine a best-fit PISN model for SDSS J0018-0939. The result was a best-fit model of a $260M_{\odot}$ ($130M_{\odot}$ He core) PISN (mean squared residual $= 159.6$). Aoki et al. (2014) discussed the discrepancies in this PISN model fit to SDSS J0018-0939, specifically mentioning that the model predicts too much Si and too large of an odd-even effect for their observed abundance pattern. However, the model does fit their measured Co

Table 4.5 Supernova Yield Model Fits to DES J025535-540643

Model	Best Fit Progenitor Mass	Mean Sq. Residual
O Shell ($S = 4$) Piston	$10\ M_{\odot}$	23.8
Fe Core (Y_e) Piston	$85\ M_{\odot}$	28.2
PISN	$260\ M_{\odot}$	64.4

abundance. Our analysis of Hor I shares a similar problem in that the model's predicted odd-even effect is too large for our observed abundance pattern. The model does fit our Si abundance well, but underpredicts the amount of Co in DES J025535-540643, mirroring the discrepancies in SDSS J0018-0939.

If it were possible to study a larger sample of member stars chemically then, if a PISN were the underlying cause of the peculiarity in the observed abundance pattern of Hor I, the α-element enhancement knee described previously would not be observed. It would require the chemical analysis of many more stars in Hor I to make any strong conclusions.

4.5.4 Possible Association with the Large Magellanic Cloud

An interesting question posed by the recent discovery of so many candidate ultra-faint dwarf galaxies in the outskirts of the Milky Way and located in the Southern hemisphere is whether they originated in the Milky Way or if rather they originated as satellites of satellites (the Magellanic Clouds). Indeed, both groups announcing the discovery of Hor I (Bechtol et al., 2015; Koposov et al., 2015a), as well as the kinematic confirmation work (Koposov et al., 2015b), note Hor I's potential association with the Large Magellanic Cloud (LMC) due to its location and measured systemic velocity. Several recent theoretical studies have shown that the existence of satellites of satellites is predicted by simulations. Specifically, Deason et al. (2015) use the ELVIS suite of N-body simulations to show that 2 to 4 of the 9 satellites discovered at the time that were found in close proximity to the LMC are expected to be associated with the LMC, while Sales et al. (2017) use the Aquarius Project suite of zoomed-in cosmological simulations to show that 2 to 3 of all 46 dwarfs located within 300 kpc of the Milky Way should be associated with the LMC. Both of

these works specifically state that Hor I has a high probability of being associated with the LMC according to their simulations. Jethwa et al. (2016) use a complementary approach to these results and construct a dynamical model to determine which, if any, of the DES-discovered satellites could have Magellanic origins assuming the Milky Way–LMC system follows the distribution of sub-haloes predicted by ΛCDM. Their model uses the satellites' observed positions and kinematic parameters to show that seven of the fourteen candidate DES satellites in the range $-7 < M_V < -1$ discovered by Bechtol et al. (2015), Koposov et al. (2015a), and Drlica-Wagner et al. (2015) are likely to be satellites of the Large Magellanic Cloud (LMC) rather than of the Milky Way. Their simulations produce predicted systemic velocities for the DES satellites, which must be confirmed by spectroscopic follow-up observations (only four of the fourteen had measured velocities at the time of publishing: Hor I, Ret II, Gru I, and Tuc II). To date, of the satellites considered by Jethwa et al. (2016), Hor I's measured systemic velocity is by far the closest to the velocity predicted if Hor I were associated with the LMC.

If Hor I is indeed a satellite of the LMC, the chemical abundance pattern of Hor I could provide further interesting information about the relationship of the satellite to its host. The LMC has an overall lower α-enhancement than the Milky Way (e.g. Pompéia et al., 2008; Lapenna et al., 2012; Van der Swaelmen et al., 2013). Van der Swaelmen et al. (2013) suggest that the lack of α-elements implies a significantly different star formation history for the LMC than that of the Milky Way halo. Hence the lower α-abundance of the Hor I stars may simply be due to its Magellanic origin, and the fact that early star formation in the LMC proceeded quite differently than in the halo of the Milky Way. The detailed abundance analysis of additional stars in Hor I, as well as of other candidate satellites of the LMC, would lend credence to this hypothesis. However, with only the three stars observed in this study, the chemical abundance pattern of Hor I does not exclude the possibility of an association with the LMC nor does it strongly suggest it. The strongest evidence that Hor I is a satellite of the LMC is the measured radial velocity of its member stars.

4.6 Conclusions

We have measured the chemical abundances of three confirmed member stars in Hor I and have shown that it is yet another example of an ultra-faint dwarf galaxy having a peculiar abundance pattern. Hor I's average metallicity of [Fe/H] ~ -2.6 is not particularly exceptional, however, the observed α abundances are much lower than expected when compared to other metal-deficient stars. In addition, the abundances of other elements, in particular the iron-peak elements, are close to the solar ratio, which is unusually high when compared to most Milky Way halo stars. We put forward the possibility that Hor I could have the earliest known transition between nucleosynthesis dominated by Type II supernovae and nucleosynthesis dominated by Type Ia supernovae. Alternatively, Hor I's chemistry could be explained by a PISN or it could be a satellite of the LMC. In either case, our small sample of three stars is not enough to confirm these suggestions and additional member stars must be studied.

Four DES-discovered ultra-faint dwarfs have been chemically studied in detail to date: Ret II (Ji et al., 2016a; Roederer et al., 2016), Tuc II (Ji et al., 2016b), Tuc III (Hansen et al., 2017), and now Hor I. In each case (with the possible exception of Tuc II), the brightest confirmed member stars show an unexpected and peculiar abundance pattern. Although a plausible explanation for the observed abundances in each system can be invoked, the variety of explanations is large, suggesting that star formation processes in the early Universe may be highly stochastic. These results suggest that study of additional ultra-faint dwarfs, and additional stars in these four previously studied ultra-faint dwarfs, may shed more light on how the first stars and galaxies were formed. However, probing the detailed chemical abundance patterns in many more confirmed member stars in Hor I will likely not be possible until the next generation of telescopes comes online in the next decade.

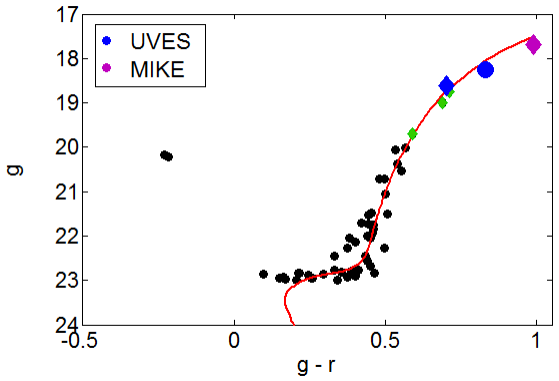

Figure 4.1 Color-magnitude diagram of high probability ($> 70\%$) candidate member stars of Hor I from Bechtol et al. (2015). A Dartmouth isochrone (Dotter et al., 2008) for a stellar population having $\tau = 12.5$ Gyrs, [Fe/H]=-2.5, [α/Fe]=$+0.0$, and distance modulus $m - M = 19.7$ as derived by Bechtol et al. (2015) is overplotted. The three stars studied in this work are indicated by larger points. The five diamond-shaped points are the confirmed member stars of Koposov et al. (2015b). Black points are unconfirmed member stars from Bechtol et al. (2015).

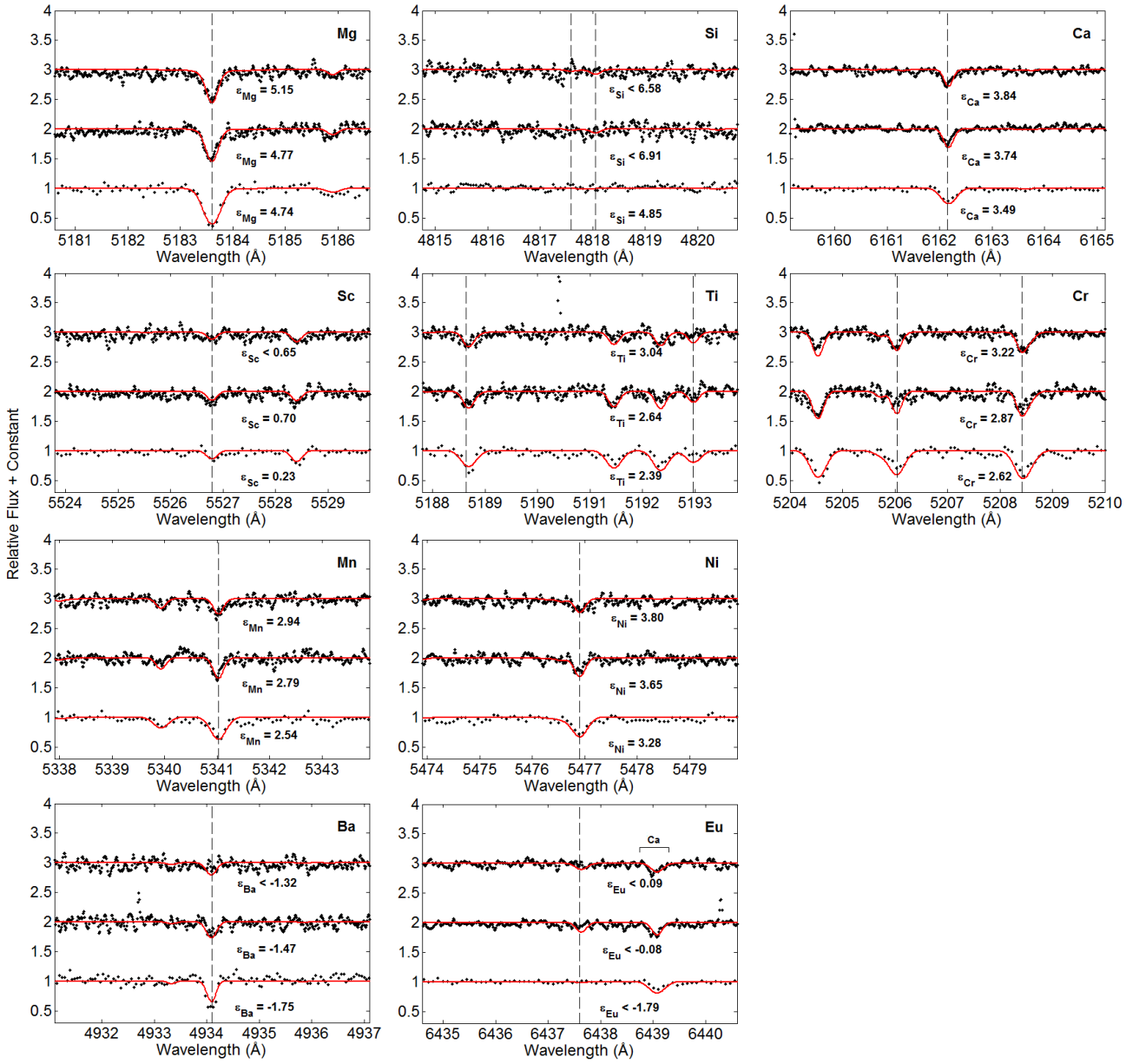

Figure 4.2 Examples of synthetic spectra showing the region around the absorption features for Ca, Mg, Si, Cr, Mn, Ti, Sc, Ni, Ba, and Eu for the ultra-faint dwarf Horologium I. In each panel, the top spectrum is DES J025540-540807, the middle spectrum is DES J025543-544349, and the bottom spectrum is DES J025535-540643. Observed data are plotted as black points, while synthetic spectra of the indicated ϵ_X are presented as red lines. Vertical dashed lines indicate the central wavelength of spectral features of the indicated element. It should be noted that the Si abundance for DES J025535-540643 was not derived from the doublet at 4817.58Å and 4818.05Å alone; other lines outside of the wavelength coverage of UVES were used to achieve a positive detection.

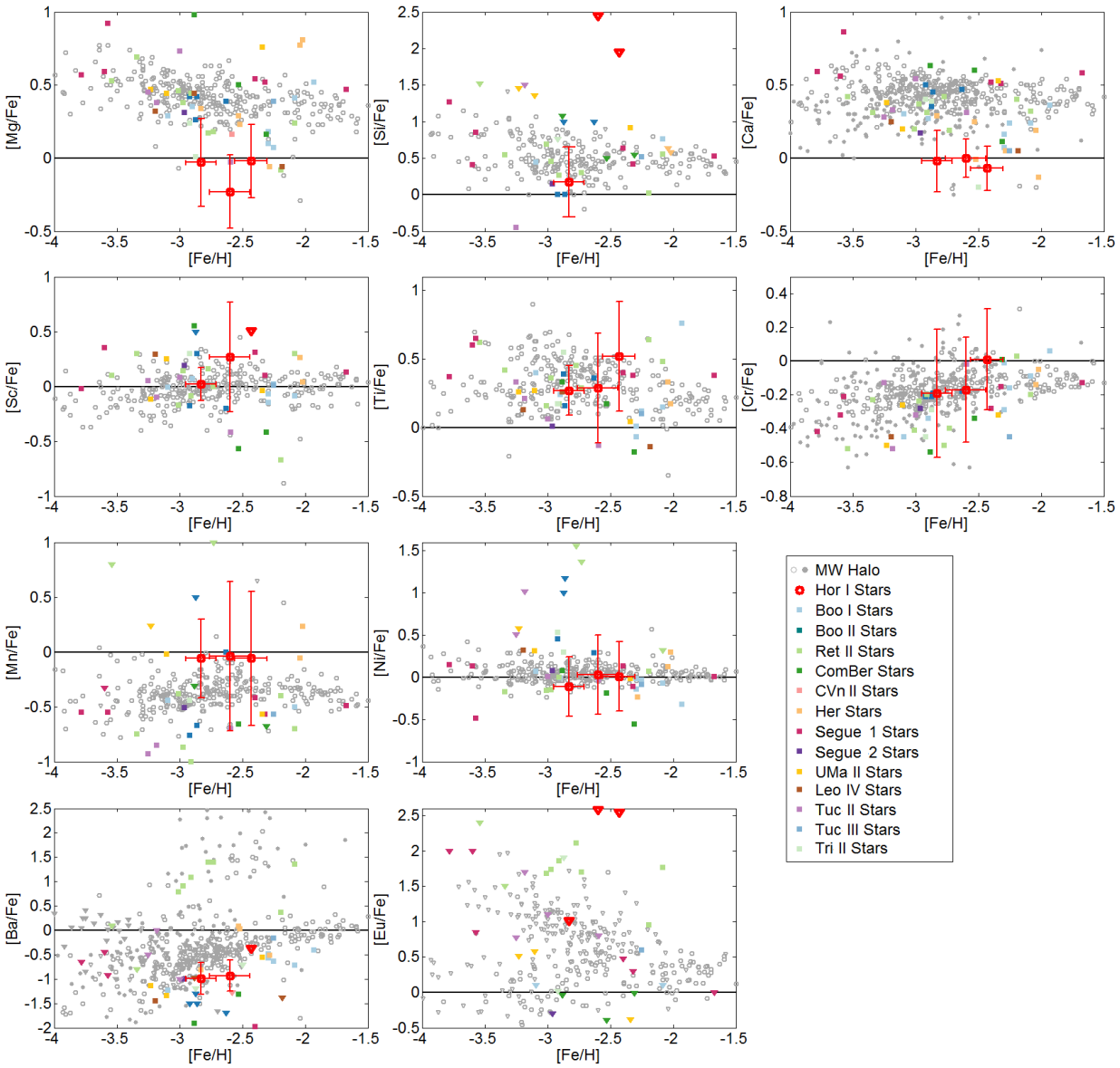

Figure 4.3 Chemical abundance measurements of three Hor I member stars (red) compared to abundance measurements of stars in the ultra-faint dwarf galaxies Boo I (Norris et al., 2010; Ishigaki et al., 2014; Gilmore et al., 2013; Frebel et al., 2016), Boo II (Ji et al., 2016d), Ret II (Ji et al., 2016c), ComBer (Frebel et al., 2010), CVn II (François et al., 2016), Her (Koch et al., 2008b, 2013; François et al., 2016), Segue 1 (Frebel et al., 2014), Segue 2 (Roederer & Kirby, 2014), UMa II (Frebel et al., 2010), Leo IV (Simon et al., 2010; François et al., 2016), Tuc II (Ji et al., 2016b), Tuc III (Hansen et al., 2017), and Tri II (Venn et al., 2017; Kirby et al., 2017) (various colored squares). Abundances of stars in the Milky Way halo from Yong et al. (2013) (filled gray) and Roederer et al. (2014) (open gray) are also shown. Error bars are shown only for the Hor I stars for clarity. Points denoted as $\bigtriangledown$ indicate an upper limit. The solar ratio ([X/Fe] = 0) is indicated by the solid black line.

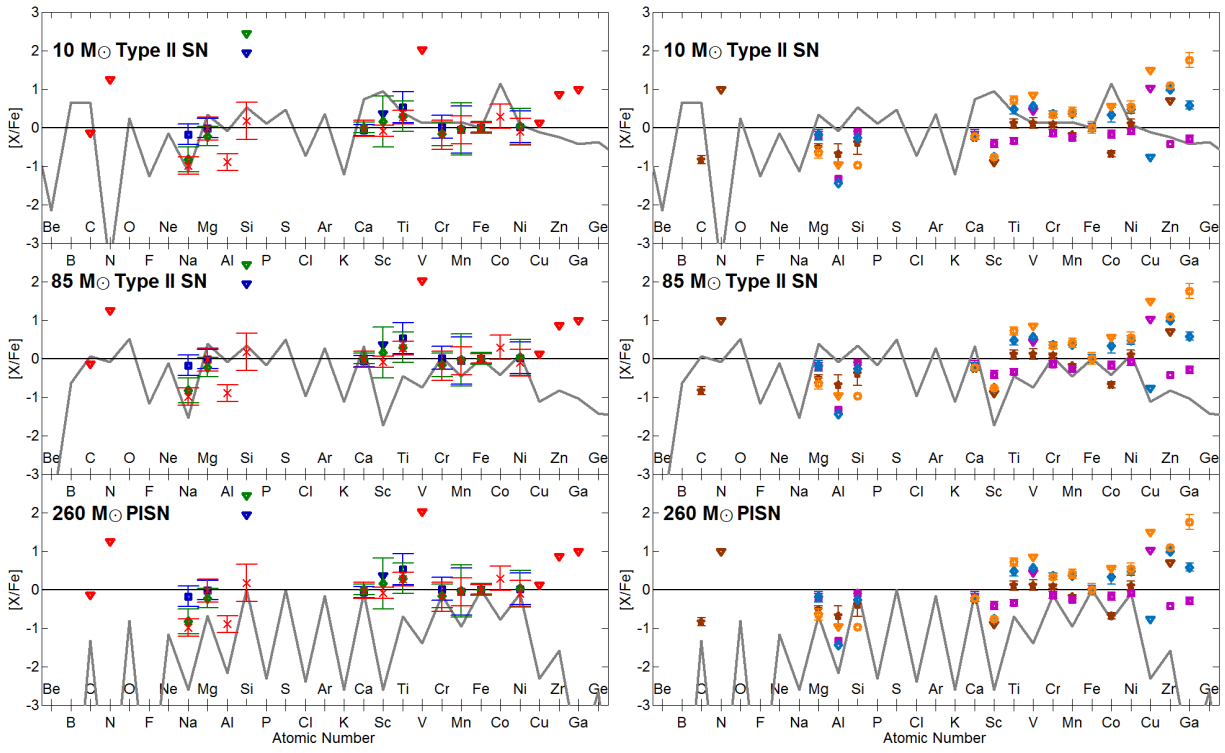

Figure 4.4 Left: The three theoretical supernova yield models (Heger & Woosley, 2002, 2010) that best fit DES J025535-540643: a 10 $M_{\odot}$ Type II SN model (top), an 85 $M_{\odot}$ Type II supernova model (middle), and a 260 $M_{\odot}$ (130 $M_{\odot}$ He core) PISN model (bottom). For comparison, our measurements of [X/Fe] for all three stars are shown: DESJ025540-540807 (dark blue squares), DES J025543-544349 (green diamonds), DES J025535-540643 (red x's). Black lines indicate the solar ratio. Right: the same three supernova yield models with abundances of SDSS J0018-0939 (brown stars; Aoki et al., 2014), CS 22966-043 (pink squares), G4-36 (light blue diamonds), and BD +80° 245 (orange circles; Ivans et al., 2003) shown for comparison. Points denoted as $\bigtriangledown$ indicate an upper limit.

5. SUMMARY AND CONCLUSIONS

The metal content of a star is an indication of how metal-poor its birth cloud was at the time of its formation. Since each star is itself a fossil record of the chemical environment in which it formed, the measurement of this metal content allows us to determine when in the chemical history of Milky Way the star formed and to study that period of time. Therefore, the study of stellar metal content is a way to understand the chemical evolution of our Galaxy.

We have approached the question of the chemical evolution of the Milky Way by two distinct approaches, each providing a different look at how the Milky Way formed. Our first approach is an attempt to enable the use of a tracer population to probe further back in the chemical history of the Galaxy than presently available. Our second approach is the direct study of the chemical abundance of an object that formed at the same time as the Milky Way progenitors, enabling the understanding of this early period of the formation of the Galaxy from a chemical perspective.

In each of our approaches, we have measured this metal content with the intent to add to the growing body of knowledge that forms the core of galactic archaeology. We summarize these approaches and their impact here.

5.1 M-dwarf Metallicity through Analysis of Binary Partners

M-dwarfs, due to the fact that they compose the majority of the main sequence stars in the Galaxy, serve a useful tracer with which to study the spatial and kinematic distribution of the Milky Way. Methods to use them as a chemical tracer have been developed using F/G/K+M binary pairs to bypass the difficulties in analysis caused by the presence of molecular species such as TiO and CaH in the M-dwarf atmosphere.

These methods to measure the metal content of M-dwarfs have used stars with [Fe/H] > -1 to calibrate their empirical relationships. This has allowed the study of the chemical evolution of the Galaxy using M-dwarfs back to a time when the birth clouds of these stars had that metallicity. In order to probe even further back in the chemical history of the Milky Way, we are motivated to

extend these empirically-calibrated relationships using a more metal-poor calibration sample. This necessitates the creation of a sample of high-fidelity F/G/K+M-dwarf binaries largely composed of metal-poor stars.

5.1.1 High Fidelity Sample of F/G/K+M-Dwarf Binary Pairs

We have measured the radial velocities of 77 F/G/K stars and 62 M-dwarfs identified by Li et al. (2014) to be potentially in F/G/K+M binaries. We used high resolution spectroscopy to measure the radial velocities of these candidate F/G/K primaries and low resolution spectroscopy to measure the radial velocity of the candidate M-dwarf secondaries. From the stars we observed, we were able to observe the primary and the secondary for 62 candidate binaries.

We compared our radial velocity measurements to existing literature values for 9 stars, 8 F/G/K type and 1 M-dwarf. In this comparison, we found that we can reproduce these literature values within error.

We selected a 2-σ agreement criterion in order to determine binarity, where σ is the combined quadrature error of the measurements in the candidate primary and secondary. Using this criterion, we identified 47 pairs as having a common radial velocity and thus consider them true binary pairs. This sample of 47 F/G/K+M binaries will be used in the next stage of analyses: to determine the metallicity of the M-dwarf secondaries by the analysis of their solar-type partners.

5.1.2 Metallicity Measurements of F/G/K Primaries with M-Dwarf Secondaries

Using the same high resolution spectra used to calculate radial velocities, we have performed chemical abundance analysis on 58 F/G/K type stars. Of this sample of 58 stars, 42 of them had previously designated as associated with an M-dwarf in a F/G/K+M binary pair.

For all stars analyzed, we determined stellar parameters using the minimization of trends in calculated abundance for Fe I and Fe II across a range of excitation potentials and transition probabilities. Once a set of stellar parameters was determined, a model atmosphere with those parameters was used in conjunction with equivalent width measurements of Fe I, Ca I, and Ti I to determine [Fe/H], [Ca/Fe], and [Ti/Fe] abundances. This gives us an first-order understanding of

the overall metallicity and α-element enhancement of these binary pairs.

In comparing the measured abundance of seven stars with previously performed measurements in the literature, we found that we can reproduce literature [Fe/H] measurements within error for six stars out of seven within 1-σ (where σ is the error associated with our determination of [Fe/H]). The measurements of the one outlier agreed within 2.2-σ. From this, we can conclude that we are in overall agreement with existing literature measurements.

Of the 42 F/G/K+M binary pairs with measured metallicity, 30% are metal-rich dwarfs based upon their proper motions and photometry while the remainder are metal-poor subdwarfs when using a criterion established by Salim & Gould (2003). This is further supported by the metallicity measurements where 71% of our sample have metallicities lower than the mean metallicity of the Milky Way halo [Fe/H] < -0.7.

This sample is intended for use in extending the existing empirically-calibrated methodologies for determining M-dwarf metallicities to more metal-poor stars. By using this new sample of 42 F/G/K+M-dwarf binaries, we can evaluate existing classification schemes and empirical relations used to identify metal-poor M-dwarfs and measure their metallicity. We can also use them to develop new ones. This will allow us to use these numerically common M-dwarfs to probe further back in the chemical history of the Milky Way.

5.2 Chemical Abundance Analysis of Ultra-Faint Dwarfs

Ultra-faint dwarf galaxies provide a laboratory with which we can explore the nucleosynthetic history of the early Universe and how that affects the chemical evolution of the Milky Way. In the last 5 years, chemical analysis of member stars in these objects have hinted at the highly variable chemical evolution histories. These nucleosynthetic histories have led to unusual abundance patterns, some of which been found in a few stars in the Milky Way halo. Based on the theory that these ultra-faint dwarfs are the progenitors of the Galaxy, it has been suggested that these unusual stars in the halo have their origins in previously disrupted ultra-faint dwarfs. Therefore, by understanding the chemical histories of the currently observable population of ultra-faint dwarfs, we can gain some understanding of the population that would eventually form the Milky Way.

The desire to understand this progenitor population motivates us to study the detailed chemical abundances of member stars in ultra-faint dwarfs. Recent efforts by the Dark Energy Survey Collaboration have identified 22 candidate ultra-faint dwarf in its first two years of operations. Follow-up spectroscopic efforts have led to the confirmation of dark matter halos around these objects and identified member stars for further study using high resolution spectroscopy.

5.2.1 Chemical Abundance Analysis of Three α-Poor, Metal-Poor Stars in the Ultra-Faint Dwarf Galaxy Horologium I

We have performed detailed chemical abundance analysis of three stars in the ultra-faint dwarf satellite galaxy Horologium I (Hor I) using high resolution spectroscopy. Our analysis shows that these stars are indeed very metal-poor ($-2.83 <$ [Fe/H] < -2.43), matching expectations that this is an old population where star formation was quenched early. We also find a lack of neutron-capture elements, indicating that Hor I was not a site for a nucleosynthetic event with high neutron-capture element output, i.e. a neutron star merger.

The key unusualness of the chemical abundance pattern of Hor I is the lack of α-element enrichment. Despite the low metallicity of the object, the three stars observed have solar levels of α-element enhancement ([α/Fe] ~ 0). This is entirely unexpected for a population where Type II supernovae are expected to dominate element formation.

This is not the first time this chemical abundance pattern has been found. Metal-poor stars without α-element enhancement was found in the Milky Way halo by Ivans et al. (2003) and by Aoki et al. (2014). However, the discovery of an ultra-faint dwarf with this chemical signature is a hint that such Milky Way stars may have originated in ultra-faint dwarf with similar chemical evolution histories to Hor I that have already been disrupted.

We have presented a few possible scenarios that may have led to the observed chemical abundance pattern. The first scenario we suggest is that an extended star formation in Hor I have led to the early transition between nucleosynthesis dominated by Type II supernovae and nucleosynthesis dominated by Type Ia supernovae. Previous work by Vargas et al. (2013) demonstrated that this transition occurs when the metallicity of the ultra-faint dwarf is [Fe/H]~ 2.3 dex. This would mean

that Hor I would be the site of the earliest observed transition between these two nucleosynthetic regimes. If this is the case, then the study of more metal-poor stars in Hor I would ultimately reveal this transition.

Another possible explanation is that this chemical abundance may be the signature of a primordial Population III supernovae, a pair-instability supernovae (PISN). In its collapse, the formation of electron/positron pairs in the stellar atmosphere immediately prior to its explosion leads the PISN to produce characteristically low numbers of α-elements. This was originally suggested by Aoki et al. (2014) in their discovery of a similar star in the Milky Way halo. We have compared nucleosynthesis models by Heger & Woosley (2002) and found that we cannot rule out the possibility. If indeed this is the first observational evidence of a PISN, then analysis of more metal-poor stars in Hor I would not show the transition between the Type II supernovae dominated regime and the Type Ia supernovae dominated nucleosynthetic regime.

One final possibility is that Hor I may not be associated with the Milky Way but is in truth a satellite of the Large Magellanic Cloud (LMC). Simulations performed by Jethwa et al. (2016) have made predictions of the kinematic of Hor I if it was associated with the LMC rather than the Milky Way, specifically identifying Hor I as the most likely candidate for being an LMC satellite. Since the LMC has a lower overall α-element enrichment than the Milky Way, then by parallel analogy, Hor I would have an overall lower overall α-element enrichment than the LMC. However, the strongest evidence that Hor I is an LMC satellite is the kinematics; the observed abundance pattern does not strongly support this conclusion nor does it exclude it.

The discovery of another ultra-faint dwarf with an unusual abundance pattern supports the evolving perception that nucleosynthesis in the early Universe was highly stochastic. Each ultra-faint dwarf studied chemically requires a different explanation for how the observed chemical abundance pattern in its member stars came to be. The variety of plausible explanations invoked suggests that nucleosynthetic processes varied from dwarf galaxy to dwarf galaxy. Further analysis of many more ultra-faint dwarfs is required to obtain a broad statistical view of the processes that produced elements in the early Universe.

5.3 Challenges and Future Work

In the course of performing this work, we have identified some challenges that offer approaches for future improvement. Here, we discuss those challenges and possible methods of addressing them in the future. We also discuss future work and other avenues that may arise from this work.

5.3.1 M-dwarf Metallicity through Analysis of Binary Partners

In this project to create a high fidelity sample of F/G/K+M binaries, there were several challenges that made analysis difficult. A key difficulty was the use of low dispersion spectra to determine binary status through radial velocity. Though low resolution spectroscopy is ultimately necessary to study the molecular features identified by Reid et al. (1995), its use lowers the precision of radial velocity measurements. This is most evident in the errors associated with the radial velocity measurement of these candidate secondaries, which range from 11.4 km s^{-1} to 73.3 km s^{-1}.

Future work to improve our identification of binaries should include a better determination of the radial velocities of these M-dwarf secondaries. This could identify more F/G/K+M binaries, enlarging our sample of binaries for use in extending the existing empirical relationships to more metal-poor stars. It would also ensure the fidelity of the stars already identified as "true binaries", increasing our confidence in their use in future analyses. However, it should be noted that the use of higher resolution spectra to measure radial velocity may be belied by the brighter limiting magnitude of high resolution spectroscopy.

Our high fidelity sample can be used to evaluate currently used classification schemes used to identify metal-poor M-dwarfs. Discrepancies found these classification schemes can lead to recalibration as Dhital et al. (2012) did for the work performed by Lépine et al. (2007). We can also evaluate how effective the ζ parameter determined by Dhital et al. (2012) is at tracing the metallicity of M-dwarfs.

We can also use this sample to extend the existing relationships developed by Rojas-Ayala et al. (2012), Newton et al. (2014), and Veyette et al. (2017) to lower metallicities. This will, of course,

require the taking of near-infrared spectra of the M-dwarf secondaries. However, this would increase how far back we can probe in the chemical history of the Milky Way using M-dwarfs as tracers.

However, our goal in creating this sample using observations performed at optical wavelengths is to create an empirically-calibrated relationship similar to Woolf & Wallerstein (2006). Using low resolution optical spectroscopy, we hope to measure the molecular indices identified by Reid et al. (1995). Using them and the accurate photometry from Li et al. (2014), we intend to be able to measure the metal content of an M-dwarf.

This will allow us to rapidly apply this newly developed methodology to the large number of M-dwarf optical spectra in the Sloan Digital Sky Survey. Using the available spectra in this and similar surveys, we can attempt to chemically trace nearby Milky Way structures using M-dwarfs.

5.3.2 Chemical Abundance Analysis of Ultra-Faint Dwarfs

In our analysis of Hor I, the key challenges that determined the elements we could measure and the accuracy of our measurements was the wavelength range available from UVES and the S/N of our observations. The use of the UVES spectrograph in multi-fiber mode, while efficient considering the inclusion of GIRAFFE measurements taken at the same time for a separate project, limited the available wavelength range, preventing the measurement of useful key elements such as those in the neutron capture sequence. This would also allow us to forgo the assumption that we made that the abundance of elements not measured using UVES in these stars can be approximated by the abundance measured in the star observed with MIKE. This can easily be resolved by a follow-up observation using a single-target Echelle spectrograph with a wider wavelength coverage.

A more serious problem is the low S/N of these spectra, which prevented definitive detections of certain element species that would have been useful in ruling out some of our proposed scenarios. For instance, the positive detection and measurement of [Cu/Fe] could allow us to exclude the possibility that Hor I is associated with the LMC (Pompéia et al., 2008). Admittedly, the low S/N also made the determination of stellar parameters difficult due to the faintness of the Fe II lines used to determine the surface gravity of these stars.

A related problem is the low number of member stars for which this analysis was performed. It is somewhat audacious to draw strong conclusions based on the chemical abundance analysis of the three brightest stars in galaxy. Such a small sample may bias our results and may lead to conclusions that are eventually overturned by analysis of more member stars.

However, achieving higher S/N at the present moment is a challenging prospect. With these stars, we are approaching the magnitude limit of high resolution spectroscopy; achieving higher S/N may require an unfeasibly large amount of telescope time. Though there are two more confirmed members of Hor I identified using medium resolution spectroscopy by Koposov et al. (2015b). However, these are faint objects at a g magnitude of 19.08 and 19.31, both difficult to achieve with current high resolution spectrographs even at the largest telescopes available. It may be due to this technological limit that further work on additional members of Hor I will not be completed until the next generation of large telescopes such as the Giant Magellan Telescope (Bernstein et al., 2014) are completed in the coming decade.

This does not mean that further work cannot be done in performing chemical abundance analysis of other ultra-faint dwarfs. Performing detailed metallicity measurements of other ultra-faint dwarfs can hint at how stochastic early Universe nucleosynthesis was. Of particular interest are other ultra-faint dwarfs in the vicinity of the LMC which might share a similar chemical evolution history to Hor I if these dwarfs are indeed satellites of the LMC.

From a theoretical standpoint, better models of nucleosynthesis would be beneficial in understanding these ultra-faint dwarfs. It is a acknowledged problem that Sc and Cr in particular are under-produced in nucleosynthetic models. Heger & Woosley (2010) presume that their underproduction of these elements may be due to unaccounted for production sites in the atmosphere. Accounting for this would make Fe-peak elements a better discriminator between various nucleosynthetic models. Should such models be developed, we would like to apply them to Hor I to see if the scenario where this chemical abundance signature is the preserved fossil record of an PISN can be excluded or supported.

5.4 Concluding Remarks

It has been the goal of this dissertation to contribute to the understanding of the assembly of the Milky Way from a chemical evolution standpoint. We have approached this goal in two ways.

In the first, we provide an avenue of improvement to existing methodologies by creating a sample of high fidelity F/G/K+M binaries. These can be used to extend empirically-calibrated methods of determining M-dwarf metallicity to more metal-poor stars, allowing us to probe further back in the chemical history of the Galaxy than currently possible using M-dwarf as tracers. In the second, we have performed the first detailed chemical abundance analysis of the ultra-faint dwarf Hor I, learning that the overall element abundance pattern is unusual especially with regards to the α-elements. This gives us a glimpse at the chemical evolution of the objects that would eventually merge to become the Milky Way.

The goal of galactic archaeology is to untangle the complex history of the Galaxy's formation and understand how it came to be as it is in the present. This is no small task and requires a variety of approaches both observational and theoretical. However, the current prospects of probing the Galaxy spatially, kinematically, and chemically using both observations and simulations is promising.

Through chemical abundance analysis of various populations, we gain insight on how numerous small dwarf galaxies, each with its own history of star formation and nucleosynthesis, formed the heterogeneous mix that composes our Galaxy today. We can, through the element signature preserved in stars, probe the chemical environment of the disk and halo and learn how element abundances evolved over time. Finally, we can explore the earliest history of the Universe by studying metal-poor stars, giving us glimpse at the origin of the elements.

It is the author's hope that this knowledge, this understanding of the formation of Galaxy in which we exist and the elements that compose us, gives humanity a deeper connection to the Universe and a new perspective of how we came to be.

REFERENCES

Allard, F. 2016, in SF2A-2016: Proceedings of the Annual meeting of the French Society of Astronomy and Astrophysics, ed. C. Reylé, J. Richard, L. Cambrésy, M. Deleuil, E. Pécontal, L. Tresse, & I. Vauglin, 223–227

Alpaslan, M. 2009, ArXiv e-prints. https://arxiv.org/abs/0912.4755

Aoki, W., Tominaga, N., Beers, T. C., Honda, S., & Lee, Y. S. 2014, Science, 345, 912, doi: 10.1126/science.1252633

Asplund, M., Grevesse, N., Sauval, A. J., & Scott, P. 2009, ARA&A, 47, 481, doi: 10.1146/annurev.astro.46.060407.145222

Axer, M., Fuhrmann, K., & Gehren, T. 1994, A&A, 291, 895

Battistini, C., & Bensby, T. 2016, A&A, 586, A49, doi: 10.1051/0004-6361/201527385

Bean, J. L., Sneden, C., Hauschildt, P. H., Johns-Krull, C. M., & Benedict, G. F. 2006, ApJ, 652, 1604, doi: 10.1086/508321

Bechtol, K., Drlica-Wagner, A., Balbinot, E., et al. 2015, ApJ, 807, 50, doi: 10.1088/0004-637X/807/1/50

Beers, T. C., & Christlieb, N. 2005, ARA&A, 43, 531, doi: 10.1146/annurev.astro.42.053102.134057

Belokurov, V. 2013, NewAR, 57, 100, doi: 10.1016/j.newar.2013.07.001

Belokurov, V., Zucker, D. B., Evans, N. W., et al. 2006, ApJ, 647, L111, doi: 10.1086/507324

Bensby, T., Feltzing, S., & Lundström, I. 2003, A&A, 410, 527, doi: 10.1051/0004-6361:20031213

Bergfors, C., Brandner, W., Janson, M., et al. 2010, A&A, 520, A54, doi: 10.1051/0004-6361/201014114

Bernstein, R., Shectman, S. A., Gunnels, S. M., Mochnacki, S., & Athey, A. E. 2003, in Proc. SPIE, Vol. 4841, Instrument Design and Performance for Optical/Infrared Ground-based Telescopes, ed. M. Iye & A. F. M. Moorwood, 1694–1704

Bernstein, R. A., McCarthy, P. J., Raybould, K., et al. 2014, in Proc. SPIE, Vol. 9145, Ground-based and Airborne Telescopes V, 91451C

Bessell, M. S. 1982, Proceedings of the Astronomical Society of Australia, 4, 417

—. 1991, AJ, 101, 662, doi: 10.1086/115714

Biemont, E., Grevesse, N., Hannaford, P., & Lowe, R. M. 1981, ApJ, 248, 867, doi: 10.1086/159213

Biémont, É., Blagoev, K., Engström, L., et al. 2011, MNRAS, 414, 3350, doi: 10.1111/j.1365-2966.2011.18637.x

Bochanski, J. J., Hawley, S. L., Covey, K. R., et al. 2010, AJ, 139, 2679, doi: 10.1088/0004-6256/139/6/2679

Bochanski, J. J., Munn, J. A., Hawley, S. L., et al. 2007, AJ, 134, 2418, doi: 10.1086/522053

Bonfils, X., Delfosse, X., Udry, S., et al. 2005, A&A, 442, 635, doi: 10.1051/0004-6361:20053046

Bromm, V., Coppi, P. S., & Larson, R. B. 1999, ApJ, 527, L5, doi: 10.1086/312385

Brown, T. M., Tumlinson, J., Geha, M., et al. 2014, ApJ, 796, 91, doi: 10.1088/0004-637X/796/2/91

Bullock, J. S., & Johnston, K. V. 2005, ApJ, 635, 931, doi: 10.1086/497422

Caffau, E., Bonifacio, P., François, P., et al. 2013, A&A, 560, A15, doi: 10.1051/0004-6361/201322213

Castelli, F., & Kurucz, R. L. 2004a, ArXiv Astrophysics e-prints

—. 2004b, ArXiv Astrophysics e-prints

Chabrier, G. 2003, PASP, 115, 763, doi: 10.1086/376392

Chanamé, J., & Gould, A. 2004, ApJ, 601, 289, doi: 10.1086/380442

Charbonneau, D., Berta, Z. K., Irwin, J., et al. 2009, Nature, 462, 891, doi: 10.1038/nature08679

Chiti, A., Frebel, A., Ji, A. P., et al. 2018, ApJ, 857, 74, doi: 10.3847/1538-4357/aab4fc

Cohen, J. G., Christlieb, N., McWilliam, A., et al. 2008, ApJ, 672, 320, doi: 10.1086/523638

Cyburt, R. H., Fields, B. D., & Olive, K. A. 2001, NewA, 6, 215, doi: 10.1016/S1384-1076(01)00053-7

Deason, A. J., Wetzel, A. R., Garrison-Kimmel, S., & Belokurov, V. 2015, MNRAS, 453, 3568, doi: 10.1093/mnras/stv1939

Dekker, H., D'Odorico, S., Kaufer, A., Delabre, B., & Kotzlowski, H. 2000, in Proc. SPIE, Vol. 4008, Optical and IR Telescope Instrumentation and Detectors, ed. M. Iye & A. F. Moorwood, 534–545

Den Hartog, E. A., Lawler, J. E., Sneden, C., & Cowan, J. J. 2003, ApJS, 148, 543, doi: 10.1086/376940

—. 2006, ApJS, 167, 292, doi: 10.1086/508262

Den Hartog, E. A., Lawler, J. E., Sobeck, J. S., Sneden, C., & Cowan, J. J. 2011, ApJS, 194, 35, doi: 10.1088/0067-0049/194/2/35

Dhital, S., West, A. A., Stassun, K. G., et al. 2012, AJ, 143, 67, doi: 10.1088/0004-6256/143/3/67

Dotter, A., Chaboyer, B., Jevremović, D., et al. 2008, ApJS, 178, 89, doi: 10.1086/589654

Drlica-Wagner, A., Bechtol, K., Rykoff, E. S., et al. 2015, ApJ, 813, 109, doi: 10.1088/0004-637X/813/2/109

Fischer, D. A., & Valenti, J. 2005, ApJ, 622, 1102, doi: 10.1086/428383

François, P., Monaco, L., Bonifacio, P., et al. 2016, A&A, 588, A7, doi: 10.1051/0004-6361/201527181

Franchini, M., Morossi, C., di Marcantonio, P., Malagnini, M. L., & Chavez, M. 2014, MNRAS, 442, 220, doi: 10.1093/mnras/stu873

Fraunhofer, J. 1905, Bestimmung des Brechungs- und Farbenzerstreuungsvermoegens verschiedener Glasarten. In bezug auf die Vervollkommung achromatischer Fernroehre

Frebel, A., & Bromm, V. 2012, ApJ, 759, 115, doi: 10.1088/0004-637X/759/2/115

Frebel, A., Casey, A. R., Jacobson, H. R., & Yu, Q. 2013, ApJ, 769, 57, doi: 10.1088/0004-637X/769/1/57

Frebel, A., & Norris, J. E. 2015, ARA&A, 53, 631, doi: 10.1146/annurev-astro-082214-122423

Frebel, A., Norris, J. E., Gilmore, G., & Wyse, R. F. G. 2016, ApJ, 826, 110, doi: 10.3847/0004-637X/826/2/110

Frebel, A., Simon, J. D., Geha, M., & Willman, B. 2010, ApJ, 708, 560, doi: 10.1088/0004-637X/708/1/560

Frebel, A., Simon, J. D., & Kirby, E. N. 2014, ApJ, 786, 74, doi: 10.1088/0004-637X/786/1/74

Freeman, K., & Bland-Hawthorn, J. 2002, ARA&A, 40, 487, doi: 10.1146/annurev.astro.40.060401.093840

Fuchs, B., Dettbarn, C., Rix, H.-W., et al. 2009, AJ, 137, 4149, doi: 10.1088/0004-6256/137/5/4149

Gallagher, A. J. 2012, PhD thesis, Centre for Astrophysics Research, Science and Technology Research Institute, University of Hertfordshire <EMAIL>andrew.gallagher@obspm.fr</EMAIL>

Gallagher, A. J., Ryan, S. G., García Pérez, A. E., & Aoki, W. 2010, A&A, 523, A24, doi: 10.1051/0004-6361/201014970

Gilmore, G., Norris, J. E., Monaco, L., et al. 2013, ApJ, 763, 61, doi: 10.1088/0004-637X/763/1/61

Gould, A., Pepper, J., & DePoy, D. L. 2003, ApJ, 594, 533, doi: 10.1086/376852

Hansen, T. T., Simon, J. D., Marshall, J. L., et al. 2017, ApJ, 838, 44, doi: 10.3847/1538-4357/aa634a

Haschke, R., Grebel, E. K., Frebel, A., et al. 2012, AJ, 144, 88, doi: 10.1088/0004-6256/144/3/88

Hayden, M. R., Recio-Blanco, A., de Laverny, P., Mikolaitis, S., & Worley, C. C. 2017, A&A, 608, L1, doi: 10.1051/0004-6361/201731494

Heger, A., & Woosley, S. E. 2002, ApJ, 567, 532, doi: 10.1086/338487

—. 2010, ApJ, 724, 341, doi: 10.1088/0004-637X/724/1/341

Hendricks, B., Koch, A., Lanfranchi, G. A., et al. 2014, ApJ, 785, 102, doi: 10.1088/0004-637X/785/2/102

Hogg, D. W., Casey, A. R., Ness, M., et al. 2016, ApJ, 833, 262, doi: 10.3847/1538-4357/833/2/262

Huggins, W. 1868, Philosophical Transactions of the Royal Society of London Series I, 158, 529

Irwin, J., Charbonneau, D., Nutzman, P., & Falco, E. 2009, 253, 37, doi: 10.1017/S1743921308026215

Ishigaki, M. N., Aoki, W., Arimoto, N., & Okamoto, S. 2014, A&A, 562, A146, doi: 10.1051/0004-6361/201322796

Ivans, I. I., Sneden, C., James, C. R., et al. 2003, ApJ, 592, 906, doi: 10.1086/375812

Janson, M., Hormuth, F., Bergfors, C., et al. 2012, ApJ, 754, 44, doi: 10.1088/0004-637X/754/1/44

Jeon, M., Besla, G., & Bromm, V. 2017, ApJ, 848, 85, doi: 10.3847/1538-4357/aa8c80

Jethwa, P., Erkal, D., & Belokurov, V. 2016, MNRAS, 461, 2212, doi: 10.1093/mnras/stw1343

Ji, A. P., Frebel, A., & Bromm, V. 2015, MNRAS, 454, 659, doi: 10.1093/mnras/stv2052

Ji, A. P., Frebel, A., Chiti, A., & Simon, J. D. 2016a, Nature, 531, 610, doi: 10.1038/nature17425

Ji, A. P., Frebel, A., Ezzeddine, R., & Casey, A. R. 2016b, ApJ, 832, L3, doi: 10.3847/2041-8205/832/1/L3

Ji, A. P., Frebel, A., Simon, J. D., & Chiti, A. 2016c, ApJ, 830, 93, doi: 10.3847/0004-637X/830/2/93

Ji, A. P., Frebel, A., Simon, J. D., & Geha, M. 2016d, ApJ, 817, 41, doi: 10.3847/0004-637X/817/1/41

Johnston, K. V., Bullock, J. S., Sharma, S., et al. 2008, ApJ, 689, 936, doi: 10.1086/592228

Johnston, K. V., Hernquist, L., & Bolte, M. 1996, ApJ, 465, 278, doi: 10.1086/177418

Karlsson, T., Johnson, J. L., & Bromm, V. 2008, ApJ, 679, 6, doi: 10.1086/533520

Kelson, D. D. 2003, PASP, 115, 688, doi: 10.1086/375502

Kim, D., & Jerjen, H. 2015, ApJ, 808, L39, doi: 10.1088/2041-8205/808/2/L39

Kim, D., Jerjen, H., Milone, A. P., Mackey, D., & Da Costa, G. S. 2015, ApJ, 803, 63, doi: 10.1088/0004-637X/803/2/63

Kirby, E. N., Cohen, J. G., Simon, J. D., et al. 2017, ApJ, 838, 83, doi: 10.3847/1538-4357/aa6570

Kirby, E. N., Cohen, J. G., Smith, G. H., et al. 2011, ApJ, 727, 79, doi: 10.1088/0004-637X/727/2/79

Kirby, E. N., Guhathakurta, P., Bolte, M., Sneden, C., & Geha, M. C. 2009, ApJ, 705, 328, doi: 10.1088/0004-637X/705/1/328

Kirchhoff, G. 1860, Annalen der Physik, 185, 148, doi: 10.1002/andp.18601850115

Kirchhoff, G., & Bunsen, R. 1860, Annalen der Physik, 186, 161, doi: 10.1002/andp.18601860602

Kirkpatrick, J. D., Henry, T. J., & Simons, D. A. 1995, AJ, 109, 797, doi: 10.1086/117323

Koch, A., Feltzing, S., Adén, D., & Matteucci, F. 2013, A&A, 554, A5, doi: 10.1051/0004-6361/201220742

Koch, A., Grebel, E. K., Gilmore, G. F., et al. 2008a, AJ, 135, 1580, doi: 10.1088/0004-6256/135/4/1580

Koch, A., McWilliam, A., Grebel, E. K., Zucker, D. B., & Belokurov, V. 2008b, ApJ, 688, L13, doi: 10.1086/595001

Koposov, S. E., Belokurov, V., Torrealba, G., & Evans, N. W. 2015a, ApJ, 805, 130, doi: 10.1088/0004-637X/805/2/130

Koposov, S. E., Casey, A. R., Belokurov, V., et al. 2015b, ApJ, 811, 62, doi: 10.1088/0004-637X/811/1/62

Kordopatis, G., Gilmore, G., Steinmetz, M., et al. 2013, AJ, 146, 134, doi: 10.1088/0004-6256/146/5/134

Kramida, A., Yu. Ralchenko, Reader, J., & and NIST ASD Team. 2018, NIST Atomic Spectra Database (ver. 5.5.2), [Online]. Available: `https://physics.nist.gov/asd` [2018, February 1]. National Institute of Standards and Technology, Gaithersburg, MD.

Kunder, A., Kordopatis, G., Steinmetz, M., et al. 2017, AJ, 153, 75, doi: 10.3847/1538-3881/153/2/75

Kurucz, R. L., & Bell, B. 1995, Atomic line list

Lapenna, E., Mucciarelli, A., Origlia, L., & Ferraro, F. R. 2012, ApJ, 761, 33, doi: 10.1088/0004-637X/761/1/33

Latham, D. W., Stefanik, R. P., Torres, G., et al. 2002, AJ, 124, 1144, doi: 10.1086/341384

Laughlin, G., Bodenheimer, P., & Adams, F. C. 1997, ApJ, 482, 420, doi: 10.1086/304125

Lawler, J. E., Bonvallet, G., & Sneden, C. 2001a, ApJ, 556, 452, doi: 10.1086/321549

Lawler, J. E., & Dakin, J. T. 1989, Journal of the Optical Society of America B Optical Physics, 6, 1457, doi: 10.1364/JOSAB.6.001457

Lawler, J. E., Den Hartog, E. A., Sneden, C., & Cowan, J. J. 2006, ApJS, 162, 227, doi: 10.1086/498213

Lawler, J. E., Guzman, A., Wood, M. P., Sneden, C., & Cowan, J. J. 2013, ApJS, 205, 11, doi: 10.1088/0067-0049/205/2/11

Lawler, J. E., Sneden, C., & Cowan, J. J. 2015, ApJS, 220, 13, doi: 10.1088/0067-0049/220/1/13

Lawler, J. E., Sneden, C., Cowan, J. J., Ivans, I. I., & Den Hartog, E. A. 2009, ApJS, 182, 51, doi: 10.1088/0067-0049/182/1/51

Lawler, J. E., Sneden, C., Cowan, J. J., et al. 2008, ApJS, 178, 71, doi: 10.1086/589834

Lawler, J. E., Wickliffe, M. E., Cowley, C. R., & Sneden, C. 2001b, ApJS, 137, 341, doi: 10.1086/323001

Lawler, J. E., Wickliffe, M. E., den Hartog, E. A., & Sneden, C. 2001c, ApJ, 563, 1075, doi: 10.1086/323407

Lawler, J. E., Wood, M. P., Den Hartog, E. A., et al. 2014, ApJS, 215, 20, doi: 10.1088/0067-0049/215/2/20

Lawler, J. E., Wyart, J.-F., & Blaise, J. 2001d, ApJS, 137, 351, doi: 10.1086/323000

Lépine, S. 2005, AJ, 130, 1680, doi: 10.1086/432792

—. 2008, AJ, 135, 2177, doi: 10.1088/0004-6256/135/6/2177

Lépine, S., Rich, R. M., & Shara, M. M. 2003, AJ, 125, 1598, doi: 10.1086/345972

—. 2007, ApJ, 669, 1235, doi: 10.1086/521614

Lépine, S., & Shara, M. M. 2005a, AJ, 129, 1483, doi: 10.1086/427854

—. 2005b, AJ, 129, 1483, doi: 10.1086/427854

Li, R., Chatelain, R., Holt, R. A., et al. 2007, Phys. Scr, 76, 577, doi: 10.1088/0031-8949/76/5/028

Li, T., Marshall, J. L., Lépine, S., Williams, P., & Chavez, J. 2014, AJ, 148, 60, doi: 10.1088/0004-6256/148/4/60

Li, T. S., Simon, J. D., Drlica-Wagner, A., et al. 2017, ApJ, 838, 8, doi: 10.3847/1538-4357/aa6113

Lind, K., Asplund, M., Barklem, P. S., & Belyaev, A. K. 2011, A&A, 528, A103, doi: 10.1051/0004-6361/201016095

Luque, E., Queiroz, A., Santiago, B., et al. 2016, MNRAS, 458, 603, doi: 10.1093/mnras/stw302

Luque, E., Pieres, A., Santiago, B., et al. 2017, MNRAS, 468, 97, doi: 10.1093/mnras/stx405

Majewski, S. R., Schiavon, R. P., Frinchaboy, P. M., et al. 2017, AJ, 154, 94, doi: 10.3847/1538-3881/aa784d

Mann, A. W., Brewer, J. M., Gaidos, E., Lépine, S., & Hilton, E. J. 2013, AJ, 145, 52, doi: 10.1088/0004-6256/145/2/52

Marshall, J. L. 2008, AJ, 135, 1000, doi: 10.1088/0004-6256/135/3/1000

Massarotti, A., Latham, D. W., Stefanik, R. P., & Fogel, J. 2008, AJ, 135, 209, doi: 10.1088/0004-6256/135/1/209

Masseron, T., Plez, B., Van Eck, S., et al. 2014, A&A, 571, A47, doi: 10.1051/0004-6361/201423956

McConnachie, A. W. 2012, AJ, 144, 4, doi: 10.1088/0004-6256/144/1/4

McWilliam, A. 1997, ARA&A, 35, 503, doi: 10.1146/annurev.astro.35.1.503

McWilliam, A., & Rich, R. M. 1994, ApJS, 91, 749, doi: 10.1086/191954

Modigliani, A., Mulas, G., Porceddu, I., et al. 2004, The Messenger, 118, 8

Mould, J. R. 1976, ApJ, 207, 535, doi: 10.1086/154521

Newton, E. R., Charbonneau, D., Irwin, J., et al. 2014, AJ, 147, 20, doi: 10.1088/0004-6256/147/1/20

Nidever, D. L., Marcy, G. W., Butler, R. P., Fischer, D. A., & Vogt, S. S. 2002, ApJS, 141, 503, doi: 10.1086/340570

Norris, J. E., Wyse, R. F. G., Gilmore, G., et al. 2010, ApJ, 723, 1632, doi: 10.1088/0004-637X/723/2/1632

Nutzman, P., & Charbonneau, D. 2008a, PASP, 120, 317, doi: 10.1086/533420

—. 2008b, PASP, 120, 317, doi: 10.1086/533420

Palmeri, P., Fischer, C. F., Wyart, J.-F., & Godefroid, M. R. 2005, MNRAS, 363, 452, doi: 10.1111/j.1365-2966.2005.09410.x

Pasquini, L., Avila, G., Allaert, E., et al. 2000, in Proc. SPIE, Vol. 4008, Optical and IR Telescope

Instrumentation and Detectors, ed. M. Iye & A. F. Moorwood, 129–140

Payne, C. H. 1925, PhD thesis, RADCLIFFE COLLEGE.

Pompéia, L., Hill, V., Spite, M., et al. 2008, A&A, 480, 379, doi: 10.1051/0004-6361:20064854

Ramírez, I., Allende Prieto, C., & Lambert, D. L. 2013, ApJ, 764, 78, doi: 10.1088/0004-637X/764/1/78

Reid, I. N., Hawley, S. L., & Gizis, J. E. 1995, AJ, 110, 1838, doi: 10.1086/117655

Robertson, B., Bullock, J. S., Font, A. S., Johnston, K. V., & Hernquist, L. 2005, ApJ, 632, 872, doi: 10.1086/452619

Roederer, I. U., & Kirby, E. N. 2014, MNRAS, 440, 2665, doi: 10.1093/mnras/stu491

Roederer, I. U., Preston, G. W., Thompson, I. B., et al. 2014, AJ, 147, 136, doi: 10.1088/0004-6256/147/6/136

Roederer, I. U., Mateo, M., Bailey, III, J. I., et al. 2016, AJ, 151, 82, doi: 10.3847/0004-6256/151/3/82

Rojas-Ayala, B., Covey, K. R., Muirhead, P. S., & Lloyd, J. P. 2012, ApJ, 748, 93, doi: 10.1088/0004-637X/748/2/93

Ruffoni, M. P., Den Hartog, E. A., Lawler, J. E., et al. 2014, MNRAS, 441, 3127, doi: 10.1093/mnras/stu780

Saha, M. N. 1921, Proceedings of the Royal Society of London Series A, 99, 135, doi: 10.1098/rspa.1921.0029

Sales, L. V., Navarro, J. F., Kallivayalil, N., & Frenk, C. S. 2017, MNRAS, 465, 1879, doi: 10.1093/mnras/stw2816

Salim, S., & Gould, A. 2003, ApJ, 582, 1011, doi: 10.1086/344822

Schlaufman, K. C., & Laughlin, G. 2011, ApJ, 738, 177, doi: 10.1088/0004-637X/738/2/177

Searle, L., & Zinn, R. 1978, ApJ, 225, 357, doi: 10.1086/156499

Simon, J. D., Frebel, A., McWilliam, A., Kirby, E. N., & Thompson, I. B. 2010, ApJ, 716, 446, doi: 10.1088/0004-637X/716/1/446

Simon, J. D., Jacobson, H. R., Frebel, A., et al. 2015a, ApJ, 802, 93, doi: 10.1088/0004-637X/802/

2/93

—. 2015b, ApJ, 802, 93, doi: 10.1088/0004-637X/802/2/93

Simon, J. D., Li, T. S., Drlica-Wagner, A., et al. 2017, ApJ, 838, 11, doi: 10.3847/1538-4357/aa5be7

Skrutskie, M. F., Cutri, R. M., Stiening, R., et al. 2006, AJ, 131, 1163, doi: 10.1086/498708

Sneden, C. 1973, ApJ, 184, 839, doi: 10.1086/152374

Sneden, C., Cowan, J. J., Kobayashi, C., et al. 2016, ApJ, 817, 53, doi: 10.3847/0004-637X/817/1/53

Sneden, C., Lawler, J. E., Cowan, J. J., Ivans, I. I., & Den Hartog, E. A. 2009, ApJS, 182, 80, doi: 10.1088/0067-0049/182/1/80

Sneden, C., Lucatello, S., Ram, R. S., Brooke, J. S. A., & Bernath, P. 2014, ApJS, 214, 26, doi: 10.1088/0067-0049/214/2/26

Sneden, C., Uomoto, A., Cottrell, P., & Fitzpatrick, M. 2012, SPECTRE: Manipulation of single-order spectra, Astrophysics Source Code Library. http://ascl.net/1202.010

Sobeck, J. S., Lawler, J. E., & Sneden, C. 2007, ApJ, 667, 1267, doi: 10.1086/519987

Sobeck, J. S., Kraft, R. P., Sneden, C., et al. 2011, AJ, 141, 175, doi: 10.1088/0004-6256/141/6/175

Soubiran, C., Jasniewicz, G., Chemin, L., et al. 2013, A&A, 552, A64, doi: 10.1051/0004-6361/201220927

The Dark Energy Survey Collaboration. 2005, ArXiv Astrophysics e-prints

Tian, H.-J., Gupta, P., Sesar, B., et al. 2017, ApJS, 232, 4, doi: 10.3847/1538-4365/aa826a

Tinsley, B. M. 1979, ApJ, 229, 1046, doi: 10.1086/157039

Tonry, J., & Davis, M. 1979, AJ, 84, 1511, doi: 10.1086/112569

Van der Swaelmen, M., Hill, V., Primas, F., & Cole, A. A. 2013, A&A, 560, A44, doi: 10.1051/0004-6361/201321109

Vargas, L. C., Geha, M., Kirby, E. N., & Simon, J. D. 2013, ApJ, 767, 134, doi: 10.1088/0004-637X/767/2/134

Venn, K. A., Irwin, M., Shetrone, M. D., et al. 2004, AJ, 128, 1177, doi: 10.1086/422734

Venn, K. A., Starkenburg, E., Malo, L., Martin, N., & Laevens, B. P. M. 2017, MNRAS, 466, 3741, doi: 10.1093/mnras/stw3198

Veyette, M. J., Muirhead, P. S., Mann, A. W., et al. 2017, ApJ, 851, 26, doi: 10.3847/1538-4357/aa96aa

Walker, M. G., Mateo, M., Olszewski, E. W., et al. 2016, ApJ, 819, 53, doi: 10.3847/0004-637X/819/1/53

Ward-Duong, K., Patience, J., De Rosa, R. J., et al. 2015, MNRAS, 449, 2618, doi: 10.1093/mnras/stv384

Wenger, M., Ochsenbein, F., Egret, D., et al. 2000, A&AS, 143, 9, doi: 10.1051/aas:2000332

West, A. A., Morgan, D. P., Bochanski, J. J., et al. 2011, AJ, 141, 97, doi: 10.1088/0004-6256/141/3/97

Wetzel, A. R., Deason, A. J., & Garrison-Kimmel, S. 2015, ApJ, 807, 49, doi: 10.1088/0004-637X/807/1/49

Wickliffe, M. E., Lawler, J. E., & Nave, G. 2000, J. Quant. Spec. Radiat. Transf., 66, 363, doi: 10.1016/S0022-4073(99)00173-9

Wickliffe, M. E., Salih, S., & Lawler, J. E. 1994, J. Quant. Spec. Radiat. Transf., 51, 545, doi: 10.1016/0022-4073(94)90108-2

Willman, B., & Strader, J. 2012, AJ, 144, 76, doi: 10.1088/0004-6256/144/3/76

Wood, M. P., Lawler, J. E., Sneden, C., & Cowan, J. J. 2014, ApJS, 211, 20, doi: 10.1088/0067-0049/211/2/20

Woolf, V. M., & Wallerstein, G. 2005, MNRAS, 356, 963, doi: 10.1111/j.1365-2966.2004.08515.x

—. 2006, PASP, 118, 218, doi: 10.1086/498459

Yong, D., Norris, J. E., Bessell, M. S., et al. 2013, ApJ, 762, 26, doi: 10.1088/0004-637X/762/1/26

York, D. G., Adelman, J., Anderson, Jr., J. E., et al. 2000, AJ, 120, 1579, doi: 10.1086/301513

APPENDIX A

ATOMIC SPECIES LINE LIST FOR USE IN STELLAR CHEMICAL ABUNDANCE ANALYSIS

Table A.1: Atomic Line Data

Species	λ (Å)	E.P. (eV)	log(gf) (dex)	Reference
Fe I	4045.81	1.48	0.28	Castelli & Kurucz (2004b)
Fe I	4063.59	1.56	0.06	Kramida et al. (2018)
Fe I	4071.74	1.61	−0.02	Castelli & Kurucz (2004b)
Fe I	4147.67	1.48	−2.10	Castelli & Kurucz (2004b)
Fe I	4216.18	0.00	−3.36	Castelli & Kurucz (2004b)
Fe I	4250.13	2.47	−0.41	Kramida et al. (2018)
Fe I	4260.47	2.40	0.08	Kramida et al. (2018)
Fe I	4415.12	1.61	−0.62	Castelli & Kurucz (2004b)
Fe I	4427.31	0.05	−3.04	Castelli & Kurucz (2004b)
Fe I	4430.61	2.22	−1.73	Kramida et al. (2018)
Fe I	4442.34	2.22	−1.26	Castelli & Kurucz (2004b)
Fe I	4447.72	2.22	−1.34	Kramida et al. (2018)
Fe I	4459.12	2.17	−1.28	Kramida et al. (2018)
Fe I	4461.65	0.09	−3.21	Kramida et al. (2018)
Fe I	4466.55	2.83	−0.59	Kramida et al. (2018)
Fe I	4489.74	0.12	−3.97	Kramida et al. (2018)
Fe I	4494.56	2.20	−1.14	Kramida et al. (2018)
Fe I	4528.61	2.18	−0.82	Castelli & Kurucz (2004b)
Fe I	4531.15	1.48	−2.16	Castelli & Kurucz (2004b)
Fe I	4592.65	1.56	−2.45	Kramida et al. (2018)
Fe I	4602.94	1.48	−1.95	Castelli & Kurucz (2004b)
Fe I	4707.27	3.24	−1.08	Castelli & Kurucz (2004b)
Fe I	4736.77	3.21	−0.74	Castelli & Kurucz (2004b)
Fe I	4802.88	3.64	−1.51	Castelli & Kurucz (2004b)
Fe I	4871.32	2.86	−0.36	Kramida et al. (2018)
Fe I	4872.14	2.88	−0.57	Kramida et al. (2018)
Fe I	4890.76	2.88	−0.38	Ruffoni et al. (2014)
Fe I	4891.49	2.85	−0.14	Kramida et al. (2018)
Fe I	4903.31	2.88	−0.93	Kramida et al. (2018)
Fe I	4918.99	2.87	−0.34	Kramida et al. (2018)
Fe I	4920.50	2.83	0.06	Kramida et al. (2018)

Table A.1: Atomic Line Data *(continued)*

Species	λ (Å)	E.P. (eV)	log(gf) (dex)	Reference
Fe I	4938.81	2.88	−1.08	Kramida et al. (2018)
Fe I	4939.69	0.86	−3.34	Castelli & Kurucz (2004b)
Fe I	5051.63	0.92	−2.80	Castelli & Kurucz (2004b)
Fe I	5083.34	0.96	−2.96	Castelli & Kurucz (2004b)
Fe I	5098.70	2.17	−2.03	Castelli & Kurucz (2004b)
Fe I	5110.41	0.00	−3.76	Castelli & Kurucz (2004b)
Fe I	5127.36	0.91	−3.31	Castelli & Kurucz (2004b)
Fe I	5150.84	0.99	−3.07	Castelli & Kurucz (2004b)
Fe I	5166.28	0.00	−4.20	Castelli & Kurucz (2004b)
Fe I	5171.60	1.48	−1.79	Castelli & Kurucz (2004b)
Fe I	5191.45	3.04	−0.55	Kramida et al. (2018)
Fe I	5194.94	1.56	−2.09	Castelli & Kurucz (2004b)
Fe I	5215.18	3.26	−0.87	Kramida et al. (2018)
Fe I	5266.56	3.00	−0.39	Kramida et al. (2018)
Fe I	5324.18	3.21	−0.11	Ruffoni et al. (2014)
Fe I	5328.04	0.91	−1.47	Castelli & Kurucz (2004b)
Fe I	5328.53	1.56	−1.85	Castelli & Kurucz (2004b)
Fe I	5371.49	0.96	−1.64	Castelli & Kurucz (2004b)
Fe I	5397.13	0.91	−1.98	Castelli & Kurucz (2004b)
Fe I	5405.78	0.99	−1.85	Castelli & Kurucz (2004b)
Fe I	5415.20	4.39	0.64	Kramida et al. (2018)
Fe I	5429.70	0.96	−1.88	Castelli & Kurucz (2004b)
Fe I	5434.52	1.01	−2.13	Castelli & Kurucz (2004b)
Fe I	5455.61	1.01	−2.09	Castelli & Kurucz (2004b)
Fe I	5497.52	1.01	−2.85	Castelli & Kurucz (2004b)
Fe I	5501.47	0.96	−3.05	Kramida et al. (2018)
Fe I	5506.78	0.99	−2.79	Castelli & Kurucz (2004b)
Fe I	5615.64	3.33	0.05	Kramida et al. (2018)
Fe I	6173.34	2.22	−2.88	Castelli & Kurucz (2004b)
Fe I	6200.32	2.61	−2.44	Castelli & Kurucz (2004b)
Fe I	6213.44	2.22	−2.56	Castelli & Kurucz (2004b)
Fe I	6240.65	2.22	−3.23	Castelli & Kurucz (2004b)
Fe I	6265.14	2.18	−2.55	Castelli & Kurucz (2004b)
Fe I	6322.69	2.59	−2.43	Castelli & Kurucz (2004b)
Fe I	6481.88	2.28	−2.97	Castelli & Kurucz (2004b)
Fe I	6518.37	2.83	−2.45	Castelli & Kurucz (2004b)
Fe I	6581.21	1.48	−4.68	Castelli & Kurucz (2004b)
Fe I	8387.77	2.17	−1.49	Castelli & Kurucz (2004b)
Fe I	8688.62	2.17	−1.20	Castelli & Kurucz (2004b)
Fe II	4508.29	2.85	−2.21	Castelli & Kurucz (2004b)

Table A.1: Atomic Line Data *(continued)*

Species	λ (Å)	E.P. (eV)	log(gf) (dex)	Reference
Fe II	4583.84	2.81	−2.02	Castelli & Kurucz (2004b)
Fe II	4923.93	2.89	−1.32	Castelli & Kurucz (2004b)
Fe II	5197.57	3.23	−2.10	Castelli & Kurucz (2004b)
Fe II	6149.25	3.89	−2.63	Castelli & Kurucz (2004b)
Fe II	6247.56	3.89	−2.27	Castelli & Kurucz (2004b)
Fe II	6432.68	2.89	−3.52	Castelli & Kurucz (2004b)
Fe II	6456.39	3.90	−2.06	Castelli & Kurucz (2004b)
CH	4310.00	band	band	Masseron et al. (2014)
CN	3880.00	band	band	Sneden et al. (2014)
Na I	5889.95	0.00	0.12	Castelli & Kurucz (2004b)
Na I	5895.93	0.00	−0.18	Castelli & Kurucz (2004b)
Mg I	4571.10	0.00	−5.62	Kramida et al. (2018)
Mg I	4702.99	4.33	−0.38	Kramida et al. (2018)
Mg I	5172.68	2.71	−0.40	Castelli & Kurucz (2004b)
Mg I	5183.60	2.71	−0.18	Castelli & Kurucz (2004b)
Mg I	5528.40	4.34	−0.50	Castelli & Kurucz (2004b)
Al I	3944.01	0.00	−0.62	Castelli & Kurucz (2004b)
Al I	3961.52	0.01	−0.32	Castelli & Kurucz (2004b)
Si I	4102.94	1.91	−3.14	Castelli & Kurucz (2004b)
Si I	4817.58	4.95	−1.91	Castelli & Kurucz (2004b)
Si I	4818.05	4.95	−1.38	Castelli & Kurucz (2004b)
Si I	5258.84	5.61	−0.18	Castelli & Kurucz (2004b)
Si I	5660.68	5.61	−1.16	Castelli & Kurucz (2004b)
Si I	5665.23	4.92	−2.04	Castelli & Kurucz (2004b)
Si I	5701.10	4.93	−2.05	Castelli & Kurucz (2004b)
Si I	5708.40	4.95	−1.47	Castelli & Kurucz (2004b)
Ca I	4425.39	1.88	−0.39	Kramida et al. (2018)
Ca I	4434.96	1.89	−0.01	Kramida et al. (2018)
Ca I	4455.89	1.90	−0.51	Kramida et al. (2018)
Ca I	6122.17	1.89	−0.32	Kramida et al. (2018)
Ca I	6162.17	1.90	0.10	Kramida et al. (2018)
Ca I	6439.03	2.52	0.47	Kramida et al. (2018)
Sc II	4400.39	0.61	−1.76	Lawler & Dakin (1989); Kurucz & Bell (1995)
Sc II	4415.54	0.60	−1.29	Lawler & Dakin (1989); Kurucz & Bell (1995)
Sc II	4420.66	0.62	−2.94	Lawler & Dakin (1989); Kurucz & Bell (1995)
Sc II	5526.79	1.77	−0.52	Lawler & Dakin (1989); Kurucz & Bell (1995)
Ti I	4870.13	2.25	0.44	Lawler et al. (2013)
Ti I	4981.73	0.85	0.57	Lawler et al. (2013)
Ti I	5173.74	0.00	−1.06	Lawler et al. (2013)
Ti I	5186.32	2.12	−1.05	Castelli & Kurucz (2004b)

Table A.1: Atomic Line Data *(continued)*

Species	λ (Å)	E.P. (eV)	log(gf) (dex)	Reference
Ti I	5192.97	0.02	−0.95	Lawler et al. (2013)
Ti I	5193.88	2.34	−1.15	Lawler et al. (2013)
V I	4005.26	1.87	−3.58	Lawler et al. (2014)
V I	6274.65	0.27	−2.13	Lawler et al. (2014)
V I	6285.15	0.28	−2.08	Lawler et al. (2014)
V I	6531.43	1.22	−1.78	Lawler et al. (2014)
Cr I	4540.49	2.54	−0.52	Sobeck et al. (2007)
Cr I	4541.06	2.54	−1.15	Sobeck et al. (2007)
Cr I	4544.60	2.54	−0.59	Sobeck et al. (2007)
Cr I	4545.95	0.94	−1.37	Sobeck et al. (2007)
Cr I	5206.04	0.94	0.02	Sobeck et al. (2007)
Cr I	5208.42	0.94	0.17	Sobeck et al. (2007)
Cr I	5296.69	0.98	−1.36	Sobeck et al. (2007)
Cr I	5298.28	0.98	−1.14	Sobeck et al. (2007)
Mn I	4502.22	2.92	−1.48	Den Hartog et al. (2011)
Mn I	4754.04	2.28	−0.79	Den Hartog et al. (2011)
Mn I	4826.50	3.13	−10.54	Den Hartog et al. (2011)
Mn I	5341.05	2.11	−2.66	Den Hartog et al. (2011)
Mn I	5537.71	2.19	−2.81	Den Hartog et al. (2011)
Co I	3995.30	0.92	−1.11	Lawler et al. (2015)
Co I	4110.54	1.05	−2.21	Lawler et al. (2015)
Co I	4118.77	1.05	−1.12	Lawler et al. (2015)
Co I	4121.32	0.92	−1.66	Lawler et al. (2015)
Ni I	5115.00	3.09	−4.45	Castelli & Kurucz (2004b)
Ni I	5476.90	1.83	−0.78	Wood et al. (2014)
Ni I	6643.63	1.68	−2.22	Wood et al. (2014)
Ni I	6767.77	1.83	−2.14	Wood et al. (2014)
Cu I	5015.54	1.39	−2.15	Kurucz & Bell (1995)
Cu I	5218.20	3.81	−0.66	Kurucz & Bell (1995)
Cu I	5782.13	1.64	−2.08	Kurucz & Bell (1995)
Zn I	4722.15	4.03	−0.34	Castelli & Kurucz (2004b)
Zn I	4810.53	4.08	−0.14	Castelli & Kurucz (2004b)
Ga I	4172.04	0.10	−0.27	Castelli & Kurucz (2004b)
Rb I	7800.26	0.00	0.14	Castelli & Kurucz (2004b)
Rb I	7947.60	0.00	−0.17	Castelli & Kurucz (2004b)
Sr II	4077.71	0.00	0.17	Castelli & Kurucz (2004b)
Sr II	4161.79	2.94	−0.50	Castelli & Kurucz (2004b)
Sr II	4215.52	0.00	−0.14	Castelli & Kurucz (2004b)
Y II	5119.11	0.99	−1.36	Biémont et al. (2011)
Y II	5200.41	0.99	−0.57	Biémont et al. (2011)

Table A.1: Atomic Line Data *(continued)*

Species	λ (Å)	E.P. (eV)	log(gf) (dex)	Reference
Y II	5205.73	1.03	−0.34	Biémont et al. (2011)
Y II	5289.82	1.03	−1.85	Biémont et al. (2011)
Zr II	4149.20	0.80	−0.03	Biemont et al. (1981)
Zr II	4161.21	0.71	−0.72	Biemont et al. (1981)
Zr II	4208.99	0.71	−0.46	Biemont et al. (1981)
Zr II	4211.91	0.53	−1.08	Castelli & Kurucz (2004b)
Nb II	3818.78	1.59	−0.14	Castelli & Kurucz (2004b)
Mo I	3864.10	0.00	−0.01	Castelli & Kurucz (2004b)
Tc I	4262.27	0.00	−0.35	Palmeri et al. (2005)
Ru I	4709.48	1.13	−0.33	Wickliffe et al. (1994)
Ba II	4554.00	0.00	0.17	Gallagher et al. (2010)
Ba II	4934.07	0.00	−2.36	Gallagher et al. (2010)
Ba II	5853.69	0.60	−1.01	Gallagher (2012)
Ba II	6141.73	0.70	−0.08	Gallagher (2012)
La II	4662.50	0.00	−1.76	Lawler et al. (2001a)
La II	4748.73	0.93	−0.54	Lawler et al. (2001a)
La II	5290.82	0.00	−1.65	Lawler et al. (2001a)
La II	5303.51	0.32	−1.87	Lawler et al. (2001a)
La II	6262.29	0.40	−2.13	Lawler et al. (2001a)
Ce II	4418.78	0.86	0.27	Lawler et al. (2009)
Ce II	4486.90	0.32	−1.87	Lawler et al. (2009)
Ce II	4562.36	0.48	0.21	Lawler et al. (2009)
Ce II	4628.16	0.52	0.14	Lawler et al. (2009)
Ce II	5274.23	1.04	0.13	Lawler et al. (2009)
Pr II	4408.82	0.00	−0.75	Li et al. (2007); Sneden et al. (2009)
Pr II	4510.15	0.42	−0.46	Li et al. (2007); Sneden et al. (2009)
Pr II	5259.73	0.63	−0.54	Li et al. (2007); Sneden et al. (2009)
Pr II	5322.77	0.48	−0.92	Li et al. (2007); Sneden et al. (2009)
Nd II	4706.54	0.00	−0.71	Den Hartog et al. (2003)
Nd II	4825.48	0.18	−0.42	Den Hartog et al. (2003)
Nd II	4914.38	0.38	−0.70	Den Hartog et al. (2003)
Nd II	5255.51	0.20	−0.67	Den Hartog et al. (2003)
Nd II	5293.16	0.82	0.10	Den Hartog et al. (2003)
Nd II	5319.81	0.55	−0.14	Den Hartog et al. (2003)
Sm II	4318.93	0.28	−0.25	Lawler et al. (2006)
Sm II	4424.34	0.48	0.14	Lawler et al. (2006)
Sm II	4537.94	0.48	−0.48	Lawler et al. (2006)
Sm II	4715.27	0.10	−1.46	Lawler et al. (2006)
Sm II	4719.84	0.04	−1.24	Lawler et al. (2006)
Eu II	4129.60	0.00	−1.03	Lawler et al. (2001c)

Table A.1: Atomic Line Data *(continued)*

Species	λ (Å)	E.P. (eV)	log(gf) (dex)	Reference
Eu II	4205.01	0.00	−0.77	Lawler et al. (2001c)
Eu II	4522.56	0.21	−1.27	Lawler et al. (2001c)
Eu II	5966.05	1.25	−1.75	Lawler et al. (2001c)
Eu II	6437.63	1.32	−1.07	Lawler et al. (2001c)
Gd II	4215.02	0.43	−0.44	Den Hartog et al. (2006)
Gd II	4251.73	0.38	−0.22	Den Hartog et al. (2006)
Gd II	4498.29	0.43	−1.08	Den Hartog et al. (2006)
Tb II	4002.57	0.64	−0.49	Lawler et al. (2001b,d)
Tb II	4005.47	0.13	−0.02	Lawler et al. (2001b)
Tb II	4752.53	0.00	−0.55	Lawler et al. (2001b)
Dy II	3944.68	0.00	0.11	Wickliffe et al. (2000)
Dy II	4103.31	0.10	−0.38	Wickliffe et al. (2000)
Dy II	4449.70	0.00	−1.03	Wickliffe et al. (2000)
Er II	3896.23	0.06	−0.12	Lawler et al. (2008)
Er II	3938.63	0.00	−0.52	Castelli & Kurucz (2004b)

This table is available in its entirety in machine-readable form.

APPENDIX B

EQUIVALENT WIDTH MEASUREMENTS

Table B.1: Equivalent Width Measurements for F/G/K Primaries

Species	λ	E.P.	log(gf)	PM I00025-4644	
	(Å)	(eV)	(dex)	EW (mÅ)	Abundance
Fe I	5141.750	2.424	−2.18	124.5	6.93
Fe I	5247.060	0.087	−4.94	85.9	6.40
Fe I	5358.120	3.300	−3.16	···	···
Fe I	5412.788	4.440	−1.71	···	···
Fe I	5661.348	4.280	−1.75	···	···
Fe I	5778.458	2.590	−3.45	40.4	7.08
Fe I	5784.660	3.400	−2.53	···	···
Fe I	5809.220	3.884	−1.61	31.7	6.59
Fe I	5849.690	3.695	−2.93	···	···
Fe I	5852.230	4.549	−1.17	30.6	6.89
Fe I	5855.090	4.608	−1.48	···	···
Fe I	5856.100	4.294	−1.56	···	···
Fe I	5858.790	4.220	−2.18	···	···
Fe I	5859.600	4.550	−0.61	46.0	6.60
Fe I	5862.370	4.550	−0.25	71.3	6.60
Fe I	5956.700	0.859	−4.60	77.2	6.76
Fe I	6027.060	4.070	−1.17	34.9	6.43
Fe I	6151.620	2.176	−3.28	55.2	6.66
Fe I	6159.380	4.610	−1.83	···	···
Fe I	6165.360	4.143	−1.46	···	···
Fe I	6173.340	2.223	−2.88	77.9	6.69
Fe I	6200.320	2.609	−2.44	86.0	6.84
Fe I	6213.440	2.223	−2.56	103.8	6.76
Fe I	6240.652	2.220	−3.23	54.3	6.64
Fe I	6265.140	2.176	−2.55	115.1	6.83
Fe I	6271.283	3.330	−2.70	···	···
Fe I	6297.801	2.223	−2.73	80.7	6.59
Fe I	6322.694	2.588	−2.43	75.3	6.63
Fe I	6358.690	0.859	−4.00	92.2	6.39
Fe I	6436.410	4.186	−2.36	···	···
Fe I	6481.878	2.279	−2.97	65.5	6.63
Fe I	6498.950	0.958	−4.69	69.2	6.78
Fe I	6518.370	2.830	−2.45	57.3	6.64
Fe I	6574.233	0.990	−5.00	51.6	6.82

Table B.1: Equivalent Width Measurements for F/G/K Primaries *(continued)*

Species	λ	E.P.	log(gf)	PM I00025-4644	
	(Å)	(eV)	(dex)	EW (mÅ)	Abundance
Fe I	6581.214	1.480	−4.68	26.0	6.62
Fe I	6591.330	4.593	−1.95	···	···
Fe I	6608.040	2.279	−3.91	···	···
Fe I	6625.027	1.010	−5.34	40.6	6.98
Fe I	6699.142	4.590	−2.10	···	···
Fe I	6713.750	4.795	−1.39	···	···
Fe I	6725.360	4.103	−2.17	···	···
Fe I	6733.150	4.638	−1.40	···	···
Fe I	6739.524	1.560	−4.79	···	···
Fe I	6750.160	2.424	−2.62	74.5	6.59
Fe I	6752.711	4.640	−1.20	···	···
Fe I	6837.009	4.590	−1.69	···	···
Fe I	6857.250	4.076	−2.04	···	···
Fe I	6971.936	3.020	−3.34	···	···
Fe I	7112.170	2.990	−2.99	···	···
Fe I	7751.120	4.990	−0.73	···	···
Fe I	7802.510	5.080	−1.31	···	···
Fe I	7807.920	4.990	−0.73	19.0	6.65
Fe I	8365.644	3.250	−2.04	56.9	6.63
Fe I	8757.200	2.845	−2.12	···	···
Fe II	5234.620	3.221	−2.22	···	···
Fe II	5425.260	3.200	−3.16	···	···
Fe II	6149.250	3.889	−2.63	···	···
Fe II	6247.560	3.892	−2.27	···	···
Fe II	6369.490	2.891	−4.02	···	···
Fe II	6432.680	2.891	−3.52	···	···
Fe II	6456.390	3.903	−2.06	···	···
Fe II	7479.700	3.892	−3.53	···	···
Fe II	7515.840	3.903	−3.42	···	···
Ca I	5867.570	2.930	−1.57	41.4	5.80
Ca I	6166.440	2.520	−1.14	132.5	6.01
Ca I	6169.040	2.520	−0.80	211.8	6.20
Ca I	6455.610	2.520	−1.29	93.5	5.74
Ca I	6572.800	0.000	−4.28	137.9	6.34
Ti I	5024.850	0.818	−0.56	150.6	4.50
Ti I	5113.450	1.443	−0.73	124.2	5.10
Ti I	5219.710	0.021	−2.24	115.7	4.82
Ti I	5866.460	1.066	−0.76	124.0	4.61
Ti I	6091.180	2.267	−0.37	52.7	4.56
Ti I	6126.220	1.066	−1.37	74.6	4.44

Table B.1: Equivalent Width Measurements for F/G/K Primaries *(continued)*

Species	λ (Å)	E.P. (eV)	log(gf) (dex)	PM I00025-4644 EW (mÅ)	PM I00025-4644 Abundance
Ti I	6258.090	1.443	−0.31	133.6	4.66

Table B.1: Equivalent Width Measurements for F/G/K Primaries *(continued)*

Species	λ	E.P.	log(gf)	PM I00329+1805	
	(Å)	(eV)	(dex)	EW (mÅ)	Abundance
Fe I	5141.750	2.424	−2.18	···	···
Fe I	5247.060	0.087	−4.94	104.8	6.72
Fe I	5358.120	3.300	−3.16	···	···
Fe I	5412.788	4.440	−1.71	···	···
Fe I	5661.348	4.280	−1.75	···	···
Fe I	5778.458	2.590	−3.45	40.0	7.12
Fe I	5784.660	3.400	−2.53	···	···
Fe I	5809.220	3.884	−1.61	···	···
Fe I	5849.690	3.695	−2.93	···	···
Fe I	5852.230	4.549	−1.17	42.7	7.15
Fe I	5855.090	4.608	−1.48	···	···
Fe I	5856.100	4.294	−1.56	···	···
Fe I	5858.790	4.220	−2.18	···	···
Fe I	5859.600	4.550	−0.61	46.6	6.65
Fe I	5862.370	4.550	−0.25	62.2	6.51
Fe I	5956.700	0.859	−4.60	81.1	6.85
Fe I	6027.060	4.070	−1.17	35.4	6.49
Fe I	6151.620	2.176	−3.28	51.0	6.63
Fe I	6159.380	4.610	−1.83	···	···
Fe I	6165.360	4.143	−1.46	···	···
Fe I	6173.340	2.223	−2.88	73.1	6.64
Fe I	6200.320	2.609	−2.44	78.0	6.73
Fe I	6213.440	2.223	−2.56	88.3	6.55
Fe I	6240.652	2.220	−3.23	85.0	7.17
Fe I	6265.140	2.176	−2.55	105.3	6.71
Fe I	6271.283	3.330	−2.70	···	···
Fe I	6297.801	2.223	−2.73	100.9	6.89
Fe I	6322.694	2.588	−2.43	66.0	6.50
Fe I	6358.690	0.859	−4.00	81.7	6.22
Fe I	6436.410	4.186	−2.36	···	···
Fe I	6481.878	2.279	−2.97	74.8	6.81
Fe I	6498.950	0.958	−4.69	65.4	6.75
Fe I	6518.370	2.830	−2.45	45.0	6.47
Fe I	6574.233	0.990	−5.00	52.3	6.88
Fe I	6581.214	1.480	−4.68	···	···
Fe I	6591.330	4.593	−1.95	···	···
Fe I	6608.040	2.279	−3.91	···	···
Fe I	6625.027	1.010	−5.34	···	···
Fe I	6699.142	4.590	−2.10	···	···
Fe I	6713.750	4.795	−1.39	···	···
Fe I	6725.360	4.103	−2.17	···	···

Table B.1: Equivalent Width Measurements for F/G/K Primaries *(continued)*

Species	λ	E.P.	log(gf)	PM I00329+1805	
	(Å)	(eV)	(dex)	EW (mÅ)	Abundance
Fe I	6733.150	4.638	−1.40	···	···
Fe I	6739.524	1.560	−4.79	···	···
Fe I	6750.160	2.424	−2.62	77.5	6.66
Fe I	6752.711	4.640	−1.20	···	···
Fe I	6837.009	4.590	−1.69	···	···
Fe I	6857.250	4.076	−2.04	···	···
Fe I	6971.936	3.020	−3.34	···	···
Fe I	7112.170	2.990	−2.99	···	···
Fe I	7751.120	4.990	−0.73	···	···
Fe I	7802.510	5.080	−1.31	···	···
Fe I	7807.920	4.990	−0.73	···	···
Fe I	8365.644	3.250	−2.04	···	···
Fe I	8757.200	2.845	−2.12	···	···
Fe II	5234.620	3.221	−2.22	···	···
Fe II	5425.260	3.200	−3.16	···	···
Fe II	6149.250	3.889	−2.63	···	···
Fe II	6247.560	3.892	−2.27	···	···
Fe II	6369.490	2.891	−4.02	···	···
Fe II	6432.680	2.891	−3.52	···	···
Fe II	6456.390	3.903	−2.06	···	···
Fe II	7479.700	3.892	−3.53	···	···
Fe II	7515.840	3.903	−3.42	···	···
Ca I	5867.570	2.930	−1.57	66.5	6.12
Ca I	6166.440	2.520	−1.14	···	···
Ca I	6169.040	2.520	−0.80	···	···
Ca I	6455.610	2.520	−1.29	113.8	5.91
Ca I	6572.800	0.000	−4.28	···	···
Ti I	5024.850	0.818	−0.56	···	···
Ti I	5113.450	1.443	−0.73	···	···
Ti I	5219.710	0.021	−2.24	···	···
Ti I	5866.460	1.066	−0.76	···	···
Ti I	6091.180	2.267	−0.37	69.5	4.80
Ti I	6126.220	1.066	−1.37	97.8	4.77
Ti I	6258.090	1.443	−0.31	···	···

Table B.1: Equivalent Width Measurements for F/G/K Primaries *(continued)*

Species	λ	E.P.	log(gf)	PM I00422+0731E	
	(Å)	(eV)	(dex)	EW (mÅ)	Abundance
Fe I	5141.750	2.424	−2.18	95.7	6.81
Fe I	5247.060	0.087	−4.94	70.7	6.57
Fe I	5358.120	3.300	−3.16	···	···
Fe I	5412.788	4.440	−1.71	···	···
Fe I	5661.348	4.280	−1.75	···	···
Fe I	5778.458	2.590	−3.45	14.8	6.66
Fe I	5784.660	3.400	−2.53	···	···
Fe I	5809.220	3.884	−1.61	30.0	6.61
Fe I	5849.690	3.695	−2.93	···	···
Fe I	5852.230	4.549	−1.17	26.2	6.79
Fe I	5855.090	4.608	−1.48	7.8	6.54
Fe I	5856.100	4.294	−1.56	···	···
Fe I	5858.790	4.220	−2.18	···	···
Fe I	5859.600	4.550	−0.61	48.0	6.62
Fe I	5862.370	4.550	−0.25	54.2	6.35
Fe I	5956.700	0.859	−4.60	47.8	6.61
Fe I	6027.060	4.070	−1.17	40.4	6.55
Fe I	6151.620	2.176	−3.28	45.0	6.70
Fe I	6159.380	4.610	−1.83	···	···
Fe I	6165.360	4.143	−1.46	31.1	6.74
Fe I	6173.340	2.223	−2.88	65.3	6.69
Fe I	6200.320	2.609	−2.44	71.9	6.79
Fe I	6213.440	2.223	−2.56	79.4	6.61
Fe I	6240.652	2.220	−3.23	37.4	6.55
Fe I	6265.140	2.176	−2.55	···	···
Fe I	6271.283	3.330	−2.70	76.9	6.50
Fe I	6297.801	2.223	−2.73	65.1	6.54
Fe I	6322.694	2.588	−2.43	60.3	6.55
Fe I	6358.690	0.859	−4.00	76.4	6.48
Fe I	6436.410	4.186	−2.36	···	···
Fe I	6481.878	2.279	−2.97	57.3	6.69
Fe I	6498.950	0.958	−4.69	46.8	6.76
Fe I	6518.370	2.830	−2.45	43.9	6.54
Fe I	6574.233	0.990	−5.00	21.5	6.60
Fe I	6581.214	1.480	−4.68	···	···
Fe I	6591.330	4.593	−1.95	···	···
Fe I	6608.040	2.279	−3.91	10.9	6.59
Fe I	6625.027	1.010	−5.34	···	···
Fe I	6699.142	4.590	−2.10	···	···
Fe I	6713.750	4.795	−1.39	···	···
Fe I	6725.360	4.103	−2.17	···	···

Table B.1: Equivalent Width Measurements for F/G/K Primaries *(continued)*

Species	λ	E.P.	log(gf)	PM I00422+0731E	
	(Å)	(eV)	(dex)	EW (mÅ)	Abundance
Fe I	6733.150	4.638	−1.40	···	···
Fe I	6739.524	1.560	−4.79	···	···
Fe I	6750.160	2.424	−2.62	59.8	6.53
Fe I	6752.711	4.640	−1.20	···	···
Fe I	6837.009	4.590	−1.69	···	···
Fe I	6857.250	4.076	−2.04	11.5	6.69
Fe I	6971.936	3.020	−3.34	···	···
Fe I	7112.170	2.990	−2.99	···	···
Fe I	7751.120	4.990	−0.73	···	···
Fe I	7802.510	5.080	−1.31	···	···
Fe I	7807.920	4.990	−0.73	···	···
Fe I	8365.644	3.250	−2.04	53.9	6.65
Fe I	8757.200	2.845	−2.12	···	···
Fe II	5234.620	3.221	−2.22	52.9	6.58
Fe II	5425.260	3.200	−3.16	···	···
Fe II	6149.250	3.889	−2.63	14.0	6.72
Fe II	6247.560	3.892	−2.27	12.8	6.31
Fe II	6369.490	2.891	−4.02	7.2	6.74
Fe II	6432.680	2.891	−3.52	19.6	6.75
Fe II	6456.390	3.903	−2.06	29.2	6.61
Fe II	7479.700	3.892	−3.53	···	···
Fe II	7515.840	3.903	−3.42	···	···
Ca I	5867.570	2.930	−1.57	···	···
Ca I	6166.440	2.520	−1.14	71.2	5.83
Ca I	6169.040	2.520	−0.80	110.1	5.98
Ca I	6455.610	2.520	−1.29	54.5	5.73
Ca I	6572.800	0.000	−4.28	45.5	5.83
Ti I	5024.850	0.818	−0.56	96.2	4.63
Ti I	5113.450	1.443	−0.73	52.5	4.69
Ti I	5219.710	0.021	−2.24	46.3	4.52
Ti I	5866.460	1.066	−0.76	72.7	4.60
Ti I	6091.180	2.267	−0.37	25.8	4.67
Ti I	6126.220	1.066	−1.37	39.1	4.62
Ti I	6258.090	1.443	−0.31	66.2	4.42

Table B.1: Equivalent Width Measurements for F/G/K Primaries *(continued)*

Species	λ	E.P.	log(gf)	PM I01227+1409	
	(Å)	(eV)	(dex)	EW (mÅ)	Abundance
Fe I	5141.750	2.424	−2.18	54.2	6.60
Fe I	5247.060	0.087	−4.94	31.4	6.60
Fe I	5358.120	3.300	−3.16	···	···
Fe I	5412.788	4.440	−1.71	···	···
Fe I	5661.348	4.280	−1.75	···	···
Fe I	5778.458	2.590	−3.45	···	···
Fe I	5784.660	3.400	−2.53	···	···
Fe I	5809.220	3.884	−1.61	14.8	6.56
Fe I	5849.690	3.695	−2.93	···	···
Fe I	5852.230	4.549	−1.17	10.1	6.56
Fe I	5855.090	4.608	−1.48	···	···
Fe I	5856.100	4.294	−1.56	···	···
Fe I	5858.790	4.220	−2.18	···	···
Fe I	5859.600	4.550	−0.61	36.1	6.72
Fe I	5862.370	4.550	−0.25	50.3	6.62
Fe I	5956.700	0.859	−4.60	18.5	6.69
Fe I	6027.060	4.070	−1.17	28.9	6.67
Fe I	6151.620	2.176	−3.28	15.2	6.56
Fe I	6159.380	4.610	−1.83	···	···
Fe I	6165.360	4.143	−1.46	12.1	6.54
Fe I	6173.340	2.223	−2.88	31.9	6.63
Fe I	6200.320	2.609	−2.44	39.4	6.72
Fe I	6213.440	2.223	−2.56	48.5	6.62
Fe I	6240.652	2.220	−3.23	18.2	6.65
Fe I	6265.140	2.176	−2.55	53.2	6.64
Fe I	6271.283	3.330	−2.70	···	···
Fe I	6297.801	2.223	−2.73	36.3	6.56
Fe I	6322.694	2.588	−2.43	38.3	6.66
Fe I	6358.690	0.859	−4.00	···	···
Fe I	6436.410	4.186	−2.36	···	···
Fe I	6481.878	2.279	−2.97	27.5	6.67
Fe I	6498.950	0.958	−4.69	···	···
Fe I	6518.370	2.830	−2.45	27.0	6.68
Fe I	6574.233	0.990	−5.00	···	···
Fe I	6581.214	1.480	−4.68	···	···
Fe I	6591.330	4.593	−1.95	···	···
Fe I	6608.040	2.279	−3.91	···	···
Fe I	6625.027	1.010	−5.34	···	···
Fe I	6699.142	4.590	−2.10	···	···
Fe I	6713.750	4.795	−1.39	···	···
Fe I	6725.360	4.103	−2.17	···	···

Table B.1: Equivalent Width Measurements for F/G/K Primaries *(continued)*

Species	λ	E.P.	log(gf)	PM I01227+1409	
	(Å)	(eV)	(dex)	EW (mÅ)	Abundance
Fe I	6733.150	4.638	−1.40	···	···
Fe I	6739.524	1.560	−4.79	···	···
Fe I	6750.160	2.424	−2.62	37.4	6.65
Fe I	6752.711	4.640	−1.20	13.3	6.79
Fe I	6837.009	4.590	−1.69	···	···
Fe I	6857.250	4.076	−2.04	···	···
Fe I	6971.936	3.020	−3.34	···	···
Fe I	7112.170	2.990	−2.99	···	···
Fe I	7751.120	4.990	−0.73	···	···
Fe I	7802.510	5.080	−1.31	···	···
Fe I	7807.920	4.990	−0.73	···	···
Fe I	8365.644	3.250	−2.04	···	···
Fe I	8757.200	2.845	−2.12	···	···
Fe II	5234.620	3.221	−2.22	71.7	6.71
Fe II	5425.260	3.200	−3.16	25.6	6.68
Fe II	6149.250	3.889	−2.63	21.2	6.68
Fe II	6247.560	3.892	−2.27	35.0	6.65
Fe II	6369.490	2.891	−4.02	···	···
Fe II	6432.680	2.891	−3.52	23.7	6.67
Fe II	6456.390	3.903	−2.06	42.8	6.60
Fe II	7479.700	3.892	−3.53	···	···
Fe II	7515.840	3.903	−3.42	···	···
Ca I	5867.570	2.930	−1.57	···	···
Ca I	6166.440	2.520	−1.14	38.8	5.73
Ca I	6169.040	2.520	−0.80	61.7	5.78
Ca I	6455.610	2.520	−1.29	27.8	5.66
Ca I	6572.800	0.000	−4.28	···	···
Ti I	5024.850	0.818	−0.56	44.6	4.35
Ti I	5113.450	1.443	−0.73	···	···
Ti I	5219.710	0.021	−2.24	···	···
Ti I	5866.460	1.066	−0.76	21.8	4.28
Ti I	6091.180	2.267	−0.37	···	···
Ti I	6126.220	1.066	−1.37	···	···
Ti I	6258.090	1.443	−0.31	28.1	4.33

Table B.1: Equivalent Width Measurements for F/G/K Primaries *(continued)*

Species	λ	E.P.	log(gf)	PM I01266-4842W	
	(Å)	(eV)	(dex)	EW (mÅ)	Abundance
Fe I	5141.750	2.424	−2.18	···	···
Fe I	5247.060	0.087	−4.94	···	···
Fe I	5358.120	3.300	−3.16	···	···
Fe I	5412.788	4.440	−1.71	···	···
Fe I	5661.348	4.280	−1.75	···	···
Fe I	5778.458	2.590	−3.45	30.3	7.05
Fe I	5784.660	3.400	−2.53	···	···
Fe I	5809.220	3.884	−1.61	41.6	7.00
Fe I	5849.690	3.695	−2.93	···	···
Fe I	5852.230	4.549	−1.17	43.7	7.34
Fe I	5855.090	4.608	−1.48	···	···
Fe I	5856.100	4.294	−1.56	···	···
Fe I	5858.790	4.220	−2.18	···	···
Fe I	5859.600	4.550	−0.61	47.3	6.84
Fe I	5862.370	4.550	−0.25	54.8	6.60
Fe I	5956.700	0.859	−4.60	75.6	6.99
Fe I	6027.060	4.070	−1.17	39.1	6.73
Fe I	6151.620	2.176	−3.28	54.4	6.88
Fe I	6159.380	4.610	−1.83	···	···
Fe I	6165.360	4.143	−1.46	···	···
Fe I	6173.340	2.223	−2.88	69.0	6.80
Fe I	6200.320	2.609	−2.44	72.1	6.87
Fe I	6213.440	2.223	−2.56	90.6	6.81
Fe I	6240.652	2.220	−3.23	···	···
Fe I	6265.140	2.176	−2.55	103.9	6.91
Fe I	6271.283	3.330	−2.70	39.0	7.39
Fe I	6297.801	2.223	−2.73	108.2	7.19
Fe I	6322.694	2.588	−2.43	65.1	6.71
Fe I	6358.690	0.859	−4.00	96.9	6.70
Fe I	6436.410	4.186	−2.36	···	···
Fe I	6481.878	2.279	−2.97	75.5	7.05
Fe I	6498.950	0.958	−4.69	73.5	7.11
Fe I	6518.370	2.830	−2.45	50.5	6.76
Fe I	6574.233	0.990	−5.00	60.9	7.21
Fe I	6581.214	1.480	−4.68	48.0	7.25
Fe I	6591.330	4.593	−1.95	···	···
Fe I	6608.040	2.279	−3.91	···	···
Fe I	6625.027	1.010	−5.34	···	···
Fe I	6699.142	4.590	−2.10	···	···
Fe I	6713.750	4.795	−1.39	···	···
Fe I	6725.360	4.103	−2.17	···	···

Table B.1: Equivalent Width Measurements for F/G/K Primaries *(continued)*

Species	λ	E.P.	log(gf)	PM I01266-4842W	
	(Å)	(eV)	(dex)	EW (mÅ)	Abundance
Fe I	6733.150	4.638	−1.40	···	···
Fe I	6739.524	1.560	−4.79	···	···
Fe I	6750.160	2.424	−2.62	85.2	7.00
Fe I	6752.711	4.640	−1.20	···	···
Fe I	6837.009	4.590	−1.69	···	···
Fe I	6857.250	4.076	−2.04	···	···
Fe I	6971.936	3.020	−3.34	···	···
Fe I	7112.170	2.990	−2.99	···	···
Fe I	7751.120	4.990	−0.73	···	···
Fe I	7802.510	5.080	−1.31	···	···
Fe I	7807.920	4.990	−0.73	···	···
Fe I	8365.644	3.250	−2.04	···	···
Fe I	8757.200	2.845	−2.12	···	···
Fe II	5234.620	3.221	−2.22	···	···
Fe II	5425.260	3.200	−3.16	···	···
Fe II	6149.250	3.889	−2.63	···	···
Fe II	6247.560	3.892	−2.27	···	···
Fe II	6369.490	2.891	−4.02	···	···
Fe II	6432.680	2.891	−3.52	···	···
Fe II	6456.390	3.903	−2.06	···	···
Fe II	7479.700	3.892	−3.53	···	···
Fe II	7515.840	3.903	−3.42	···	···
Ca I	5867.570	2.930	−1.57	73.9	6.14
Ca I	6166.440	2.520	−1.14	···	···
Ca I	6169.040	2.520	−0.80	···	···
Ca I	6455.610	2.520	−1.29	122.1	5.93
Ca I	6572.800	0.000	−4.28	···	···
Ti I	5024.850	0.818	−0.56	···	···
Ti I	5113.450	1.443	−0.73	···	···
Ti I	5219.710	0.021	−2.24	109.0	4.63
Ti I	5866.460	1.066	−0.76	155.3	4.76
Ti I	6091.180	2.267	−0.37	66.6	4.75
Ti I	6126.220	1.066	−1.37	102.8	4.84
Ti I	6258.090	1.443	−0.31	173.4	4.83

Table B.1: Equivalent Width Measurements for F/G/K Primaries *(continued)*

Species	λ	E.P.	log(gf)	NLTT 4817	
	(Å)	(eV)	(dex)	EW (mÅ)	Abundance
Fe I	5141.750	2.424	−2.18	18.4	5.76
Fe I	5247.060	0.087	−4.94	···	···
Fe I	5358.120	3.300	−3.16	···	···
Fe I	5412.788	4.440	−1.71	···	···
Fe I	5661.348	4.280	−1.75	···	···
Fe I	5778.458	2.590	−3.45	···	···
Fe I	5784.660	3.400	−2.53	···	···
Fe I	5809.220	3.884	−1.61	···	···
Fe I	5849.690	3.695	−2.93	···	···
Fe I	5852.230	4.549	−1.17	···	···
Fe I	5855.090	4.608	−1.48	···	···
Fe I	5856.100	4.294	−1.56	···	···
Fe I	5858.790	4.220	−2.18	···	···
Fe I	5859.600	4.550	−0.61	11.3	6.00
Fe I	5862.370	4.550	−0.25	17.9	5.88
Fe I	5956.700	0.859	−4.60	···	···
Fe I	6027.060	4.070	−1.17	10.5	6.05
Fe I	6151.620	2.176	−3.28	···	···
Fe I	6159.380	4.610	−1.83	···	···
Fe I	6165.360	4.143	−1.46	···	···
Fe I	6173.340	2.223	−2.88	11.2	5.96
Fe I	6200.320	2.609	−2.44	13.4	5.99
Fe I	6213.440	2.223	−2.56	17.1	5.85
Fe I	6240.652	2.220	−3.23	···	···
Fe I	6265.140	2.176	−2.55	21.1	5.91
Fe I	6271.283	3.330	−2.70	···	···
Fe I	6297.801	2.223	−2.73	···	···
Fe I	6322.694	2.588	−2.43	···	···
Fe I	6358.690	0.859	−4.00	8.0	5.52
Fe I	6436.410	4.186	−2.36	···	···
Fe I	6481.878	2.279	−2.97	···	···
Fe I	6498.950	0.958	−4.69	13.6	6.57
Fe I	6518.370	2.830	−2.45	···	···
Fe I	6574.233	0.990	−5.00	···	···
Fe I	6581.214	1.480	−4.68	···	···
Fe I	6591.330	4.593	−1.95	···	···
Fe I	6608.040	2.279	−3.91	···	···
Fe I	6625.027	1.010	−5.34	···	···
Fe I	6699.142	4.590	−2.10	···	···
Fe I	6713.750	4.795	−1.39	···	···
Fe I	6725.360	4.103	−2.17	···	···

Table B.1: Equivalent Width Measurements for F/G/K Primaries *(continued)*

Species	λ	E.P.	log(gf)	NLTT 4817	
	(Å)	(eV)	(dex)	EW (mÅ)	Abundance
Fe I	6733.150	4.638	−1.40	···	···
Fe I	6739.524	1.560	−4.79	···	···
Fe I	6750.160	2.424	−2.62	11.1	5.87
Fe I	6752.711	4.640	−1.20	···	···
Fe I	6837.009	4.590	−1.69	···	···
Fe I	6857.250	4.076	−2.04	···	···
Fe I	6971.936	3.020	−3.34	···	···
Fe I	7112.170	2.990	−2.99	···	···
Fe I	7751.120	4.990	−0.73	···	···
Fe I	7802.510	5.080	−1.31	···	···
Fe I	7807.920	4.990	−0.73	···	···
Fe I	8365.644	3.250	−2.04	···	···
Fe I	8757.200	2.845	−2.12	···	···
Fe II	5234.620	3.221	−2.22	39.1	5.96
Fe II	5425.260	3.200	−3.16	···	···
Fe II	6149.250	3.889	−2.63	5.9	5.94
Fe II	6247.560	3.892	−2.27	10.8	5.87
Fe II	6369.490	2.891	−4.02	···	···
Fe II	6432.680	2.891	−3.52	···	···
Fe II	6456.390	3.903	−2.06	16.5	5.89
Fe II	7479.700	3.892	−3.53	···	···
Fe II	7515.840	3.903	−3.42	···	···
Ca I	5867.570	2.930	−1.57	···	···
Ca I	6166.440	2.520	−1.14	15.4	5.13
Ca I	6169.040	2.520	−0.80	27.4	5.11
Ca I	6455.610	2.520	−1.29	8.1	4.96
Ca I	6572.800	0.000	−4.28	···	···
Ti I	5024.850	0.818	−0.56	16.4	3.63
Ti I	5113.450	1.443	−0.73	···	···
Ti I	5219.710	0.021	−2.24	···	···
Ti I	5866.460	1.066	−0.76	···	···
Ti I	6091.180	2.267	−0.37	···	···
Ti I	6126.220	1.066	−1.37	···	···
Ti I	6258.090	1.443	−0.31	6.8	3.51

Table B.1: Equivalent Width Measurements for F/G/K Primaries *(continued)*

Species	λ	E.P.	log(gf)	PM I01352+0538N	
	(Å)	(eV)	(dex)	EW (mÅ)	Abundance
Fe I	5141.750	2.424	−2.18	73.4	6.75
Fe I	5247.060	0.087	−4.94	75.1	7.09
Fe I	5358.120	3.300	−3.16	···	···
Fe I	5412.788	4.440	−1.71	···	···
Fe I	5661.348	4.280	−1.75	···	···
Fe I	5778.458	2.590	−3.45	20.5	6.92
Fe I	5784.660	3.400	−2.53	···	···
Fe I	5809.220	3.884	−1.61	32.8	6.77
Fe I	5849.690	3.695	−2.93	···	···
Fe I	5852.230	4.549	−1.17	26.5	6.87
Fe I	5855.090	4.608	−1.48	11.2	6.76
Fe I	5856.100	4.294	−1.56	21.8	6.88
Fe I	5858.790	4.220	−2.18	···	···
Fe I	5859.600	4.550	−0.61	48.7	6.75
Fe I	5862.370	4.550	−0.25	66.1	6.68
Fe I	5956.700	0.859	−4.60	44.4	6.76
Fe I	6027.060	4.070	−1.17	47.8	6.83
Fe I	6151.620	2.176	−3.28	37.4	6.71
Fe I	6159.380	4.610	−1.83	···	···
Fe I	6165.360	4.143	−1.46	31.1	6.84
Fe I	6173.340	2.223	−2.88	61.1	6.90
Fe I	6200.320	2.609	−2.44	62.9	6.91
Fe I	6213.440	2.223	−2.56	73.8	6.84
Fe I	6240.652	2.220	−3.23	38.6	6.73
Fe I	6265.140	2.176	−2.55	72.1	6.74
Fe I	6271.283	3.330	−2.70	···	···
Fe I	6297.801	2.223	−2.73	82.6	7.16
Fe I	6322.694	2.588	−2.43	61.4	6.83
Fe I	6358.690	0.859	−4.00	68.3	6.69
Fe I	6436.410	4.186	−2.36	···	···
Fe I	6481.878	2.279	−2.97	50.3	6.79
Fe I	6498.950	0.958	−4.69	45.6	6.94
Fe I	6518.370	2.830	−2.45	47.6	6.80
Fe I	6574.233	0.990	−5.00	33.9	7.01
Fe I	6581.214	1.480	−4.68	···	···
Fe I	6591.330	4.593	−1.95	···	···
Fe I	6608.040	2.279	−3.91	···	···
Fe I	6625.027	1.010	−5.34	15.8	6.86
Fe I	6699.142	4.590	−2.10	···	···
Fe I	6713.750	4.795	−1.39	13.9	6.95
Fe I	6725.360	4.103	−2.17	···	···

Table B.1: Equivalent Width Measurements for F/G/K Primaries *(continued)*

Species	λ	E.P.	log(gf)	PM I01352+0538N	
	(Å)	(eV)	(dex)	EW (mÅ)	Abundance
Fe I	6733.150	4.638	−1.40	···	···
Fe I	6739.524	1.560	−4.79	···	···
Fe I	6750.160	2.424	−2.62	62.9	6.85
Fe I	6752.711	4.640	−1.20	23.9	6.90
Fe I	6837.009	4.590	−1.69	···	···
Fe I	6857.250	4.076	−2.04	···	···
Fe I	6971.936	3.020	−3.34	···	···
Fe I	7112.170	2.990	−2.99	21.9	6.87
Fe I	7751.120	4.990	−0.73	28.3	6.86
Fe I	7802.510	5.080	−1.31	···	···
Fe I	7807.920	4.990	−0.73	37.3	7.04
Fe I	8365.644	3.250	−2.04	···	···
Fe I	8757.200	2.845	−2.12	···	···
Fe II	5234.620	3.221	−2.22	51.4	6.93
Fe II	5425.260	3.200	−3.16	16.3	6.82
Fe II	6149.250	3.889	−2.63	13.2	6.87
Fe II	6247.560	3.892	−2.27	20.9	6.81
Fe II	6369.490	2.891	−4.02	···	···
Fe II	6432.680	2.891	−3.52	12.2	6.69
Fe II	6456.390	3.903	−2.06	27.7	6.82
Fe II	7479.700	3.892	−3.53	···	···
Fe II	7515.840	3.903	−3.42	···	···
Ca I	5867.570	2.930	−1.57	21.2	5.88
Ca I	6166.440	2.520	−1.14	67.3	5.89
Ca I	6169.040	2.520	−0.80	104.2	6.05
Ca I	6455.610	2.520	−1.29	51.6	5.77
Ca I	6572.800	0.000	−4.28	45.8	5.94
Ti I	5024.850	0.818	−0.56	74.7	4.54
Ti I	5113.450	1.443	−0.73	···	···
Ti I	5219.710	0.021	−2.24	44.8	4.64
Ti I	5866.460	1.066	−0.76	59.0	4.57
Ti I	6091.180	2.267	−0.37	20.9	4.59
Ti I	6126.220	1.066	−1.37	32.1	4.56
Ti I	6258.090	1.443	−0.31	66.2	4.65

Table B.1: Equivalent Width Measurements for F/G/K Primaries *(continued)*

Species	λ	E.P.	log(gf)	PM I01430-4959W	
	(Å)	(eV)	(dex)	EW (mÅ)	Abundance
Fe I	5141.750	2.424	−2.18	66.3	6.34
Fe I	5247.060	0.087	−4.94	62.8	6.40
Fe I	5358.120	3.300	−3.16	···	···
Fe I	5412.788	4.440	−1.71	···	···
Fe I	5661.348	4.280	−1.75	···	···
Fe I	5778.458	2.590	−3.45	···	···
Fe I	5784.660	3.400	−2.53	···	···
Fe I	5809.220	3.884	−1.61	···	···
Fe I	5849.690	3.695	−2.93	···	···
Fe I	5852.230	4.549	−1.17	···	···
Fe I	5855.090	4.608	−1.48	···	···
Fe I	5856.100	4.294	−1.56	···	···
Fe I	5858.790	4.220	−2.18	···	···
Fe I	5859.600	4.550	−0.61	24.2	6.12
Fe I	5862.370	4.550	−0.25	58.8	6.42
Fe I	5956.700	0.859	−4.60	40.1	6.31
Fe I	6027.060	4.070	−1.17	33.0	6.37
Fe I	6151.620	2.176	−3.28	48.0	6.70
Fe I	6159.380	4.610	−1.83	···	···
Fe I	6165.360	4.143	−1.46	···	···
Fe I	6173.340	2.223	−2.88	52.6	6.45
Fe I	6200.320	2.609	−2.44	51.9	6.43
Fe I	6213.440	2.223	−2.56	73.7	6.56
Fe I	6240.652	2.220	−3.23	···	···
Fe I	6265.140	2.176	−2.55	70.5	6.44
Fe I	6271.283	3.330	−2.70	···	···
Fe I	6297.801	2.223	−2.73	56.1	6.37
Fe I	6322.694	2.588	−2.43	40.9	6.14
Fe I	6358.690	0.859	−4.00	51.9	5.97
Fe I	6436.410	4.186	−2.36	···	···
Fe I	6481.878	2.279	−2.97	41.3	6.33
Fe I	6498.950	0.958	−4.69	···	···
Fe I	6518.370	2.830	−2.45	30.3	6.18
Fe I	6574.233	0.990	−5.00	···	···
Fe I	6581.214	1.480	−4.68	···	···
Fe I	6591.330	4.593	−1.95	···	···
Fe I	6608.040	2.279	−3.91	···	···
Fe I	6625.027	1.010	−5.34	···	···
Fe I	6699.142	4.590	−2.10	···	···
Fe I	6713.750	4.795	−1.39	···	···
Fe I	6725.360	4.103	−2.17	···	···

Table B.1: Equivalent Width Measurements for F/G/K Primaries *(continued)*

Species	λ	E.P.	log(gf)	PM I01430-4959W	
	(Å)	(eV)	(dex)	EW (mÅ)	Abundance
Fe I	6733.150	4.638	−1.40	···	···
Fe I	6739.524	1.560	−4.79	···	···
Fe I	6750.160	2.424	−2.62	47.3	6.27
Fe I	6752.711	4.640	−1.20	···	···
Fe I	6837.009	4.590	−1.69	···	···
Fe I	6857.250	4.076	−2.04	···	···
Fe I	6971.936	3.020	−3.34	···	···
Fe I	7112.170	2.990	−2.99	···	···
Fe I	7751.120	4.990	−0.73	···	···
Fe I	7802.510	5.080	−1.31	···	···
Fe I	7807.920	4.990	−0.73	···	···
Fe I	8365.644	3.250	−2.04	···	···
Fe I	8757.200	2.845	−2.12	···	···
Fe II	5234.620	3.221	−2.22	33.2	6.53
Fe II	5425.260	3.200	−3.16	···	···
Fe II	6149.250	3.889	−2.63	···	···
Fe II	6247.560	3.892	−2.27	···	···
Fe II	6369.490	2.891	−4.02	···	···
Fe II	6432.680	2.891	−3.52	···	···
Fe II	6456.390	3.903	−2.06	10.8	6.32
Fe II	7479.700	3.892	−3.53	···	···
Fe II	7515.840	3.903	−3.42	···	···
Ca I	5867.570	2.930	−1.57	···	···
Ca I	6166.440	2.520	−1.14	46.0	5.29
Ca I	6169.040	2.520	−0.80	85.5	5.56
Ca I	6455.610	2.520	−1.29	44.7	5.41
Ca I	6572.800	0.000	−4.28	40.5	5.42
Ti I	5024.850	0.818	−0.56	88.8	4.37
Ti I	5113.450	1.443	−0.73	···	···
Ti I	5219.710	0.021	−2.24	31.6	3.86
Ti I	5866.460	1.066	−0.76	44.0	3.85
Ti I	6091.180	2.267	−0.37	···	···
Ti I	6126.220	1.066	−1.37	31.3	4.15
Ti I	6258.090	1.443	−0.31	59.5	4.15

Table B.1: Equivalent Width Measurements for F/G/K Primaries *(continued)*

Species	λ	E.P.	log(gf)	PM I02012+0218	
	(Å)	(eV)	(dex)	EW (mÅ)	Abundance
Fe I	5141.750	2.424	−2.18	41.9	6.09
Fe I	5247.060	0.087	−4.94	41.6	6.34
Fe I	5358.120	3.300	−3.16	···	···
Fe I	5412.788	4.440	−1.71	···	···
Fe I	5661.348	4.280	−1.75	···	···
Fe I	5778.458	2.590	−3.45	···	···
Fe I	5784.660	3.400	−2.53	···	···
Fe I	5809.220	3.884	−1.61	10.7	6.13
Fe I	5849.690	3.695	−2.93	···	···
Fe I	5852.230	4.549	−1.17	···	···
Fe I	5855.090	4.608	−1.48	···	···
Fe I	5856.100	4.294	−1.56	···	···
Fe I	5858.790	4.220	−2.18	···	···
Fe I	5859.600	4.550	−0.61	20.4	6.16
Fe I	5862.370	4.550	−0.25	24.8	5.91
Fe I	5956.700	0.859	−4.60	15.0	6.05
Fe I	6027.060	4.070	−1.17	15.2	6.06
Fe I	6151.620	2.176	−3.28	11.2	5.99
Fe I	6159.380	4.610	−1.83	···	···
Fe I	6165.360	4.143	−1.46	11.4	6.26
Fe I	6173.340	2.223	−2.88	27.1	6.16
Fe I	6200.320	2.609	−2.44	31.1	6.23
Fe I	6213.440	2.223	−2.56	···	···
Fe I	6240.652	2.220	−3.23	13.8	6.09
Fe I	6265.140	2.176	−2.55	40.9	6.10
Fe I	6271.283	3.330	−2.70	···	···
Fe I	6297.801	2.223	−2.73	30.3	6.08
Fe I	6322.694	2.588	−2.43	25.7	6.05
Fe I	6358.690	0.859	−4.00	32.0	5.92
Fe I	6436.410	4.186	−2.36	···	···
Fe I	6481.878	2.279	−2.97	22.7	6.17
Fe I	6498.950	0.958	−4.69	···	···
Fe I	6518.370	2.830	−2.45	19.1	6.14
Fe I	6574.233	0.990	−5.00	···	···
Fe I	6581.214	1.480	−4.68	···	···
Fe I	6591.330	4.593	−1.95	···	···
Fe I	6608.040	2.279	−3.91	···	···
Fe I	6625.027	1.010	−5.34	···	···
Fe I	6699.142	4.590	−2.10	···	···
Fe I	6713.750	4.795	−1.39	···	···
Fe I	6725.360	4.103	−2.17	···	···

Table B.1: Equivalent Width Measurements for F/G/K Primaries *(continued)*

Species	λ	E.P.	log(gf)	PM I02012+0218	
	(Å)	(eV)	(dex)	EW (mÅ)	Abundance
Fe I	6733.150	4.638	−1.40	···	···
Fe I	6739.524	1.560	−4.79	···	···
Fe I	6750.160	2.424	−2.62	29.6	6.15
Fe I	6752.711	4.640	−1.20	···	···
Fe I	6837.009	4.590	−1.69	···	···
Fe I	6857.250	4.076	−2.04	···	···
Fe I	6971.936	3.020	−3.34	···	···
Fe I	7112.170	2.990	−2.99	···	···
Fe I	7751.120	4.990	−0.73	···	···
Fe I	7802.510	5.080	−1.31	···	···
Fe I	7807.920	4.990	−0.73	12.4	6.39
Fe I	8365.644	3.250	−2.04	···	···
Fe I	8757.200	2.845	−2.12	···	···
Fe II	5234.620	3.221	−2.22	19.8	5.85
Fe II	5425.260	3.200	−3.16	···	···
Fe II	6149.250	3.889	−2.63	6.0	6.27
Fe II	6247.560	3.892	−2.27	8.2	6.06
Fe II	6369.490	2.891	−4.02	···	···
Fe II	6432.680	2.891	−3.52	···	···
Fe II	6456.390	3.903	−2.06	10.5	5.99
Fe II	7479.700	3.892	−3.53	···	···
Fe II	7515.840	3.903	−3.42	···	···
Ca I	5867.570	2.930	−1.57	···	···
Ca I	6166.440	2.520	−1.14	34.9	5.39
Ca I	6169.040	2.520	−0.80	66.3	5.58
Ca I	6455.610	2.520	−1.29	19.7	5.18
Ca I	6572.800	0.000	−4.28	···	···
Ti I	5024.850	0.818	−0.56	39.5	3.86
Ti I	5113.450	1.443	−0.73	···	···
Ti I	5219.710	0.021	−2.24	···	···
Ti I	5866.460	1.066	−0.76	31.7	4.08
Ti I	6091.180	2.267	−0.37	···	···
Ti I	6126.220	1.066	−1.37	6.9	3.82
Ti I	6258.090	1.443	−0.31	24.7	3.84

Table B.1: Equivalent Width Measurements for F/G/K Primaries *(continued)*

Species	λ	E.P.	log(gf)	PM I02225+1531S	
	(Å)	(eV)	(dex)	EW (mÅ)	Abundance
Fe I	5141.750	2.424	−2.18	41.9	6.09
Fe I	5247.060	0.087	−4.94	41.6	6.34
Fe I	5358.120	3.300	−3.16	···	···
Fe I	5412.788	4.440	−1.71	···	···
Fe I	5661.348	4.280	−1.75	···	···
Fe I	5778.458	2.590	−3.45	···	···
Fe I	5784.660	3.400	−2.53	···	···
Fe I	5809.220	3.884	−1.61	10.7	6.13
Fe I	5849.690	3.695	−2.93	···	···
Fe I	5852.230	4.549	−1.17	···	···
Fe I	5855.090	4.608	−1.48	···	···
Fe I	5856.100	4.294	−1.56	···	···
Fe I	5858.790	4.220	−2.18	···	···
Fe I	5859.600	4.550	−0.61	20.4	6.16
Fe I	5862.370	4.550	−0.25	24.8	5.91
Fe I	5956.700	0.859	−4.60	15.0	6.05
Fe I	6027.060	4.070	−1.17	15.2	6.06
Fe I	6151.620	2.176	−3.28	11.2	5.99
Fe I	6159.380	4.610	−1.83	···	···
Fe I	6165.360	4.143	−1.46	11.4	6.26
Fe I	6173.340	2.223	−2.88	27.1	6.16
Fe I	6200.320	2.609	−2.44	31.1	6.23
Fe I	6213.440	2.223	−2.56	···	···
Fe I	6240.652	2.220	−3.23	13.8	6.09
Fe I	6265.140	2.176	−2.55	40.9	6.10
Fe I	6271.283	3.330	−2.70	···	···
Fe I	6297.801	2.223	−2.73	30.3	6.08
Fe I	6322.694	2.588	−2.43	25.7	6.05
Fe I	6358.690	0.859	−4.00	32.0	5.92
Fe I	6436.410	4.186	−2.36	···	···
Fe I	6481.878	2.279	−2.97	22.7	6.17
Fe I	6498.950	0.958	−4.69	···	···
Fe I	6518.370	2.830	−2.45	19.1	6.14
Fe I	6574.233	0.990	−5.00	···	···
Fe I	6581.214	1.480	−4.68	···	···
Fe I	6591.330	4.593	−1.95	···	···
Fe I	6608.040	2.279	−3.91	···	···
Fe I	6625.027	1.010	−5.34	···	···
Fe I	6699.142	4.590	−2.10	···	···
Fe I	6713.750	4.795	−1.39	···	···
Fe I	6725.360	4.103	−2.17	···	···

Table B.1: Equivalent Width Measurements for F/G/K Primaries *(continued)*

Species	λ	E.P.	log(gf)	PM I02225+1531S	
	(Å)	(eV)	(dex)	EW (mÅ)	Abundance
Fe I	6733.150	4.638	−1.40	···	···
Fe I	6739.524	1.560	−4.79	···	···
Fe I	6750.160	2.424	−2.62	29.6	6.15
Fe I	6752.711	4.640	−1.20	···	···
Fe I	6837.009	4.590	−1.69	···	···
Fe I	6857.250	4.076	−2.04	···	···
Fe I	6971.936	3.020	−3.34	···	···
Fe I	7112.170	2.990	−2.99	···	···
Fe I	7751.120	4.990	−0.73	···	···
Fe I	7802.510	5.080	−1.31	···	···
Fe I	7807.920	4.990	−0.73	12.4	6.39
Fe I	8365.644	3.250	−2.04	···	···
Fe I	8757.200	2.845	−2.12	···	···
Fe II	5234.620	3.221	−2.22	19.8	5.85
Fe II	5425.260	3.200	−3.16	···	···
Fe II	6149.250	3.889	−2.63	6.0	6.27
Fe II	6247.560	3.892	−2.27	8.2	6.06
Fe II	6369.490	2.891	−4.02	···	···
Fe II	6432.680	2.891	−3.52	···	···
Fe II	6456.390	3.903	−2.06	10.5	5.99
Fe II	7479.700	3.892	−3.53	···	···
Fe II	7515.840	3.903	−3.42	···	···
Ca I	5867.570	2.930	−1.57	···	···
Ca I	6166.440	2.520	−1.14	34.9	5.39
Ca I	6169.040	2.520	−0.80	66.3	5.58
Ca I	6455.610	2.520	−1.29	19.7	5.18
Ca I	6572.800	0.000	−4.28	···	···
Ti I	5024.850	0.818	−0.56	39.5	3.86
Ti I	5113.450	1.443	−0.73	···	···
Ti I	5219.710	0.021	−2.24	···	···
Ti I	5866.460	1.066	−0.76	31.7	4.08
Ti I	6091.180	2.267	−0.37	···	···
Ti I	6126.220	1.066	−1.37	6.9	3.82
Ti I	6258.090	1.443	−0.31	24.7	3.84

Table B.1: Equivalent Width Measurements for F/G/K Primaries *(continued)*

Species	λ	E.P.	log(gf)	PM I02548+2057W	
	(Å)	(eV)	(dex)	EW (mÅ)	Abundance
Fe I	5141.750	2.424	−2.18	···	···
Fe I	5247.060	0.087	−4.94	72.2	6.04
Fe I	5358.120	3.300	−3.16	···	···
Fe I	5412.788	4.440	−1.71	···	···
Fe I	5661.348	4.280	−1.75	···	···
Fe I	5778.458	2.590	−3.45	···	···
Fe I	5784.660	3.400	−2.53	···	···
Fe I	5809.220	3.884	−1.61	···	···
Fe I	5849.690	3.695	−2.93	···	···
Fe I	5852.230	4.549	−1.17	···	···
Fe I	5855.090	4.608	−1.48	···	···
Fe I	5856.100	4.294	−1.56	···	···
Fe I	5858.790	4.220	−2.18	···	···
Fe I	5859.600	4.550	−0.61	22.8	6.03
Fe I	5862.370	4.550	−0.25	38.5	5.95
Fe I	5956.700	0.859	−4.60	41.2	6.07
Fe I	6027.060	4.070	−1.17	23.2	6.05
Fe I	6151.620	2.176	−3.28	22.7	5.95
Fe I	6159.380	4.610	−1.83	···	···
Fe I	6165.360	4.143	−1.46	···	···
Fe I	6173.340	2.223	−2.88	37.9	5.90
Fe I	6200.320	2.609	−2.44	60.4	6.26
Fe I	6213.440	2.223	−2.56	63.3	5.97
Fe I	6240.652	2.220	−3.23	23.2	5.96
Fe I	6265.140	2.176	−2.55	68.3	5.97
Fe I	6271.283	3.330	−2.70	···	···
Fe I	6297.801	2.223	−2.73	55.9	6.03
Fe I	6322.694	2.588	−2.43	49.2	6.05
Fe I	6358.690	0.859	−4.00	52.6	5.63
Fe I	6436.410	4.186	−2.36	···	···
Fe I	6481.878	2.279	−2.97	37.9	6.05
Fe I	6498.950	0.958	−4.69	33.3	6.11
Fe I	6518.370	2.830	−2.45	···	···
Fe I	6574.233	0.990	−5.00	···	···
Fe I	6581.214	1.480	−4.68	···	···
Fe I	6591.330	4.593	−1.95	···	···
Fe I	6608.040	2.279	−3.91	···	···
Fe I	6625.027	1.010	−5.34	···	···
Fe I	6699.142	4.590	−2.10	···	···
Fe I	6713.750	4.795	−1.39	···	···
Fe I	6725.360	4.103	−2.17	···	···

Table B.1: Equivalent Width Measurements for F/G/K Primaries *(continued)*

Species	λ	E.P.	log(gf)	PM I02548+2057W	
	(Å)	(eV)	(dex)	EW (mÅ)	Abundance
Fe I	6733.150	4.638	−1.40	···	···
Fe I	6739.524	1.560	−4.79	···	···
Fe I	6750.160	2.424	−2.62	49.7	6.04
Fe I	6752.711	4.640	−1.20	···	···
Fe I	6837.009	4.590	−1.69	···	···
Fe I	6857.250	4.076	−2.04	···	···
Fe I	6971.936	3.020	−3.34	···	···
Fe I	7112.170	2.990	−2.99	···	···
Fe I	7751.120	4.990	−0.73	···	···
Fe I	7802.510	5.080	−1.31	···	···
Fe I	7807.920	4.990	−0.73	···	···
Fe I	8365.644	3.250	−2.04	25.3	5.92
Fe I	8757.200	2.845	−2.12	···	···
Fe II	5234.620	3.221	−2.22	15.7	6.01
Fe II	5425.260	3.200	−3.16	···	···
Fe II	6149.250	3.889	−2.63	···	···
Fe II	6247.560	3.892	−2.27	···	···
Fe II	6369.490	2.891	−4.02	···	···
Fe II	6432.680	2.891	−3.52	···	···
Fe II	6456.390	3.903	−2.06	···	···
Fe II	7479.700	3.892	−3.53	···	···
Fe II	7515.840	3.903	−3.42	···	···
Ca I	5867.570	2.930	−1.57	···	···
Ca I	6166.440	2.520	−1.14	56.3	5.22
Ca I	6169.040	2.520	−0.80	113.5	5.46
Ca I	6455.610	2.520	−1.29	43.3	5.18
Ca I	6572.800	0.000	−4.28	63.8	5.51
Ti I	5024.850	0.818	−0.56	102.9	3.99
Ti I	5113.450	1.443	−0.73	···	···
Ti I	5219.710	0.021	−2.24	62.3	4.12
Ti I	5866.460	1.066	−0.76	67.0	3.90
Ti I	6091.180	2.267	−0.37	···	···
Ti I	6126.220	1.066	−1.37	36.0	4.02
Ti I	6258.090	1.443	−0.31	70.9	3.92

Table B.1: Equivalent Width Measurements for F/G/K Primaries *(continued)*

Species	λ	E.P.	log(gf)	PM I02569-5831N	
	(Å)	(eV)	(dex)	EW (mÅ)	Abundance
Fe I	5141.750	2.424	−2.18	···	···
Fe I	5247.060	0.087	−4.94	···	···
Fe I	5358.120	3.300	−3.16	···	···
Fe I	5412.788	4.440	−1.71	···	···
Fe I	5661.348	4.280	−1.75	···	···
Fe I	5778.458	2.590	−3.45	28.4	6.96
Fe I	5784.660	3.400	−2.53	···	···
Fe I	5809.220	3.884	−1.61	45.4	6.96
Fe I	5849.690	3.695	−2.93	···	···
Fe I	5852.230	4.549	−1.17	43.2	7.21
Fe I	5855.090	4.608	−1.48	···	···
Fe I	5856.100	4.294	−1.56	···	···
Fe I	5858.790	4.220	−2.18	···	···
Fe I	5859.600	4.550	−0.61	47.0	6.71
Fe I	5862.370	4.550	−0.25	68.7	6.65
Fe I	5956.700	0.859	−4.60	76.6	6.97
Fe I	6027.060	4.070	−1.17	42.0	6.67
Fe I	6151.620	2.176	−3.28	55.6	6.83
Fe I	6159.380	4.610	−1.83	···	···
Fe I	6165.360	4.143	−1.46	···	···
Fe I	6173.340	2.223	−2.88	75.3	6.83
Fe I	6200.320	2.609	−2.44	81.8	6.93
Fe I	6213.440	2.223	−2.56	97.9	6.84
Fe I	6240.652	2.220	−3.23	···	···
Fe I	6265.140	2.176	−2.55	97.6	6.77
Fe I	6271.283	3.330	−2.70	···	···
Fe I	6297.801	2.223	−2.73	105.4	7.09
Fe I	6322.694	2.588	−2.43	79.7	6.86
Fe I	6358.690	0.859	−4.00	98.0	6.69
Fe I	6436.410	4.186	−2.36	···	···
Fe I	6481.878	2.279	−2.97	68.8	6.86
Fe I	6498.950	0.958	−4.69	···	···
Fe I	6518.370	2.830	−2.45	50.2	6.66
Fe I	6574.233	0.990	−5.00	···	···
Fe I	6581.214	1.480	−4.68	···	···
Fe I	6591.330	4.593	−1.95	···	···
Fe I	6608.040	2.279	−3.91	···	···
Fe I	6625.027	1.010	−5.34	···	···
Fe I	6699.142	4.590	−2.10	···	···
Fe I	6713.750	4.795	−1.39	···	···
Fe I	6725.360	4.103	−2.17	···	···

Table B.1: Equivalent Width Measurements for F/G/K Primaries *(continued)*

Species	λ	E.P.	log(gf)	PM I02569-5831N	
	(Å)	(eV)	(dex)	EW (mÅ)	Abundance
Fe I	6733.150	4.638	−1.40	···	···
Fe I	6739.524	1.560	−4.79	···	···
Fe I	6750.160	2.424	−2.62	79.4	6.84
Fe I	6752.711	4.640	−1.20	···	···
Fe I	6837.009	4.590	−1.69	···	···
Fe I	6857.250	4.076	−2.04	···	···
Fe I	6971.936	3.020	−3.34	···	···
Fe I	7112.170	2.990	−2.99	···	···
Fe I	7751.120	4.990	−0.73	···	···
Fe I	7802.510	5.080	−1.31	···	···
Fe I	7807.920	4.990	−0.73	21.5	6.81
Fe I	8365.644	3.250	−2.04	···	···
Fe I	8757.200	2.845	−2.12	···	···
Fe II	5234.620	3.221	−2.22	···	···
Fe II	5425.260	3.200	−3.16	···	···
Fe II	6149.250	3.889	−2.63	···	···
Fe II	6247.560	3.892	−2.27	···	···
Fe II	6369.490	2.891	−4.02	···	···
Fe II	6432.680	2.891	−3.52	···	···
Fe II	6456.390	3.903	−2.06	···	···
Fe II	7479.700	3.892	−3.53	···	···
Fe II	7515.840	3.903	−3.42	···	···
Ca I	5867.570	2.930	−1.57	···	···
Ca I	6166.440	2.520	−1.14	151.2	6.14
Ca I	6169.040	2.520	−0.80	···	···
Ca I	6455.610	2.520	−1.29	106.7	5.91
Ca I	6572.800	0.000	−4.28	···	···
Ti I	5024.850	0.818	−0.56	147.7	4.48
Ti I	5113.450	1.443	−0.73	···	···
Ti I	5219.710	0.021	−2.24	108.2	4.82
Ti I	5866.460	1.066	−0.76	143.8	4.84
Ti I	6091.180	2.267	−0.37	68.1	4.88
Ti I	6126.220	1.066	−1.37	93.9	4.88
Ti I	6258.090	1.443	−0.31	···	···

Table B.1: Equivalent Width Measurements for F/G/K Primaries *(continued)*

Species	λ	E.P.	log(gf)	PM I03150+0102	
	(Å)	(eV)	(dex)	EW (mÅ)	Abundance
Fe I	5141.750	2.424	−2.18	58.7	6.44
Fe I	5247.060	0.087	−4.94	46.6	6.47
Fe I	5358.120	3.300	−3.16	···	···
Fe I	5412.788	4.440	−1.71	···	···
Fe I	5661.348	4.280	−1.75	···	···
Fe I	5778.458	2.590	−3.45	···	···
Fe I	5784.660	3.400	−2.53	···	···
Fe I	5809.220	3.884	−1.61	18.3	6.47
Fe I	5849.690	3.695	−2.93	···	···
Fe I	5852.230	4.549	−1.17	13.5	6.55
Fe I	5855.090	4.608	−1.48	···	···
Fe I	5856.100	4.294	−1.56	···	···
Fe I	5858.790	4.220	−2.18	···	···
Fe I	5859.600	4.550	−0.61	35.1	6.53
Fe I	5862.370	4.550	−0.25	48.1	6.40
Fe I	5956.700	0.859	−4.60	34.9	6.67
Fe I	6027.060	4.070	−1.17	33.9	6.59
Fe I	6151.620	2.176	−3.28	26.7	6.57
Fe I	6159.380	4.610	−1.83	···	···
Fe I	6165.360	4.143	−1.46	18.1	6.57
Fe I	6173.340	2.223	−2.88	44.3	6.58
Fe I	6200.320	2.609	−2.44	45.9	6.58
Fe I	6213.440	2.223	−2.56	59.8	6.56
Fe I	6240.652	2.220	−3.23	···	···
Fe I	6265.140	2.176	−2.55	61.9	6.54
Fe I	6271.283	3.330	−2.70	···	···
Fe I	6297.801	2.223	−2.73	72.9	6.98
Fe I	6322.694	2.588	−2.43	49.3	6.60
Fe I	6358.690	0.859	−4.00	48.7	6.33
Fe I	6436.410	4.186	−2.36	···	···
Fe I	6481.878	2.279	−2.97	45.1	6.73
Fe I	6498.950	0.958	−4.69	···	···
Fe I	6518.370	2.830	−2.45	39.2	6.68
Fe I	6574.233	0.990	−5.00	···	···
Fe I	6581.214	1.480	−4.68	···	···
Fe I	6591.330	4.593	−1.95	···	···
Fe I	6608.040	2.279	−3.91	···	···
Fe I	6625.027	1.010	−5.34	···	···
Fe I	6699.142	4.590	−2.10	···	···
Fe I	6713.750	4.795	−1.39	···	···
Fe I	6725.360	4.103	−2.17	···	···

Table B.1: Equivalent Width Measurements for F/G/K Primaries *(continued)*

Species	λ	E.P.	log(gf)	PM I03150+0102	
	(Å)	(eV)	(dex)	EW (mÅ)	Abundance
Fe I	6733.150	4.638	−1.40	···	···
Fe I	6739.524	1.560	−4.79	···	···
Fe I	6750.160	2.424	−2.62	48.3	6.58
Fe I	6752.711	4.640	−1.20	···	···
Fe I	6837.009	4.590	−1.69	···	···
Fe I	6857.250	4.076	−2.04	···	···
Fe I	6971.936	3.020	−3.34	···	···
Fe I	7112.170	2.990	−2.99	···	···
Fe I	7751.120	4.990	−0.73	···	···
Fe I	7802.510	5.080	−1.31	···	···
Fe I	7807.920	4.990	−0.73	30.3	6.93
Fe I	8365.644	3.250	−2.04	···	···
Fe I	8757.200	2.845	−2.12	···	···
Fe II	5234.620	3.221	−2.22	41.3	6.50
Fe II	5425.260	3.200	−3.16	11.0	6.54
Fe II	6149.250	3.889	−2.63	···	···
Fe II	6247.560	3.892	−2.27	18.0	6.61
Fe II	6369.490	2.891	−4.02	···	···
Fe II	6432.680	2.891	−3.52	···	···
Fe II	6456.390	3.903	−2.06	20.5	6.49
Fe II	7479.700	3.892	−3.53	···	···
Fe II	7515.840	3.903	−3.42	···	···
Ca I	5867.570	2.930	−1.57	···	···
Ca I	6166.440	2.520	−1.14	49.1	5.67
Ca I	6169.040	2.520	−0.80	82.4	5.82
Ca I	6455.610	2.520	−1.29	34.1	5.55
Ca I	6572.800	0.000	−4.28	···	···
Ti I	5024.850	0.818	−0.56	59.0	4.26
Ti I	5113.450	1.443	−0.73	···	···
Ti I	5219.710	0.021	−2.24	···	···
Ti I	5866.460	1.066	−0.76	41.2	4.32
Ti I	6091.180	2.267	−0.37	10.2	4.36
Ti I	6126.220	1.066	−1.37	19.7	4.44
Ti I	6258.090	1.443	−0.31	43.2	4.29

Table B.1: Equivalent Width Measurements for F/G/K Primaries *(continued)*

Species	λ	E.P.	log(gf)	PM I03256-3333E	
	(Å)	(eV)	(dex)	EW (mÅ)	Abundance
Fe I	5141.750	2.424	−2.18	···	···
Fe I	5247.060	0.087	−4.94	120.0	7.07
Fe I	5358.120	3.300	−3.16	···	···
Fe I	5412.788	4.440	−1.71	···	···
Fe I	5661.348	4.280	−1.75	···	···
Fe I	5778.458	2.590	−3.45	···	···
Fe I	5784.660	3.400	−2.53	···	···
Fe I	5809.220	3.884	−1.61	33.0	6.74
Fe I	5849.690	3.695	−2.93	···	···
Fe I	5852.230	4.549	−1.17	···	···
Fe I	5855.090	4.608	−1.48	···	···
Fe I	5856.100	4.294	−1.56	···	···
Fe I	5858.790	4.220	−2.18	···	···
Fe I	5859.600	4.550	−0.61	52.3	6.81
Fe I	5862.370	4.550	−0.25	54.4	6.48
Fe I	5956.700	0.859	−4.60	62.0	6.69
Fe I	6027.060	4.070	−1.17	41.6	6.68
Fe I	6151.620	2.176	−3.28	···	···
Fe I	6159.380	4.610	−1.83	···	···
Fe I	6165.360	4.143	−1.46	···	···
Fe I	6173.340	2.223	−2.88	68.0	6.72
Fe I	6200.320	2.609	−2.44	79.0	6.90
Fe I	6213.440	2.223	−2.56	···	···
Fe I	6240.652	2.220	−3.23	···	···
Fe I	6265.140	2.176	−2.55	97.7	6.77
Fe I	6271.283	3.330	−2.70	···	···
Fe I	6297.801	2.223	−2.73	77.5	6.72
Fe I	6322.694	2.588	−2.43	61.9	6.58
Fe I	6358.690	0.859	−4.00	90.9	6.58
Fe I	6436.410	4.186	−2.36	···	···
Fe I	6481.878	2.279	−2.97	61.6	6.75
Fe I	6498.950	0.958	−4.69	···	···
Fe I	6518.370	2.830	−2.45	46.1	6.59
Fe I	6574.233	0.990	−5.00	47.4	6.89
Fe I	6581.214	1.480	−4.68	39.0	7.01
Fe I	6591.330	4.593	−1.95	···	···
Fe I	6608.040	2.279	−3.91	···	···
Fe I	6625.027	1.010	−5.34	···	···
Fe I	6699.142	4.590	−2.10	···	···
Fe I	6713.750	4.795	−1.39	···	···
Fe I	6725.360	4.103	−2.17	···	···

Table B.1: Equivalent Width Measurements for F/G/K Primaries *(continued)*

Species	λ	E.P.	log(gf)	PM I03256-3333E	
	(Å)	(eV)	(dex)	EW (mÅ)	Abundance
Fe I	6733.150	4.638	−1.40	···	···
Fe I	6739.524	1.560	−4.79	···	···
Fe I	6750.160	2.424	−2.62	76.1	6.80
Fe I	6752.711	4.640	−1.20	···	···
Fe I	6837.009	4.590	−1.69	···	···
Fe I	6857.250	4.076	−2.04	···	···
Fe I	6971.936	3.020	−3.34	···	···
Fe I	7112.170	2.990	−2.99	···	···
Fe I	7751.120	4.990	−0.73	33.8	7.11
Fe I	7802.510	5.080	−1.31	···	···
Fe I	7807.920	4.990	−0.73	30.7	7.05
Fe I	8365.644	3.250	−2.04	···	···
Fe I	8757.200	2.845	−2.12	···	···
Fe II	5234.620	3.221	−2.22	···	···
Fe II	5425.260	3.200	−3.16	···	···
Fe II	6149.250	3.889	−2.63	···	···
Fe II	6247.560	3.892	−2.27	···	···
Fe II	6369.490	2.891	−4.02	···	···
Fe II	6432.680	2.891	−3.52	···	···
Fe II	6456.390	3.903	−2.06	···	···
Fe II	7479.700	3.892	−3.53	···	···
Fe II	7515.840	3.903	−3.42	···	···
Ca I	5867.570	2.930	−1.57	53.9	5.92
Ca I	6166.440	2.520	−1.14	148.3	6.04
Ca I	6169.040	2.520	−0.80	···	···
Ca I	6455.610	2.520	−1.29	101.7	5.78
Ca I	6572.800	0.000	−4.28	···	···
Ti I	5024.850	0.818	−0.56	···	···
Ti I	5113.450	1.443	−0.73	···	···
Ti I	5219.710	0.021	−2.24	101.2	4.62
Ti I	5866.460	1.066	−0.76	134.9	4.66
Ti I	6091.180	2.267	−0.37	58.0	4.65
Ti I	6126.220	1.066	−1.37	86.4	4.69
Ti I	6258.090	1.443	−0.31	137.9	4.64

Table B.1: Equivalent Width Measurements for F/G/K Primaries *(continued)*

Species	λ	E.P.	log(gf)	NLTT 12296	
	(Å)	(eV)	(dex)	EW (mÅ)	Abundance
Fe I	5141.750	2.424	−2.18	···	···
Fe I	5247.060	0.087	−4.94	82.4	6.48
Fe I	5358.120	3.300	−3.16	···	···
Fe I	5412.788	4.440	−1.71	···	···
Fe I	5661.348	4.280	−1.75	···	···
Fe I	5778.458	2.590	−3.45	···	···
Fe I	5784.660	3.400	−2.53	···	···
Fe I	5809.220	3.884	−1.61	22.4	6.36
Fe I	5849.690	3.695	−2.93	···	···
Fe I	5852.230	4.549	−1.17	···	···
Fe I	5855.090	4.608	−1.48	···	···
Fe I	5856.100	4.294	−1.56	···	···
Fe I	5858.790	4.220	−2.18	···	···
Fe I	5859.600	4.550	−0.61	36.7	6.40
Fe I	5862.370	4.550	−0.25	55.7	6.32
Fe I	5956.700	0.859	−4.60	···	···
Fe I	6027.060	4.070	−1.17	34.2	6.38
Fe I	6151.620	2.176	−3.28	38.9	6.39
Fe I	6159.380	4.610	−1.83	···	···
Fe I	6165.360	4.143	−1.46	···	···
Fe I	6173.340	2.223	−2.88	61.4	6.46
Fe I	6200.320	2.609	−2.44	65.5	6.54
Fe I	6213.440	2.223	−2.56	83.9	6.50
Fe I	6240.652	2.220	−3.23	···	···
Fe I	6265.140	2.176	−2.55	93.4	6.56
Fe I	6271.283	3.330	−2.70	···	···
Fe I	6297.801	2.223	−2.73	···	···
Fe I	6322.694	2.588	−2.43	71.5	6.59
Fe I	6358.690	0.859	−4.00	74.9	6.21
Fe I	6436.410	4.186	−2.36	···	···
Fe I	6481.878	2.279	−2.97	55.6	6.50
Fe I	6498.950	0.958	−4.69	···	···
Fe I	6518.370	2.830	−2.45	44.5	6.43
Fe I	6574.233	0.990	−5.00	···	···
Fe I	6581.214	1.480	−4.68	···	···
Fe I	6591.330	4.593	−1.95	···	···
Fe I	6608.040	2.279	−3.91	···	···
Fe I	6625.027	1.010	−5.34	···	···
Fe I	6699.142	4.590	−2.10	···	···
Fe I	6713.750	4.795	−1.39	···	···
Fe I	6725.360	4.103	−2.17	···	···

Table B.1: Equivalent Width Measurements for F/G/K Primaries *(continued)*

Species	λ	E.P.	log(gf)	NLTT 12296	
	(Å)	(eV)	(dex)	EW (mÅ)	Abundance
Fe I	6733.150	4.638	−1.40	···	···
Fe I	6739.524	1.560	−4.79	···	···
Fe I	6750.160	2.424	−2.62	65.1	6.47
Fe I	6752.711	4.640	−1.20	···	···
Fe I	6837.009	4.590	−1.69	···	···
Fe I	6857.250	4.076	−2.04	···	···
Fe I	6971.936	3.020	−3.34	···	···
Fe I	7112.170	2.990	−2.99	···	···
Fe I	7751.120	4.990	−0.73	···	···
Fe I	7802.510	5.080	−1.31	···	···
Fe I	7807.920	4.990	−0.73	19.4	6.61
Fe I	8365.644	3.250	−2.04	···	···
Fe I	8757.200	2.845	−2.12	···	···
Fe II	5234.620	3.221	−2.22	···	···
Fe II	5425.260	3.200	−3.16	···	···
Fe II	6149.250	3.889	−2.63	···	···
Fe II	6247.560	3.892	−2.27	···	···
Fe II	6369.490	2.891	−4.02	···	···
Fe II	6432.680	2.891	−3.52	···	···
Fe II	6456.390	3.903	−2.06	···	···
Fe II	7479.700	3.892	−3.53	···	···
Fe II	7515.840	3.903	−3.42	···	···
Ca I	5867.570	2.930	−1.57	···	···
Ca I	6166.440	2.520	−1.14	99.7	5.71
Ca I	6169.040	2.520	−0.80	151.4	5.80
Ca I	6455.610	2.520	−1.29	61.5	5.40
Ca I	6572.800	0.000	−4.28	···	···
Ti I	5024.850	0.818	−0.56	···	···
Ti I	5113.450	1.443	−0.73	···	···
Ti I	5219.710	0.021	−2.24	65.9	4.20
Ti I	5866.460	1.066	−0.76	104.7	4.49
Ti I	6091.180	2.267	−0.37	34.2	4.35
Ti I	6126.220	1.066	−1.37	57.1	4.34
Ti I	6258.090	1.443	−0.31	92.7	4.28

Table B.1: Equivalent Width Measurements for F/G/K Primaries *(continued)*

Species	λ	E.P.	log(gf)	PM I04072+1526N	
	(Å)	(eV)	(dex)	EW (mÅ)	Abundance
Fe I	5141.750	2.424	−2.18	75.4	7.09
Fe I	5247.060	0.087	−4.94	59.5	7.12
Fe I	5358.120	3.300	−3.16	···	···
Fe I	5412.788	4.440	−1.71	···	···
Fe I	5661.348	4.280	−1.75	···	···
Fe I	5778.458	2.590	−3.45	···	···
Fe I	5784.660	3.400	−2.53	···	···
Fe I	5809.220	3.884	−1.61	46.4	7.28
Fe I	5849.690	3.695	−2.93	···	···
Fe I	5852.230	4.549	−1.17	33.6	7.21
Fe I	5855.090	4.608	−1.48	15.7	7.11
Fe I	5856.100	4.294	−1.56	27.3	7.21
Fe I	5858.790	4.220	−2.18	···	···
Fe I	5859.600	4.550	−0.61	62.5	7.18
Fe I	5862.370	4.550	−0.25	75.3	7.01
Fe I	5956.700	0.859	−4.60	51.5	7.33
Fe I	6027.060	4.070	−1.17	59.3	7.25
Fe I	6151.620	2.176	−3.28	46.2	7.23
Fe I	6159.380	4.610	−1.83	···	···
Fe I	6165.360	4.143	−1.46	33.3	7.09
Fe I	6173.340	2.223	−2.88	62.2	7.22
Fe I	6200.320	2.609	−2.44	65.8	7.24
Fe I	6213.440	2.223	−2.56	73.5	7.13
Fe I	6240.652	2.220	−3.23	45.8	7.21
Fe I	6265.140	2.176	−2.55	79.0	7.18
Fe I	6271.283	3.330	−2.70	···	···
Fe I	6297.801	2.223	−2.73	···	···
Fe I	6322.694	2.588	−2.43	69.6	7.28
Fe I	6358.690	0.859	−4.00	72.3	7.15
Fe I	6436.410	4.186	−2.36	···	···
Fe I	6481.878	2.279	−2.97	58.6	7.27
Fe I	6498.950	0.958	−4.69	44.1	7.31
Fe I	6518.370	2.830	−2.45	59.2	7.31
Fe I	6574.233	0.990	−5.00	···	···
Fe I	6581.214	1.480	−4.68	···	···
Fe I	6591.330	4.593	−1.95	···	···
Fe I	6608.040	2.279	−3.91	···	···
Fe I	6625.027	1.010	−5.34	···	···
Fe I	6699.142	4.590	−2.10	···	···
Fe I	6713.750	4.795	−1.39	···	···
Fe I	6725.360	4.103	−2.17	···	···

Table B.1: Equivalent Width Measurements for F/G/K Primaries *(continued)*

Species	λ	E.P.	log(gf)	PM I04072+1526N	
	(Å)	(eV)	(dex)	EW (mÅ)	Abundance
Fe I	6733.150	4.638	−1.40	···	···
Fe I	6739.524	1.560	−4.79	···	···
Fe I	6750.160	2.424	−2.62	63.5	7.15
Fe I	6752.711	4.640	−1.20	22.8	7.05
Fe I	6837.009	4.590	−1.69	···	···
Fe I	6857.250	4.076	−2.04	19.7	7.24
Fe I	6971.936	3.020	−3.34	···	···
Fe I	7112.170	2.990	−2.99	···	···
Fe I	7751.120	4.990	−0.73	40.9	7.26
Fe I	7802.510	5.080	−1.31	···	···
Fe I	7807.920	4.990	−0.73	49.6	7.41
Fe I	8365.644	3.250	−2.04	···	···
Fe I	8757.200	2.845	−2.12	···	···
Fe II	5234.620	3.221	−2.22	64.8	7.16
Fe II	5425.260	3.200	−3.16	29.9	7.21
Fe II	6149.250	3.889	−2.63	28.4	7.30
Fe II	6247.560	3.892	−2.27	33.4	7.08
Fe II	6369.490	2.891	−4.02	···	···
Fe II	6432.680	2.891	−3.52	24.7	7.10
Fe II	6456.390	3.903	−2.06	42.7	7.10
Fe II	7479.700	3.892	−3.53	···	···
Fe II	7515.840	3.903	−3.42	69.3	4.81
Ca I	5867.570	2.930	−1.57	21.1	6.11
Ca I	6166.440	2.520	−1.14	67.2	6.16
Ca I	6169.040	2.520	−0.80	90.2	6.16
Ca I	6455.610	2.520	−1.29	53.1	6.06
Ca I	6572.800	0.000	−4.28	···	···
Ti I	5024.850	0.818	−0.56	···	···
Ti I	5113.450	1.443	−0.73	···	···
Ti I	5219.710	0.021	−2.24	···	···
Ti I	5866.460	1.066	−0.76	52.0	4.81
Ti I	6091.180	2.267	−0.37	···	···
Ti I	6126.220	1.066	−1.37	27.6	4.88
Ti I	6258.090	1.443	−0.31	53.6	4.75

Table B.1: Equivalent Width Measurements for F/G/K Primaries *(continued)*

Species	λ	E.P.	log(gf)	PM I04099+0942E	
	(Å)	(eV)	(dex)	EW (mÅ)	Abundance
Fe I	5141.750	2.424	−2.18	···	···
Fe I	5247.060	0.087	−4.94	···	···
Fe I	5358.120	3.300	−3.16	···	···
Fe I	5412.788	4.440	−1.71	···	···
Fe I	5661.348	4.280	−1.75	···	···
Fe I	5778.458	2.590	−3.45	···	···
Fe I	5784.660	3.400	−2.53	···	···
Fe I	5809.220	3.884	−1.61	15.1	6.20
Fe I	5849.690	3.695	−2.93	···	···
Fe I	5852.230	4.549	−1.17	···	···
Fe I	5855.090	4.608	−1.48	···	···
Fe I	5856.100	4.294	−1.56	···	···
Fe I	5858.790	4.220	−2.18	···	···
Fe I	5859.600	4.550	−0.61	···	···
Fe I	5862.370	4.550	−0.25	37.4	6.05
Fe I	5956.700	0.859	−4.60	33.0	6.29
Fe I	6027.060	4.070	−1.17	···	···
Fe I	6151.620	2.176	−3.28	···	···
Fe I	6159.380	4.610	−1.83	···	···
Fe I	6165.360	4.143	−1.46	14.4	6.29
Fe I	6173.340	2.223	−2.88	33.4	6.10
Fe I	6200.320	2.609	−2.44	···	···
Fe I	6213.440	2.223	−2.56	···	···
Fe I	6240.652	2.220	−3.23	···	···
Fe I	6265.140	2.176	−2.55	57.5	6.17
Fe I	6271.283	3.330	−2.70	···	···
Fe I	6297.801	2.223	−2.73	43.8	6.15
Fe I	6322.694	2.588	−2.43	34.8	6.07
Fe I	6358.690	0.859	−4.00	48.8	5.99
Fe I	6436.410	4.186	−2.36	···	···
Fe I	6481.878	2.279	−2.97	33.1	6.23
Fe I	6498.950	0.958	−4.69	20.0	6.14
Fe I	6518.370	2.830	−2.45	···	···
Fe I	6574.233	0.990	−5.00	···	···
Fe I	6581.214	1.480	−4.68	···	···
Fe I	6591.330	4.593	−1.95	···	···
Fe I	6608.040	2.279	−3.91	···	···
Fe I	6625.027	1.010	−5.34	···	···
Fe I	6699.142	4.590	−2.10	···	···
Fe I	6713.750	4.795	−1.39	···	···
Fe I	6725.360	4.103	−2.17	···	···

Table B.1: Equivalent Width Measurements for F/G/K Primaries *(continued)*

Species	λ	E.P.	log(gf)	PM I04099+0942E	
	(Å)	(eV)	(dex)	EW (mÅ)	Abundance
Fe I	6733.150	4.638	−1.40	···	···
Fe I	6739.524	1.560	−4.79	···	···
Fe I	6750.160	2.424	−2.62	44.0	6.24
Fe I	6752.711	4.640	−1.20	···	···
Fe I	6837.009	4.590	−1.69	···	···
Fe I	6857.250	4.076	−2.04	···	···
Fe I	6971.936	3.020	−3.34	···	···
Fe I	7112.170	2.990	−2.99	···	···
Fe I	7751.120	4.990	−0.73	···	···
Fe I	7802.510	5.080	−1.31	···	···
Fe I	7807.920	4.990	−0.73	···	···
Fe I	8365.644	3.250	−2.04	···	···
Fe I	8757.200	2.845	−2.12	···	···
Fe II	5234.620	3.221	−2.22	···	···
Fe II	5425.260	3.200	−3.16	···	···
Fe II	6149.250	3.889	−2.63	···	···
Fe II	6247.560	3.892	−2.27	···	···
Fe II	6369.490	2.891	−4.02	···	···
Fe II	6432.680	2.891	−3.52	···	···
Fe II	6456.390	3.903	−2.06	···	···
Fe II	7479.700	3.892	−3.53	···	···
Fe II	7515.840	3.903	−3.42	···	···
Ca I	5867.570	2.930	−1.57	···	···
Ca I	6166.440	2.520	−1.14	27.7	5.05
Ca I	6169.040	2.520	−0.80	58.6	5.22
Ca I	6455.610	2.520	−1.29	26.1	5.16
Ca I	6572.800	0.000	−4.28	···	···
Ti I	5024.850	0.818	−0.56	···	···
Ti I	5113.450	1.443	−0.73	···	···
Ti I	5219.710	0.021	−2.24	···	···
Ti I	5866.460	1.066	−0.76	43.6	4.02
Ti I	6091.180	2.267	−0.37	···	···
Ti I	6126.220	1.066	−1.37	···	···
Ti I	6258.090	1.443	−0.31	32.8	3.75

Table B.1: Equivalent Width Measurements for F/G/K Primaries *(continued)*

Species	λ	E.P.	log(gf)	PM I04254-4601	
	(Å)	(eV)	(dex)	EW (mÅ)	Abundance
Fe I	5141.750	2.424	−2.18	68.4	6.22
Fe I	5247.060	0.087	−4.94	58.4	6.21
Fe I	5358.120	3.300	−3.16	···	···
Fe I	5412.788	4.440	−1.71	···	···
Fe I	5661.348	4.280	−1.75	···	···
Fe I	5778.458	2.590	−3.45	···	···
Fe I	5784.660	3.400	−2.53	···	···
Fe I	5809.220	3.884	−1.61	9.2	5.94
Fe I	5849.690	3.695	−2.93	···	···
Fe I	5852.230	4.549	−1.17	···	···
Fe I	5855.090	4.608	−1.48	···	···
Fe I	5856.100	4.294	−1.56	···	···
Fe I	5858.790	4.220	−2.18	···	···
Fe I	5859.600	4.550	−0.61	26.1	6.18
Fe I	5862.370	4.550	−0.25	39.5	6.06
Fe I	5956.700	0.859	−4.60	34.0	6.26
Fe I	6027.060	4.070	−1.17	23.7	6.17
Fe I	6151.620	2.176	−3.28	24.8	6.22
Fe I	6159.380	4.610	−1.83	···	···
Fe I	6165.360	4.143	−1.46	···	···
Fe I	6173.340	2.223	−2.88	42.5	6.22
Fe I	6200.320	2.609	−2.44	45.5	6.26
Fe I	6213.440	2.223	−2.56	56.6	6.13
Fe I	6240.652	2.220	−3.23	21.0	6.12
Fe I	6265.140	2.176	−2.55	64.6	6.19
Fe I	6271.283	3.330	−2.70	···	···
Fe I	6297.801	2.223	−2.73	68.2	6.48
Fe I	6322.694	2.588	−2.43	47.7	6.25
Fe I	6358.690	0.859	−4.00	50.6	5.93
Fe I	6436.410	4.186	−2.36	···	···
Fe I	6481.878	2.279	−2.97	34.8	6.22
Fe I	6498.950	0.958	−4.69	27.2	6.29
Fe I	6518.370	2.830	−2.45	30.0	6.22
Fe I	6574.233	0.990	−5.00	···	···
Fe I	6581.214	1.480	−4.68	···	···
Fe I	6591.330	4.593	−1.95	···	···
Fe I	6608.040	2.279	−3.91	···	···
Fe I	6625.027	1.010	−5.34	···	···
Fe I	6699.142	4.590	−2.10	···	···
Fe I	6713.750	4.795	−1.39	···	···
Fe I	6725.360	4.103	−2.17	···	···

Table B.1: Equivalent Width Measurements for F/G/K Primaries *(continued)*

Species	λ	E.P.	log(gf)	PM I04254-4601	
	(Å)	(eV)	(dex)	EW (mÅ)	Abundance
Fe I	6733.150	4.638	−1.40	···	···
Fe I	6739.524	1.560	−4.79	···	···
Fe I	6750.160	2.424	−2.62	44.4	6.19
Fe I	6752.711	4.640	−1.20	···	···
Fe I	6837.009	4.590	−1.69	···	···
Fe I	6857.250	4.076	−2.04	···	···
Fe I	6971.936	3.020	−3.34	···	···
Fe I	7112.170	2.990	−2.99	···	···
Fe I	7751.120	4.990	−0.73	···	···
Fe I	7802.510	5.080	−1.31	···	···
Fe I	7807.920	4.990	−0.73	16.4	6.47
Fe I	8365.644	3.250	−2.04	···	···
Fe I	8757.200	2.845	−2.12	···	···
Fe II	5234.620	3.221	−2.22	23.7	6.11
Fe II	5425.260	3.200	−3.16	···	···
Fe II	6149.250	3.889	−2.63	···	···
Fe II	6247.560	3.892	−2.27	···	···
Fe II	6369.490	2.891	−4.02	···	···
Fe II	6432.680	2.891	−3.52	···	···
Fe II	6456.390	3.903	−2.06	10.0	6.18
Fe II	7479.700	3.892	−3.53	···	···
Fe II	7515.840	3.903	−3.42	···	···
Ca I	5867.570	2.930	−1.57	···	···
Ca I	6166.440	2.520	−1.14	59.2	5.53
Ca I	6169.040	2.520	−0.80	93.2	5.59
Ca I	6455.610	2.520	−1.29	41.9	5.42
Ca I	6572.800	0.000	−4.28	···	···
Ti I	5024.850	0.818	−0.56	75.0	4.06
Ti I	5113.450	1.443	−0.73	···	···
Ti I	5219.710	0.021	−2.24	33.1	4.11
Ti I	5866.460	1.066	−0.76	59.8	4.22
Ti I	6091.180	2.267	−0.37	···	···
Ti I	6126.220	1.066	−1.37	···	···
Ti I	6258.090	1.443	−0.31	61.7	4.19

Table B.1: Equivalent Width Measurements for F/G/K Primaries *(continued)*

Species	λ	E.P.	log(gf)	PM I04325-5657N	
	(Å)	(eV)	(dex)	EW (mÅ)	Abundance
Fe I	5141.750	2.424	−2.18	58.2	6.50
Fe I	5247.060	0.087	−4.94	48.7	6.59
Fe I	5358.120	3.300	−3.16	···	···
Fe I	5412.788	4.440	−1.71	···	···
Fe I	5661.348	4.280	−1.75	···	···
Fe I	5778.458	2.590	−3.45	···	···
Fe I	5784.660	3.400	−2.53	···	···
Fe I	5809.220	3.884	−1.61	16.3	6.43
Fe I	5849.690	3.695	−2.93	···	···
Fe I	5852.230	4.549	−1.17	20.9	6.79
Fe I	5855.090	4.608	−1.48	···	···
Fe I	5856.100	4.294	−1.56	···	···
Fe I	5858.790	4.220	−2.18	···	···
Fe I	5859.600	4.550	−0.61	34.2	6.53
Fe I	5862.370	4.550	−0.25	57.2	6.56
Fe I	5956.700	0.859	−4.60	29.1	6.58
Fe I	6027.060	4.070	−1.17	31.0	6.55
Fe I	6151.620	2.176	−3.28	24.5	6.54
Fe I	6159.380	4.610	−1.83	···	···
Fe I	6165.360	4.143	−1.46	···	···
Fe I	6173.340	2.223	−2.88	45.5	6.66
Fe I	6200.320	2.609	−2.44	···	···
Fe I	6213.440	2.223	−2.56	58.8	6.61
Fe I	6240.652	2.220	−3.23	···	···
Fe I	6265.140	2.176	−2.55	55.4	6.48
Fe I	6271.283	3.330	−2.70	···	···
Fe I	6297.801	2.223	−2.73	···	···
Fe I	6322.694	2.588	−2.43	50.6	6.69
Fe I	6358.690	0.859	−4.00	···	···
Fe I	6436.410	4.186	−2.36	···	···
Fe I	6481.878	2.279	−2.97	···	···
Fe I	6498.950	0.958	−4.69	···	···
Fe I	6518.370	2.830	−2.45	···	···
Fe I	6574.233	0.990	−5.00	···	···
Fe I	6581.214	1.480	−4.68	···	···
Fe I	6591.330	4.593	−1.95	···	···
Fe I	6608.040	2.279	−3.91	···	···
Fe I	6625.027	1.010	−5.34	···	···
Fe I	6699.142	4.590	−2.10	···	···
Fe I	6713.750	4.795	−1.39	···	···
Fe I	6725.360	4.103	−2.17	···	···

Table B.1: Equivalent Width Measurements for F/G/K Primaries *(continued)*

Species	λ	E.P.	log(gf)	PM I04325-5657N	
	(Å)	(eV)	(dex)	EW (mÅ)	Abundance
Fe I	6733.150	4.638	−1.40	···	···
Fe I	6739.524	1.560	−4.79	···	···
Fe I	6750.160	2.424	−2.62	47.8	6.63
Fe I	6752.711	4.640	−1.20	···	···
Fe I	6837.009	4.590	−1.69	···	···
Fe I	6857.250	4.076	−2.04	···	···
Fe I	6971.936	3.020	−3.34	···	···
Fe I	7112.170	2.990	−2.99	···	···
Fe I	7751.120	4.990	−0.73	···	···
Fe I	7802.510	5.080	−1.31	···	···
Fe I	7807.920	4.990	−0.73	···	···
Fe I	8365.644	3.250	−2.04	···	···
Fe I	8757.200	2.845	−2.12	···	···
Fe II	5234.620	3.221	−2.22	38.9	6.56
Fe II	5425.260	3.200	−3.16	···	···
Fe II	6149.250	3.889	−2.63	···	···
Fe II	6247.560	3.892	−2.27	···	···
Fe II	6369.490	2.891	−4.02	···	···
Fe II	6432.680	2.891	−3.52	···	···
Fe II	6456.390	3.903	−2.06	21.3	6.60
Fe II	7479.700	3.892	−3.53	···	···
Fe II	7515.840	3.903	−3.42	···	···
Ca I	5867.570	2.930	−1.57	···	···
Ca I	6166.440	2.520	−1.14	58.2	5.82
Ca I	6169.040	2.520	−0.80	86.9	5.88
Ca I	6455.610	2.520	−1.29	49.7	5.82
Ca I	6572.800	0.000	−4.28	···	···
Ti I	5024.850	0.818	−0.56	55.6	4.25
Ti I	5113.450	1.443	−0.73	···	···
Ti I	5219.710	0.021	−2.24	···	···
Ti I	5866.460	1.066	−0.76	47.3	4.47
Ti I	6091.180	2.267	−0.37	···	···
Ti I	6126.220	1.066	−1.37	···	···
Ti I	6258.090	1.443	−0.31	54.3	4.53

Table B.1: Equivalent Width Measurements for F/G/K Primaries *(continued)*

Species	λ	E.P.	log(gf)	PM I04327+0820	
	(Å)	(eV)	(dex)	EW (mÅ)	Abundance
Fe I	5141.750	2.424	−2.18	33.8	6.11
Fe I	5247.060	0.087	−4.94	23.1	6.21
Fe I	5358.120	3.300	−3.16	···	···
Fe I	5412.788	4.440	−1.71	···	···
Fe I	5661.348	4.280	−1.75	···	···
Fe I	5778.458	2.590	−3.45	···	···
Fe I	5784.660	3.400	−2.53	···	···
Fe I	5809.220	3.884	−1.61	10.6	6.29
Fe I	5849.690	3.695	−2.93	···	···
Fe I	5852.230	4.549	−1.17	···	···
Fe I	5855.090	4.608	−1.48	···	···
Fe I	5856.100	4.294	−1.56	···	···
Fe I	5858.790	4.220	−2.18	···	···
Fe I	5859.600	4.550	−0.61	18.6	6.24
Fe I	5862.370	4.550	−0.25	28.3	6.12
Fe I	5956.700	0.859	−4.60	11.9	6.26
Fe I	6027.060	4.070	−1.17	12.1	6.10
Fe I	6151.620	2.176	−3.28	···	···
Fe I	6159.380	4.610	−1.83	···	···
Fe I	6165.360	4.143	−1.46	···	···
Fe I	6173.340	2.223	−2.88	23.3	6.30
Fe I	6200.320	2.609	−2.44	27.0	6.34
Fe I	6213.440	2.223	−2.56	32.6	6.20
Fe I	6240.652	2.220	−3.23	···	···
Fe I	6265.140	2.176	−2.55	34.7	6.19
Fe I	6271.283	3.330	−2.70	···	···
Fe I	6297.801	2.223	−2.73	28.7	6.28
Fe I	6322.694	2.588	−2.43	35.4	6.49
Fe I	6358.690	0.859	−4.00	22.0	5.97
Fe I	6436.410	4.186	−2.36	···	···
Fe I	6481.878	2.279	−2.97	16.9	6.25
Fe I	6498.950	0.958	−4.69	···	···
Fe I	6518.370	2.830	−2.45	···	···
Fe I	6574.233	0.990	−5.00	···	···
Fe I	6581.214	1.480	−4.68	···	···
Fe I	6591.330	4.593	−1.95	···	···
Fe I	6608.040	2.279	−3.91	···	···
Fe I	6625.027	1.010	−5.34	···	···
Fe I	6699.142	4.590	−2.10	···	···
Fe I	6713.750	4.795	−1.39	···	···
Fe I	6725.360	4.103	−2.17	···	···

Table B.1: Equivalent Width Measurements for F/G/K Primaries *(continued)*

Species	λ	E.P.	log(gf)	PM I04327+0820	
	(Å)	(eV)	(dex)	EW (mÅ)	Abundance
Fe I	6733.150	4.638	−1.40	···	···
Fe I	6739.524	1.560	−4.79	···	···
Fe I	6750.160	2.424	−2.62	26.1	6.29
Fe I	6752.711	4.640	−1.20	···	···
Fe I	6837.009	4.590	−1.69	···	···
Fe I	6857.250	4.076	−2.04	···	···
Fe I	6971.936	3.020	−3.34	···	···
Fe I	7112.170	2.990	−2.99	···	···
Fe I	7751.120	4.990	−0.73	···	···
Fe I	7802.510	5.080	−1.31	···	···
Fe I	7807.920	4.990	−0.73	9.3	6.37
Fe I	8365.644	3.250	−2.04	···	···
Fe I	8757.200	2.845	−2.12	···	···
Fe II	5234.620	3.221	−2.22	37.3	6.25
Fe II	5425.260	3.200	−3.16	9.7	6.33
Fe II	6149.250	3.889	−2.63	···	···
Fe II	6247.560	3.892	−2.27	11.7	6.19
Fe II	6369.490	2.891	−4.02	···	···
Fe II	6432.680	2.891	−3.52	···	···
Fe II	6456.390	3.903	−2.06	14.1	6.09
Fe II	7479.700	3.892	−3.53	···	···
Fe II	7515.840	3.903	−3.42	···	···
Ca I	5867.570	2.930	−1.57	···	···
Ca I	6166.440	2.520	−1.14	36.1	5.58
Ca I	6169.040	2.520	−0.80	58.8	5.62
Ca I	6455.610	2.520	−1.29	17.4	5.29
Ca I	6572.800	0.000	−4.28	···	···
Ti I	5024.850	0.818	−0.56	···	···
Ti I	5113.450	1.443	−0.73	31.9	3.95
Ti I	5219.710	0.021	−2.24	···	···
Ti I	5866.460	1.066	−0.76	24.8	4.19
Ti I	6091.180	2.267	−0.37	···	···
Ti I	6126.220	1.066	−1.37	10.3	4.31
Ti I	6258.090	1.443	−0.31	28.9	4.21

Table B.1: Equivalent Width Measurements for F/G/K Primaries *(continued)*

Species	λ	E.P.	log(gf)	NLTT 14407	
	(Å)	(eV)	(dex)	EW (mÅ)	Abundance
Fe I	5141.750	2.424	−2.18	···	···
Fe I	5247.060	0.087	−4.94	···	···
Fe I	5358.120	3.300	−3.16	···	···
Fe I	5412.788	4.440	−1.71	···	···
Fe I	5661.348	4.280	−1.75	···	···
Fe I	5778.458	2.590	−3.45	···	···
Fe I	5784.660	3.400	−2.53	···	···
Fe I	5809.220	3.884	−1.61	28.0	6.50
Fe I	5849.690	3.695	−2.93	···	···
Fe I	5852.230	4.549	−1.17	···	···
Fe I	5855.090	4.608	−1.48	···	···
Fe I	5856.100	4.294	−1.56	···	···
Fe I	5858.790	4.220	−2.18	···	···
Fe I	5859.600	4.550	−0.61	35.4	6.39
Fe I	5862.370	4.550	−0.25	57.3	6.35
Fe I	5956.700	0.859	−4.60	62.4	6.48
Fe I	6027.060	4.070	−1.17	36.2	6.43
Fe I	6151.620	2.176	−3.28	40.3	6.38
Fe I	6159.380	4.610	−1.83	···	···
Fe I	6165.360	4.143	−1.46	···	···
Fe I	6173.340	2.223	−2.88	64.4	6.44
Fe I	6200.320	2.609	−2.44	72.4	6.58
Fe I	6213.440	2.223	−2.56	88.4	6.47
Fe I	6240.652	2.220	−3.23	···	···
Fe I	6265.140	2.176	−2.55	91.7	6.45
Fe I	6271.283	3.330	−2.70	···	···
Fe I	6297.801	2.223	−2.73	72.9	6.42
Fe I	6322.694	2.588	−2.43	68.3	6.47
Fe I	6358.690	0.859	−4.00	···	···
Fe I	6436.410	4.186	−2.36	···	···
Fe I	6481.878	2.279	−2.97	59.8	6.51
Fe I	6498.950	0.958	−4.69	···	···
Fe I	6518.370	2.830	−2.45	41.1	6.33
Fe I	6574.233	0.990	−5.00	34.5	6.50
Fe I	6581.214	1.480	−4.68	···	···
Fe I	6591.330	4.593	−1.95	···	···
Fe I	6608.040	2.279	−3.91	···	···
Fe I	6625.027	1.010	−5.34	···	···
Fe I	6699.142	4.590	−2.10	···	···
Fe I	6713.750	4.795	−1.39	···	···
Fe I	6725.360	4.103	−2.17	···	···

Table B.1: Equivalent Width Measurements for F/G/K Primaries *(continued)*

Species	λ	E.P.	log(gf)	NLTT 14407	
	(Å)	(eV)	(dex)	EW (mÅ)	Abundance
Fe I	6733.150	4.638	−1.40	···	···
Fe I	6739.524	1.560	−4.79	···	···
Fe I	6750.160	2.424	−2.62	66.8	6.43
Fe I	6752.711	4.640	−1.20	···	···
Fe I	6837.009	4.590	−1.69	···	···
Fe I	6857.250	4.076	−2.04	···	···
Fe I	6971.936	3.020	−3.34	···	···
Fe I	7112.170	2.990	−2.99	···	···
Fe I	7751.120	4.990	−0.73	···	···
Fe I	7802.510	5.080	−1.31	···	···
Fe I	7807.920	4.990	−0.73	···	···
Fe I	8365.644	3.250	−2.04	···	···
Fe I	8757.200	2.845	−2.12	···	···
Fe II	5234.620	3.221	−2.22	···	···
Fe II	5425.260	3.200	−3.16	···	···
Fe II	6149.250	3.889	−2.63	···	···
Fe II	6247.560	3.892	−2.27	···	···
Fe II	6369.490	2.891	−4.02	···	···
Fe II	6432.680	2.891	−3.52	···	···
Fe II	6456.390	3.903	−2.06	···	···
Fe II	7479.700	3.892	−3.53	···	···
Fe II	7515.840	3.903	−3.42	···	···
Ca I	5867.570	2.930	−1.57	33.1	5.65
Ca I	6166.440	2.520	−1.14	117.2	5.76
Ca I	6169.040	2.520	−0.80	174.1	5.83
Ca I	6455.610	2.520	−1.29	84.0	5.56
Ca I	6572.800	0.000	−4.28	···	···
Ti I	5024.850	0.818	−0.56	···	···
Ti I	5113.450	1.443	−0.73	···	···
Ti I	5219.710	0.021	−2.24	82.7	4.25
Ti I	5866.460	1.066	−0.76	109.4	4.34
Ti I	6091.180	2.267	−0.37	42.1	4.37
Ti I	6126.220	1.066	−1.37	77.1	4.47
Ti I	6258.090	1.443	−0.31	118.3	4.40

Table B.1: Equivalent Width Measurements for F/G/K Primaries *(continued)*

Species	λ (Å)	E.P. (eV)	log(gf) (dex)	PM I05484-3617Nn EW (mÅ)	Abundance
Fe I	5141.750	2.424	−2.18	89.7	6.61
Fe I	5247.060	0.087	−4.94	66.5	6.37
Fe I	5358.120	3.300	−3.16	···	···
Fe I	5412.788	4.440	−1.71	···	···
Fe I	5661.348	4.280	−1.75	···	···
Fe I	5778.458	2.590	−3.45	···	···
Fe I	5784.660	3.400	−2.53	···	···
Fe I	5809.220	3.884	−1.61	22.0	6.38
Fe I	5849.690	3.695	−2.93	···	···
Fe I	5852.230	4.549	−1.17	···	···
Fe I	5855.090	4.608	−1.48	···	···
Fe I	5856.100	4.294	−1.56	···	···
Fe I	5858.790	4.220	−2.18	···	···
Fe I	5859.600	4.550	−0.61	38.0	6.42
Fe I	5862.370	4.550	−0.25	48.8	6.23
Fe I	5956.700	0.859	−4.60	53.0	6.59
Fe I	6027.060	4.070	−1.17	37.7	6.47
Fe I	6151.620	2.176	−3.28	32.4	6.37
Fe I	6159.380	4.610	−1.83	···	···
Fe I	6165.360	4.143	−1.46	24.5	6.56
Fe I	6173.340	2.223	−2.88	52.2	6.39
Fe I	6200.320	2.609	−2.44	63.7	6.59
Fe I	6213.440	2.223	−2.56	72.1	6.42
Fe I	6240.652	2.220	−3.23	32.2	6.36
Fe I	6265.140	2.176	−2.55	77.5	6.44
Fe I	6271.283	3.330	−2.70	···	···
Fe I	6297.801	2.223	−2.73	78.5	6.69
Fe I	6322.694	2.588	−2.43	59.1	6.46
Fe I	6358.690	0.859	−4.00	61.7	6.13
Fe I	6436.410	4.186	−2.36	···	···
Fe I	6481.878	2.279	−2.97	51.5	6.52
Fe I	6498.950	0.958	−4.69	44.3	6.60
Fe I	6518.370	2.830	−2.45	39.9	6.41
Fe I	6574.233	0.990	−5.00	22.1	6.47
Fe I	6581.214	1.480	−4.68	···	···
Fe I	6591.330	4.593	−1.95	···	···
Fe I	6608.040	2.279	−3.91	···	···
Fe I	6625.027	1.010	−5.34	···	···
Fe I	6699.142	4.590	−2.10	···	···
Fe I	6713.750	4.795	−1.39	···	···
Fe I	6725.360	4.103	−2.17	···	···

Table B.1: Equivalent Width Measurements for F/G/K Primaries *(continued)*

Species	λ	E.P.	log(gf)	PM I05484-3617Nn	
	(Å)	(eV)	(dex)	EW (mÅ)	Abundance
Fe I	6733.150	4.638	−1.40	···	···
Fe I	6739.524	1.560	−4.79	···	···
Fe I	6750.160	2.424	−2.62	57.1	6.42
Fe I	6752.711	4.640	−1.20	···	···
Fe I	6837.009	4.590	−1.69	···	···
Fe I	6857.250	4.076	−2.04	···	···
Fe I	6971.936	3.020	−3.34	···	···
Fe I	7112.170	2.990	−2.99	···	···
Fe I	7751.120	4.990	−0.73	···	···
Fe I	7802.510	5.080	−1.31	···	···
Fe I	7807.920	4.990	−0.73	21.5	6.62
Fe I	8365.644	3.250	−2.04	···	···
Fe I	8757.200	2.845	−2.12	···	···
Fe II	5234.620	3.221	−2.22	25.0	6.30
Fe II	5425.260	3.200	−3.16	···	···
Fe II	6149.250	3.889	−2.63	···	···
Fe II	6247.560	3.892	−2.27	7.3	6.36
Fe II	6369.490	2.891	−4.02	···	···
Fe II	6432.680	2.891	−3.52	···	···
Fe II	6456.390	3.903	−2.06	13.4	6.49
Fe II	7479.700	3.892	−3.53	···	···
Fe II	7515.840	3.903	−3.42	···	···
Ca I	5867.570	2.930	−1.57	16.4	5.58
Ca I	6166.440	2.520	−1.14	74.5	5.68
Ca I	6169.040	2.520	−0.80	112.3	5.77
Ca I	6455.610	2.520	−1.29	54.5	5.55
Ca I	6572.800	0.000	−4.28	···	···
Ti I	5024.850	0.818	−0.56	81.6	4.13
Ti I	5113.450	1.443	−0.73	···	···
Ti I	5219.710	0.021	−2.24	44.3	4.20
Ti I	5866.460	1.066	−0.76	70.7	4.34
Ti I	6091.180	2.267	−0.37	15.3	4.19
Ti I	6126.220	1.066	−1.37	32.7	4.25
Ti I	6258.090	1.443	−0.31	65.0	4.19

Table B.1: Equivalent Width Measurements for F/G/K Primaries *(continued)*

Species	λ	E.P.	log(gf)	PM I06032+1921N	
	(Å)	(eV)	(dex)	EW (mÅ)	Abundance
Fe I	5141.750	2.424	−2.18	51.4	6.51
Fe I	5247.060	0.087	−4.94	34.1	6.42
Fe I	5358.120	3.300	−3.16	···	···
Fe I	5412.788	4.440	−1.71	···	···
Fe I	5661.348	4.280	−1.75	···	···
Fe I	5778.458	2.590	−3.45	···	···
Fe I	5784.660	3.400	−2.53	···	···
Fe I	5809.220	3.884	−1.61	15.0	6.44
Fe I	5849.690	3.695	−2.93	···	···
Fe I	5852.230	4.549	−1.17	···	···
Fe I	5855.090	4.608	−1.48	···	···
Fe I	5856.100	4.294	−1.56	···	···
Fe I	5858.790	4.220	−2.18	···	···
Fe I	5859.600	4.550	−0.61	28.2	6.46
Fe I	5862.370	4.550	−0.25	38.8	6.33
Fe I	5956.700	0.859	−4.60	21.3	6.50
Fe I	6027.060	4.070	−1.17	24.4	6.46
Fe I	6151.620	2.176	−3.28	16.1	6.38
Fe I	6159.380	4.610	−1.83	···	···
Fe I	6165.360	4.143	−1.46	12.4	6.43
Fe I	6173.340	2.223	−2.88	30.6	6.44
Fe I	6200.320	2.609	−2.44	33.8	6.48
Fe I	6213.440	2.223	−2.56	47.4	6.52
Fe I	6240.652	2.220	−3.23	···	···
Fe I	6265.140	2.176	−2.55	53.4	6.60
Fe I	6271.283	3.330	−2.70	···	···
Fe I	6297.801	2.223	−2.73	36.7	6.44
Fe I	6322.694	2.588	−2.43	34.0	6.44
Fe I	6358.690	0.859	−4.00	36.7	6.28
Fe I	6436.410	4.186	−2.36	···	···
Fe I	6481.878	2.279	−2.97	30.6	6.58
Fe I	6498.950	0.958	−4.69	19.5	6.61
Fe I	6518.370	2.830	−2.45	19.7	6.33
Fe I	6574.233	0.990	−5.00	···	···
Fe I	6581.214	1.480	−4.68	···	···
Fe I	6591.330	4.593	−1.95	···	···
Fe I	6608.040	2.279	−3.91	···	···
Fe I	6625.027	1.010	−5.34	···	···
Fe I	6699.142	4.590	−2.10	···	···
Fe I	6713.750	4.795	−1.39	···	···
Fe I	6725.360	4.103	−2.17	···	···

Table B.1: Equivalent Width Measurements for F/G/K Primaries *(continued)*

Species	λ	E.P.	log(gf)	PM I06032+1921N	
	(Å)	(eV)	(dex)	EW (mÅ)	Abundance
Fe I	6733.150	4.638	−1.40	···	···
Fe I	6739.524	1.560	−4.79	···	···
Fe I	6750.160	2.424	−2.62	35.5	6.48
Fe I	6752.711	4.640	−1.20	···	···
Fe I	6837.009	4.590	−1.69	···	···
Fe I	6857.250	4.076	−2.04	···	···
Fe I	6971.936	3.020	−3.34	···	···
Fe I	7112.170	2.990	−2.99	···	···
Fe I	7751.120	4.990	−0.73	···	···
Fe I	7802.510	5.080	−1.31	···	···
Fe I	7807.920	4.990	−0.73	20.4	6.75
Fe I	8365.644	3.250	−2.04	···	···
Fe I	8757.200	2.845	−2.12	···	···
Fe II	5234.620	3.221	−2.22	48.6	6.72
Fe II	5425.260	3.200	−3.16	9.0	6.37
Fe II	6149.250	3.889	−2.63	6.9	6.37
Fe II	6247.560	3.892	−2.27	17.2	6.51
Fe II	6369.490	2.891	−4.02	···	···
Fe II	6432.680	2.891	−3.52	12.5	6.57
Fe II	6456.390	3.903	−2.06	21.9	6.47
Fe II	7479.700	3.892	−3.53	···	···
Fe II	7515.840	3.903	−3.42	···	···
Ca I	5867.570	2.930	−1.57	7.3	5.51
Ca I	6166.440	2.520	−1.14	41.7	5.66
Ca I	6169.040	2.520	−0.80	62.6	5.68
Ca I	6455.610	2.520	−1.29	27.1	5.50
Ca I	6572.800	0.000	−4.28	21.6	5.76
Ti I	5024.850	0.818	−0.56	39.0	4.06
Ti I	5113.450	1.443	−0.73	···	···
Ti I	5219.710	0.021	−2.24	15.9	4.28
Ti I	5866.460	1.066	−0.76	24.7	4.12
Ti I	6091.180	2.267	−0.37	···	···
Ti I	6126.220	1.066	−1.37	10.3	4.22
Ti I	6258.090	1.443	−0.31	27.6	4.11

Table B.1: Equivalent Width Measurements for F/G/K Primaries *(continued)*

Species	λ	E.P.	log(gf)	PM I06050+0723S	
	(Å)	(eV)	(dex)	EW (mÅ)	Abundance
Fe I	5141.750	2.424	−2.18	···	···
Fe I	5247.060	0.087	−4.94	···	···
Fe I	5358.120	3.300	−3.16	···	···
Fe I	5412.788	4.440	−1.71	···	···
Fe I	5661.348	4.280	−1.75	···	···
Fe I	5778.458	2.590	−3.45	···	···
Fe I	5784.660	3.400	−2.53	···	···
Fe I	5809.220	3.884	−1.61	···	···
Fe I	5849.690	3.695	−2.93	···	···
Fe I	5852.230	4.549	−1.17	···	···
Fe I	5855.090	4.608	−1.48	···	···
Fe I	5856.100	4.294	−1.56	···	···
Fe I	5858.790	4.220	−2.18	···	···
Fe I	5859.600	4.550	−0.61	···	···
Fe I	5862.370	4.550	−0.25	···	···
Fe I	5956.700	0.859	−4.60	59.2	6.17
Fe I	6027.060	4.070	−1.17	···	···
Fe I	6151.620	2.176	−3.28	26.9	6.08
Fe I	6159.380	4.610	−1.83	···	···
Fe I	6165.360	4.143	−1.46	···	···
Fe I	6173.340	2.223	−2.88	50.4	6.16
Fe I	6200.320	2.609	−2.44	50.5	6.23
Fe I	6213.440	2.223	−2.56	···	···
Fe I	6240.652	2.220	−3.23	···	···
Fe I	6265.140	2.176	−2.55	84.1	6.21
Fe I	6271.283	3.330	−2.70	···	···
Fe I	6297.801	2.223	−2.73	···	···
Fe I	6322.694	2.588	−2.43	38.9	6.00
Fe I	6358.690	0.859	−4.00	73.6	5.74
Fe I	6436.410	4.186	−2.36	···	···
Fe I	6481.878	2.279	−2.97	42.5	6.19
Fe I	6498.950	0.958	−4.69	59.8	6.36
Fe I	6518.370	2.830	−2.45	···	···
Fe I	6574.233	0.990	−5.00	33.1	6.28
Fe I	6581.214	1.480	−4.68	···	···
Fe I	6591.330	4.593	−1.95	···	···
Fe I	6608.040	2.279	−3.91	···	···
Fe I	6625.027	1.010	−5.34	···	···
Fe I	6699.142	4.590	−2.10	···	···
Fe I	6713.750	4.795	−1.39	···	···
Fe I	6725.360	4.103	−2.17	···	···

Table B.1: Equivalent Width Measurements for F/G/K Primaries *(continued)*

Species	λ	E.P.	log(gf)	PM I06050+0723S	
	(Å)	(eV)	(dex)	EW (mÅ)	Abundance
Fe I	6733.150	4.638	−1.40	···	···
Fe I	6739.524	1.560	−4.79	···	···
Fe I	6750.160	2.424	−2.62	50.8	6.15
Fe I	6752.711	4.640	−1.20	···	···
Fe I	6837.009	4.590	−1.69	···	···
Fe I	6857.250	4.076	−2.04	···	···
Fe I	6971.936	3.020	−3.34	···	···
Fe I	7112.170	2.990	−2.99	···	···
Fe I	7751.120	4.990	−0.73	···	···
Fe I	7802.510	5.080	−1.31	···	···
Fe I	7807.920	4.990	−0.73	···	···
Fe I	8365.644	3.250	−2.04	···	···
Fe I	8757.200	2.845	−2.12	···	···
Fe II	5234.620	3.221	−2.22	···	···
Fe II	5425.260	3.200	−3.16	···	···
Fe II	6149.250	3.889	−2.63	···	···
Fe II	6247.560	3.892	−2.27	···	···
Fe II	6369.490	2.891	−4.02	···	···
Fe II	6432.680	2.891	−3.52	···	···
Fe II	6456.390	3.903	−2.06	···	···
Fe II	7479.700	3.892	−3.53	···	···
Fe II	7515.840	3.903	−3.42	···	···
Ca I	5867.570	2.930	−1.57	···	···
Ca I	6166.440	2.520	−1.14	128.1	5.34
Ca I	6169.040	2.520	−0.80	···	···
Ca I	6455.610	2.520	−1.29	100.2	5.25
Ca I	6572.800	0.000	−4.28	···	···
Ti I	5024.850	0.818	−0.56	···	···
Ti I	5113.450	1.443	−0.73	···	···
Ti I	5219.710	0.021	−2.24	100.8	3.65
Ti I	5866.460	1.066	−0.76	149.7	3.99
Ti I	6091.180	2.267	−0.37	49.9	4.10
Ti I	6126.220	1.066	−1.37	···	···
Ti I	6258.090	1.443	−0.31	···	···

Table B.1: Equivalent Width Measurements for F/G/K Primaries *(continued)*

Species	λ	E.P.	log(gf)	PM I08152-6337	
	(Å)	(eV)	(dex)	EW (mÅ)	Abundance
Fe I	5141.750	2.424	−2.18	···	···
Fe I	5247.060	0.087	−4.94	···	···
Fe I	5358.120	3.300	−3.16	···	···
Fe I	5412.788	4.440	−1.71	···	···
Fe I	5661.348	4.280	−1.75	···	···
Fe I	5778.458	2.590	−3.45	···	···
Fe I	5784.660	3.400	−2.53	···	···
Fe I	5809.220	3.884	−1.61	66.0	7.29
Fe I	5849.690	3.695	−2.93	···	···
Fe I	5852.230	4.549	−1.17	58.8	7.45
Fe I	5855.090	4.608	−1.48	···	···
Fe I	5856.100	4.294	−1.56	···	···
Fe I	5858.790	4.220	−2.18	···	···
Fe I	5859.600	4.550	−0.61	64.3	6.96
Fe I	5862.370	4.550	−0.25	98.6	7.00
Fe I	5956.700	0.859	−4.60	88.8	7.17
Fe I	6027.060	4.070	−1.17	65.1	7.04
Fe I	6151.620	2.176	−3.28	71.2	7.10
Fe I	6159.380	4.610	−1.83	···	···
Fe I	6165.360	4.143	−1.46	49.1	7.16
Fe I	6173.340	2.223	−2.88	100.9	7.20
Fe I	6200.320	2.609	−2.44	108.0	7.29
Fe I	6213.440	2.223	−2.56	···	···
Fe I	6240.652	2.220	−3.23	···	···
Fe I	6265.140	2.176	−2.55	134.3	7.19
Fe I	6271.283	3.330	−2.70	45.3	7.41
Fe I	6297.801	2.223	−2.73	···	···
Fe I	6322.694	2.588	−2.43	101.5	7.17
Fe I	6358.690	0.859	−4.00	···	···
Fe I	6436.410	4.186	−2.36	···	···
Fe I	6481.878	2.279	−2.97	87.6	7.15
Fe I	6498.950	0.958	−4.69	···	···
Fe I	6518.370	2.830	−2.45	···	···
Fe I	6574.233	0.990	−5.00	···	···
Fe I	6581.214	1.480	−4.68	···	···
Fe I	6591.330	4.593	−1.95	···	···
Fe I	6608.040	2.279	−3.91	···	···
Fe I	6625.027	1.010	−5.34	···	···
Fe I	6699.142	4.590	−2.10	···	···
Fe I	6713.750	4.795	−1.39	···	···
Fe I	6725.360	4.103	−2.17	···	···

Table B.1: Equivalent Width Measurements for F/G/K Primaries *(continued)*

Species	λ	E.P.	log(gf)	PM I08152-6337	
	(Å)	(eV)	(dex)	EW (mÅ)	Abundance
Fe I	6733.150	4.638	−1.40	···	···
Fe I	6739.524	1.560	−4.79	···	···
Fe I	6750.160	2.424	−2.62	101.4	7.14
Fe I	6752.711	4.640	−1.20	···	···
Fe I	6837.009	4.590	−1.69	···	···
Fe I	6857.250	4.076	−2.04	···	···
Fe I	6971.936	3.020	−3.34	···	···
Fe I	7112.170	2.990	−2.99	···	···
Fe I	7751.120	4.990	−0.73	···	···
Fe I	7802.510	5.080	−1.31	···	···
Fe I	7807.920	4.990	−0.73	46.2	7.28
Fe I	8365.644	3.250	−2.04	···	···
Fe I	8757.200	2.845	−2.12	···	···
Fe II	5234.620	3.221	−2.22	···	···
Fe II	5425.260	3.200	−3.16	···	···
Fe II	6149.250	3.889	−2.63	···	···
Fe II	6247.560	3.892	−2.27	···	···
Fe II	6369.490	2.891	−4.02	···	···
Fe II	6432.680	2.891	−3.52	···	···
Fe II	6456.390	3.903	−2.06	16.6	7.24
Fe II	7479.700	3.892	−3.53	···	···
Fe II	7515.840	3.903	−3.42	···	···
Ca I	5867.570	2.930	−1.57	72.3	···
Ca I	6166.440	2.520	−1.14	151.4	···
Ca I	6169.040	2.520	−0.80	···	···
Ca I	6455.610	2.520	−1.29	114.6	···
Ca I	6572.800	0.000	−4.28	···	···
Ti I	5024.850	0.818	−0.56	···	···
Ti I	5113.450	1.443	−0.73	···	···
Ti I	5219.710	0.021	−2.24	103.3	4.78
Ti I	5866.460	1.066	−0.76	132.3	4.81
Ti I	6091.180	2.267	−0.37	66.7	4.88
Ti I	6126.220	1.066	−1.37	89.6	4.82
Ti I	6258.090	1.443	−0.31	146.4	4.88

Table B.1: Equivalent Width Measurements for F/G/K Primaries *(continued)*

Species	λ	E.P.	log(gf)	PM I08239-7549W	
	(Å)	(eV)	(dex)	EW (mÅ)	Abundance
Fe I	5141.750	2.424	−2.18	103.6	7.18
Fe I	5247.060	0.087	−4.94	91.9	7.22
Fe I	5358.120	3.300	−3.16	···	···
Fe I	5412.788	4.440	−1.71	···	···
Fe I	5661.348	4.280	−1.75	25.3	7.17
Fe I	5778.458	2.590	−3.45	34.3	7.26
Fe I	5784.660	3.400	−2.53	···	···
Fe I	5809.220	3.884	−1.61	64.2	7.38
Fe I	5849.690	3.695	−2.93	···	···
Fe I	5852.230	4.549	−1.17	51.4	7.38
Fe I	5855.090	4.608	−1.48	24.8	7.22
Fe I	5856.100	4.294	−1.56	40.3	7.31
Fe I	5858.790	4.220	−2.18	···	···
Fe I	5859.600	4.550	−0.61	87.8	7.36
Fe I	5862.370	4.550	−0.25	101.6	7.17
Fe I	5956.700	0.859	−4.60	81.0	7.41
Fe I	6027.060	4.070	−1.17	71.9	7.25
Fe I	6151.620	2.176	−3.28	69.6	7.32
Fe I	6159.380	4.610	−1.83	···	···
Fe I	6165.360	4.143	−1.46	50.4	7.23
Fe I	6173.340	2.223	−2.88	87.7	7.30
Fe I	6200.320	2.609	−2.44	94.4	7.38
Fe I	6213.440	2.223	−2.56	106.2	7.27
Fe I	6240.652	2.220	−3.23	67.8	7.27
Fe I	6265.140	2.176	−2.55	109.8	7.26
Fe I	6271.283	3.330	−2.70	35.6	7.32
Fe I	6297.801	2.223	−2.73	94.4	7.25
Fe I	6322.694	2.588	−2.43	92.7	7.31
Fe I	6358.690	0.859	−4.00	108.8	7.26
Fe I	6436.410	4.186	−2.36	···	···
Fe I	6481.878	2.279	−2.97	80.7	7.30
Fe I	6498.950	0.958	−4.69	71.9	7.37
Fe I	6518.370	2.830	−2.45	73.9	7.25
Fe I	6574.233	0.990	−5.00	53.5	7.35
Fe I	6581.214	1.480	−4.68	39.5	7.31
Fe I	6591.330	4.593	−1.95	···	···
Fe I	6608.040	2.279	−3.91	30.8	7.26
Fe I	6625.027	1.010	−5.34	45.8	7.56
Fe I	6699.142	4.590	−2.10	···	···
Fe I	6713.750	4.795	−1.39	25.6	7.33
Fe I	6725.360	4.103	−2.17	···	···

Table B.1: Equivalent Width Measurements for F/G/K Primaries *(continued)*

Species	λ	E.P.	log(gf)	PM I08239-7549W	
	(Å)	(eV)	(dex)	EW (mÅ)	Abundance
Fe I	6733.150	4.638	−1.40	33.9	7.35
Fe I	6739.524	1.560	−4.79	24.6	7.18
Fe I	6750.160	2.424	−2.62	92.9	7.29
Fe I	6752.711	4.640	−1.20	49.0	7.44
Fe I	6837.009	4.590	−1.69	···	···
Fe I	6857.250	4.076	−2.04	28.2	7.28
Fe I	6971.936	3.020	−3.34	24.8	7.35
Fe I	7112.170	2.990	−2.99	38.6	7.26
Fe I	7751.120	4.990	−0.73	51.6	7.33
Fe I	7802.510	5.080	−1.31	···	···
Fe I	7807.920	4.990	−0.73	63.4	7.51
Fe I	8365.644	3.250	−2.04	···	···
Fe I	8757.200	2.845	−2.12	···	···
Fe II	5234.620	3.221	−2.22	64.4	7.35
Fe II	5425.260	3.200	−3.16	23.9	7.26
Fe II	6149.250	3.889	−2.63	···	···
Fe II	6247.560	3.892	−2.27	29.2	7.26
Fe II	6369.490	2.891	−4.02	···	···
Fe II	6432.680	2.891	−3.52	26.5	7.40
Fe II	6456.390	3.903	−2.06	35.3	7.23
Fe II	7479.700	3.892	−3.53	···	···
Fe II	7515.840	3.903	−3.42	···	···
Ca I	5867.570	2.930	−1.57	39.7	6.22
Ca I	6166.440	2.520	−1.14	100.1	6.28
Ca I	6169.040	2.520	−0.80	136.4	6.33
Ca I	6455.610	2.520	−1.29	77.5	6.10
Ca I	6572.800	0.000	−4.28	···	···
Ti I	5024.850	0.818	−0.56	83.9	4.49
Ti I	5113.450	1.443	−0.73	···	···
Ti I	5219.710	0.021	−2.24	60.2	4.76
Ti I	5866.460	1.066	−0.76	85.8	4.88
Ti I	6091.180	2.267	−0.37	33.9	4.82
Ti I	6126.220	1.066	−1.37	52.0	4.83
Ti I	6258.090	1.443	−0.31	83.5	4.77

Table B.1: Equivalent Width Measurements for F/G/K Primaries *(continued)*

Species	λ	E.P.	log(gf)	PM I08386-3856	
	(Å)	(eV)	(dex)	EW (mÅ)	Abundance
Fe I	5141.750	2.424	−2.18	110.0	7.02
Fe I	5247.060	0.087	−4.94	95.7	7.05
Fe I	5358.120	3.300	−3.16	···	···
Fe I	5412.788	4.440	−1.71	···	···
Fe I	5661.348	4.280	−1.75	···	···
Fe I	5778.458	2.590	−3.45	34.0	7.12
Fe I	5784.660	3.400	−2.53	···	···
Fe I	5809.220	3.884	−1.61	53.7	7.09
Fe I	5849.690	3.695	−2.93	···	···
Fe I	5852.230	4.549	−1.17	45.0	7.19
Fe I	5855.090	4.608	−1.48	···	···
Fe I	5856.100	4.294	−1.56	32.5	7.08
Fe I	5858.790	4.220	−2.18	···	···
Fe I	5859.600	4.550	−0.61	76.8	7.09
Fe I	5862.370	4.550	−0.25	92.3	6.91
Fe I	5956.700	0.859	−4.60	76.1	7.13
Fe I	6027.060	4.070	−1.17	63.3	6.99
Fe I	6151.620	2.176	−3.28	62.1	7.02
Fe I	6159.380	4.610	−1.83	···	···
Fe I	6165.360	4.143	−1.46	45.4	7.06
Fe I	6173.340	2.223	−2.88	84.2	7.06
Fe I	6200.320	2.609	−2.44	91.4	7.15
Fe I	6213.440	2.223	−2.56	102.3	7.01
Fe I	6240.652	2.220	−3.23	64.7	7.07
Fe I	6265.140	2.176	−2.55	109.5	7.03
Fe I	6271.283	3.330	−2.70	30.8	7.11
Fe I	6297.801	2.223	−2.73	91.0	7.01
Fe I	6322.694	2.588	−2.43	91.3	7.11
Fe I	6358.690	0.859	−4.00	104.1	6.96
Fe I	6436.410	4.186	−2.36	···	···
Fe I	6481.878	2.279	−2.97	77.5	7.09
Fe I	6498.950	0.958	−4.69	···	···
Fe I	6518.370	2.830	−2.45	66.6	6.99
Fe I	6574.233	0.990	−5.00	55.2	7.20
Fe I	6581.214	1.480	−4.68	31.6	6.97
Fe I	6591.330	4.593	−1.95	···	···
Fe I	6608.040	2.279	−3.91	26.7	7.01
Fe I	6625.027	1.010	−5.34	45.6	7.36
Fe I	6699.142	4.590	−2.10	···	···
Fe I	6713.750	4.795	−1.39	18.3	7.09
Fe I	6725.360	4.103	−2.17	16.5	7.05

Table B.1: Equivalent Width Measurements for F/G/K Primaries *(continued)*

Species	λ	E.P.	log(gf)	PM I08386-3856	
	(Å)	(eV)	(dex)	EW (mÅ)	Abundance
Fe I	6733.150	4.638	−1.40	24.7	7.10
Fe I	6739.524	1.560	−4.79	21.1	6.90
Fe I	6750.160	2.424	−2.62	87.3	7.03
Fe I	6752.711	4.640	−1.20	···	···
Fe I	6837.009	4.590	−1.69	···	···
Fe I	6857.250	4.076	−2.04	18.3	6.95
Fe I	6971.936	3.020	−3.34	···	···
Fe I	7112.170	2.990	−2.99	34.1	7.05
Fe I	7751.120	4.990	−0.73	41.7	7.11
Fe I	7802.510	5.080	−1.31	···	···
Fe I	7807.920	4.990	−0.73	50.3	7.25
Fe I	8365.644	3.250	−2.04	···	···
Fe I	8757.200	2.845	−2.12	···	···
Fe II	5234.620	3.221	−2.22	44.6	7.06
Fe II	5425.260	3.200	−3.16	16.8	7.17
Fe II	6149.250	3.889	−2.63	···	···
Fe II	6247.560	3.892	−2.27	16.0	7.00
Fe II	6369.490	2.891	−4.02	···	···
Fe II	6432.680	2.891	−3.52	···	···
Fe II	6456.390	3.903	−2.06	18.3	6.90
Fe II	7479.700	3.892	−3.53	···	···
Fe II	7515.840	3.903	−3.42	···	···
Ca I	5867.570	2.930	−1.57	···	···
Ca I	6166.440	2.520	−1.14	111.1	6.13
Ca I	6169.040	2.520	−0.80	154.3	6.16
Ca I	6455.610	2.520	−1.29	81.7	5.92
Ca I	6572.800	0.000	−4.28	···	···
Ti I	5024.850	0.818	−0.56	107.7	4.55
Ti I	5113.450	1.443	−0.73	···	···
Ti I	5219.710	0.021	−2.24	74.7	4.74
Ti I	5866.460	1.066	−0.76	100.0	4.81
Ti I	6091.180	2.267	−0.37	41.6	4.73
Ti I	6126.220	1.066	−1.37	65.6	4.79
Ti I	6258.090	1.443	−0.31	99.5	4.72

Table B.1: Equivalent Width Measurements for F/G/K Primaries *(continued)*

Species	λ	E.P.	log(gf)	PM I09502+0509E	
	(Å)	(eV)	(dex)	EW (mÅ)	Abundance
Fe I	5141.750	2.424	−2.18	90.8	6.79
Fe I	5247.060	0.087	−4.94	78.4	6.80
Fe I	5358.120	3.300	−3.16	···	···
Fe I	5412.788	4.440	−1.71	···	···
Fe I	5661.348	4.280	−1.75	···	···
Fe I	5778.458	2.590	−3.45	···	···
Fe I	5784.660	3.400	−2.53	···	···
Fe I	5809.220	3.884	−1.61	34.9	6.74
Fe I	5849.690	3.695	−2.93	···	···
Fe I	5852.230	4.549	−1.17	23.9	6.76
Fe I	5855.090	4.608	−1.48	···	···
Fe I	5856.100	4.294	−1.56	···	···
Fe I	5858.790	4.220	−2.18	···	···
Fe I	5859.600	4.550	−0.61	51.7	6.72
Fe I	5862.370	4.550	−0.25	62.2	6.52
Fe I	5956.700	0.859	−4.60	50.5	6.67
Fe I	6027.060	4.070	−1.17	46.0	6.70
Fe I	6151.620	2.176	−3.28	38.4	6.59
Fe I	6159.380	4.610	−1.83	···	···
Fe I	6165.360	4.143	−1.46	22.1	6.57
Fe I	6173.340	2.223	−2.88	60.7	6.68
Fe I	6200.320	2.609	−2.44	70.3	6.85
Fe I	6213.440	2.223	−2.56	83.3	6.77
Fe I	6240.652	2.220	−3.23	47.6	6.77
Fe I	6265.140	2.176	−2.55	81.2	6.67
Fe I	6271.283	3.330	−2.70	···	···
Fe I	6297.801	2.223	−2.73	66.2	6.64
Fe I	6322.694	2.588	−2.43	64.8	6.70
Fe I	6358.690	0.859	−4.00	73.4	6.51
Fe I	6436.410	4.186	−2.36	···	···
Fe I	6481.878	2.279	−2.97	57.0	6.75
Fe I	6498.950	0.958	−4.69	48.2	6.78
Fe I	6518.370	2.830	−2.45	41.7	6.54
Fe I	6574.233	0.990	−5.00	29.5	6.73
Fe I	6581.214	1.480	−4.68	···	···
Fe I	6591.330	4.593	−1.95	···	···
Fe I	6608.040	2.279	−3.91	···	···
Fe I	6625.027	1.010	−5.34	···	···
Fe I	6699.142	4.590	−2.10	···	···
Fe I	6713.750	4.795	−1.39	···	···
Fe I	6725.360	4.103	−2.17	···	···

Table B.1: Equivalent Width Measurements for F/G/K Primaries *(continued)*

Species	λ	E.P.	log(gf)	PM I09502+0509E	
	(Å)	(eV)	(dex)	EW (mÅ)	Abundance
Fe I	6733.150	4.638	−1.40	···	···
Fe I	6739.524	1.560	−4.79	···	···
Fe I	6750.160	2.424	−2.62	61.9	6.64
Fe I	6752.711	4.640	−1.20	21.9	6.82
Fe I	6837.009	4.590	−1.69	···	···
Fe I	6857.250	4.076	−2.04	···	···
Fe I	6971.936	3.020	−3.34	···	···
Fe I	7112.170	2.990	−2.99	···	···
Fe I	7751.120	4.990	−0.73	23.6	6.74
Fe I	7802.510	5.080	−1.31	···	···
Fe I	7807.920	4.990	−0.73	···	···
Fe I	8365.644	3.250	−2.04	47.0	6.60
Fe I	8757.200	2.845	−2.12	···	···
Fe II	5234.620	3.221	−2.22	34.4	6.71
Fe II	5425.260	3.200	−3.16	···	···
Fe II	6149.250	3.889	−2.63	···	···
Fe II	6247.560	3.892	−2.27	···	···
Fe II	6369.490	2.891	−4.02	···	···
Fe II	6432.680	2.891	−3.52	···	···
Fe II	6456.390	3.903	−2.06	13.1	6.59
Fe II	7479.700	3.892	−3.53	···	···
Fe II	7515.840	3.903	−3.42	···	···
Ca I	5867.570	2.930	−1.57	26.9	5.85
Ca I	6166.440	2.520	−1.14	79.0	5.82
Ca I	6169.040	2.520	−0.80	112.3	5.86
Ca I	6455.610	2.520	−1.29	57.0	5.64
Ca I	6572.800	0.000	−4.28	···	···
Ti I	5024.850	0.818	−0.56	72.9	4.10
Ti I	5113.450	1.443	−0.73	···	···
Ti I	5219.710	0.021	−2.24	56.6	4.51
Ti I	5866.460	1.066	−0.76	70.4	4.44
Ti I	6091.180	2.267	−0.37	23.8	4.45
Ti I	6126.220	1.066	−1.37	36.8	4.37
Ti I	6258.090	1.443	−0.31	68.9	4.35

Table B.1: Equivalent Width Measurements for F/G/K Primaries *(continued)*

Species	λ	E.P.	log(gf)	PM I10105+1203W	
	(Å)	(eV)	(dex)	EW (mÅ)	Abundance
Fe I	5141.750	2.424	−2.18	81.6	6.69
Fe I	5247.060	0.087	−4.94	69.4	6.66
Fe I	5358.120	3.300	−3.16	···	···
Fe I	5412.788	4.440	−1.71	···	···
Fe I	5661.348	4.280	−1.75	···	···
Fe I	5778.458	2.590	−3.45	···	···
Fe I	5784.660	3.400	−2.53	···	···
Fe I	5809.220	3.884	−1.61	24.8	6.55
Fe I	5849.690	3.695	−2.93	···	···
Fe I	5852.230	4.549	−1.17	···	···
Fe I	5855.090	4.608	−1.48	···	···
Fe I	5856.100	4.294	−1.56	···	···
Fe I	5858.790	4.220	−2.18	···	···
Fe I	5859.600	4.550	−0.61	46.7	6.66
Fe I	5862.370	4.550	−0.25	68.3	6.63
Fe I	5956.700	0.859	−4.60	51.0	6.76
Fe I	6027.060	4.070	−1.17	42.7	6.66
Fe I	6151.620	2.176	−3.28	39.6	6.67
Fe I	6159.380	4.610	−1.83	···	···
Fe I	6165.360	4.143	−1.46	22.4	6.60
Fe I	6173.340	2.223	−2.88	56.5	6.64
Fe I	6200.320	2.609	−2.44	62.0	6.72
Fe I	6213.440	2.223	−2.56	71.3	6.59
Fe I	6240.652	2.220	−3.23	42.7	6.73
Fe I	6265.140	2.176	−2.55	78.1	6.64
Fe I	6271.283	3.330	−2.70	···	···
Fe I	6297.801	2.223	−2.73	88.6	7.06
Fe I	6322.694	2.588	−2.43	62.1	6.68
Fe I	6358.690	0.859	−4.00	67.7	6.45
Fe I	6436.410	4.186	−2.36	···	···
Fe I	6481.878	2.279	−2.97	···	···
Fe I	6498.950	0.958	−4.69	42.9	6.77
Fe I	6518.370	2.830	−2.45	40.0	6.54
Fe I	6574.233	0.990	−5.00	26.6	6.78
Fe I	6581.214	1.480	−4.68	14.4	6.67
Fe I	6591.330	4.593	−1.95	···	···
Fe I	6608.040	2.279	−3.91	···	···
Fe I	6625.027	1.010	−5.34	···	···
Fe I	6699.142	4.590	−2.10	···	···
Fe I	6713.750	4.795	−1.39	···	···
Fe I	6725.360	4.103	−2.17	···	···

Table B.1: Equivalent Width Measurements for F/G/K Primaries *(continued)*

Species	λ	E.P.	log(gf)	PM I10105+1203W	
	(Å)	(eV)	(dex)	EW (mÅ)	Abundance
Fe I	6733.150	4.638	−1.40	···	···
Fe I	6739.524	1.560	−4.79	···	···
Fe I	6750.160	2.424	−2.62	61.1	6.65
Fe I	6752.711	4.640	−1.20	18.7	6.74
Fe I	6837.009	4.590	−1.69	···	···
Fe I	6857.250	4.076	−2.04	···	···
Fe I	6971.936	3.020	−3.34	···	···
Fe I	7112.170	2.990	−2.99	···	···
Fe I	7751.120	4.990	−0.73	···	···
Fe I	7802.510	5.080	−1.31	···	···
Fe I	7807.920	4.990	−0.73	30.9	6.89
Fe I	8365.644	3.250	−2.04	···	···
Fe I	8757.200	2.845	−2.12	···	···
Fe II	5234.620	3.221	−2.22	45.4	6.70
Fe II	5425.260	3.200	−3.16	···	···
Fe II	6149.250	3.889	−2.63	···	···
Fe II	6247.560	3.892	−2.27	13.3	6.56
Fe II	6369.490	2.891	−4.02	···	···
Fe II	6432.680	2.891	−3.52	···	···
Fe II	6456.390	3.903	−2.06	25.5	6.77
Fe II	7479.700	3.892	−3.53	···	···
Fe II	7515.840	3.903	−3.42	···	···
Ca I	5867.570	2.930	−1.57	24.9	5.94
Ca I	6166.440	2.520	−1.14	72.0	5.86
Ca I	6169.040	2.520	−0.80	102.1	5.91
Ca I	6455.610	2.520	−1.29	60.5	5.83
Ca I	6572.800	0.000	−4.28	···	···
Ti I	5024.850	0.818	−0.56	79.2	4.38
Ti I	5113.450	1.443	−0.73	···	···
Ti I	5219.710	0.021	−2.24	34.5	4.30
Ti I	5866.460	1.066	−0.76	55.4	4.33
Ti I	6091.180	2.267	−0.37	19.5	4.51
Ti I	6126.220	1.066	−1.37	36.2	4.57
Ti I	6258.090	1.443	−0.31	67.6	4.49

Table B.1: Equivalent Width Measurements for F/G/K Primaries *(continued)*

Species	λ	E.P.	log(gf)	PM I11125-3512	
	(Å)	(eV)	(dex)	EW (mÅ)	Abundance
Fe I	5141.750	2.424	−2.18	···	···
Fe I	5247.060	0.087	−4.94	95.1	6.84
Fe I	5358.120	3.300	−3.16	···	···
Fe I	5412.788	4.440	−1.71	···	···
Fe I	5661.348	4.280	−1.75	···	···
Fe I	5778.458	2.590	−3.45	···	···
Fe I	5784.660	3.400	−2.53	···	···
Fe I	5809.220	3.884	−1.61	···	···
Fe I	5849.690	3.695	−2.93	···	···
Fe I	5852.230	4.549	−1.17	···	···
Fe I	5855.090	4.608	−1.48	···	···
Fe I	5856.100	4.294	−1.56	···	···
Fe I	5858.790	4.220	−2.18	···	···
Fe I	5859.600	4.550	−0.61	44.1	6.59
Fe I	5862.370	4.550	−0.25	76.0	6.68
Fe I	5956.700	0.859	−4.60	72.6	6.91
Fe I	6027.060	4.070	−1.17	47.9	6.70
Fe I	6151.620	2.176	−3.28	50.1	6.72
Fe I	6159.380	4.610	−1.83	···	···
Fe I	6165.360	4.143	−1.46	43.3	6.99
Fe I	6173.340	2.223	−2.88	73.7	6.77
Fe I	6200.320	2.609	−2.44	90.1	7.03
Fe I	6213.440	2.223	−2.56	103.6	6.91
Fe I	6240.652	2.220	−3.23	···	···
Fe I	6265.140	2.176	−2.55	92.6	6.69
Fe I	6271.283	3.330	−2.70	···	···
Fe I	6297.801	2.223	−2.73	107.3	7.13
Fe I	6322.694	2.588	−2.43	66.3	6.60
Fe I	6358.690	0.859	−4.00	96.0	6.67
Fe I	6436.410	4.186	−2.36	···	···
Fe I	6481.878	2.279	−2.97	74.5	6.92
Fe I	6498.950	0.958	−4.69	···	···
Fe I	6518.370	2.830	−2.45	69.0	6.94
Fe I	6574.233	0.990	−5.00	43.1	6.90
Fe I	6581.214	1.480	−4.68	···	···
Fe I	6591.330	4.593	−1.95	···	···
Fe I	6608.040	2.279	−3.91	···	···
Fe I	6625.027	1.010	−5.34	···	···
Fe I	6699.142	4.590	−2.10	···	···
Fe I	6713.750	4.795	−1.39	···	···
Fe I	6725.360	4.103	−2.17	···	···

Table B.1: Equivalent Width Measurements for F/G/K Primaries *(continued)*

Species	λ	E.P.	log(gf)	PM I11125-3512	
	(Å)	(eV)	(dex)	EW (mÅ)	Abundance
Fe I	6733.150	4.638	−1.40	···	···
Fe I	6739.524	1.560	−4.79	···	···
Fe I	6750.160	2.424	−2.62	86.8	6.92
Fe I	6752.711	4.640	−1.20	31.8	7.05
Fe I	6837.009	4.590	−1.69	···	···
Fe I	6857.250	4.076	−2.04	···	···
Fe I	6971.936	3.020	−3.34	···	···
Fe I	7112.170	2.990	−2.99	···	···
Fe I	7751.120	4.990	−0.73	···	···
Fe I	7802.510	5.080	−1.31	···	···
Fe I	7807.920	4.990	−0.73	···	···
Fe I	8365.644	3.250	−2.04	···	···
Fe I	8757.200	2.845	−2.12	···	···
Fe II	5234.620	3.221	−2.22	···	···
Fe II	5425.260	3.200	−3.16	···	···
Fe II	6149.250	3.889	−2.63	···	···
Fe II	6247.560	3.892	−2.27	···	···
Fe II	6369.490	2.891	−4.02	···	···
Fe II	6432.680	2.891	−3.52	···	···
Fe II	6456.390	3.903	−2.06	···	···
Fe II	7479.700	3.892	−3.53	···	···
Fe II	7515.840	3.903	−3.42	···	···
Ca I	5867.570	2.930	−1.57	···	···
Ca I	6166.440	2.520	−1.14	139.5	6.34
Ca I	6169.040	2.520	−0.80	161.0	6.17
Ca I	6455.610	2.520	−1.29	86.5	5.92
Ca I	6572.800	0.000	−4.28	···	···
Ti I	5024.850	0.818	−0.56	···	···
Ti I	5113.450	1.443	−0.73	···	···
Ti I	5219.710	0.021	−2.24	87.7	4.81
Ti I	5866.460	1.066	−0.76	114.1	4.87
Ti I	6091.180	2.267	−0.37	···	···
Ti I	6126.220	1.066	−1.37	62.2	4.63
Ti I	6258.090	1.443	−0.31	97.0	4.56

Table B.1: Equivalent Width Measurements for F/G/K Primaries *(continued)*

Species	λ (Å)	E.P. (eV)	log(gf) (dex)	NLTT 27188 EW (mÅ)	NLTT 27188 Abundance
Fe I	5141.750	2.424	−2.18	15.3	5.94
Fe I	5247.060	0.087	−4.94	···	···
Fe I	5358.120	3.300	−3.16	···	···
Fe I	5412.788	4.440	−1.71	···	···
Fe I	5661.348	4.280	−1.75	···	···
Fe I	5778.458	2.590	−3.45	···	···
Fe I	5784.660	3.400	−2.53	···	···
Fe I	5809.220	3.884	−1.61	···	···
Fe I	5849.690	3.695	−2.93	···	···
Fe I	5852.230	4.549	−1.17	···	···
Fe I	5855.090	4.608	−1.48	···	···
Fe I	5856.100	4.294	−1.56	···	···
Fe I	5858.790	4.220	−2.18	···	···
Fe I	5859.600	4.550	−0.61	···	···
Fe I	5862.370	4.550	−0.25	21.4	6.14
Fe I	5956.700	0.859	−4.60	···	···
Fe I	6027.060	4.070	−1.17	9.0	6.16
Fe I	6151.620	2.176	−3.28	···	···
Fe I	6159.380	4.610	−1.83	···	···
Fe I	6165.360	4.143	−1.46	···	···
Fe I	6173.340	2.223	−2.88	···	···
Fe I	6200.320	2.609	−2.44	14.5	6.29
Fe I	6213.440	2.223	−2.56	···	···
Fe I	6240.652	2.220	−3.23	···	···
Fe I	6265.140	2.176	−2.55	24.1	6.28
Fe I	6271.283	3.330	−2.70	···	···
Fe I	6297.801	2.223	−2.73	···	···
Fe I	6322.694	2.588	−2.43	···	···
Fe I	6358.690	0.859	−4.00	···	···
Fe I	6436.410	4.186	−2.36	···	···
Fe I	6481.878	2.279	−2.97	···	···
Fe I	6498.950	0.958	−4.69	···	···
Fe I	6518.370	2.830	−2.45	···	···
Fe I	6574.233	0.990	−5.00	···	···
Fe I	6581.214	1.480	−4.68	···	···
Fe I	6591.330	4.593	−1.95	···	···
Fe I	6608.040	2.279	−3.91	···	···
Fe I	6625.027	1.010	−5.34	···	···
Fe I	6699.142	4.590	−2.10	···	···
Fe I	6713.750	4.795	−1.39	···	···
Fe I	6725.360	4.103	−2.17	···	···

Table B.1: Equivalent Width Measurements for F/G/K Primaries *(continued)*

Species	λ	E.P.	log(gf)	NLTT 27188	
	(Å)	(eV)	(dex)	EW (mÅ)	Abundance
Fe I	6733.150	4.638	−1.40	···	···
Fe I	6739.524	1.560	−4.79	···	···
Fe I	6750.160	2.424	−2.62	10.2	6.09
Fe I	6752.711	4.640	−1.20	···	···
Fe I	6837.009	4.590	−1.69	···	···
Fe I	6857.250	4.076	−2.04	···	···
Fe I	6971.936	3.020	−3.34	···	···
Fe I	7112.170	2.990	−2.99	···	···
Fe I	7751.120	4.990	−0.73	···	···
Fe I	7802.510	5.080	−1.31	···	···
Fe I	7807.920	4.990	−0.73	···	···
Fe I	8365.644	3.250	−2.04	···	···
Fe I	8757.200	2.845	−2.12	···	···
Fe II	5234.620	3.221	−2.22	32.5	6.11
Fe II	5425.260	3.200	−3.16	···	···
Fe II	6149.250	3.889	−2.63	···	···
Fe II	6247.560	3.892	−2.27	10.3	6.07
Fe II	6369.490	2.891	−4.02	···	···
Fe II	6432.680	2.891	−3.52	···	···
Fe II	6456.390	3.903	−2.06	15.8	6.09
Fe II	7479.700	3.892	−3.53	···	···
Fe II	7515.840	3.903	−3.42	···	···
Ca I	5867.570	2.930	−1.57	···	···
Ca I	6166.440	2.520	−1.14	14.4	5.27
Ca I	6169.040	2.520	−0.80	28.2	5.30
Ca I	6455.610	2.520	−1.29	···	···
Ca I	6572.800	0.000	−4.28	···	···
Ti I	5024.850	0.818	−0.56	···	···
Ti I	5113.450	1.443	−0.73	···	···
Ti I	5219.710	0.021	−2.24	···	···
Ti I	5866.460	1.066	−0.76	···	···
Ti I	6091.180	2.267	−0.37	···	···
Ti I	6126.220	1.066	−1.37	···	···
Ti I	6258.090	1.443	−0.31	12.3	4.06

Table B.1: Equivalent Width Measurements for F/G/K Primaries *(continued)*

Species	λ	E.P.	log(gf)	PM I11263+2047Ee	
	(Å)	(eV)	(dex)	EW (mÅ)	Abundance
Fe I	5141.750	2.424	−2.18	···	···
Fe I	5247.060	0.087	−4.94	96.5	6.60
Fe I	5358.120	3.300	−3.16	···	···
Fe I	5412.788	4.440	−1.71	···	···
Fe I	5661.348	4.280	−1.75	···	···
Fe I	5778.458	2.590	−3.45	···	···
Fe I	5784.660	3.400	−2.53	···	···
Fe I	5809.220	3.884	−1.61	···	···
Fe I	5849.690	3.695	−2.93	···	···
Fe I	5852.230	4.549	−1.17	···	···
Fe I	5855.090	4.608	−1.48	···	···
Fe I	5856.100	4.294	−1.56	···	···
Fe I	5858.790	4.220	−2.18	···	···
Fe I	5859.600	4.550	−0.61	37.2	6.65
Fe I	5862.370	4.550	−0.25	54.0	6.55
Fe I	5956.700	0.859	−4.60	74.2	6.80
Fe I	6027.060	4.070	−1.17	32.3	6.57
Fe I	6151.620	2.176	−3.28	···	···
Fe I	6159.380	4.610	−1.83	···	···
Fe I	6165.360	4.143	−1.46	···	···
Fe I	6173.340	2.223	−2.88	65.8	6.63
Fe I	6200.320	2.609	−2.44	75.7	6.80
Fe I	6213.440	2.223	−2.56	···	···
Fe I	6240.652	2.220	−3.23	···	···
Fe I	6265.140	2.176	−2.55	···	···
Fe I	6271.283	3.330	−2.70	···	···
Fe I	6297.801	2.223	−2.73	77.1	6.65
Fe I	6322.694	2.588	−2.43	63.6	6.58
Fe I	6358.690	0.859	−4.00	···	···
Fe I	6436.410	4.186	−2.36	···	···
Fe I	6481.878	2.279	−2.97	58.1	6.65
Fe I	6498.950	0.958	−4.69	···	···
Fe I	6518.370	2.830	−2.45	52.3	6.71
Fe I	6574.233	0.990	−5.00	43.5	6.73
Fe I	6581.214	1.480	−4.68	···	···
Fe I	6591.330	4.593	−1.95	···	···
Fe I	6608.040	2.279	−3.91	···	···
Fe I	6625.027	1.010	−5.34	···	···
Fe I	6699.142	4.590	−2.10	···	···
Fe I	6713.750	4.795	−1.39	···	···
Fe I	6725.360	4.103	−2.17	···	···

Table B.1: Equivalent Width Measurements for F/G/K Primaries *(continued)*

Species	λ	E.P.	log(gf)	PM I11263+2047Ee	
	(Å)	(eV)	(dex)	EW (mÅ)	Abundance
Fe I	6733.150	4.638	−1.40	···	···
Fe I	6739.524	1.560	−4.79	···	···
Fe I	6750.160	2.424	−2.62	70.7	6.67
Fe I	6752.711	4.640	−1.20	···	···
Fe I	6837.009	4.590	−1.69	···	···
Fe I	6857.250	4.076	−2.04	···	···
Fe I	6971.936	3.020	−3.34	···	···
Fe I	7112.170	2.990	−2.99	···	···
Fe I	7751.120	4.990	−0.73	···	···
Fe I	7802.510	5.080	−1.31	···	···
Fe I	7807.920	4.990	−0.73	16.2	6.80
Fe I	8365.644	3.250	−2.04	···	···
Fe I	8757.200	2.845	−2.12	···	···
Fe II	5234.620	3.221	−2.22	···	···
Fe II	5425.260	3.200	−3.16	···	···
Fe II	6149.250	3.889	−2.63	···	···
Fe II	6247.560	3.892	−2.27	···	···
Fe II	6369.490	2.891	−4.02	···	···
Fe II	6432.680	2.891	−3.52	···	···
Fe II	6456.390	3.903	−2.06	···	···
Fe II	7479.700	3.892	−3.53	···	···
Fe II	7515.840	3.903	−3.42	···	···
Ca I	5867.570	2.930	−1.57	···	···
Ca I	6166.440	2.520	−1.14	142.7	5.79
Ca I	6169.040	2.520	−0.80	···	···
Ca I	6455.610	2.520	−1.29	101.8	5.58
Ca I	6572.800	0.000	−4.28	···	···
Ti I	5024.850	0.818	−0.56	···	···
Ti I	5113.450	1.443	−0.73	···	···
Ti I	5219.710	0.021	−2.24	114.0	4.44
Ti I	5866.460	1.066	−0.76	149.3	4.49
Ti I	6091.180	2.267	−0.37	56.6	4.46
Ti I	6126.220	1.066	−1.37	89.9	4.46
Ti I	6258.090	1.443	−0.31	···	···

Table B.1: Equivalent Width Measurements for F/G/K Primaries *(continued)*

Species	λ	E.P.	log(gf)	PM I11330+1318N	
	(Å)	(eV)	(dex)	EW (mÅ)	Abundance
Fe I	5141.750	2.424	−2.18	77.2	7.18
Fe I	5247.060	0.087	−4.94	64.0	7.24
Fe I	5358.120	3.300	−3.16	···	···
Fe I	5412.788	4.440	−1.71	···	···
Fe I	5661.348	4.280	−1.75	···	···
Fe I	5778.458	2.590	−3.45	19.1	7.22
Fe I	5784.660	3.400	−2.53	···	···
Fe I	5809.220	3.884	−1.61	46.4	7.30
Fe I	5849.690	3.695	−2.93	···	···
Fe I	5852.230	4.549	−1.17	33.1	7.22
Fe I	5855.090	4.608	−1.48	21.1	7.29
Fe I	5856.100	4.294	−1.56	28.2	7.25
Fe I	5858.790	4.220	−2.18	···	···
Fe I	5859.600	4.550	−0.61	65.0	7.29
Fe I	5862.370	4.550	−0.25	77.2	7.14
Fe I	5956.700	0.859	−4.60	45.8	7.22
Fe I	6027.060	4.070	−1.17	58.7	7.29
Fe I	6151.620	2.176	−3.28	42.4	7.17
Fe I	6159.380	4.610	−1.83	···	···
Fe I	6165.360	4.143	−1.46	38.8	7.23
Fe I	6173.340	2.223	−2.88	62.8	7.25
Fe I	6200.320	2.609	−2.44	68.6	7.33
Fe I	6213.440	2.223	−2.56	78.7	7.28
Fe I	6240.652	2.220	−3.23	···	···
Fe I	6265.140	2.176	−2.55	82.1	7.29
Fe I	6271.283	3.330	−2.70	···	···
Fe I	6297.801	2.223	−2.73	···	···
Fe I	6322.694	2.588	−2.43	70.1	7.32
Fe I	6358.690	0.859	−4.00	79.6	7.33
Fe I	6436.410	4.186	−2.36	···	···
Fe I	6481.878	2.279	−2.97	56.6	7.25
Fe I	6498.950	0.958	−4.69	39.8	7.24
Fe I	6518.370	2.830	−2.45	···	···
Fe I	6574.233	0.990	−5.00	···	···
Fe I	6581.214	1.480	−4.68	···	···
Fe I	6591.330	4.593	−1.95	···	···
Fe I	6608.040	2.279	−3.91	···	···
Fe I	6625.027	1.010	−5.34	···	···
Fe I	6699.142	4.590	−2.10	···	···
Fe I	6713.750	4.795	−1.39	18.5	7.28
Fe I	6725.360	4.103	−2.17	···	···

Table B.1: Equivalent Width Measurements for F/G/K Primaries *(continued)*

Species	λ	E.P.	log(gf)	PM I11330+1318N	
	(Å)	(eV)	(dex)	EW (mÅ)	Abundance
Fe I	6733.150	4.638	−1.40	···	···
Fe I	6739.524	1.560	−4.79	···	···
Fe I	6750.160	2.424	−2.62	68.3	7.27
Fe I	6752.711	4.640	−1.20	31.0	7.26
Fe I	6837.009	4.590	−1.69	14.5	7.24
Fe I	6857.250	4.076	−2.04	···	···
Fe I	6971.936	3.020	−3.34	···	···
Fe I	7112.170	2.990	−2.99	25.8	7.28
Fe I	7751.120	4.990	−0.73	···	···
Fe I	7802.510	5.080	−1.31	···	···
Fe I	7807.920	4.990	−0.73	···	···
Fe I	8365.644	3.250	−2.04	···	···
Fe I	8757.200	2.845	−2.12	···	···
Fe II	5234.620	3.221	−2.22	71.0	7.16
Fe II	5425.260	3.200	−3.16	38.5	7.28
Fe II	6149.250	3.889	−2.63	28.2	7.14
Fe II	6247.560	3.892	−2.27	49.6	7.32
Fe II	6369.490	2.891	−4.02	···	···
Fe II	6432.680	2.891	−3.52	38.7	7.31
Fe II	6456.390	3.903	−2.06	60.7	7.37
Fe II	7479.700	3.892	−3.53	···	···
Fe II	7515.840	3.903	−3.42	···	···
Ca I	5867.570	2.930	−1.57	18.3	6.06
Ca I	6166.440	2.520	−1.14	64.0	6.17
Ca I	6169.040	2.520	−0.80	89.1	6.25
Ca I	6455.610	2.520	−1.29	50.5	6.06
Ca I	6572.800	0.000	−4.28	···	···
Ti I	5024.850	0.818	−0.56	66.4	4.79
Ti I	5113.450	1.443	−0.73	···	···
Ti I	5219.710	0.021	−2.24	···	···
Ti I	5866.460	1.066	−0.76	42.6	4.65
Ti I	6091.180	2.267	−0.37	···	···
Ti I	6126.220	1.066	−1.37	22.4	4.79
Ti I	6258.090	1.443	−0.31	48.4	4.68

Table B.1: Equivalent Width Measurements for F/G/K Primaries *(continued)*

Species	λ	E.P.	log(gf)	PM I11392-4118N	
	(Å)	(eV)	(dex)	EW (mÅ)	Abundance
Fe I	5141.750	2.424	−2.18	···	···
Fe I	5247.060	0.087	−4.94	···	···
Fe I	5358.120	3.300	−3.16	···	···
Fe I	5412.788	4.440	−1.71	···	···
Fe I	5661.348	4.280	−1.75	···	···
Fe I	5778.458	2.590	−3.45	49.6	7.51
Fe I	5784.660	3.400	−2.53	···	···
Fe I	5809.220	3.884	−1.61	···	···
Fe I	5849.690	3.695	−2.93	···	···
Fe I	5852.230	4.549	−1.17	···	···
Fe I	5855.090	4.608	−1.48	···	···
Fe I	5856.100	4.294	−1.56	···	···
Fe I	5858.790	4.220	−2.18	···	···
Fe I	5859.600	4.550	−0.61	41.1	7.02
Fe I	5862.370	4.550	−0.25	59.0	6.92
Fe I	5956.700	0.859	−4.60	101.1	7.09
Fe I	6027.060	4.070	−1.17	36.9	6.92
Fe I	6151.620	2.176	−3.28	54.3	6.85
Fe I	6159.380	4.610	−1.83	···	···
Fe I	6165.360	4.143	−1.46	···	···
Fe I	6173.340	2.223	−2.88	91.7	7.05
Fe I	6200.320	2.609	−2.44	70.5	6.84
Fe I	6213.440	2.223	−2.56	···	···
Fe I	6240.652	2.220	−3.23	···	···
Fe I	6265.140	2.176	−2.55	116.5	6.93
Fe I	6271.283	3.330	−2.70	···	···
Fe I	6297.801	2.223	−2.73	85.3	6.81
Fe I	6322.694	2.588	−2.43	64.3	6.70
Fe I	6358.690	0.859	−4.00	97.3	6.39
Fe I	6436.410	4.186	−2.36	···	···
Fe I	6481.878	2.279	−2.97	86.6	7.13
Fe I	6498.950	0.958	−4.69	98.7	7.22
Fe I	6518.370	2.830	−2.45	57.6	6.93
Fe I	6574.233	0.990	−5.00	70.5	7.15
Fe I	6581.214	1.480	−4.68	···	···
Fe I	6591.330	4.593	−1.95	···	···
Fe I	6608.040	2.279	−3.91	···	···
Fe I	6625.027	1.010	−5.34	···	···
Fe I	6699.142	4.590	−2.10	···	···
Fe I	6713.750	4.795	−1.39	···	···
Fe I	6725.360	4.103	−2.17	···	···

Table B.1: Equivalent Width Measurements for F/G/K Primaries *(continued)*

Species	λ	E.P.	log(gf)	PM I11392-4118N	
	(Å)	(eV)	(dex)	EW (mÅ)	Abundance
Fe I	6733.150	4.638	−1.40	···	···
Fe I	6739.524	1.560	−4.79	···	···
Fe I	6750.160	2.424	−2.62	88.4	6.98
Fe I	6752.711	4.640	−1.20	···	···
Fe I	6837.009	4.590	−1.69	···	···
Fe I	6857.250	4.076	−2.04	···	···
Fe I	6971.936	3.020	−3.34	···	···
Fe I	7112.170	2.990	−2.99	···	···
Fe I	7751.120	4.990	−0.73	···	···
Fe I	7802.510	5.080	−1.31	···	···
Fe I	7807.920	4.990	−0.73	···	···
Fe I	8365.644	3.250	−2.04	···	···
Fe I	8757.200	2.845	−2.12	···	···
Fe II	5234.620	3.221	−2.22	···	···
Fe II	5425.260	3.200	−3.16	···	···
Fe II	6149.250	3.889	−2.63	···	···
Fe II	6247.560	3.892	−2.27	···	···
Fe II	6369.490	2.891	−4.02	···	···
Fe II	6432.680	2.891	−3.52	···	···
Fe II	6456.390	3.903	−2.06	···	···
Fe II	7479.700	3.892	−3.53	···	···
Fe II	7515.840	3.903	−3.42	···	···
Ca I	5867.570	2.930	−1.57	86.6	5.99
Ca I	6166.440	2.520	−1.14	···	···
Ca I	6169.040	2.520	−0.80	···	···
Ca I	6455.610	2.520	−1.29	141.3	5.68
Ca I	6572.800	0.000	−4.28	···	···
Ti I	5024.850	0.818	−0.56	154.4	3.86
Ti I	5113.450	1.443	−0.73	···	···
Ti I	5219.710	0.021	−2.24	119.4	4.12
Ti I	5866.460	1.066	−0.76	160.1	4.31
Ti I	6091.180	2.267	−0.37	67.4	4.47
Ti I	6126.220	1.066	−1.37	99.1	4.26
Ti I	6258.090	1.443	−0.31	···	···

Table B.1: Equivalent Width Measurements for F/G/K Primaries *(continued)*

Species	λ	E.P.	log(gf)	PM I11584-4155E	
	(Å)	(eV)	(dex)	EW (mÅ)	Abundance
Fe I	5141.750	2.424	−2.18	95.2	6.97
Fe I	5247.060	0.087	−4.94	69.8	6.74
Fe I	5358.120	3.300	−3.16	···	···
Fe I	5412.788	4.440	−1.71	···	···
Fe I	5661.348	4.280	−1.75	···	···
Fe I	5778.458	2.590	−3.45	···	···
Fe I	5784.660	3.400	−2.53	···	···
Fe I	5809.220	3.884	−1.61	34.8	6.80
Fe I	5849.690	3.695	−2.93	···	···
Fe I	5852.230	4.549	−1.17	···	···
Fe I	5855.090	4.608	−1.48	···	···
Fe I	5856.100	4.294	−1.56	···	···
Fe I	5858.790	4.220	−2.18	···	···
Fe I	5859.600	4.550	−0.61	56.3	6.85
Fe I	5862.370	4.550	−0.25	74.6	6.76
Fe I	5956.700	0.859	−4.60	52.4	6.84
Fe I	6027.060	4.070	−1.17	43.1	6.71
Fe I	6151.620	2.176	−3.28	45.7	6.84
Fe I	6159.380	4.610	−1.83	···	···
Fe I	6165.360	4.143	−1.46	28.7	6.78
Fe I	6173.340	2.223	−2.88	63.9	6.83
Fe I	6200.320	2.609	−2.44	65.7	6.84
Fe I	6213.440	2.223	−2.56	79.7	6.80
Fe I	6240.652	2.220	−3.23	41.4	6.75
Fe I	6265.140	2.176	−2.55	83.2	6.79
Fe I	6271.283	3.330	−2.70	···	···
Fe I	6297.801	2.223	−2.73	73.2	6.85
Fe I	6322.694	2.588	−2.43	69.6	6.87
Fe I	6358.690	0.859	−4.00	77.0	6.69
Fe I	6436.410	4.186	−2.36	···	···
Fe I	6481.878	2.279	−2.97	63.3	6.96
Fe I	6498.950	0.958	−4.69	50.1	6.96
Fe I	6518.370	2.830	−2.45	48.8	6.76
Fe I	6574.233	0.990	−5.00	31.5	6.93
Fe I	6581.214	1.480	−4.68	···	···
Fe I	6591.330	4.593	−1.95	···	···
Fe I	6608.040	2.279	−3.91	···	···
Fe I	6625.027	1.010	−5.34	···	···
Fe I	6699.142	4.590	−2.10	···	···
Fe I	6713.750	4.795	−1.39	···	···
Fe I	6725.360	4.103	−2.17	···	···

Table B.1: Equivalent Width Measurements for F/G/K Primaries *(continued)*

Species	λ	E.P.	log(gf)	PM I11584-4155E	
	(Å)	(eV)	(dex)	EW (mÅ)	Abundance
Fe I	6733.150	4.638	−1.40	13.9	6.82
Fe I	6739.524	1.560	−4.79	···	···
Fe I	6750.160	2.424	−2.62	64.7	6.77
Fe I	6752.711	4.640	−1.20	···	···
Fe I	6837.009	4.590	−1.69	···	···
Fe I	6857.250	4.076	−2.04	···	···
Fe I	6971.936	3.020	−3.34	···	···
Fe I	7112.170	2.990	−2.99	18.9	6.80
Fe I	7751.120	4.990	−0.73	22.5	6.74
Fe I	7802.510	5.080	−1.31	···	···
Fe I	7807.920	4.990	−0.73	34.2	6.99
Fe I	8365.644	3.250	−2.04	···	···
Fe I	8757.200	2.845	−2.12	···	···
Fe II	5234.620	3.221	−2.22	43.1	6.78
Fe II	5425.260	3.200	−3.16	···	···
Fe II	6149.250	3.889	−2.63	···	···
Fe II	6247.560	3.892	−2.27	13.5	6.68
Fe II	6369.490	2.891	−4.02	···	···
Fe II	6432.680	2.891	−3.52	10.3	6.76
Fe II	6456.390	3.903	−2.06	21.8	6.78
Fe II	7479.700	3.892	−3.53	···	···
Fe II	7515.840	3.903	−3.42	···	···
Ca I	5867.570	2.930	−1.57	31.0	6.06
Ca I	6166.440	2.520	−1.14	84.1	6.04
Ca I	6169.040	2.520	−0.80	116.9	6.09
Ca I	6455.610	2.520	−1.29	63.1	5.88
Ca I	6572.800	0.000	−4.28	62.5	6.14
Ti I	5024.850	0.818	−0.56	88.0	4.57
Ti I	5113.450	1.443	−0.73	···	···
Ti I	5219.710	0.021	−2.24	52.1	4.65
Ti I	5866.460	1.066	−0.76	76.3	4.73
Ti I	6091.180	2.267	−0.37	27.7	4.72
Ti I	6126.220	1.066	−1.37	43.2	4.71
Ti I	6258.090	1.443	−0.31	77.8	4.69

Table B.1: Equivalent Width Measurements for F/G/K Primaries *(continued)*

Species	λ	E.P.	log(gf)	PM I12170+0742E	
	(Å)	(eV)	(dex)	EW (mÅ)	Abundance
Fe I	5141.750	2.424	−2.18	···	···
Fe I	5247.060	0.087	−4.94	···	···
Fe I	5358.120	3.300	−3.16	···	···
Fe I	5412.788	4.440	−1.71	···	···
Fe I	5661.348	4.280	−1.75	···	···
Fe I	5778.458	2.590	−3.45	···	···
Fe I	5784.660	3.400	−2.53	···	···
Fe I	5809.220	3.884	−1.61	···	···
Fe I	5849.690	3.695	−2.93	···	···
Fe I	5852.230	4.549	−1.17	···	···
Fe I	5855.090	4.608	−1.48	···	···
Fe I	5856.100	4.294	−1.56	···	···
Fe I	5858.790	4.220	−2.18	···	···
Fe I	5859.600	4.550	−0.61	···	···
Fe I	5862.370	4.550	−0.25	53.0	6.19
Fe I	5956.700	0.859	−4.60	···	···
Fe I	6027.060	4.070	−1.17	29.5	6.23
Fe I	6151.620	2.176	−3.28	···	···
Fe I	6159.380	4.610	−1.83	···	···
Fe I	6165.360	4.143	−1.46	···	···
Fe I	6173.340	2.223	−2.88	74.5	6.58
Fe I	6200.320	2.609	−2.44	···	···
Fe I	6213.440	2.223	−2.56	70.7	6.20
Fe I	6240.652	2.220	−3.23	···	···
Fe I	6265.140	2.176	−2.55	78.7	6.25
Fe I	6271.283	3.330	−2.70	···	···
Fe I	6297.801	2.223	−2.73	···	···
Fe I	6322.694	2.588	−2.43	···	···
Fe I	6358.690	0.859	−4.00	···	···
Fe I	6436.410	4.186	−2.36	···	···
Fe I	6481.878	2.279	−2.97	39.7	6.19
Fe I	6498.950	0.958	−4.69	···	···
Fe I	6518.370	2.830	−2.45	31.3	6.15
Fe I	6574.233	0.990	−5.00	···	···
Fe I	6581.214	1.480	−4.68	···	···
Fe I	6591.330	4.593	−1.95	···	···
Fe I	6608.040	2.279	−3.91	···	···
Fe I	6625.027	1.010	−5.34	···	···
Fe I	6699.142	4.590	−2.10	···	···
Fe I	6713.750	4.795	−1.39	···	···
Fe I	6725.360	4.103	−2.17	···	···

Table B.1: Equivalent Width Measurements for F/G/K Primaries *(continued)*

Species	λ	E.P.	log(gf)	PM I12170+0742E	
	(Å)	(eV)	(dex)	EW (mÅ)	Abundance
Fe I	6733.150	4.638	−1.40	···	···
Fe I	6739.524	1.560	−4.79	···	···
Fe I	6750.160	2.424	−2.62	···	···
Fe I	6752.711	4.640	−1.20	···	···
Fe I	6837.009	4.590	−1.69	···	···
Fe I	6857.250	4.076	−2.04	···	···
Fe I	6971.936	3.020	−3.34	···	···
Fe I	7112.170	2.990	−2.99	···	···
Fe I	7751.120	4.990	−0.73	···	···
Fe I	7802.510	5.080	−1.31	···	···
Fe I	7807.920	4.990	−0.73	···	···
Fe I	8365.644	3.250	−2.04	···	···
Fe I	8757.200	2.845	−2.12	···	···
Fe II	5234.620	3.221	−2.22	···	···
Fe II	5425.260	3.200	−3.16	···	···
Fe II	6149.250	3.889	−2.63	···	···
Fe II	6247.560	3.892	−2.27	···	···
Fe II	6369.490	2.891	−4.02	···	···
Fe II	6432.680	2.891	−3.52	···	···
Fe II	6456.390	3.903	−2.06	···	···
Fe II	7479.700	3.892	−3.53	···	···
Fe II	7515.840	3.903	−3.42	···	···
Ca I	5867.570	2.930	−1.57	···	···
Ca I	6166.440	2.520	−1.14	47.4	5.28
Ca I	6169.040	2.520	−0.80	93.7	5.46
Ca I	6455.610	2.520	−1.29	···	···
Ca I	6572.800	0.000	−4.28	···	···
Ti I	5024.850	0.818	−0.56	···	···
Ti I	5113.450	1.443	−0.73	···	···
Ti I	5219.710	0.021	−2.24	···	···
Ti I	5866.460	1.066	−0.76	···	···
Ti I	6091.180	2.267	−0.37	···	···
Ti I	6126.220	1.066	−1.37	···	···
Ti I	6258.090	1.443	−0.31	41.0	3.74

Table B.1: Equivalent Width Measurements for F/G/K Primaries *(continued)*

Species	λ	E.P.	log(gf)	PM I12237+0625	
	(Å)	(eV)	(dex)	EW (mÅ)	Abundance
Fe I	5141.750	2.424	−2.18	···	···
Fe I	5247.060	0.087	−4.94	111.0	6.81
Fe I	5358.120	3.300	−3.16	···	···
Fe I	5412.788	4.440	−1.71	···	···
Fe I	5661.348	4.280	−1.75	···	···
Fe I	5778.458	2.590	−3.45	···	···
Fe I	5784.660	3.400	−2.53	···	···
Fe I	5809.220	3.884	−1.61	···	···
Fe I	5849.690	3.695	−2.93	···	···
Fe I	5852.230	4.549	−1.17	···	···
Fe I	5855.090	4.608	−1.48	···	···
Fe I	5856.100	4.294	−1.56	···	···
Fe I	5858.790	4.220	−2.18	···	···
Fe I	5859.600	4.550	−0.61	43.5	6.52
Fe I	5862.370	4.550	−0.25	58.4	6.37
Fe I	5956.700	0.859	−4.60	65.9	6.58
Fe I	6027.060	4.070	−1.17	49.0	6.64
Fe I	6151.620	2.176	−3.28	52.1	6.61
Fe I	6159.380	4.610	−1.83	···	···
Fe I	6165.360	4.143	−1.46	···	···
Fe I	6173.340	2.223	−2.88	67.9	6.51
Fe I	6200.320	2.609	−2.44	87.7	6.81
Fe I	6213.440	2.223	−2.56	99.5	6.65
Fe I	6240.652	2.220	−3.23	53.2	6.63
Fe I	6265.140	2.176	−2.55	101.0	6.60
Fe I	6271.283	3.330	−2.70	···	···
Fe I	6297.801	2.223	−2.73	81.8	6.57
Fe I	6322.694	2.588	−2.43	···	···
Fe I	6358.690	0.859	−4.00	80.0	6.19
Fe I	6436.410	4.186	−2.36	···	···
Fe I	6481.878	2.279	−2.97	63.6	6.59
Fe I	6498.950	0.958	−4.69	···	···
Fe I	6518.370	2.830	−2.45	60.5	6.67
Fe I	6574.233	0.990	−5.00	39.7	6.66
Fe I	6581.214	1.480	−4.68	···	···
Fe I	6591.330	4.593	−1.95	···	···
Fe I	6608.040	2.279	−3.91	···	···
Fe I	6625.027	1.010	−5.34	···	···
Fe I	6699.142	4.590	−2.10	···	···
Fe I	6713.750	4.795	−1.39	···	···
Fe I	6725.360	4.103	−2.17	···	···

Table B.1: Equivalent Width Measurements for F/G/K Primaries *(continued)*

Species	λ	E.P.	log(gf)	PM I12237+0625	
	(Å)	(eV)	(dex)	EW (mÅ)	Abundance
Fe I	6733.150	4.638	−1.40	···	···
Fe I	6739.524	1.560	−4.79	···	···
Fe I	6750.160	2.424	−2.62	73.2	6.55
Fe I	6752.711	4.640	−1.20	···	···
Fe I	6837.009	4.590	−1.69	···	···
Fe I	6857.250	4.076	−2.04	···	···
Fe I	6971.936	3.020	−3.34	···	···
Fe I	7112.170	2.990	−2.99	···	···
Fe I	7751.120	4.990	−0.73	···	···
Fe I	7802.510	5.080	−1.31	···	···
Fe I	7807.920	4.990	−0.73	23.7	6.74
Fe I	8365.644	3.250	−2.04	52.4	6.54
Fe I	8757.200	2.845	−2.12	···	···
Fe II	5234.620	3.221	−2.22	···	···
Fe II	5425.260	3.200	−3.16	···	···
Fe II	6149.250	3.889	−2.63	···	···
Fe II	6247.560	3.892	−2.27	···	···
Fe II	6369.490	2.891	−4.02	···	···
Fe II	6432.680	2.891	−3.52	···	···
Fe II	6456.390	3.903	−2.06	···	···
Fe II	7479.700	3.892	−3.53	···	···
Fe II	7515.840	3.903	−3.42	···	···
Ca I	5867.570	2.930	−1.57	···	···
Ca I	6166.440	2.520	−1.14	118.5	···
Ca I	6169.040	2.520	−0.80	166.2	···
Ca I	6455.610	2.520	−1.29	93.0	···
Ca I	6572.800	0.000	−4.28	···	···
Ti I	5024.850	0.818	−0.56	132.5	4.34
Ti I	5113.450	1.443	−0.73	···	···
Ti I	5219.710	0.021	−2.24	91.8	4.52
Ti I	5866.460	1.066	−0.76	113.6	4.51
Ti I	6091.180	2.267	−0.37	56.3	4.69
Ti I	6126.220	1.066	−1.37	71.6	4.48
Ti I	6258.090	1.443	−0.31	···	···

Table B.1: Equivalent Width Measurements for F/G/K Primaries *(continued)*

Species	λ	E.P.	log(gf)	PM I12508+0757	
	(Å)	(eV)	(dex)	EW (mÅ)	Abundance
Fe I	5141.750	2.424	−2.18	52.0	6.57
Fe I	5247.060	0.087	−4.94	36.8	6.77
Fe I	5358.120	3.300	−3.16	···	···
Fe I	5412.788	4.440	−1.71	···	···
Fe I	5661.348	4.280	−1.75	···	···
Fe I	5778.458	2.590	−3.45	···	···
Fe I	5784.660	3.400	−2.53	···	···
Fe I	5809.220	3.884	−1.61	21.2	6.79
Fe I	5849.690	3.695	−2.93	···	···
Fe I	5852.230	4.549	−1.17	···	···
Fe I	5855.090	4.608	−1.48	···	···
Fe I	5856.100	4.294	−1.56	···	···
Fe I	5858.790	4.220	−2.18	···	···
Fe I	5859.600	4.550	−0.61	40.9	6.80
Fe I	5862.370	4.550	−0.25	53.6	6.64
Fe I	5956.700	0.859	−4.60	24.9	6.92
Fe I	6027.060	4.070	−1.17	30.9	6.73
Fe I	6151.620	2.176	−3.28	20.6	6.78
Fe I	6159.380	4.610	−1.83	···	···
Fe I	6165.360	4.143	−1.46	19.7	6.83
Fe I	6173.340	2.223	−2.88	38.9	6.80
Fe I	6200.320	2.609	−2.44	38.5	6.73
Fe I	6213.440	2.223	−2.56	52.2	6.69
Fe I	6240.652	2.220	−3.23	16.3	6.65
Fe I	6265.140	2.176	−2.55	52.2	6.63
Fe I	6271.283	3.330	−2.70	···	···
Fe I	6297.801	2.223	−2.73	43.3	6.72
Fe I	6322.694	2.588	−2.43	38.6	6.69
Fe I	6358.690	0.859	−4.00	38.3	6.55
Fe I	6436.410	4.186	−2.36	···	···
Fe I	6481.878	2.279	−2.97	32.4	6.81
Fe I	6498.950	0.958	−4.69	···	···
Fe I	6518.370	2.830	−2.45	···	···
Fe I	6574.233	0.990	−5.00	···	···
Fe I	6581.214	1.480	−4.68	···	···
Fe I	6591.330	4.593	−1.95	···	···
Fe I	6608.040	2.279	−3.91	···	···
Fe I	6625.027	1.010	−5.34	···	···
Fe I	6699.142	4.590	−2.10	···	···
Fe I	6713.750	4.795	−1.39	···	···
Fe I	6725.360	4.103	−2.17	···	···

Table B.1: Equivalent Width Measurements for F/G/K Primaries *(continued)*

Species	λ	E.P.	log(gf)	PM I12508+0757	
	(Å)	(eV)	(dex)	EW (mÅ)	Abundance
Fe I	6733.150	4.638	−1.40	5.2	6.58
Fe I	6739.524	1.560	−4.79	···	···
Fe I	6750.160	2.424	−2.62	45.1	6.81
Fe I	6752.711	4.640	−1.20	11.8	6.76
Fe I	6837.009	4.590	−1.69	···	···
Fe I	6857.250	4.076	−2.04	···	···
Fe I	6971.936	3.020	−3.34	···	···
Fe I	7112.170	2.990	−2.99	···	···
Fe I	7751.120	4.990	−0.73	···	···
Fe I	7802.510	5.080	−1.31	···	···
Fe I	7807.920	4.990	−0.73	···	···
Fe I	8365.644	3.250	−2.04	···	···
Fe I	8757.200	2.845	−2.12	···	···
Fe II	5234.620	3.221	−2.22	···	···
Fe II	5425.260	3.200	−3.16	22.1	6.74
Fe II	6149.250	3.889	−2.63	19.0	6.76
Fe II	6247.560	3.892	−2.27	30.6	6.68
Fe II	6369.490	2.891	−4.02	···	···
Fe II	6432.680	2.891	−3.52	21.7	6.76
Fe II	6456.390	3.903	−2.06	39.1	6.64
Fe II	7479.700	3.892	−3.53	···	···
Fe II	7515.840	3.903	−3.42	···	···
Ca I	5867.570	2.930	−1.57	···	···
Ca I	6166.440	2.520	−1.14	41.7	5.78
Ca I	6169.040	2.520	−0.80	61.6	5.73
Ca I	6455.610	2.520	−1.29	30.2	5.72
Ca I	6572.800	0.000	−4.28	···	···
Ti I	5024.850	0.818	−0.56	40.7	4.31
Ti I	5113.450	1.443	−0.73	···	···
Ti I	5219.710	0.021	−2.24	···	···
Ti I	5866.460	1.066	−0.76	26.7	4.44
Ti I	6091.180	2.267	−0.37	···	···
Ti I	6126.220	1.066	−1.37	8.4	4.45
Ti I	6258.090	1.443	−0.31	31.2	4.43

Table B.1: Equivalent Width Measurements for F/G/K Primaries *(continued)*

Species	λ	E.P.	log(gf)	PM I13133-4153N	
	(Å)	(eV)	(dex)	EW (mÅ)	Abundance
Fe I	5141.750	2.424	−2.18	···	···
Fe I	5247.060	0.087	−4.94	104.3	6.53
Fe I	5358.120	3.300	−3.16	···	···
Fe I	5412.788	4.440	−1.71	···	···
Fe I	5661.348	4.280	−1.75	···	···
Fe I	5778.458	2.590	−3.45	···	···
Fe I	5784.660	3.400	−2.53	···	···
Fe I	5809.220	3.884	−1.61	25.1	6.33
Fe I	5849.690	3.695	−2.93	···	···
Fe I	5852.230	4.549	−1.17	···	···
Fe I	5855.090	4.608	−1.48	···	···
Fe I	5856.100	4.294	−1.56	···	···
Fe I	5858.790	4.220	−2.18	···	···
Fe I	5859.600	4.550	−0.61	34.9	6.26
Fe I	5862.370	4.550	−0.25	58.5	6.22
Fe I	5956.700	0.859	−4.60	55.0	6.29
Fe I	6027.060	4.070	−1.17	···	···
Fe I	6151.620	2.176	−3.28	27.8	6.06
Fe I	6159.380	4.610	−1.83	···	···
Fe I	6165.360	4.143	−1.46	···	···
Fe I	6173.340	2.223	−2.88	59.0	6.23
Fe I	6200.320	2.609	−2.44	53.9	6.16
Fe I	6213.440	2.223	−2.56	···	···
Fe I	6240.652	2.220	−3.23	44.1	6.35
Fe I	6265.140	2.176	−2.55	67.3	5.95
Fe I	6271.283	3.330	−2.70	···	···
Fe I	6297.801	2.223	−2.73	···	···
Fe I	6322.694	2.588	−2.43	59.7	6.21
Fe I	6358.690	0.859	−4.00	73.0	5.93
Fe I	6436.410	4.186	−2.36	···	···
Fe I	6481.878	2.279	−2.97	···	···
Fe I	6498.950	0.958	−4.69	···	···
Fe I	6518.370	2.830	−2.45	···	···
Fe I	6574.233	0.990	−5.00	···	···
Fe I	6581.214	1.480	−4.68	···	···
Fe I	6591.330	4.593	−1.95	···	···
Fe I	6608.040	2.279	−3.91	···	···
Fe I	6625.027	1.010	−5.34	···	···
Fe I	6699.142	4.590	−2.10	···	···
Fe I	6713.750	4.795	−1.39	···	···
Fe I	6725.360	4.103	−2.17	···	···

Table B.1: Equivalent Width Measurements for F/G/K Primaries *(continued)*

Species	λ	E.P.	log(gf)	PM I13133-4153N	
	(Å)	(eV)	(dex)	EW (mÅ)	Abundance
Fe I	6733.150	4.638	−1.40	···	···
Fe I	6739.524	1.560	−4.79	···	···
Fe I	6750.160	2.424	−2.62	61.1	6.20
Fe I	6752.711	4.640	−1.20	···	···
Fe I	6837.009	4.590	−1.69	···	···
Fe I	6857.250	4.076	−2.04	···	···
Fe I	6971.936	3.020	−3.34	···	···
Fe I	7112.170	2.990	−2.99	···	···
Fe I	7751.120	4.990	−0.73	···	···
Fe I	7802.510	5.080	−1.31	···	···
Fe I	7807.920	4.990	−0.73	···	···
Fe I	8365.644	3.250	−2.04	···	···
Fe I	8757.200	2.845	−2.12	···	···
Fe II	5234.620	3.221	−2.22	···	···
Fe II	5425.260	3.200	−3.16	···	···
Fe II	6149.250	3.889	−2.63	···	···
Fe II	6247.560	3.892	−2.27	···	···
Fe II	6369.490	2.891	−4.02	···	···
Fe II	6432.680	2.891	−3.52	···	···
Fe II	6456.390	3.903	−2.06	···	···
Fe II	7479.700	3.892	−3.53	···	···
Fe II	7515.840	3.903	−3.42	···	···
Ca I	5867.570	2.930	−1.57	···	···
Ca I	6166.440	2.520	−1.14	85.7	5.54
Ca I	6169.040	2.520	−0.80	122.2	5.53
Ca I	6455.610	2.520	−1.29	63.5	5.44
Ca I	6572.800	0.000	−4.28	···	···
Ti I	5024.850	0.818	−0.56	100.3	3.95
Ti I	5113.450	1.443	−0.73	···	···
Ti I	5219.710	0.021	−2.24	68.0	4.20
Ti I	5866.460	1.066	−0.76	87.4	4.17
Ti I	6091.180	2.267	−0.37	28.8	4.31
Ti I	6126.220	1.066	−1.37	50.6	4.24
Ti I	6258.090	1.443	−0.31	97.2	4.25

Table B.1: Equivalent Width Measurements for F/G/K Primaries *(continued)*

Species	λ	E.P.	log(gf)	PM I13167+0810E	
	(Å)	(eV)	(dex)	EW (mÅ)	Abundance
Fe I	5141.750	2.424	−2.18	93.6	6.80
Fe I	5247.060	0.087	−4.94	75.2	6.76
Fe I	5358.120	3.300	−3.16	···	···
Fe I	5412.788	4.440	−1.71	···	···
Fe I	5661.348	4.280	−1.75	···	···
Fe I	5778.458	2.590	−3.45	21.6	6.85
Fe I	5784.660	3.400	−2.53	···	···
Fe I	5809.220	3.884	−1.61	42.5	6.88
Fe I	5849.690	3.695	−2.93	···	···
Fe I	5852.230	4.549	−1.17	31.2	6.92
Fe I	5855.090	4.608	−1.48	···	···
Fe I	5856.100	4.294	−1.56	27.9	6.97
Fe I	5858.790	4.220	−2.18	···	···
Fe I	5859.600	4.550	−0.61	61.2	6.84
Fe I	5862.370	4.550	−0.25	75.9	6.67
Fe I	5956.700	0.859	−4.60	69.2	7.08
Fe I	6027.060	4.070	−1.17	53.4	6.81
Fe I	6151.620	2.176	−3.28	48.2	6.79
Fe I	6159.380	4.610	−1.83	···	···
Fe I	6165.360	4.143	−1.46	34.1	6.83
Fe I	6173.340	2.223	−2.88	68.3	6.82
Fe I	6200.320	2.609	−2.44	76.4	6.93
Fe I	6213.440	2.223	−2.56	86.0	6.79
Fe I	6240.652	2.220	−3.23	53.8	6.90
Fe I	6265.140	2.176	−2.55	91.4	6.80
Fe I	6271.283	3.330	−2.70	···	···
Fe I	6297.801	2.223	−2.73	98.0	7.12
Fe I	6322.694	2.588	−2.43	79.0	6.93
Fe I	6358.690	0.859	−4.00	87.9	6.77
Fe I	6436.410	4.186	−2.36	···	···
Fe I	6481.878	2.279	−2.97	···	···
Fe I	6498.950	0.958	−4.69	56.0	6.96
Fe I	6518.370	2.830	−2.45	69.2	7.04
Fe I	6574.233	0.990	−5.00	40.3	6.97
Fe I	6581.214	1.480	−4.68	24.5	6.86
Fe I	6591.330	4.593	−1.95	···	···
Fe I	6608.040	2.279	−3.91	···	···
Fe I	6625.027	1.010	−5.34	···	···
Fe I	6699.142	4.590	−2.10	···	···
Fe I	6713.750	4.795	−1.39	12.1	6.86
Fe I	6725.360	4.103	−2.17	···	···

Table B.1: Equivalent Width Measurements for F/G/K Primaries *(continued)*

Species	λ	E.P.	log(gf)	PM I13167+0810E	
	(Å)	(eV)	(dex)	EW (mÅ)	Abundance
Fe I	6733.150	4.638	−1.40	···	···
Fe I	6739.524	1.560	−4.79	···	···
Fe I	6750.160	2.424	−2.62	75.1	6.86
Fe I	6752.711	4.640	−1.20	···	···
Fe I	6837.009	4.590	−1.69	···	···
Fe I	6857.250	4.076	−2.04	13.9	6.80
Fe I	6971.936	3.020	−3.34	···	···
Fe I	7112.170	2.990	−2.99	···	···
Fe I	7751.120	4.990	−0.73	···	···
Fe I	7802.510	5.080	−1.31	···	···
Fe I	7807.920	4.990	−0.73	···	···
Fe I	8365.644	3.250	−2.04	···	···
Fe I	8757.200	2.845	−2.12	···	···
Fe II	5234.620	3.221	−2.22	35.1	6.74
Fe II	5425.260	3.200	−3.16	11.6	6.88
Fe II	6149.250	3.889	−2.63	···	···
Fe II	6247.560	3.892	−2.27	16.3	6.92
Fe II	6369.490	2.891	−4.02	···	···
Fe II	6432.680	2.891	−3.52	···	···
Fe II	6456.390	3.903	−2.06	20.1	6.87
Fe II	7479.700	3.892	−3.53	···	···
Fe II	7515.840	3.903	−3.42	···	···
Ca I	5867.570	2.930	−1.57	26.7	5.84
Ca I	6166.440	2.520	−1.14	85.0	5.86
Ca I	6169.040	2.520	−0.80	119.7	5.88
Ca I	6455.610	2.520	−1.29	69.0	5.79
Ca I	6572.800	0.000	−4.28	···	···
Ti I	5024.850	0.818	−0.56	89.5	4.38
Ti I	5113.450	1.443	−0.73	···	···
Ti I	5219.710	0.021	−2.24	···	···
Ti I	5866.460	1.066	−0.76	77.6	4.56
Ti I	6091.180	2.267	−0.37	26.8	4.52
Ti I	6126.220	1.066	−1.37	47.5	4.59
Ti I	6258.090	1.443	−0.31	76.4	4.47

Table B.1: Equivalent Width Measurements for F/G/K Primaries *(continued)*

Species	λ	E.P.	log(gf)	PM I14055+0244S	
	(Å)	(eV)	(dex)	EW (mÅ)	Abundance
Fe I	5141.750	2.424	−2.18	···	···
Fe I	5247.060	0.087	−4.94	···	···
Fe I	5358.120	3.300	−3.16	···	···
Fe I	5412.788	4.440	−1.71	···	···
Fe I	5661.348	4.280	−1.75	···	···
Fe I	5778.458	2.590	−3.45	···	···
Fe I	5784.660	3.400	−2.53	···	···
Fe I	5809.220	3.884	−1.61	···	···
Fe I	5849.690	3.695	−2.93	···	···
Fe I	5852.230	4.549	−1.17	···	···
Fe I	5855.090	4.608	−1.48	···	···
Fe I	5856.100	4.294	−1.56	···	···
Fe I	5858.790	4.220	−2.18	···	···
Fe I	5859.600	4.550	−0.61	···	···
Fe I	5862.370	4.550	−0.25	70.3	6.68
Fe I	5956.700	0.859	−4.60	96.1	7.34
Fe I	6027.060	4.070	−1.17	···	···
Fe I	6151.620	2.176	−3.28	···	···
Fe I	6159.380	4.610	−1.83	···	···
Fe I	6165.360	4.143	−1.46	···	···
Fe I	6173.340	2.223	−2.88	75.5	6.85
Fe I	6200.320	2.609	−2.44	92.2	7.10
Fe I	6213.440	2.223	−2.56	118.0	7.12
Fe I	6240.652	2.220	−3.23	···	···
Fe I	6265.140	2.176	−2.55	128.2	7.16
Fe I	6271.283	3.330	−2.70	···	···
Fe I	6297.801	2.223	−2.73	105.4	7.14
Fe I	6322.694	2.588	−2.43	110.7	7.30
Fe I	6358.690	0.859	−4.00	92.3	6.63
Fe I	6436.410	4.186	−2.36	···	···
Fe I	6481.878	2.279	−2.97	65.4	6.81
Fe I	6498.950	0.958	−4.69	···	···
Fe I	6518.370	2.830	−2.45	53.3	6.72
Fe I	6574.233	0.990	−5.00	···	···
Fe I	6581.214	1.480	−4.68	···	···
Fe I	6591.330	4.593	−1.95	···	···
Fe I	6608.040	2.279	−3.91	···	···
Fe I	6625.027	1.010	−5.34	···	···
Fe I	6699.142	4.590	−2.10	···	···
Fe I	6713.750	4.795	−1.39	···	···
Fe I	6725.360	4.103	−2.17	···	···

Table B.1: Equivalent Width Measurements for F/G/K Primaries *(continued)*

Species	λ	E.P.	log(gf)	PM I14055+0244S	
	(Å)	(eV)	(dex)	EW (mÅ)	Abundance
Fe I	6733.150	4.638	−1.40	···	···
Fe I	6739.524	1.560	−4.79	···	···
Fe I	6750.160	2.424	−2.62	62.5	6.56
Fe I	6752.711	4.640	−1.20	···	···
Fe I	6837.009	4.590	−1.69	···	···
Fe I	6857.250	4.076	−2.04	···	···
Fe I	6971.936	3.020	−3.34	···	···
Fe I	7112.170	2.990	−2.99	···	···
Fe I	7751.120	4.990	−0.73	···	···
Fe I	7802.510	5.080	−1.31	···	···
Fe I	7807.920	4.990	−0.73	···	···
Fe I	8365.644	3.250	−2.04	···	···
Fe I	8757.200	2.845	−2.12	···	···
Fe II	5234.620	3.221	−2.22	···	···
Fe II	5425.260	3.200	−3.16	···	···
Fe II	6149.250	3.889	−2.63	···	···
Fe II	6247.560	3.892	−2.27	···	···
Fe II	6369.490	2.891	−4.02	···	···
Fe II	6432.680	2.891	−3.52	···	···
Fe II	6456.390	3.903	−2.06	···	···
Fe II	7479.700	3.892	−3.53	···	···
Fe II	7515.840	3.903	−3.42	···	···
Ca I	5867.570	2.930	−1.57	···	···
Ca I	6166.440	2.520	−1.14	154.6	6.31
Ca I	6169.040	2.520	−0.80	···	···
Ca I	6455.610	2.520	−1.29	112.6	6.09
Ca I	6572.800	0.000	−4.28	···	···
Ti I	5024.850	0.818	−0.56	···	···
Ti I	5113.450	1.443	−0.73	···	···
Ti I	5219.710	0.021	−2.24	120.1	5.14
Ti I	5866.460	1.066	−0.76	156.8	5.13
Ti I	6091.180	2.267	−0.37	46.6	4.60
Ti I	6126.220	1.066	−1.37	77.1	4.70
Ti I	6258.090	1.443	−0.31	128.7	4.80

Table B.1: Equivalent Width Measurements for F/G/K Primaries *(continued)*

Species	λ	E.P.	log(gf)	PM I14124+0517S	
	(Å)	(eV)	(dex)	EW (mÅ)	Abundance
Fe I	5141.750	2.424	−2.18	72.6	6.59
Fe I	5247.060	0.087	−4.94	59.4	6.58
Fe I	5358.120	3.300	−3.16	···	···
Fe I	5412.788	4.440	−1.71	···	···
Fe I	5661.348	4.280	−1.75	···	···
Fe I	5778.458	2.590	−3.45	···	···
Fe I	5784.660	3.400	−2.53	···	···
Fe I	5809.220	3.884	−1.61	20.3	6.48
Fe I	5849.690	3.695	−2.93	···	···
Fe I	5852.230	4.549	−1.17	···	···
Fe I	5855.090	4.608	−1.48	···	···
Fe I	5856.100	4.294	−1.56	···	···
Fe I	5858.790	4.220	−2.18	···	···
Fe I	5859.600	4.550	−0.61	43.4	6.63
Fe I	5862.370	4.550	−0.25	56.4	6.48
Fe I	5956.700	0.859	−4.60	27.8	6.41
Fe I	6027.060	4.070	−1.17	36.0	6.57
Fe I	6151.620	2.176	−3.28	34.5	6.65
Fe I	6159.380	4.610	−1.83	···	···
Fe I	6165.360	4.143	−1.46	···	···
Fe I	6173.340	2.223	−2.88	54.5	6.68
Fe I	6200.320	2.609	−2.44	51.5	6.60
Fe I	6213.440	2.223	−2.56	70.5	6.65
Fe I	6240.652	2.220	−3.23	35.3	6.66
Fe I	6265.140	2.176	−2.55	72.8	6.62
Fe I	6271.283	3.330	−2.70	···	···
Fe I	6297.801	2.223	−2.73	62.5	6.67
Fe I	6322.694	2.588	−2.43	55.7	6.63
Fe I	6358.690	0.859	−4.00	59.2	6.40
Fe I	6436.410	4.186	−2.36	···	···
Fe I	6481.878	2.279	−2.97	40.0	6.54
Fe I	6498.950	0.958	−4.69	35.8	6.74
Fe I	6518.370	2.830	−2.45	···	···
Fe I	6574.233	0.990	−5.00	···	···
Fe I	6581.214	1.480	−4.68	···	···
Fe I	6591.330	4.593	−1.95	···	···
Fe I	6608.040	2.279	−3.91	···	···
Fe I	6625.027	1.010	−5.34	···	···
Fe I	6699.142	4.590	−2.10	···	···
Fe I	6713.750	4.795	−1.39	···	···
Fe I	6725.360	4.103	−2.17	···	···

Table B.1: Equivalent Width Measurements for F/G/K Primaries *(continued)*

Species	λ	E.P.	log(gf)	PM I14124+0517S	
	(Å)	(eV)	(dex)	EW (mÅ)	Abundance
Fe I	6733.150	4.638	−1.40	···	···
Fe I	6739.524	1.560	−4.79	···	···
Fe I	6750.160	2.424	−2.62	61.0	6.72
Fe I	6752.711	4.640	−1.20	···	···
Fe I	6837.009	4.590	−1.69	···	···
Fe I	6857.250	4.076	−2.04	···	···
Fe I	6971.936	3.020	−3.34	···	···
Fe I	7112.170	2.990	−2.99	···	···
Fe I	7751.120	4.990	−0.73	···	···
Fe I	7802.510	5.080	−1.31	···	···
Fe I	7807.920	4.990	−0.73	26.4	6.82
Fe I	8365.644	3.250	−2.04	···	···
Fe I	8757.200	2.845	−2.12	···	···
Fe II	5234.620	3.221	−2.22	46.2	6.68
Fe II	5425.260	3.200	−3.16	···	···
Fe II	6149.250	3.889	−2.63	···	···
Fe II	6247.560	3.892	−2.27	13.6	6.54
Fe II	6369.490	2.891	−4.02	···	···
Fe II	6432.680	2.891	−3.52	···	···
Fe II	6456.390	3.903	−2.06	23.1	6.66
Fe II	7479.700	3.892	−3.53	···	···
Fe II	7515.840	3.903	−3.42	···	···
Ca I	5867.570	2.930	−1.57	20.4	5.89
Ca I	6166.440	2.520	−1.14	55.7	5.68
Ca I	6169.040	2.520	−0.80	81.1	5.70
Ca I	6455.610	2.520	−1.29	44.3	5.64
Ca I	6572.800	0.000	−4.28	33.8	5.75
Ti I	5024.850	0.818	−0.56	58.1	4.09
Ti I	5113.450	1.443	−0.73	···	···
Ti I	5219.710	0.021	−2.24	···	···
Ti I	5866.460	1.066	−0.76	42.9	4.22
Ti I	6091.180	2.267	−0.37	···	···
Ti I	6126.220	1.066	−1.37	20.6	4.34
Ti I	6258.090	1.443	−0.31	51.2	4.30

Table B.1: Equivalent Width Measurements for F/G/K Primaries *(continued)*

Species	λ (Å)	E.P. (eV)	log(gf) (dex)	PM I14136-3634E EW (mÅ)	Abundance
Fe I	5141.750	2.424	−2.18	···	···
Fe I	5247.060	0.087	−4.94	···	···
Fe I	5358.120	3.300	−3.16	···	···
Fe I	5412.788	4.440	−1.71	···	···
Fe I	5661.348	4.280	−1.75	···	···
Fe I	5778.458	2.590	−3.45	···	···
Fe I	5784.660	3.400	−2.53	···	···
Fe I	5809.220	3.884	−1.61	···	···
Fe I	5849.690	3.695	−2.93	···	···
Fe I	5852.230	4.549	−1.17	···	···
Fe I	5855.090	4.608	−1.48	···	···
Fe I	5856.100	4.294	−1.56	···	···
Fe I	5858.790	4.220	−2.18	···	···
Fe I	5859.600	4.550	−0.61	···	···
Fe I	5862.370	4.550	−0.25	65.5	6.37
Fe I	5956.700	0.859	−4.60	59.0	6.42
Fe I	6027.060	4.070	−1.17	36.0	6.36
Fe I	6151.620	2.176	−3.28	···	···
Fe I	6159.380	4.610	−1.83	···	···
Fe I	6165.360	4.143	−1.46	···	···
Fe I	6173.340	2.223	−2.88	56.5	6.27
Fe I	6200.320	2.609	−2.44	68.4	6.45
Fe I	6213.440	2.223	−2.56	77.1	6.25
Fe I	6240.652	2.220	−3.23	50.4	6.51
Fe I	6265.140	2.176	−2.55	78.4	6.20
Fe I	6271.283	3.330	−2.70	···	···
Fe I	6297.801	2.223	−2.73	75.0	6.38
Fe I	6322.694	2.588	−2.43	48.4	6.11
Fe I	6358.690	0.859	−4.00	···	···
Fe I	6436.410	4.186	−2.36	···	···
Fe I	6481.878	2.279	−2.97	49.4	6.30
Fe I	6498.950	0.958	−4.69	···	···
Fe I	6518.370	2.830	−2.45	···	···
Fe I	6574.233	0.990	−5.00	···	···
Fe I	6581.214	1.480	−4.68	···	···
Fe I	6591.330	4.593	−1.95	···	···
Fe I	6608.040	2.279	−3.91	···	···
Fe I	6625.027	1.010	−5.34	···	···
Fe I	6699.142	4.590	−2.10	···	···
Fe I	6713.750	4.795	−1.39	···	···
Fe I	6725.360	4.103	−2.17	···	···

Table B.1: Equivalent Width Measurements for F/G/K Primaries *(continued)*

Species	λ	E.P.	log(gf)	PM I14136-3634E	
	(Å)	(eV)	(dex)	EW (mÅ)	Abundance
Fe I	6733.150	4.638	−1.40	···	···
Fe I	6739.524	1.560	−4.79	···	···
Fe I	6750.160	2.424	−2.62	65.6	6.35
Fe I	6752.711	4.640	−1.20	···	···
Fe I	6837.009	4.590	−1.69	···	···
Fe I	6857.250	4.076	−2.04	···	···
Fe I	6971.936	3.020	−3.34	···	···
Fe I	7112.170	2.990	−2.99	···	···
Fe I	7751.120	4.990	−0.73	···	···
Fe I	7802.510	5.080	−1.31	···	···
Fe I	7807.920	4.990	−0.73	···	···
Fe I	8365.644	3.250	−2.04	···	···
Fe I	8757.200	2.845	−2.12	···	···
Fe II	5234.620	3.221	−2.22	···	···
Fe II	5425.260	3.200	−3.16	···	···
Fe II	6149.250	3.889	−2.63	···	···
Fe II	6247.560	3.892	−2.27	···	···
Fe II	6369.490	2.891	−4.02	···	···
Fe II	6432.680	2.891	−3.52	···	···
Fe II	6456.390	3.903	−2.06	···	···
Fe II	7479.700	3.892	−3.53	···	···
Fe II	7515.840	3.903	−3.42	···	···
Ca I	5867.570	2.930	−1.57	···	···
Ca I	6166.440	2.520	−1.14	71.1	5.40
Ca I	6169.040	2.520	−0.80	137.6	5.71
Ca I	6455.610	2.520	−1.29	72.5	5.56
Ca I	6572.800	0.000	−4.28	···	···
Ti I	5024.850	0.818	−0.56	133.5	4.39
Ti I	5113.450	1.443	−0.73	···	···
Ti I	5219.710	0.021	−2.24	100.7	4.73
Ti I	5866.460	1.066	−0.76	85.9	4.18
Ti I	6091.180	2.267	−0.37	···	···
Ti I	6126.220	1.066	−1.37	51.4	4.26
Ti I	6258.090	1.443	−0.31	···	···

Table B.1: Equivalent Width Measurements for F/G/K Primaries *(continued)*

Species	λ	E.P.	log(gf)	PM I14475+1134	
	(Å)	(eV)	(dex)	EW (mÅ)	Abundance
Fe I	5141.750	2.424	−2.18	80.6	6.78
Fe I	5247.060	0.087	−4.94	75.6	6.89
Fe I	5358.120	3.300	−3.16	···	···
Fe I	5412.788	4.440	−1.71	···	···
Fe I	5661.348	4.280	−1.75	···	···
Fe I	5778.458	2.590	−3.45	22.4	6.93
Fe I	5784.660	3.400	−2.53	···	···
Fe I	5809.220	3.884	−1.61	30.4	6.68
Fe I	5849.690	3.695	−2.93	···	···
Fe I	5852.230	4.549	−1.17	24.0	6.78
Fe I	5855.090	4.608	−1.48	···	···
Fe I	5856.100	4.294	−1.56	22.9	6.88
Fe I	5858.790	4.220	−2.18	···	···
Fe I	5859.600	4.550	−0.61	46.8	6.69
Fe I	5862.370	4.550	−0.25	64.6	6.64
Fe I	5956.700	0.859	−4.60	62.8	7.05
Fe I	6027.060	4.070	−1.17	40.6	6.64
Fe I	6151.620	2.176	−3.28	38.4	6.66
Fe I	6159.380	4.610	−1.83	···	···
Fe I	6165.360	4.143	−1.46	21.9	6.58
Fe I	6173.340	2.223	−2.88	53.6	6.63
Fe I	6200.320	2.609	−2.44	57.3	6.69
Fe I	6213.440	2.223	−2.56	71.2	6.67
Fe I	6240.652	2.220	−3.23	40.9	6.71
Fe I	6265.140	2.176	−2.55	74.5	6.67
Fe I	6271.283	3.330	−2.70	···	···
Fe I	6297.801	2.223	−2.73	62.2	6.65
Fe I	6322.694	2.588	−2.43	60.8	6.71
Fe I	6358.690	0.859	−4.00	63.7	6.43
Fe I	6436.410	4.186	−2.36	···	···
Fe I	6481.878	2.279	−2.97	69.5	7.09
Fe I	6498.950	0.958	−4.69	40.5	6.74
Fe I	6518.370	2.830	−2.45	37.6	6.51
Fe I	6574.233	0.990	−5.00	24.9	6.73
Fe I	6581.214	1.480	−4.68	···	···
Fe I	6591.330	4.593	−1.95	···	···
Fe I	6608.040	2.279	−3.91	···	···
Fe I	6625.027	1.010	−5.34	···	···
Fe I	6699.142	4.590	−2.10	···	···
Fe I	6713.750	4.795	−1.39	···	···
Fe I	6725.360	4.103	−2.17	···	···

Table B.1: Equivalent Width Measurements for F/G/K Primaries *(continued)*

Species	λ	E.P.	log(gf)	PM I14475+1134	
	(Å)	(eV)	(dex)	EW (mÅ)	Abundance
Fe I	6733.150	4.638	−1.40	···	···
Fe I	6739.524	1.560	−4.79	···	···
Fe I	6750.160	2.424	−2.62	61.5	6.72
Fe I	6752.711	4.640	−1.20	17.9	6.72
Fe I	6837.009	4.590	−1.69	···	···
Fe I	6857.250	4.076	−2.04	···	···
Fe I	6971.936	3.020	−3.34	···	···
Fe I	7112.170	2.990	−2.99	···	···
Fe I	7751.120	4.990	−0.73	···	···
Fe I	7802.510	5.080	−1.31	···	···
Fe I	7807.920	4.990	−0.73	29.4	6.87
Fe I	8365.644	3.250	−2.04	···	···
Fe I	8757.200	2.845	−2.12	···	···
Fe II	5234.620	3.221	−2.22	53.1	6.86
Fe II	5425.260	3.200	−3.16	20.4	6.92
Fe II	6149.250	3.889	−2.63	···	···
Fe II	6247.560	3.892	−2.27	15.0	6.55
Fe II	6369.490	2.891	−4.02	···	···
Fe II	6432.680	2.891	−3.52	···	···
Fe II	6456.390	3.903	−2.06	22.6	6.62
Fe II	7479.700	3.892	−3.53	···	···
Fe II	7515.840	3.903	−3.42	···	···
Ca I	5867.570	2.930	−1.57	21.7	5.87
Ca I	6166.440	2.520	−1.14	77.5	6.03
Ca I	6169.040	2.520	−0.80	105.9	6.08
Ca I	6455.610	2.520	−1.29	60.3	5.89
Ca I	6572.800	0.000	−4.28	···	···
Ti I	5024.850	0.818	−0.56	83.3	4.58
Ti I	5113.450	1.443	−0.73	43.9	4.59
Ti I	5219.710	0.021	−2.24	42.3	4.48
Ti I	5866.460	1.066	−0.76	66.5	4.61
Ti I	6091.180	2.267	−0.37	···	···
Ti I	6126.220	1.066	−1.37	33.4	4.53
Ti I	6258.090	1.443	−0.31	65.9	4.53

Table B.1: Equivalent Width Measurements for F/G/K Primaries *(continued)*

Species	λ	E.P.	log(gf)	PM I15413+1349N	
	(Å)	(eV)	(dex)	EW (mÅ)	Abundance
Fe I	5141.750	2.424	−2.18	···	···
Fe I	5247.060	0.087	−4.94	···	···
Fe I	5358.120	3.300	−3.16	···	···
Fe I	5412.788	4.440	−1.71	···	···
Fe I	5661.348	4.280	−1.75	···	···
Fe I	5778.458	2.590	−3.45	···	···
Fe I	5784.660	3.400	−2.53	···	···
Fe I	5809.220	3.884	−1.61	···	···
Fe I	5849.690	3.695	−2.93	···	···
Fe I	5852.230	4.549	−1.17	···	···
Fe I	5855.090	4.608	−1.48	···	···
Fe I	5856.100	4.294	−1.56	···	···
Fe I	5858.790	4.220	−2.18	···	···
Fe I	5859.600	4.550	−0.61	···	···
Fe I	5862.370	4.550	−0.25	···	···
Fe I	5956.700	0.859	−4.60	···	···
Fe I	6027.060	4.070	−1.17	···	···
Fe I	6151.620	2.176	−3.28	···	···
Fe I	6159.380	4.610	−1.83	···	···
Fe I	6165.360	4.143	−1.46	···	···
Fe I	6173.340	2.223	−2.88	64.8	6.53
Fe I	6200.320	2.609	−2.44	···	···
Fe I	6213.440	2.223	−2.56	···	···
Fe I	6240.652	2.220	−3.23	···	···
Fe I	6265.140	2.176	−2.55	95.6	6.52
Fe I	6271.283	3.330	−2.70	···	···
Fe I	6297.801	2.223	−2.73	···	···
Fe I	6322.694	2.588	−2.43	···	···
Fe I	6358.690	0.859	−4.00	···	···
Fe I	6436.410	4.186	−2.36	···	···
Fe I	6481.878	2.279	−2.97	70.2	6.75
Fe I	6498.950	0.958	−4.69	···	···
Fe I	6518.370	2.830	−2.45	···	···
Fe I	6574.233	0.990	−5.00	39.0	6.47
Fe I	6581.214	1.480	−4.68	···	···
Fe I	6591.330	4.593	−1.95	···	···
Fe I	6608.040	2.279	−3.91	···	···
Fe I	6625.027	1.010	−5.34	···	···
Fe I	6699.142	4.590	−2.10	···	···
Fe I	6713.750	4.795	−1.39	···	···
Fe I	6725.360	4.103	−2.17	···	···

Table B.1: Equivalent Width Measurements for F/G/K Primaries *(continued)*

Species	λ	E.P.	log(gf)	PM I15413+1349N	
	(Å)	(eV)	(dex)	EW (mÅ)	Abundance
Fe I	6733.150	4.638	−1.40	···	···
Fe I	6739.524	1.560	−4.79	···	···
Fe I	6750.160	2.424	−2.62	···	···
Fe I	6752.711	4.640	−1.20	···	···
Fe I	6837.009	4.590	−1.69	···	···
Fe I	6857.250	4.076	−2.04	···	···
Fe I	6971.936	3.020	−3.34	···	···
Fe I	7112.170	2.990	−2.99	···	···
Fe I	7751.120	4.990	−0.73	···	···
Fe I	7802.510	5.080	−1.31	···	···
Fe I	7807.920	4.990	−0.73	···	···
Fe I	8365.644	3.250	−2.04	···	···
Fe I	8757.200	2.845	−2.12	62.2	6.40
Fe II	5234.620	3.221	−2.22	···	···
Fe II	5425.260	3.200	−3.16	···	···
Fe II	6149.250	3.889	−2.63	···	···
Fe II	6247.560	3.892	−2.27	···	···
Fe II	6369.490	2.891	−4.02	···	···
Fe II	6432.680	2.891	−3.52	···	···
Fe II	6456.390	3.903	−2.06	···	···
Fe II	7479.700	3.892	−3.53	···	···
Fe II	7515.840	3.903	−3.42	···	···
Ca I	5867.570	2.930	−1.57	···	···
Ca I	6166.440	2.520	−1.14	161.7	5.58
Ca I	6169.040	2.520	−0.80	···	···
Ca I	6455.610	2.520	−1.29	122.4	5.42
Ca I	6572.800	0.000	−4.28	···	···
Ti I	5024.850	0.818	−0.56	···	···
Ti I	5113.450	1.443	−0.73	···	···
Ti I	5219.710	0.021	−2.24	143.6	4.20
Ti I	5866.460	1.066	−0.76	···	···
Ti I	6091.180	2.267	−0.37	···	···
Ti I	6126.220	1.066	−1.37	98.9	4.10
Ti I	6258.090	1.443	−0.31	···	···

Table B.1: Equivalent Width Measurements for F/G/K Primaries *(continued)*

Species	λ	E.P.	log(gf)	PM I16008+0146E	
	(Å)	(eV)	(dex)	EW (mÅ)	Abundance
Fe I	5141.750	2.424	−2.18	···	···
Fe I	5247.060	0.087	−4.94	81.5	6.59
Fe I	5358.120	3.300	−3.16	···	···
Fe I	5412.788	4.440	−1.71	···	···
Fe I	5661.348	4.280	−1.75	···	···
Fe I	5778.458	2.590	−3.45	28.1	6.86
Fe I	5784.660	3.400	−2.53	···	···
Fe I	5809.220	3.884	−1.61	28.4	6.53
Fe I	5849.690	3.695	−2.93	···	···
Fe I	5852.230	4.549	−1.17	31.4	6.90
Fe I	5855.090	4.608	−1.48	···	···
Fe I	5856.100	4.294	−1.56	···	···
Fe I	5858.790	4.220	−2.18	···	···
Fe I	5859.600	4.550	−0.61	43.0	6.57
Fe I	5862.370	4.550	−0.25	72.2	6.67
Fe I	5956.700	0.859	−4.60	59.4	6.61
Fe I	6027.060	4.070	−1.17	43.4	6.62
Fe I	6151.620	2.176	−3.28	43.1	6.52
Fe I	6159.380	4.610	−1.83	···	···
Fe I	6165.360	4.143	−1.46	···	···
Fe I	6173.340	2.223	−2.88	66.7	6.66
Fe I	6200.320	2.609	−2.44	66.7	6.67
Fe I	6213.440	2.223	−2.56	88.8	6.73
Fe I	6240.652	2.220	−3.23	43.3	6.52
Fe I	6265.140	2.176	−2.55	88.4	6.65
Fe I	6271.283	3.330	−2.70	···	···
Fe I	6297.801	2.223	−2.73	92.5	6.95
Fe I	6322.694	2.588	−2.43	66.9	6.63
Fe I	6358.690	0.859	−4.00	82.6	6.46
Fe I	6436.410	4.186	−2.36	···	···
Fe I	6481.878	2.279	−2.97	62.6	6.72
Fe I	6498.950	0.958	−4.69	55.8	6.70
Fe I	6518.370	2.830	−2.45	49.0	6.57
Fe I	6574.233	0.990	−5.00	56.1	7.05
Fe I	6581.214	1.480	−4.68	···	···
Fe I	6591.330	4.593	−1.95	···	···
Fe I	6608.040	2.279	−3.91	···	···
Fe I	6625.027	1.010	−5.34	23.7	6.69
Fe I	6699.142	4.590	−2.10	···	···
Fe I	6713.750	4.795	−1.39	···	···
Fe I	6725.360	4.103	−2.17	···	···

Table B.1: Equivalent Width Measurements for F/G/K Primaries *(continued)*

Species	λ	E.P.	log(gf)	PM I16008+0146E	
	(Å)	(eV)	(dex)	EW (mÅ)	Abundance
Fe I	6733.150	4.638	−1.40	···	···
Fe I	6739.524	1.560	−4.79	···	···
Fe I	6750.160	2.424	−2.62	72.1	6.70
Fe I	6752.711	4.640	−1.20	···	···
Fe I	6837.009	4.590	−1.69	···	···
Fe I	6857.250	4.076	−2.04	···	···
Fe I	6971.936	3.020	−3.34	···	···
Fe I	7112.170	2.990	−2.99	···	···
Fe I	7751.120	4.990	−0.73	16.3	6.54
Fe I	7802.510	5.080	−1.31	···	···
Fe I	7807.920	4.990	−0.73	25.1	6.78
Fe I	8365.644	3.250	−2.04	66.3	6.87
Fe I	8757.200	2.845	−2.12	···	···
Fe II	5234.620	3.221	−2.22	28.4	6.72
Fe II	5425.260	3.200	−3.16	···	···
Fe II	6149.250	3.889	−2.63	···	···
Fe II	6247.560	3.892	−2.27	···	···
Fe II	6369.490	2.891	−4.02	···	···
Fe II	6432.680	2.891	−3.52	···	···
Fe II	6456.390	3.903	−2.06	11.0	6.68
Fe II	7479.700	3.892	−3.53	···	···
Fe II	7515.840	3.903	−3.42	···	···
Ca I	5867.570	2.930	−1.57	29.7	5.70
Ca I	6166.440	2.520	−1.14	88.4	5.75
Ca I	6169.040	2.520	−0.80	140.5	5.96
Ca I	6455.610	2.520	−1.29	65.6	5.56
Ca I	6572.800	0.000	−4.28	79.6	5.83
Ti I	5024.850	0.818	−0.56	105.5	4.30
Ti I	5113.450	1.443	−0.73	88.6	4.90
Ti I	5219.710	0.021	−2.24	73.9	4.44
Ti I	5866.460	1.066	−0.76	90.7	4.45
Ti I	6091.180	2.267	−0.37	27.9	4.24
Ti I	6126.220	1.066	−1.37	58.4	4.42
Ti I	6258.090	1.443	−0.31	90.9	4.41

Table B.1: Equivalent Width Measurements for F/G/K Primaries *(continued)*

Species	λ	E.P.	log(gf)	PM I16519-4806N	
	(Å)	(eV)	(dex)	EW (mÅ)	Abundance
Fe I	5141.750	2.424	−2.18	72.9	5.89
Fe I	5247.060	0.087	−4.94	···	···
Fe I	5358.120	3.300	−3.16	···	···
Fe I	5412.788	4.440	−1.71	···	···
Fe I	5661.348	4.280	−1.75	···	···
Fe I	5778.458	2.590	−3.45	···	···
Fe I	5784.660	3.400	−2.53	···	···
Fe I	5809.220	3.884	−1.61	···	···
Fe I	5849.690	3.695	−2.93	···	···
Fe I	5852.230	4.549	−1.17	···	···
Fe I	5855.090	4.608	−1.48	···	···
Fe I	5856.100	4.294	−1.56	···	···
Fe I	5858.790	4.220	−2.18	···	···
Fe I	5859.600	4.550	−0.61	···	···
Fe I	5862.370	4.550	−0.25	···	···
Fe I	5956.700	0.859	−4.60	···	···
Fe I	6027.060	4.070	−1.17	···	···
Fe I	6151.620	2.176	−3.28	21.6	5.77
Fe I	6159.380	4.610	−1.83	···	···
Fe I	6165.360	4.143	−1.46	···	···
Fe I	6173.340	2.223	−2.88	23.3	5.47
Fe I	6200.320	2.609	−2.44	···	···
Fe I	6213.440	2.223	−2.56	23.5	5.15
Fe I	6240.652	2.220	−3.23	···	···
Fe I	6265.140	2.176	−2.55	55.9	5.66
Fe I	6271.283	3.330	−2.70	···	···
Fe I	6297.801	2.223	−2.73	···	···
Fe I	6322.694	2.588	−2.43	29.9	5.62
Fe I	6358.690	0.859	−4.00	···	···
Fe I	6436.410	4.186	−2.36	···	···
Fe I	6481.878	2.279	−2.97	···	···
Fe I	6498.950	0.958	−4.69	···	···
Fe I	6518.370	2.830	−2.45	···	···
Fe I	6574.233	0.990	−5.00	···	···
Fe I	6581.214	1.480	−4.68	···	···
Fe I	6591.330	4.593	−1.95	···	···
Fe I	6608.040	2.279	−3.91	···	···
Fe I	6625.027	1.010	−5.34	···	···
Fe I	6699.142	4.590	−2.10	···	···
Fe I	6713.750	4.795	−1.39	···	···
Fe I	6725.360	4.103	−2.17	···	···

Table B.1: Equivalent Width Measurements for F/G/K Primaries *(continued)*

Species	λ	E.P.	log(gf)	PM I16519-4806N	
	(Å)	(eV)	(dex)	EW (mÅ)	Abundance
Fe I	6733.150	4.638	−1.40	···	···
Fe I	6739.524	1.560	−4.79	···	···
Fe I	6750.160	2.424	−2.62	25.3	5.48
Fe I	6752.711	4.640	−1.20	···	···
Fe I	6837.009	4.590	−1.69	···	···
Fe I	6857.250	4.076	−2.04	···	···
Fe I	6971.936	3.020	−3.34	···	···
Fe I	7112.170	2.990	−2.99	···	···
Fe I	7751.120	4.990	−0.73	···	···
Fe I	7802.510	5.080	−1.31	···	···
Fe I	7807.920	4.990	−0.73	···	···
Fe I	8365.644	3.250	−2.04	···	···
Fe I	8757.200	2.845	−2.12	···	···
Fe II	5234.620	3.221	−2.22	···	···
Fe II	5425.260	3.200	−3.16	···	···
Fe II	6149.250	3.889	−2.63	···	···
Fe II	6247.560	3.892	−2.27	···	···
Fe II	6369.490	2.891	−4.02	···	···
Fe II	6432.680	2.891	−3.52	···	···
Fe II	6456.390	3.903	−2.06	···	···
Fe II	7479.700	3.892	−3.53	···	···
Fe II	7515.840	3.903	−3.42	···	···
Ca I	5867.570	2.930	−1.57	···	···
Ca I	6166.440	2.520	−1.14	···	···
Ca I	6169.040	2.520	−0.80	50.0	4.50
Ca I	6455.610	2.520	−1.29	···	···
Ca I	6572.800	0.000	−4.28	···	···
Ti I	5024.850	0.818	−0.56	···	···
Ti I	5113.450	1.443	−0.73	···	···
Ti I	5219.710	0.021	−2.24	49.8	3.36
Ti I	5866.460	1.066	−0.76	···	···
Ti I	6091.180	2.267	−0.37	···	···
Ti I	6126.220	1.066	−1.37	···	···
Ti I	6258.090	1.443	−0.31	···	···

Table B.1: Equivalent Width Measurements for F/G/K Primaries *(continued)*

Species	λ	E.P.	log(gf)	PM I17135+1909	
	(Å)	(eV)	(dex)	EW (mÅ)	Abundance
Fe I	5141.750	2.424	−2.18	107.4	7.19
Fe I	5247.060	0.087	−4.94	97.7	7.25
Fe I	5358.120	3.300	−3.16	···	···
Fe I	5412.788	4.440	−1.71	···	···
Fe I	5661.348	4.280	−1.75	···	···
Fe I	5778.458	2.590	−3.45	33.2	7.19
Fe I	5784.660	3.400	−2.53	···	···
Fe I	5809.220	3.884	−1.61	52.6	7.12
Fe I	5849.690	3.695	−2.93	···	···
Fe I	5852.230	4.549	−1.17	41.6	7.16
Fe I	5855.090	4.608	−1.48	31.0	7.32
Fe I	5856.100	4.294	−1.56	···	···
Fe I	5858.790	4.220	−2.18	···	···
Fe I	5859.600	4.550	−0.61	83.4	7.28
Fe I	5862.370	4.550	−0.25	99.5	7.13
Fe I	5956.700	0.859	−4.60	63.8	7.00
Fe I	6027.060	4.070	−1.17	69.4	7.16
Fe I	6151.620	2.176	−3.28	61.7	7.10
Fe I	6159.380	4.610	−1.83	···	···
Fe I	6165.360	4.143	−1.46	44.6	7.08
Fe I	6173.340	2.223	−2.88	82.8	7.14
Fe I	6200.320	2.609	−2.44	79.9	7.07
Fe I	6213.440	2.223	−2.56	···	···
Fe I	6240.652	2.220	−3.23	58.1	7.02
Fe I	6265.140	2.176	−2.55	93.0	6.93
Fe I	6271.283	3.330	−2.70	29.0	7.14
Fe I	6297.801	2.223	−2.73	105.5	7.37
Fe I	6322.694	2.588	−2.43	87.4	7.16
Fe I	6358.690	0.859	−4.00	99.1	7.03
Fe I	6436.410	4.186	−2.36	···	···
Fe I	6481.878	2.279	−2.97	73.6	7.10
Fe I	6498.950	0.958	−4.69	62.6	7.12
Fe I	6518.370	2.830	−2.45	69.7	7.11
Fe I	6574.233	0.990	−5.00	60.2	7.42
Fe I	6581.214	1.480	−4.68	···	···
Fe I	6591.330	4.593	−1.95	···	···
Fe I	6608.040	2.279	−3.91	···	···
Fe I	6625.027	1.010	−5.34	52.3	7.64
Fe I	6699.142	4.590	−2.10	···	···
Fe I	6713.750	4.795	−1.39	26.5	7.31
Fe I	6725.360	4.103	−2.17	···	···

Table B.1: Equivalent Width Measurements for F/G/K Primaries *(continued)*

Species	λ	E.P.	log(gf)	PM I17135+1909	
	(Å)	(eV)	(dex)	EW (mÅ)	Abundance
Fe I	6733.150	4.638	−1.40	20.5	7.00
Fe I	6739.524	1.560	−4.79	···	···
Fe I	6750.160	2.424	−2.62	95.6	7.27
Fe I	6752.711	4.640	−1.20	30.7	7.05
Fe I	6837.009	4.590	−1.69	···	···
Fe I	6857.250	4.076	−2.04	···	···
Fe I	6971.936	3.020	−3.34	···	···
Fe I	7112.170	2.990	−2.99	24.6	6.91
Fe I	7751.120	4.990	−0.73	33.0	6.95
Fe I	7802.510	5.080	−1.31	···	···
Fe I	7807.920	4.990	−0.73	54.4	7.33
Fe I	8365.644	3.250	−2.04	···	···
Fe I	8757.200	2.845	−2.12	···	···
Fe II	5234.620	3.221	−2.22	83.7	7.48
Fe II	5425.260	3.200	−3.16	20.3	6.94
Fe II	6149.250	3.889	−2.63	···	···
Fe II	6247.560	3.892	−2.27	51.9	7.57
Fe II	6369.490	2.891	−4.02	···	···
Fe II	6432.680	2.891	−3.52	···	···
Fe II	6456.390	3.903	−2.06	29.2	6.82
Fe II	7479.700	3.892	−3.53	···	···
Fe II	7515.840	3.903	−3.42	···	···
Ca I	5867.570	2.930	−1.57	41.7	6.28
Ca I	6166.440	2.520	−1.14	99.2	6.31
Ca I	6169.040	2.520	−0.80	142.1	6.44
Ca I	6455.610	2.520	−1.29	72.6	6.06
Ca I	6572.800	0.000	−4.28	79.0	6.41
Ti I	5024.850	0.818	−0.56	106.3	4.92
Ti I	5113.450	1.443	−0.73	63.9	4.94
Ti I	5219.710	0.021	−2.24	69.8	4.98
Ti I	5866.460	1.066	−0.76	91.7	5.01
Ti I	6091.180	2.267	−0.37	42.7	5.02
Ti I	6126.220	1.066	−1.37	50.1	4.83
Ti I	6258.090	1.443	−0.31	82.6	4.77

Table B.1: Equivalent Width Measurements for F/G/K Primaries *(continued)*

Species	λ	E.P.	log(gf)	PM I19207+0506S	
	(Å)	(eV)	(dex)	EW (mÅ)	Abundance
Fe I	5141.750	2.424	−2.18	47.6	6.50
Fe I	5247.060	0.087	−4.94	···	···
Fe I	5358.120	3.300	−3.16	···	···
Fe I	5412.788	4.440	−1.71	···	···
Fe I	5661.348	4.280	−1.75	···	···
Fe I	5778.458	2.590	−3.45	···	···
Fe I	5784.660	3.400	−2.53	···	···
Fe I	5809.220	3.884	−1.61	11.7	6.45
Fe I	5849.690	3.695	−2.93	···	···
Fe I	5852.230	4.549	−1.17	···	···
Fe I	5855.090	4.608	−1.48	···	···
Fe I	5856.100	4.294	−1.56	···	···
Fe I	5858.790	4.220	−2.18	···	···
Fe I	5859.600	4.550	−0.61	28.8	6.58
Fe I	5862.370	4.550	−0.25	43.0	6.49
Fe I	5956.700	0.859	−4.60	18.7	6.71
Fe I	6027.060	4.070	−1.17	23.4	6.55
Fe I	6151.620	2.176	−3.28	11.6	6.44
Fe I	6159.380	4.610	−1.83	···	···
Fe I	6165.360	4.143	−1.46	11.6	6.53
Fe I	6173.340	2.223	−2.88	28.1	6.56
Fe I	6200.320	2.609	−2.44	30.1	6.55
Fe I	6213.440	2.223	−2.56	42.1	6.52
Fe I	6240.652	2.220	−3.23	···	···
Fe I	6265.140	2.176	−2.55	45.3	6.53
Fe I	6271.283	3.330	−2.70	···	···
Fe I	6297.801	2.223	−2.73	30.6	6.47
Fe I	6322.694	2.588	−2.43	30.2	6.51
Fe I	6358.690	0.859	−4.00	28.6	6.33
Fe I	6436.410	4.186	−2.36	···	···
Fe I	6481.878	2.279	−2.97	20.9	6.52
Fe I	6498.950	0.958	−4.69	···	···
Fe I	6518.370	2.830	−2.45	···	···
Fe I	6574.233	0.990	−5.00	···	···
Fe I	6581.214	1.480	−4.68	···	···
Fe I	6591.330	4.593	−1.95	···	···
Fe I	6608.040	2.279	−3.91	···	···
Fe I	6625.027	1.010	−5.34	···	···
Fe I	6699.142	4.590	−2.10	···	···
Fe I	6713.750	4.795	−1.39	···	···
Fe I	6725.360	4.103	−2.17	···	···

Table B.1: Equivalent Width Measurements for F/G/K Primaries *(continued)*

Species	λ	E.P.	log(gf)	PM I19207+0506S	
	(Å)	(eV)	(dex)	EW (mÅ)	Abundance
Fe I	6733.150	4.638	−1.40	···	···
Fe I	6739.524	1.560	−4.79	···	···
Fe I	6750.160	2.424	−2.62	31.3	6.55
Fe I	6752.711	4.640	−1.20	···	···
Fe I	6837.009	4.590	−1.69	···	···
Fe I	6857.250	4.076	−2.04	···	···
Fe I	6971.936	3.020	−3.34	···	···
Fe I	7112.170	2.990	−2.99	···	···
Fe I	7751.120	4.990	−0.73	11.8	6.57
Fe I	7802.510	5.080	−1.31	···	···
Fe I	7807.920	4.990	−0.73	···	···
Fe I	8365.644	3.250	−2.04	18.4	6.39
Fe I	8757.200	2.845	−2.12	···	···
Fe II	5234.620	3.221	−2.22	···	···
Fe II	5425.260	3.200	−3.16	···	···
Fe II	6149.250	3.889	−2.63	···	···
Fe II	6247.560	3.892	−2.27	···	···
Fe II	6369.490	2.891	−4.02	···	···
Fe II	6432.680	2.891	−3.52	···	···
Fe II	6456.390	3.903	−2.06	···	···
Fe II	7479.700	3.892	−3.53	···	···
Fe II	7515.840	3.903	−3.42	···	···
Ca I	5867.570	2.930	−1.57	···	···
Ca I	6166.440	2.520	−1.14	31.4	5.60
Ca I	6169.040	2.520	−0.80	51.4	5.61
Ca I	6455.610	2.520	−1.29	22.9	5.55
Ca I	6572.800	0.000	−4.28	···	···
Ti I	5024.850	0.818	−0.56	37.0	4.23
Ti I	5113.450	1.443	−0.73	···	···
Ti I	5219.710	0.021	−2.24	···	···
Ti I	5866.460	1.066	−0.76	25.0	4.37
Ti I	6091.180	2.267	−0.37	···	···
Ti I	6126.220	1.066	−1.37	···	···
Ti I	6258.090	1.443	−0.31	19.4	4.13

Table B.1: Equivalent Width Measurements for F/G/K Primaries *(continued)*

Species	λ	E.P.	log(gf)	PM I20343+1151	
	(Å)	(eV)	(dex)	EW (mÅ)	Abundance
Fe I	5141.750	2.424	−2.18	92.1	6.83
Fe I	5247.060	0.087	−4.94	75.6	6.80
Fe I	5358.120	3.300	−3.16	···	···
Fe I	5412.788	4.440	−1.71	···	···
Fe I	5661.348	4.280	−1.75	···	···
Fe I	5778.458	2.590	−3.45	33.1	7.15
Fe I	5784.660	3.400	−2.53	···	···
Fe I	5809.220	3.884	−1.61	54.5	7.13
Fe I	5849.690	3.695	−2.93	···	···
Fe I	5852.230	4.549	−1.17	43.0	7.16
Fe I	5855.090	4.608	−1.48	···	···
Fe I	5856.100	4.294	−1.56	36.9	7.18
Fe I	5858.790	4.220	−2.18	···	···
Fe I	5859.600	4.550	−0.61	63.8	6.92
Fe I	5862.370	4.550	−0.25	85.7	6.83
Fe I	5956.700	0.859	−4.60	67.1	7.07
Fe I	6027.060	4.070	−1.17	60.7	6.97
Fe I	6151.620	2.176	−3.28	55.1	6.97
Fe I	6159.380	4.610	−1.83	···	···
Fe I	6165.360	4.143	−1.46	44.5	7.06
Fe I	6173.340	2.223	−2.88	72.5	6.94
Fe I	6200.320	2.609	−2.44	78.4	7.01
Fe I	6213.440	2.223	−2.56	···	···
Fe I	6240.652	2.220	−3.23	···	···
Fe I	6265.140	2.176	−2.55	102.1	6.99
Fe I	6271.283	3.330	−2.70	27.4	7.07
Fe I	6297.801	2.223	−2.73	107.8	7.28
Fe I	6322.694	2.588	−2.43	75.9	6.93
Fe I	6358.690	0.859	−4.00	100.5	6.99
Fe I	6436.410	4.186	−2.36	···	···
Fe I	6481.878	2.279	−2.97	70.5	7.04
Fe I	6498.950	0.958	−4.69	65.8	7.19
Fe I	6518.370	2.830	−2.45	64.1	7.00
Fe I	6574.233	0.990	−5.00	···	···
Fe I	6581.214	1.480	−4.68	···	···
Fe I	6591.330	4.593	−1.95	···	···
Fe I	6608.040	2.279	−3.91	···	···
Fe I	6625.027	1.010	−5.34	···	···
Fe I	6699.142	4.590	−2.10	···	···
Fe I	6713.750	4.795	−1.39	···	···
Fe I	6725.360	4.103	−2.17	···	···

Table B.1: Equivalent Width Measurements for F/G/K Primaries *(continued)*

Species	λ	E.P.	log(gf)	PM I20343+1151	
	(Å)	(eV)	(dex)	EW (mÅ)	Abundance
Fe I	6733.150	4.638	−1.40	···	···
Fe I	6739.524	1.560	−4.79	···	···
Fe I	6750.160	2.424	−2.62	78.5	6.96
Fe I	6752.711	4.640	−1.20	···	···
Fe I	6837.009	4.590	−1.69	···	···
Fe I	6857.250	4.076	−2.04	22.3	7.09
Fe I	6971.936	3.020	−3.34	···	···
Fe I	7112.170	2.990	−2.99	33.6	7.09
Fe I	7751.120	4.990	−0.73	···	···
Fe I	7802.510	5.080	−1.31	···	···
Fe I	7807.920	4.990	−0.73	50.2	7.24
Fe I	8365.644	3.250	−2.04	···	···
Fe I	8757.200	2.845	−2.12	···	···
Fe II	5234.620	3.221	−2.22	39.6	6.97
Fe II	5425.260	3.200	−3.16	15.2	7.13
Fe II	6149.250	3.889	−2.63	···	···
Fe II	6247.560	3.892	−2.27	···	···
Fe II	6369.490	2.891	−4.02	···	···
Fe II	6432.680	2.891	−3.52	···	···
Fe II	6456.390	3.903	−2.06	16.4	6.84
Fe II	7479.700	3.892	−3.53	···	···
Fe II	7515.840	3.903	−3.42	···	···
Ca I	5867.570	2.930	−1.57	38.0	6.03
Ca I	6166.440	2.520	−1.14	98.6	6.01
Ca I	6169.040	2.520	−0.80	137.2	6.02
Ca I	6455.610	2.520	−1.29	77.2	5.89
Ca I	6572.800	0.000	−4.28	···	···
Ti I	5024.850	0.818	−0.56	···	···
Ti I	5113.450	1.443	−0.73	···	···
Ti I	5219.710	0.021	−2.24	70.0	4.78
Ti I	5866.460	1.066	−0.76	93.4	4.79
Ti I	6091.180	2.267	−0.37	41.3	4.79
Ti I	6126.220	1.066	−1.37	61.1	4.82
Ti I	6258.090	1.443	−0.31	93.2	4.71

Table B.1: Equivalent Width Measurements for F/G/K Primaries *(continued)*

Species	λ	E.P.	log(gf)	NLTT 49474	
	(Å)	(eV)	(dex)	EW (mÅ)	Abundance
Fe I	5141.750	2.424	−2.18	42.4	6.69
Fe I	5247.060	0.087	−4.94	30.5	6.86
Fe I	5358.120	3.300	−3.16	···	···
Fe I	5412.788	4.440	−1.71	···	···
Fe I	5661.348	4.280	−1.75	···	···
Fe I	5778.458	2.590	−3.45	···	···
Fe I	5784.660	3.400	−2.53	···	···
Fe I	5809.220	3.884	−1.61	···	···
Fe I	5849.690	3.695	−2.93	···	···
Fe I	5852.230	4.549	−1.17	···	···
Fe I	5855.090	4.608	−1.48	···	···
Fe I	5856.100	4.294	−1.56	···	···
Fe I	5858.790	4.220	−2.18	···	···
Fe I	5859.600	4.550	−0.61	30.6	6.74
Fe I	5862.370	4.550	−0.25	44.9	6.68
Fe I	5956.700	0.859	−4.60	16.6	6.82
Fe I	6027.060	4.070	−1.17	31.4	6.89
Fe I	6151.620	2.176	−3.28	16.0	6.75
Fe I	6159.380	4.610	−1.83	···	···
Fe I	6165.360	4.143	−1.46	18.9	6.90
Fe I	6173.340	2.223	−2.88	32.8	6.89
Fe I	6200.320	2.609	−2.44	···	···
Fe I	6213.440	2.223	−2.56	46.2	6.91
Fe I	6240.652	2.220	−3.23	17.1	6.78
Fe I	6265.140	2.176	−2.55	45.1	6.83
Fe I	6271.283	3.330	−2.70	···	···
Fe I	6297.801	2.223	−2.73	35.2	6.80
Fe I	6322.694	2.588	−2.43	40.4	6.97
Fe I	6358.690	0.859	−4.00	29.6	6.59
Fe I	6436.410	4.186	−2.36	···	···
Fe I	6481.878	2.279	−2.97	26.8	6.86
Fe I	6498.950	0.958	−4.69	···	···
Fe I	6518.370	2.830	−2.45	···	···
Fe I	6574.233	0.990	−5.00	···	···
Fe I	6581.214	1.480	−4.68	···	···
Fe I	6591.330	4.593	−1.95	···	···
Fe I	6608.040	2.279	−3.91	···	···
Fe I	6625.027	1.010	−5.34	···	···
Fe I	6699.142	4.590	−2.10	···	···
Fe I	6713.750	4.795	−1.39	···	···
Fe I	6725.360	4.103	−2.17	···	···

Table B.1: Equivalent Width Measurements for F/G/K Primaries *(continued)*

Species	λ	E.P.	log(gf)	NLTT 49474	
	(Å)	(eV)	(dex)	EW (mÅ)	Abundance
Fe I	6733.150	4.638	−1.40	···	···
Fe I	6739.524	1.560	−4.79	···	···
Fe I	6750.160	2.424	−2.62	36.0	6.87
Fe I	6752.711	4.640	−1.20	···	···
Fe I	6837.009	4.590	−1.69	···	···
Fe I	6857.250	4.076	−2.04	···	···
Fe I	6971.936	3.020	−3.34	···	···
Fe I	7112.170	2.990	−2.99	···	···
Fe I	7751.120	4.990	−0.73	···	···
Fe I	7802.510	5.080	−1.31	···	···
Fe I	7807.920	4.990	−0.73	···	···
Fe I	8365.644	3.250	−2.04	···	···
Fe I	8757.200	2.845	−2.12	···	···
Fe II	5234.620	3.221	−2.22	57.6	6.98
Fe II	5425.260	3.200	−3.16	···	···
Fe II	6149.250	3.889	−2.63	···	···
Fe II	6247.560	3.892	−2.27	24.3	6.68
Fe II	6369.490	2.891	−4.02	···	···
Fe II	6432.680	2.891	−3.52	15.1	6.66
Fe II	6456.390	3.903	−2.06	31.9	6.70
Fe II	7479.700	3.892	−3.53	···	···
Fe II	7515.840	3.903	−3.42	···	···
Ca I	5867.570	2.930	−1.57	···	···
Ca I	6166.440	2.520	−1.14	40.8	5.91
Ca I	6169.040	2.520	−0.80	58.8	5.91
Ca I	6455.610	2.520	−1.29	25.4	5.71
Ca I	6572.800	0.000	−4.28	···	···
Ti I	5024.850	0.818	−0.56	40.1	4.54
Ti I	5113.450	1.443	−0.73	···	···
Ti I	5219.710	0.021	−2.24	···	···
Ti I	5866.460	1.066	−0.76	20.1	4.40
Ti I	6091.180	2.267	−0.37	···	···
Ti I	6126.220	1.066	−1.37	···	···
Ti I	6258.090	1.443	−0.31	30.7	4.59

Table B.1: Equivalent Width Measurements for F/G/K Primaries *(continued)*

Species	λ	E.P.	log(gf)	PM I20487+1406	
	(Å)	(eV)	(dex)	EW (mÅ)	Abundance
Fe I	5141.750	2.424	−2.18	126.3	7.50
Fe I	5247.060	0.087	−4.94	132.6	7.79
Fe I	5358.120	3.300	−3.16	28.6	7.54
Fe I	5412.788	4.440	−1.71	···	···
Fe I	5661.348	4.280	−1.75	···	···
Fe I	5778.458	2.590	−3.45	58.5	7.61
Fe I	5784.660	3.400	−2.53	···	···
Fe I	5809.220	3.884	−1.61	76.3	7.54
Fe I	5849.690	3.695	−2.93	17.8	7.45
Fe I	5852.230	4.549	−1.17	61.4	7.52
Fe I	5855.090	4.608	−1.48	···	···
Fe I	5856.100	4.294	−1.56	56.3	7.55
Fe I	5858.790	4.220	−2.18	···	···
Fe I	5859.600	4.550	−0.61	91.7	7.47
Fe I	5862.370	4.550	−0.25	···	···
Fe I	5956.700	0.859	−4.60	99.7	7.55
Fe I	6027.060	4.070	−1.17	88.3	7.49
Fe I	6151.620	2.176	−3.28	86.4	7.48
Fe I	6159.380	4.610	−1.83	···	···
Fe I	6165.360	4.143	−1.46	63.9	7.42
Fe I	6173.340	2.223	−2.88	103.0	7.43
Fe I	6200.320	2.609	−2.44	106.7	7.49
Fe I	6213.440	2.223	−2.56	126.3	7.50
Fe I	6240.652	2.220	−3.23	···	···
Fe I	6265.140	2.176	−2.55	123.5	7.39
Fe I	6271.283	3.330	−2.70	47.8	7.46
Fe I	6297.801	2.223	−2.73	108.3	7.37
Fe I	6322.694	2.588	−2.43	109.7	7.49
Fe I	6358.690	0.859	−4.00	···	···
Fe I	6436.410	4.186	−2.36	25.4	7.59
Fe I	6481.878	2.279	−2.97	103.4	7.56
Fe I	6498.950	0.958	−4.69	98.3	7.64
Fe I	6518.370	2.830	−2.45	···	···
Fe I	6574.233	0.990	−5.00	78.0	7.60
Fe I	6581.214	1.480	−4.68	67.1	7.65
Fe I	6591.330	4.593	−1.95	···	···
Fe I	6608.040	2.279	−3.91	45.9	7.42
Fe I	6625.027	1.010	−5.34	76.3	7.92
Fe I	6699.142	4.590	−2.10	···	···
Fe I	6713.750	4.795	−1.39	36.2	7.51
Fe I	6725.360	4.103	−2.17	···	···

Table B.1: Equivalent Width Measurements for F/G/K Primaries *(continued)*

Species	λ	E.P.	log(gf)	PM I20487+1406	
	(Å)	(eV)	(dex)	EW (mÅ)	Abundance
Fe I	6733.150	4.638	−1.40	···	···
Fe I	6739.524	1.560	−4.79	···	···
Fe I	6750.160	2.424	−2.62	108.5	7.43
Fe I	6752.711	4.640	−1.20	61.2	7.61
Fe I	6837.009	4.590	−1.69	···	···
Fe I	6857.250	4.076	−2.04	42.3	7.49
Fe I	6971.936	3.020	−3.34	···	···
Fe I	7112.170	2.990	−2.99	63.0	7.59
Fe I	7751.120	4.990	−0.73	63.1	7.50
Fe I	7802.510	5.080	−1.31	27.3	7.50
Fe I	7807.920	4.990	−0.73	76.1	7.70
Fe I	8365.644	3.250	−2.04	96.8	7.41
Fe I	8757.200	2.845	−2.12	···	···
Fe II	5234.620	3.221	−2.22	77.0	7.47
Fe II	5425.260	3.200	−3.16	42.2	7.60
Fe II	6149.250	3.889	−2.63	32.2	7.55
Fe II	6247.560	3.892	−2.27	···	···
Fe II	6369.490	2.891	−4.02	···	···
Fe II	6432.680	2.891	−3.52	35.0	7.47
Fe II	6456.390	3.903	−2.06	50.6	7.46
Fe II	7479.700	3.892	−3.53	···	···
Fe II	7515.840	3.903	−3.42	···	···
Ca I	5867.570	2.930	−1.57	43.8	6.24
Ca I	6166.440	2.520	−1.14	94.4	6.19
Ca I	6169.040	2.520	−0.80	120.6	6.23
Ca I	6455.610	2.520	−1.29	88.0	6.22
Ca I	6572.800	0.000	−4.28	···	···
Ti I	5024.850	0.818	−0.56	122.9	5.09
Ti I	5113.450	1.443	−0.73	···	···
Ti I	5219.710	0.021	−2.24	76.2	4.85
Ti I	5866.460	1.066	−0.76	95.7	4.89
Ti I	6091.180	2.267	−0.37	44.0	4.91
Ti I	6126.220	1.066	−1.37	67.6	4.93
Ti I	6258.090	1.443	−0.31	90.8	4.73

Table B.1: Equivalent Width Measurements for F/G/K Primaries *(continued)*

Species	λ	E.P.	log(gf)	PM I21175-4142E	
	(Å)	(eV)	(dex)	EW (mÅ)	Abundance
Fe I	5141.750	2.424	−2.18	42.0	6.27
Fe I	5247.060	0.087	−4.94	···	···
Fe I	5358.120	3.300	−3.16	···	···
Fe I	5412.788	4.440	−1.71	···	···
Fe I	5661.348	4.280	−1.75	···	···
Fe I	5778.458	2.590	−3.45	···	···
Fe I	5784.660	3.400	−2.53	15.0	6.88
Fe I	5809.220	3.884	−1.61	23.3	6.69
Fe I	5849.690	3.695	−2.93	···	···
Fe I	5852.230	4.549	−1.17	···	···
Fe I	5855.090	4.608	−1.48	···	···
Fe I	5856.100	4.294	−1.56	···	···
Fe I	5858.790	4.220	−2.18	···	···
Fe I	5859.600	4.550	−0.61	19.4	6.24
Fe I	5862.370	4.550	−0.25	47.4	6.44
Fe I	5956.700	0.859	−4.60	28.4	6.71
Fe I	6027.060	4.070	−1.17	20.7	6.36
Fe I	6151.620	2.176	−3.28	23.2	6.61
Fe I	6159.380	4.610	−1.83	···	···
Fe I	6165.360	4.143	−1.46	15.8	6.56
Fe I	6173.340	2.223	−2.88	33.6	6.51
Fe I	6200.320	2.609	−2.44	38.0	6.56
Fe I	6213.440	2.223	−2.56	54.7	6.64
Fe I	6240.652	2.220	−3.23	22.9	6.59
Fe I	6265.140	2.176	−2.55	45.4	6.39
Fe I	6271.283	3.330	−2.70	···	···
Fe I	6297.801	2.223	−2.73	39.1	6.48
Fe I	6322.694	2.588	−2.43	44.5	6.66
Fe I	6358.690	0.859	−4.00	41.3	6.39
Fe I	6436.410	4.186	−2.36	···	···
Fe I	6481.878	2.279	−2.97	31.6	6.60
Fe I	6498.950	0.958	−4.69	···	···
Fe I	6518.370	2.830	−2.45	33.4	6.68
Fe I	6574.233	0.990	−5.00	···	···
Fe I	6581.214	1.480	−4.68	···	···
Fe I	6591.330	4.593	−1.95	···	···
Fe I	6608.040	2.279	−3.91	···	···
Fe I	6625.027	1.010	−5.34	···	···
Fe I	6699.142	4.590	−2.10	···	···
Fe I	6713.750	4.795	−1.39	···	···
Fe I	6725.360	4.103	−2.17	···	···

Table B.1: Equivalent Width Measurements for F/G/K Primaries *(continued)*

Species	λ	E.P.	log(gf)	PM I21175-4142E	
	(Å)	(eV)	(dex)	EW (mÅ)	Abundance
Fe I	6733.150	4.638	−1.40	···	···
Fe I	6739.524	1.560	−4.79	···	···
Fe I	6750.160	2.424	−2.62	37.8	6.52
Fe I	6752.711	4.640	−1.20	13.1	6.68
Fe I	6837.009	4.590	−1.69	···	···
Fe I	6857.250	4.076	−2.04	···	···
Fe I	6971.936	3.020	−3.34	···	···
Fe I	7112.170	2.990	−2.99	···	···
Fe I	7751.120	4.990	−0.73	···	···
Fe I	7802.510	5.080	−1.31	···	···
Fe I	7807.920	4.990	−0.73	···	···
Fe I	8365.644	3.250	−2.04	···	···
Fe I	8757.200	2.845	−2.12	···	···
Fe II	5234.620	3.221	−2.22	34.9	6.35
Fe II	5425.260	3.200	−3.16	···	···
Fe II	6149.250	3.889	−2.63	7.9	6.46
Fe II	6247.560	3.892	−2.27	15.7	6.47
Fe II	6369.490	2.891	−4.02	···	···
Fe II	6432.680	2.891	−3.52	···	···
Fe II	6456.390	3.903	−2.06	21.0	6.45
Fe II	7479.700	3.892	−3.53	···	···
Fe II	7515.840	3.903	−3.42	···	···
Ca I	5867.570	2.930	−1.57	···	···
Ca I	6166.440	2.520	−1.14	42.8	5.65
Ca I	6169.040	2.520	−0.80	···	···
Ca I	6455.610	2.520	−1.29	25.2	5.45
Ca I	6572.800	0.000	−4.28	···	···
Ti I	5024.850	0.818	−0.56	42.1	4.13
Ti I	5113.450	1.443	−0.73	···	···
Ti I	5219.710	0.021	−2.24	···	···
Ti I	5866.460	1.066	−0.76	37.2	4.42
Ti I	6091.180	2.267	−0.37	···	···
Ti I	6126.220	1.066	−1.37	···	···
Ti I	6258.090	1.443	−0.31	···	···

Table B.1: Equivalent Width Measurements for F/G/K Primaries *(continued)*

Species	λ	E.P.	log(gf)	PM I21442+0102N	
	(Å)	(eV)	(dex)	EW (mÅ)	Abundance
Fe I	5141.750	2.424	−2.18	···	···
Fe I	5247.060	0.087	−4.94	81.6	6.48
Fe I	5358.120	3.300	−3.16	···	···
Fe I	5412.788	4.440	−1.71	···	···
Fe I	5661.348	4.280	−1.75	···	···
Fe I	5778.458	2.590	−3.45	23.2	6.77
Fe I	5784.660	3.400	−2.53	···	···
Fe I	5809.220	3.884	−1.61	···	···
Fe I	5849.690	3.695	−2.93	···	···
Fe I	5852.230	4.549	−1.17	···	···
Fe I	5855.090	4.608	−1.48	···	···
Fe I	5856.100	4.294	−1.56	···	···
Fe I	5858.790	4.220	−2.18	···	···
Fe I	5859.600	4.550	−0.61	33.4	6.45
Fe I	5862.370	4.550	−0.25	56.5	6.45
Fe I	5956.700	0.859	−4.60	61.1	6.62
Fe I	6027.060	4.070	−1.17	42.2	6.64
Fe I	6151.620	2.176	−3.28	45.1	6.58
Fe I	6159.380	4.610	−1.83	···	···
Fe I	6165.360	4.143	−1.46	···	···
Fe I	6173.340	2.223	−2.88	65.8	6.61
Fe I	6200.320	2.609	−2.44	75.6	6.78
Fe I	6213.440	2.223	−2.56	···	···
Fe I	6240.652	2.220	−3.23	···	···
Fe I	6265.140	2.176	−2.55	98.6	6.69
Fe I	6271.283	3.330	−2.70	···	···
Fe I	6297.801	2.223	−2.73	70.1	6.53
Fe I	6322.694	2.588	−2.43	67.4	6.61
Fe I	6358.690	0.859	−4.00	87.8	6.45
Fe I	6436.410	4.186	−2.36	···	···
Fe I	6481.878	2.279	−2.97	61.4	6.68
Fe I	6498.950	0.958	−4.69	···	···
Fe I	6518.370	2.830	−2.45	···	···
Fe I	6574.233	0.990	−5.00	50.0	6.90
Fe I	6581.214	1.480	−4.68	···	···
Fe I	6591.330	4.593	−1.95	···	···
Fe I	6608.040	2.279	−3.91	···	···
Fe I	6625.027	1.010	−5.34	···	···
Fe I	6699.142	4.590	−2.10	···	···
Fe I	6713.750	4.795	−1.39	···	···
Fe I	6725.360	4.103	−2.17	···	···

Table B.1: Equivalent Width Measurements for F/G/K Primaries *(continued)*

Species	λ	E.P.	log(gf)	PM I21442+0102N	
	(Å)	(eV)	(dex)	EW (mÅ)	Abundance
Fe I	6733.150	4.638	−1.40	···	···
Fe I	6739.524	1.560	−4.79	···	···
Fe I	6750.160	2.424	−2.62	69.4	6.62
Fe I	6752.711	4.640	−1.20	···	···
Fe I	6837.009	4.590	−1.69	···	···
Fe I	6857.250	4.076	−2.04	···	···
Fe I	6971.936	3.020	−3.34	···	···
Fe I	7112.170	2.990	−2.99	···	···
Fe I	7751.120	4.990	−0.73	···	···
Fe I	7802.510	5.080	−1.31	···	···
Fe I	7807.920	4.990	−0.73	···	···
Fe I	8365.644	3.250	−2.04	···	···
Fe I	8757.200	2.845	−2.12	···	···
Fe II	5234.620	3.221	−2.22	···	···
Fe II	5425.260	3.200	−3.16	···	···
Fe II	6149.250	3.889	−2.63	···	···
Fe II	6247.560	3.892	−2.27	···	···
Fe II	6369.490	2.891	−4.02	···	···
Fe II	6432.680	2.891	−3.52	···	···
Fe II	6456.390	3.903	−2.06	···	···
Fe II	7479.700	3.892	−3.53	···	···
Fe II	7515.840	3.903	−3.42	···	···
Ca I	5867.570	2.930	−1.57	51.2	5.87
Ca I	6166.440	2.520	−1.14	146.9	5.97
Ca I	6169.040	2.520	−0.80	···	···
Ca I	6455.610	2.520	−1.29	102.4	5.74
Ca I	6572.800	0.000	−4.28	···	···
Ti I	5024.850	0.818	−0.56	134.5	4.19
Ti I	5113.450	1.443	−0.73	···	···
Ti I	5219.710	0.021	−2.24	97.9	4.52
Ti I	5866.460	1.066	−0.76	137.6	4.62
Ti I	6091.180	2.267	−0.37	55.1	4.57
Ti I	6126.220	1.066	−1.37	96.5	4.78
Ti I	6258.090	1.443	−0.31	···	···

Table B.1: Equivalent Width Measurements for F/G/K Primaries *(continued)*

Species	λ (Å)	E.P. (eV)	log(gf) (dex)	NLTT 52532 EW (mÅ)	NLTT 52532 Abundance
Fe I	5141.750	2.424	−2.18	···	···
Fe I	5247.060	0.087	−4.94	···	···
Fe I	5358.120	3.300	−3.16	···	···
Fe I	5412.788	4.440	−1.71	···	···
Fe I	5661.348	4.280	−1.75	···	···
Fe I	5778.458	2.590	−3.45	···	···
Fe I	5784.660	3.400	−2.53	···	···
Fe I	5809.220	3.884	−1.61	···	···
Fe I	5849.690	3.695	−2.93	···	···
Fe I	5852.230	4.549	−1.17	···	···
Fe I	5855.090	4.608	−1.48	···	···
Fe I	5856.100	4.294	−1.56	···	···
Fe I	5858.790	4.220	−2.18	···	···
Fe I	5859.600	4.550	−0.61	···	···
Fe I	5862.370	4.550	−0.25	···	···
Fe I	5956.700	0.859	−4.60	60.1	6.15
Fe I	6027.060	4.070	−1.17	···	···
Fe I	6151.620	2.176	−3.28	16.7	5.76
Fe I	6159.380	4.610	−1.83	···	···
Fe I	6165.360	4.143	−1.46	···	···
Fe I	6173.340	2.223	−2.88	43.2	6.00
Fe I	6200.320	2.609	−2.44	55.0	6.25
Fe I	6213.440	2.223	−2.56	49.4	5.78
Fe I	6240.652	2.220	−3.23	···	···
Fe I	6265.140	2.176	−2.55	78.0	6.09
Fe I	6271.283	3.330	−2.70	···	···
Fe I	6297.801	2.223	−2.73	···	···
Fe I	6322.694	2.588	−2.43	···	···
Fe I	6358.690	0.859	−4.00	64.1	5.58
Fe I	6436.410	4.186	−2.36	···	···
Fe I	6481.878	2.279	−2.97	···	···
Fe I	6498.950	0.958	−4.69	···	···
Fe I	6518.370	2.830	−2.45	21.1	5.92
Fe I	6574.233	0.990	−5.00	38.2	6.33
Fe I	6581.214	1.480	−4.68	···	···
Fe I	6591.330	4.593	−1.95	···	···
Fe I	6608.040	2.279	−3.91	···	···
Fe I	6625.027	1.010	−5.34	···	···
Fe I	6699.142	4.590	−2.10	···	···
Fe I	6713.750	4.795	−1.39	···	···
Fe I	6725.360	4.103	−2.17	···	···

Table B.1: Equivalent Width Measurements for F/G/K Primaries *(continued)*

Species	λ	E.P.	log(gf)	NLTT 52532	
	(Å)	(eV)	(dex)	EW (mÅ)	Abundance
Fe I	6733.150	4.638	−1.40	···	···
Fe I	6739.524	1.560	−4.79	···	···
Fe I	6750.160	2.424	−2.62	46.0	6.03
Fe I	6752.711	4.640	−1.20	···	···
Fe I	6837.009	4.590	−1.69	···	···
Fe I	6857.250	4.076	−2.04	···	···
Fe I	6971.936	3.020	−3.34	···	···
Fe I	7112.170	2.990	−2.99	···	···
Fe I	7751.120	4.990	−0.73	···	···
Fe I	7802.510	5.080	−1.31	···	···
Fe I	7807.920	4.990	−0.73	···	···
Fe I	8365.644	3.250	−2.04	···	···
Fe I	8757.200	2.845	−2.12	···	···
Fe II	5234.620	3.221	−2.22	···	···
Fe II	5425.260	3.200	−3.16	···	···
Fe II	6149.250	3.889	−2.63	···	···
Fe II	6247.560	3.892	−2.27	···	···
Fe II	6369.490	2.891	−4.02	···	···
Fe II	6432.680	2.891	−3.52	···	···
Fe II	6456.390	3.903	−2.06	···	···
Fe II	7479.700	3.892	−3.53	···	···
Fe II	7515.840	3.903	−3.42	···	···
Ca I	5867.570	2.930	−1.57	···	···
Ca I	6166.440	2.520	−1.14	130.3	5.34
Ca I	6169.040	2.520	−0.80	···	···
Ca I	6455.610	2.520	−1.29	90.4	5.15
Ca I	6572.800	0.000	−4.28	···	···
Ti I	5024.850	0.818	−0.56	···	···
Ti I	5113.450	1.443	−0.73	···	···
Ti I	5219.710	0.021	−2.24	125.3	3.96
Ti I	5866.460	1.066	−0.76	130.7	3.81
Ti I	6091.180	2.267	−0.37	···	···
Ti I	6126.220	1.066	−1.37	85.3	3.89
Ti I	6258.090	1.443	−0.31	···	···

Table B.1: Equivalent Width Measurements for F/G/K Primaries *(continued)*

Species	λ	E.P.	log(gf)	PM I22487-5613W	
	(Å)	(eV)	(dex)	EW (mÅ)	Abundance
Fe I	5141.750	2.424	−2.18	115.0	7.20
Fe I	5247.060	0.087	−4.94	100.3	7.14
Fe I	5358.120	3.300	−3.16	···	···
Fe I	5412.788	4.440	−1.71	35.3	7.46
Fe I	5661.348	4.280	−1.75	29.9	7.21
Fe I	5778.458	2.590	−3.45	44.8	7.33
Fe I	5784.660	3.400	−2.53	···	···
Fe I	5809.220	3.884	−1.61	69.6	7.40
Fe I	5849.690	3.695	−2.93	···	···
Fe I	5852.230	4.549	−1.17	52.6	7.36
Fe I	5855.090	4.608	−1.48	27.6	7.24
Fe I	5856.100	4.294	−1.56	40.4	7.25
Fe I	5858.790	4.220	−2.18	15.3	7.18
Fe I	5859.600	4.550	−0.61	88.4	7.34
Fe I	5862.370	4.550	−0.25	103.8	7.17
Fe I	5956.700	0.859	−4.60	84.9	7.27
Fe I	6027.060	4.070	−1.17	78.2	7.29
Fe I	6151.620	2.176	−3.28	73.8	7.24
Fe I	6159.380	4.610	−1.83	···	···
Fe I	6165.360	4.143	−1.46	53.0	7.22
Fe I	6173.340	2.223	−2.88	97.7	7.32
Fe I	6200.320	2.609	−2.44	96.9	7.30
Fe I	6213.440	2.223	−2.56	117.8	7.29
Fe I	6240.652	2.220	−3.23	71.7	7.20
Fe I	6265.140	2.176	−2.55	123.9	7.30
Fe I	6271.283	3.330	−2.70	40.1	7.31
Fe I	6297.801	2.223	−2.73	103.4	7.25
Fe I	6322.694	2.588	−2.43	103.2	7.35
Fe I	6358.690	0.859	−4.00	116.4	7.17
Fe I	6436.410	4.186	−2.36	15.1	7.30
Fe I	6481.878	2.279	−2.97	90.4	7.33
Fe I	6498.950	0.958	−4.69	82.6	7.36
Fe I	6518.370	2.830	−2.45	81.9	7.28
Fe I	6574.233	0.990	−5.00	63.2	7.32
Fe I	6581.214	1.480	−4.68	48.5	7.29
Fe I	6591.330	4.593	−1.95	···	···
Fe I	6608.040	2.279	−3.91	35.8	7.21
Fe I	6625.027	1.010	−5.34	63.1	7.67
Fe I	6699.142	4.590	−2.10	···	···
Fe I	6713.750	4.795	−1.39	26.9	7.32
Fe I	6725.360	4.103	−2.17	26.7	7.34

Table B.1: Equivalent Width Measurements for F/G/K Primaries *(continued)*

Species	λ	E.P.	log(gf)	PM I22487-5613W	
	(Å)	(eV)	(dex)	EW (mÅ)	Abundance
Fe I	6733.150	4.638	−1.40	32.1	7.28
Fe I	6739.524	1.560	−4.79	28.8	7.08
Fe I	6750.160	2.424	−2.62	101.7	7.30
Fe I	6752.711	4.640	−1.20	53.8	7.49
Fe I	6837.009	4.590	−1.69	···	···
Fe I	6857.250	4.076	−2.04	···	···
Fe I	6971.936	3.020	−3.34	···	···
Fe I	7112.170	2.990	−2.99	···	···
Fe I	7751.120	4.990	−0.73	···	···
Fe I	7802.510	5.080	−1.31	···	···
Fe I	7807.920	4.990	−0.73	···	···
Fe I	8365.644	3.250	−2.04	···	···
Fe I	8757.200	2.845	−2.12	···	···
Fe II	5234.620	3.221	−2.22	45.6	7.05
Fe II	5425.260	3.200	−3.16	33.3	7.66
Fe II	6149.250	3.889	−2.63	15.3	7.28
Fe II	6247.560	3.892	−2.27	24.5	7.28
Fe II	6369.490	2.891	−4.02	···	···
Fe II	6432.680	2.891	−3.52	18.5	7.26
Fe II	6456.390	3.903	−2.06	27.0	7.16
Fe II	7479.700	3.892	−3.53	···	···
Fe II	7515.840	3.903	−3.42	···	···
Ca I	5867.570	2.930	−1.57	56.1	6.32
Ca I	6166.440	2.520	−1.14	115.5	6.30
Ca I	6169.040	2.520	−0.80	165.5	6.41
Ca I	6455.610	2.520	−1.29	93.4	6.15
Ca I	6572.800	0.000	−4.28	102.7	6.44
Ti I	5024.850	0.818	−0.56	112.1	4.69
Ti I	5113.450	1.443	−0.73	···	···
Ti I	5219.710	0.021	−2.24	78.3	4.76
Ti I	5866.460	1.066	−0.76	101.5	4.86
Ti I	6091.180	2.267	−0.37	45.2	4.79
Ti I	6126.220	1.066	−1.37	72.0	4.89
Ti I	6258.090	1.443	−0.31	104.4	4.84

Table B.1: Equivalent Width Measurements for F/G/K Primaries *(continued)*

Species	λ	E.P.	log(gf)	PM I23033-5311	
	(Å)	(eV)	(dex)	EW (mÅ)	Abundance
Fe I	5141.750	2.424	−2.18	42.0	6.64
Fe I	5247.060	0.087	−4.94	23.9	6.74
Fe I	5358.120	3.300	−3.16	···	···
Fe I	5412.788	4.440	−1.71	···	···
Fe I	5661.348	4.280	−1.75	···	···
Fe I	5778.458	2.590	−3.45	···	···
Fe I	5784.660	3.400	−2.53	···	···
Fe I	5809.220	3.884	−1.61	···	···
Fe I	5849.690	3.695	−2.93	···	···
Fe I	5852.230	4.549	−1.17	···	···
Fe I	5855.090	4.608	−1.48	···	···
Fe I	5856.100	4.294	−1.56	···	···
Fe I	5858.790	4.220	−2.18	···	···
Fe I	5859.600	4.550	−0.61	25.3	6.62
Fe I	5862.370	4.550	−0.25	40.5	6.58
Fe I	5956.700	0.859	−4.60	···	···
Fe I	6027.060	4.070	−1.17	21.3	6.64
Fe I	6151.620	2.176	−3.28	16.0	6.80
Fe I	6159.380	4.610	−1.83	···	···
Fe I	6165.360	4.143	−1.46	16.5	6.85
Fe I	6173.340	2.223	−2.88	26.6	6.75
Fe I	6200.320	2.609	−2.44	28.2	6.71
Fe I	6213.440	2.223	−2.56	43.6	6.81
Fe I	6240.652	2.220	−3.23	···	···
Fe I	6265.140	2.176	−2.55	47.1	6.83
Fe I	6271.283	3.330	−2.70	···	···
Fe I	6297.801	2.223	−2.73	31.6	6.71
Fe I	6322.694	2.588	−2.43	31.4	6.75
Fe I	6358.690	0.859	−4.00	20.2	6.38
Fe I	6436.410	4.186	−2.36	···	···
Fe I	6481.878	2.279	−2.97	20.8	6.73
Fe I	6498.950	0.958	−4.69	10.2	6.79
Fe I	6518.370	2.830	−2.45	···	···
Fe I	6574.233	0.990	−5.00	···	···
Fe I	6581.214	1.480	−4.68	···	···
Fe I	6591.330	4.593	−1.95	···	···
Fe I	6608.040	2.279	−3.91	···	···
Fe I	6625.027	1.010	−5.34	···	···
Fe I	6699.142	4.590	−2.10	···	···
Fe I	6713.750	4.795	−1.39	···	···
Fe I	6725.360	4.103	−2.17	···	···

Table B.1: Equivalent Width Measurements for F/G/K Primaries *(continued)*

Species	λ	E.P.	log(gf)	PM I23033-5311	
	(Å)	(eV)	(dex)	EW (mÅ)	Abundance
Fe I	6733.150	4.638	−1.40	···	···
Fe I	6739.524	1.560	−4.79	···	···
Fe I	6750.160	2.424	−2.62	31.8	6.78
Fe I	6752.711	4.640	−1.20	9.5	6.74
Fe I	6837.009	4.590	−1.69	···	···
Fe I	6857.250	4.076	−2.04	···	···
Fe I	6971.936	3.020	−3.34	···	···
Fe I	7112.170	2.990	−2.99	···	···
Fe I	7751.120	4.990	−0.73	···	···
Fe I	7802.510	5.080	−1.31	···	···
Fe I	7807.920	4.990	−0.73	···	···
Fe I	8365.644	3.250	−2.04	···	···
Fe I	8757.200	2.845	−2.12	···	···
Fe II	5234.620	3.221	−2.22	60.8	6.82
Fe II	5425.260	3.200	−3.16	···	···
Fe II	6149.250	3.889	−2.63	16.0	6.69
Fe II	6247.560	3.892	−2.27	24.9	6.60
Fe II	6369.490	2.891	−4.02	···	···
Fe II	6432.680	2.891	−3.52	17.7	6.69
Fe II	6456.390	3.903	−2.06	33.7	6.61
Fe II	7479.700	3.892	−3.53	···	···
Fe II	7515.840	3.903	−3.42	···	···
Ca I	5867.570	2.930	−1.57	···	···
Ca I	6166.440	2.520	−1.14	27.6	5.65
Ca I	6169.040	2.520	−0.80	45.6	5.66
Ca I	6455.610	2.520	−1.29	16.7	5.50
Ca I	6572.800	0.000	−4.28	···	···
Ti I	5024.850	0.818	−0.56	23.9	4.17
Ti I	5113.450	1.443	−0.73	···	···
Ti I	5219.710	0.021	−2.24	···	···
Ti I	5866.460	1.066	−0.76	14.1	4.26
Ti I	6091.180	2.267	−0.37	···	···
Ti I	6126.220	1.066	−1.37	6.3	4.46
Ti I	6258.090	1.443	−0.31	15.7	4.21

Table B.1: Equivalent Width Measurements for F/G/K Primaries *(continued)*

Species	λ (Å)	E.P. (eV)	log(gf) (dex)	NLTT 57827 EW (mÅ)	NLTT 57827 Abundance
Fe I	5141.750	2.424	−2.18	···	···
Fe I	5247.060	0.087	−4.94	71.9	5.98
Fe I	5358.120	3.300	−3.16	···	···
Fe I	5412.788	4.440	−1.71	···	···
Fe I	5661.348	4.280	−1.75	···	···
Fe I	5778.458	2.590	−3.45	···	···
Fe I	5784.660	3.400	−2.53	···	···
Fe I	5809.220	3.884	−1.61	···	···
Fe I	5849.690	3.695	−2.93	···	···
Fe I	5852.230	4.549	−1.17	···	···
Fe I	5855.090	4.608	−1.48	···	···
Fe I	5856.100	4.294	−1.56	···	···
Fe I	5858.790	4.220	−2.18	···	···
Fe I	5859.600	4.550	−0.61	···	···
Fe I	5862.370	4.550	−0.25	···	···
Fe I	5956.700	0.859	−4.60	49.6	6.15
Fe I	6027.060	4.070	−1.17	···	···
Fe I	6151.620	2.176	−3.28	···	···
Fe I	6159.380	4.610	−1.83	···	···
Fe I	6165.360	4.143	−1.46	···	···
Fe I	6173.340	2.223	−2.88	26.2	5.64
Fe I	6200.320	2.609	−2.44	44.4	5.99
Fe I	6213.440	2.223	−2.56	56.6	5.84
Fe I	6240.652	2.220	−3.23	26.6	5.99
Fe I	6265.140	2.176	−2.55	73.9	6.02
Fe I	6271.283	3.330	−2.70	···	···
Fe I	6297.801	2.223	−2.73	···	···
Fe I	6322.694	2.588	−2.43	···	···
Fe I	6358.690	0.859	−4.00	57.3	5.65
Fe I	6436.410	4.186	−2.36	···	···
Fe I	6481.878	2.279	−2.97	39.9	6.04
Fe I	6498.950	0.958	−4.69	···	···
Fe I	6518.370	2.830	−2.45	32.4	6.04
Fe I	6574.233	0.990	−5.00	···	···
Fe I	6581.214	1.480	−4.68	···	···
Fe I	6591.330	4.593	−1.95	···	···
Fe I	6608.040	2.279	−3.91	···	···
Fe I	6625.027	1.010	−5.34	···	···
Fe I	6699.142	4.590	−2.10	···	···
Fe I	6713.750	4.795	−1.39	···	···
Fe I	6725.360	4.103	−2.17	···	···

Table B.1: Equivalent Width Measurements for F/G/K Primaries *(continued)*

Species	λ	E.P.	log(gf)	NLTT 57827	
	(Å)	(eV)	(dex)	EW (mÅ)	Abundance
Fe I	6733.150	4.638	−1.40	···	···
Fe I	6739.524	1.560	−4.79	···	···
Fe I	6750.160	2.424	−2.62	45.3	5.94
Fe I	6752.711	4.640	−1.20	···	···
Fe I	6837.009	4.590	−1.69	···	···
Fe I	6857.250	4.076	−2.04	···	···
Fe I	6971.936	3.020	−3.34	···	···
Fe I	7112.170	2.990	−2.99	···	···
Fe I	7751.120	4.990	−0.73	···	···
Fe I	7802.510	5.080	−1.31	···	···
Fe I	7807.920	4.990	−0.73	···	···
Fe I	8365.644	3.250	−2.04	···	···
Fe I	8757.200	2.845	−2.12	···	···
Fe II	5234.620	3.221	−2.22	···	···
Fe II	5425.260	3.200	−3.16	···	···
Fe II	6149.250	3.889	−2.63	···	···
Fe II	6247.560	3.892	−2.27	···	···
Fe II	6369.490	2.891	−4.02	···	···
Fe II	6432.680	2.891	−3.52	···	···
Fe II	6456.390	3.903	−2.06	···	···
Fe II	7479.700	3.892	−3.53	···	···
Fe II	7515.840	3.903	−3.42	···	···
Ca I	5867.570	2.930	−1.57	···	···
Ca I	6166.440	2.520	−1.14	48.3	5.04
Ca I	6169.040	2.520	−0.80	99.7	5.26
Ca I	6455.610	2.520	−1.29	38.9	5.04
Ca I	6572.800	0.000	−4.28	···	···
Ti I	5024.850	0.818	−0.56	···	···
Ti I	5113.450	1.443	−0.73	···	···
Ti I	5219.710	0.021	−2.24	···	···
Ti I	5866.460	1.066	−0.76	86.6	4.07
Ti I	6091.180	2.267	−0.37	···	···
Ti I	6126.220	1.066	−1.37	44.3	4.04
Ti I	6258.090	1.443	−0.31	82.7	3.98

Table B.59: Equivalent Widths Measurements of DES J025540-540807

Species	λ (Å)	E.P. (eV)	log(gf) (dex)	DES J025540-540807 EW (mÅ)	DES J025540-540807 Abundance
Fe I	4045.81	1.48	0.28	···	···
Fe I	4063.59	1.56	0.06	···	···
Fe I	4071.74	1.61	−0.02	···	···
Fe I	4147.67	1.48	−2.10	···	···
Fe I	4216.18	0.00	−3.36	···	···
Fe I	4250.13	2.47	−0.41	···	···
Fe I	4260.47	2.40	0.08	···	···
Fe I	4415.12	1.61	−0.62	···	···
Fe I	4427.31	0.05	−3.04	···	···
Fe I	4430.61	2.22	−1.73	···	···
Fe I	4442.34	2.22	−1.26	···	···
Fe I	4447.72	2.22	−1.34	···	···
Fe I	4459.12	2.17	−1.28	···	···
Fe I	4461.65	0.09	−3.21	···	···
Fe I	4466.55	2.83	−0.59	···	···
Fe I	4489.74	0.12	−3.97	···	···
Fe I	4494.56	2.20	−1.14	···	···
Fe I	4528.61	2.18	−0.82	···	···
Fe I	4531.15	1.48	−2.16	···	···
Fe I	4592.65	1.56	−2.45	···	···
Fe I	4602.94	1.48	−1.95	···	···
Fe I	4707.27	3.24	−1.08	···	···
Fe I	4736.77	3.21	−0.74	···	···
Fe I	4802.88	3.64	−1.51	4.3	5.1
Fe I	4871.32	2.86	−0.36	···	···
Fe I	4872.14	2.88	−0.57	···	···
Fe I	4890.76	2.88	−0.38	···	···
Fe I	4891.49	2.85	−0.14	···	···
Fe I	4903.31	2.88	−0.93	···	···
Fe I	4918.99	2.87	−0.34	···	···
Fe I	4920.50	2.83	0.06	···	···
Fe I	4938.81	2.88	−1.08	···	···
Fe I	4939.69	0.86	−3.34	···	···
Fe I	5051.63	0.92	−2.80	···	···
Fe I	5083.34	0.96	−2.96	···	···
Fe I	5098.70	2.17	−2.03	···	···
Fe I	5110.41	0.00	−3.76	···	···
Fe I	5127.36	0.91	−3.31	···	···
Fe I	5150.84	0.99	−3.07	···	···
Fe I	5166.28	0.00	−4.20	···	···

Table B.59 *(continued)*

Species	λ (Å)	E.P. (eV)	log(gf) (dex)	DES J025540-540807 EW (mÅ)	Abundance
Fe I	5171.60	1.48	−1.79	···	···
Fe I	5191.45	3.04	−0.55	···	···
Fe I	5194.94	1.56	−2.09	···	···
Fe I	5215.18	3.26	−0.87	···	···
Fe I	5266.56	3.00	−0.39	···	···
Fe I	5324.18	3.21	−0.11	···	···
Fe I	5328.04	0.91	−1.47	···	···
Fe I	5328.53	1.56	−1.85	···	···
Fe I	5371.49	0.96	−1.64	···	···
Fe I	5397.13	0.91	−1.98	···	···
Fe I	5405.78	0.99	−1.85	···	···
Fe I	5415.20	4.39	0.64	21	4.71
Fe I	5429.70	0.96	−1.88	···	···
Fe I	5434.52	1.01	−2.13	···	···
Fe I	5455.61	1.01	−2.09	···	···
Fe I	5497.52	1.01	−2.85	···	···
Fe I	5501.47	0.96	−3.05	46.9	4.99
Fe I	5506.78	0.99	−2.79	60.7	5.31
Fe I	5615.64	3.33	0.05	···	···
Fe I	6173.34	2.22	−2.88	6.3	4.98
Fe I	6200.32	2.61	−2.44	7	5.03
Fe I	6213.44	2.22	−2.56	13.5	5.05
Fe I	6240.65	2.22	−3.23	7.6	5.41
Fe I	6265.14	2.18	−2.55	8.6	4.75
Fe I	6322.69	2.59	−2.43	8.4	5.08
Fe I	6481.88	2.28	−2.97	5.3	5.04
Fe I	6518.37	2.83	−2.45	···	···
Fe I	6581.21	1.48	−4.68	8.2	5.35
Fe I	8387.77	2.17	−1.49	···	···
Fe I	8688.62	2.17	−1.20	···	···
Fe II	4508.29	2.85	−2.21	···	···
Fe II	4583.84	2.81	−2.02	···	···
Fe II	4923.93	2.89	−1.32	···	···
Fe II	5197.57	3.23	−2.10	···	···
Fe II	6149.25	3.89	−2.63	3.5	4.94
Fe II	6247.56	3.89	−2.27	8.2	4.99
Fe II	6432.68	2.89	−3.52	7.6	5.07
Fe II	6456.39	3.90	−2.06	7.5	4.73
Na I	5889.95	0.00	0.12	128.8	3.46
Na I	5895.93	0.00	−0.18	159.7	3.61

Table B.59 *(continued)*

Species	λ (Å)	E.P. (eV)	log(gf) (dex)	DES J025540-540807 EW (mÅ)	DES J025540-540807 Abundance
Mg I	4571.10	0.00	−5.62	···	···
Mg I	4702.99	4.33	−0.38	···	···
Mg I	5172.68	2.71	−0.40	128.8	5.05
Mg I	5183.60	2.71	−0.18	159.7	5.25
Mg I	5528.40	4.34	−0.50	···	···
Ca I	4425.39	1.88	−0.39	···	···
Ca I	4434.96	1.89	−0.01	···	···
Ca I	4455.89	1.90	−0.51	···	···
Ca I	6122.17	1.89	−0.32	···	···
Ca I	6162.17	1.90	0.10	56.1	3.87
Ca I	6439.03	2.52	0.47	40.5	3.8

Table B.60: Equivalent Widths Measurements of DES J025543-544349

Species	λ (Å)	E.P. (eV)	log(gf) (dex)	DES J025543-544349 EW (mÅ)	Abundance
Fe I	4045.81	1.48	0.28	···	···
Fe I	4063.59	1.56	0.06	···	···
Fe I	4071.74	1.61	−0.02	···	···
Fe I	4147.67	1.48	−2.10	···	···
Fe I	4216.18	0.00	−3.36	···	···
Fe I	4250.13	2.47	−0.41	···	···
Fe I	4260.47	2.40	0.08	···	···
Fe I	4415.12	1.61	−0.62	···	···
Fe I	4427.31	0.05	−3.04	···	···
Fe I	4430.61	2.22	−1.73	···	···
Fe I	4442.34	2.22	−1.26	···	···
Fe I	4447.72	2.22	−1.34	···	···
Fe I	4459.12	2.17	−1.28	···	···
Fe I	4461.65	0.09	−3.21	···	···
Fe I	4466.55	2.83	−0.59	···	···
Fe I	4489.74	0.12	−3.97	···	···
Fe I	4494.56	2.20	−1.14	···	···
Fe I	4528.61	2.18	−0.82	···	···
Fe I	4531.15	1.48	−2.16	···	···
Fe I	4592.65	1.56	−2.45	···	···
Fe I	4602.94	1.48	−1.95	···	···
Fe I	4707.27	3.24	−1.08	···	···
Fe I	4736.77	3.21	−0.74	···	···
Fe I	4802.88	3.64	−1.51	4.9	5.01
Fe I	4871.32	2.86	−0.36	···	···
Fe I	4872.14	2.88	−0.57	···	···
Fe I	4890.76	2.88	−0.38	···	···
Fe I	4891.49	2.85	−0.14	···	···
Fe I	4903.31	2.88	−0.93	···	···
Fe I	4918.99	2.87	−0.34	···	···
Fe I	4920.50	2.83	0.06	···	···
Fe I	4938.81	2.88	−1.08	···	···
Fe I	4939.69	0.86	−3.34	···	···
Fe I	5051.63	0.92	−2.80	···	···
Fe I	5083.34	0.96	−2.96	···	···
Fe I	5098.70	2.17	−2.03	···	···
Fe I	5110.41	0.00	−3.76	···	···
Fe I	5127.36	0.91	−3.31	···	···
Fe I	5150.84	0.99	−3.07	···	···
Fe I	5166.28	0.00	−4.20	···	···

Table B.60 *(continued)*

Species	λ (Å)	E.P. (eV)	log(gf) (dex)	DES J025543-544349 EW (mÅ)	Abundance
Fe I	5171.60	1.48	−1.79	···	···
Fe I	5191.45	3.04	−0.55	···	···
Fe I	5194.94	1.56	−2.09	···	···
Fe I	5215.18	3.26	−0.87	···	···
Fe I	5266.56	3.00	−0.39	···	···
Fe I	5324.18	3.21	−0.11	···	···
Fe I	5328.04	0.91	−1.47	···	···
Fe I	5328.53	1.56	−1.85	···	···
Fe I	5371.49	0.96	−1.64	···	···
Fe I	5397.13	0.91	−1.98	···	···
Fe I	5405.78	0.99	−1.85	···	···
Fe I	5415.20	4.39	0.64	19.7	4.5
Fe I	5429.70	0.96	−1.88	···	···
Fe I	5434.52	1.01	−2.13	···	···
Fe I	5455.61	1.01	−2.09	···	···
Fe I	5497.52	1.01	−2.85	···	···
Fe I	5501.47	0.96	−3.05	73.6	4.96
Fe I	5506.78	0.99	−2.79	79.3	4.95
Fe I	5615.64	3.33	0.05	···	···
Fe I	6173.34	2.22	−2.88	7.9	4.86
Fe I	6200.32	2.61	−2.44	5	4.66
Fe I	6213.44	2.22	−2.56	7.7	4.53
Fe I	6240.65	2.22	−3.23	···	···
Fe I	6265.14	2.18	−2.55	17.8	4.87
Fe I	6322.69	2.59	−2.43	7.8	4.83
Fe I	6481.88	2.28	−2.97	13	5.24
Fe I	6518.37	2.83	−2.45	17	5.5
Fe I	6581.21	1.48	−4.68	7.2	5.1
Fe I	8387.77	2.17	−1.49	···	···
Fe I	8688.62	2.17	−1.20	···	···
Fe II	4508.29	2.85	−2.21	···	···
Fe II	4583.84	2.81	−2.02	···	···
Fe II	4923.93	2.89	−1.32	···	···
Fe II	5197.57	3.23	−2.10	···	···
Fe II	6149.25	3.89	−2.63	2.5	4.63
Fe II	6247.56	3.89	−2.27	5.4	4.62
Fe II	6432.68	2.89	−3.52	10.6	5.02
Fe II	6456.39	3.90	−2.06	13.2	4.84
Na I	5889.95	0.00	0.12	138.6	2.86
Na I	5895.93	0.00	−0.18	109.4	2.6

Table B.60 *(continued)*

Species	λ (Å)	E.P. (eV)	log(gf) (dex)	DES J025543-544349 EW (mÅ)	DES J025543-544349 Abundance
Mg I	4571.10	0.00	−5.62	···	···
Mg I	4702.99	4.33	−0.38	···	···
Mg I	5172.68	2.71	−0.40	142.9	4.73
Mg I	5183.60	2.71	−0.18	155.3	4.73
Mg I	5528.40	4.34	−0.50	42.4	4.86
Ca I	4425.39	1.88	−0.39	···	···
Ca I	4434.96	1.89	−0.01	···	···
Ca I	4455.89	1.90	−0.51	···	···
Ca I	6122.17	1.89	−0.32	48.6	3.76
Ca I	6162.17	1.90	0.10	69	3.7
Ca I	6439.03	2.52	0.47	52.1	3.75

Table B.61: Equivalent Widths Measurements of DES J025535-540643

Species	λ	E.P.	log(gf)	DES J025535-540643	
	(Å)	(eV)	(dex)	EW (mÅ)	Abundance
Fe I	4045.81	1.48	0.28	265.3	4.42
Fe I	4063.59	1.56	0.06	241.2	4.51
Fe I	4071.74	1.61	−0.02	228.6	4.5
Fe I	4147.67	1.48	−2.10	126	4.84
Fe I	4216.18	0.00	−3.36	208.2	5.38
Fe I	4250.13	2.47	−0.41	141.9	4.64
Fe I	4260.47	2.40	0.08	187.8	4.77
Fe I	4415.12	1.61	−0.62	216.7	4.76
Fe I	4427.31	0.05	−3.04	209.6	4.89
Fe I	4430.61	2.22	−1.73	69.1	4.64
Fe I	4442.34	2.22	−1.26	96.7	4.45
Fe I	4447.72	2.22	−1.34	83.5	4.41
Fe I	4459.12	2.17	−1.28	112.9	4.68
Fe I	4461.65	0.09	−3.21	192.2	4.97
Fe I	4466.55	2.83	−0.59	151.7	5.32
Fe I	4489.74	0.12	−3.97	158.4	5.27
Fe I	4494.56	2.20	−1.14	164.6	5.25
Fe I	4528.61	2.18	−0.82	160	4.88
Fe I	4531.15	1.48	−2.16	137.8	4.87
Fe I	4592.65	1.56	−2.45	131.7	5.22
Fe I	4602.94	1.48	−1.95	169.4	5.16
Fe I	4707.27	3.24	−1.08	31.7	4.73
Fe I	4736.77	3.21	−0.74	54.4	4.67
Fe I	4802.88	3.64	−1.51	...	...
Fe I	4871.32	2.86	−0.36	100.7	4.39
Fe I	4872.14	2.88	−0.57	76.4	4.34
Fe I	4890.76	2.88	−0.38	114.1	4.58
Fe I	4891.49	2.85	−0.14	109.6	4.2
Fe I	4903.31	2.88	−0.93	64.6	4.69
Fe I	4918.99	2.87	−0.34	66.2	3.98
Fe I	4920.50	2.83	0.06	90.7	3.77
Fe I	4938.81	2.88	−1.08	55	4.57
Fe I	4939.69	0.86	−3.34	116.4	4.92
Fe I	5051.63	0.92	−2.80	150.9	4.85
Fe I	5083.34	0.96	−2.96	125.4	4.63
Fe I	5098.70	2.17	−2.03	115.9	5.25
Fe I	5110.41	0.00	−3.76	161.7	4.71
Fe I	5127.36	0.91	−3.31	86.5	5.06
Fe I	5150.84	0.99	−3.07	87.6	4.45
Fe I	5166.28	0.00	−4.20	180	5.28

Table B.61 *(continued)*

Species	λ (Å)	E.P. (eV)	log(gf) (dex)	DES J025535-540643 EW (mÅ)	Abundance
Fe I	5171.60	1.48	−1.79	147.2	4.42
Fe I	5191.45	3.04	−0.55	80.3	4.49
Fe I	5194.94	1.56	−2.09	102.7	4.31
Fe I	5215.18	3.26	−0.87	49.6	4.63
Fe I	5266.56	3.00	−0.39	81.1	4.28
Fe I	5324.18	3.21	−0.11	86.8	4.31
Fe I	5328.04	0.91	−1.47	246.3	4.63
Fe I	5328.53	1.56	−1.85	135.6	4.47
Fe I	5371.49	0.96	−1.64	209.4	4.41
Fe I	5397.13	0.91	−1.98	219.2	4.79
Fe I	5405.78	0.99	−1.85	214	4.71
Fe I	5415.20	4.39	0.64	63.7	4.78
Fe I	5429.70	0.96	−1.88	207.2	4.6
Fe I	5434.52	1.01	−2.13	197.2	4.79
Fe I	5455.61	1.01	−2.09	199.6	4.78
Fe I	5497.52	1.01	−2.85	119.1	4.53
Fe I	5501.47	0.96	−3.05	119.4	4.69
Fe I	5506.78	0.99	−2.79	135.2	4.64
Fe I	5615.64	3.33	0.05	83.3	4.25
Fe I	6173.34	2.22	−2.88	···	···
Fe I	6200.32	2.61	−2.44	···	···
Fe I	6213.44	2.22	−2.56	···	···
Fe I	6240.65	2.22	−3.23	···	···
Fe I	6265.14	2.18	−2.55	···	···
Fe I	6322.69	2.59	−2.43	···	···
Fe I	6481.88	2.28	−2.97	···	···
Fe I	6518.37	2.83	−2.45	···	···
Fe I	6581.21	1.48	−4.68	···	···
Fe I	8387.77	2.17	−1.49	119	4.42
Fe I	8688.62	2.17	−1.20	177.1	4.63
Fe II	4508.29	2.85	−2.21	64.7	4.76
Fe II	4583.84	2.81	−2.02	84.5	4.72
Fe II	4923.93	2.89	−1.32	96	4.2
Fe II	5197.57	3.23	−2.10	37.1	4.66
Fe II	6149.25	3.89	−2.63	···	···
Fe II	6247.56	3.89	−2.27	···	···
Fe II	6432.68	2.89	−3.52	···	···
Fe II	6456.39	3.90	−2.06	···	···
Na I	5889.95	0.00	0.12	···	···
Na I	5895.93	0.00	−0.18	···	···

Table B.61 *(continued)*

Species	λ (Å)	E.P. (eV)	log(gf) (dex)	DES J025535-540643 EW (mÅ)	DES J025535-540643 Abundance
Mg I	4571.10	0.00	−5.62	74	4.73
Mg I	4702.99	4.33	−0.38	76.5	4.93
Mg I	5172.68	2.71	−0.40	209.6	4.43
Mg I	5183.60	2.71	−0.18	256.5	4.75
Mg I	5528.40	4.34	−0.50	···	···
Ca I	4425.39	1.88	−0.39	44.4	3.51
Ca I	4434.96	1.89	−0.01	69.7	3.46
Ca I	4455.89	1.90	−0.51	40.4	3.6
Ca I	6122.17	1.89	−0.32	···	···
Ca I	6162.17	1.90	0.10	82	3.29
Ca I	6439.03	2.52	0.47	···	···